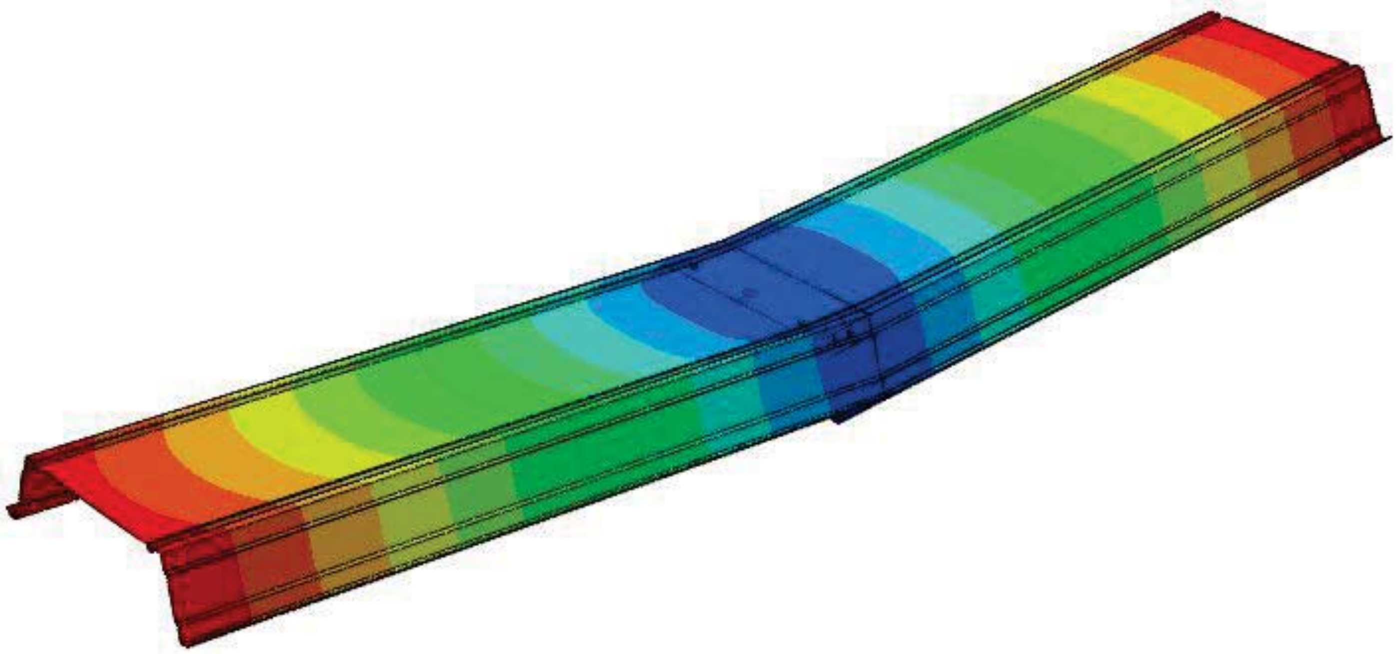

Gerber Splicing in Thin Steel Sheeting of Roofs

A Study of Rotational Stiffness in the Joint

Master's Thesis in the Master's Programme Structural Engineering and Building Technology

JOSEFINE SJÖLANDER
EMY TIDERMAN

Department of Civil and Environmental Engineering
Division of Structural Engineering
Steel and Timber Structures
CHALMERS UNIVERSITY OF TECHNOLOGY
Gothenburg, Sweden 2016
Master's Thesis BOMX02-16-107

MASTER'S THESIS BOMX02-16-107

Gerber Splicing in Thin Steel Sheeting of Roofs

A Study of Rotational Stiffness in the Joint

Master's Thesis in the Master's Programme Structural Engineering and Building Technology

JOSEFINE SJÖLANDER

EMY TIDERMAN

Department of Civil and Environmental Engineering

Division of Structural Engineering

Steel and Timber Structures

CHALMERS UNIVERSITY OF TECHNOLOGY

Göteborg, Sweden 2016

Gerber Splicing in Thin Steel Sheeting of Roofs
A Study of Rotational Stiffness in the Joint

Master's Thesis in the Master's Programme Structural Engineering and Building Technology

JOSEFINE SJÖLANDER

EMY TIDERMAN

Examensarbete BOMX02-16-107/ Institutionen för bygg- och miljöteknik,
Chalmers tekniska högskola 2016

Department of Civil and Environmental Engineering
Division of Structural Engineering
Steel and Timber Structures
Chalmers University of Technology
SE-412 96 Göteborg
Sweden
Telephone: + 46 (0)31-772 1000

Cover:
Deflection of spliced trapezoidal profile steel sheet, modelled in Abaqus

Chalmers Reproservice Göteborg, Sweden, 2016

Gerber Splicing in Thin Steel Sheeting of Roofs

A Study of Rotational Stiffness in the Joint

Master's thesis in the Master's Programme Structural Engineering and Building Technology

JOSEFINE SJÖLANDER
EMY TIDERMAN
Department of Civil and Environmental Engineering
Division of Structural Engineering
Steel and Timber Structures
Chalmers University of Technology

ABSTRACT

In Sweden during the winters of 2009/2010 and 2010/2011 roofs collapsed all around the country. The theory that was first adopted assumed heavy snow fall to be the reason for the failures. Previous research showed that this was not the case and Boverket instead found the common denominator to be the trapezoidal thin steel sheet, TRP, with Gerber system design. In general, the other collapses rather failed due to design or construction errors.

The building industry chooses to build roofs with Gerber system design mostly for its economic benefits due to better material utilisation. The design utilises the sheets in an optimal manner, both in span and over the support, by having joints located where the moment is theoretically zero. This makes the system statically determined.

Previous investigations indicated that the joint did not perform as intended and therefore the purpose of this study is to analyse the behaviour of the sheets' splicing in detail as well as the moment distribution of the sheet. The overall goal is to understand the real behaviour of the Gerber system and present an answer to what may have caused the roof collapses subjected to this study.

Initially, an extensive literature study was performed, which gave a profound understanding about the problematics regarding the Gerber system. Furthermore, several numerical models were computed and compared to analytical values in order to validate the results.

The results showed that the splice does display a rotational stiffness, but it could be concluded that it would have to be higher in order to affect the moment distribution. Even though the results differ from the expected effects of including a stiffness in the design, the method is presumed suitable for the analysis and the results are considered reliable.

Key words: Gerber system, Trapezoidal thin steel sheet, Rotational stiffness, Arbitrary profile, Collapsed roofs, Numerical models, Abaqus

Gerberskarvning av profilerad tunnplåt
En studie om rotationsstyvhet i leden

Examensarbete inom masterprogrammet Structural Engineering and Building Technology

JOSEFINE SJÖLANDER
EMY TIDERMAN
Institutionen för bygg- och miljöteknik
Avdelningen för Konstruktionsteknik
Stål- och träbyggnad
Chalmers tekniska högskola

SAMMANFATTNING

Under vintrarna 2009/2010 och 2010/2011 kollapsade tak runt om i hela Sverige. De kraftiga snöfallen antogs till en början vara orsaken, dock visade undersökningar på att så inte var fallet. Boverket kunde istället fastställa att trapetsprofilerad tunnplåt monterad enligt Gerbersystemet var en gemensam nämnare bland de kollapsade taken. Övriga ras berodde snarare på konstruktion- och produktionsfel.

Byggbranschen väljer att bygga tak med Gerbersystem främst för dess ekonomiska fördelar i form av bättre materialutnyttjande. Systemet använder plåtarna på ett optimalt sätt, både i fält och över stöd, genom att ha skarvar placerade där momentet teoretiskt sett är noll. Detta gör systemet statiskt bestämt.

Tidigare undersökningar antydde att skarvens beteende inte stämde överrens med vad som var förväntat. I och med detta är syftet med denna studie att analysera beteendet av plåtens skarvning i detalj och dessutom studera momentfördelningen i plåten. Det övergripande målet är att förstå det riktiga beteendet hos Gerbersystem och presentera ett svar till vad som kan ha orsakat dessa specifika takkollapser.

Inledningsvis genomfördes en omfattande litteraturstudie, vilket gav en djupare förståelse i problematiken gällande Gerbersystem. Dessutom gjordes ett flertal analyser av numeriska modeller som sedan, i validerande syfte, jämfördes med analytiska värden.

Resultaten visade att en rotationsstyvhet i skarven bör beaktas, men att den skulle behöva vara mycket högre för att påverka momentfördelningen nämnevärt. Även om resultatet skiljer sig från den förväntade effekten av att inkludera en styvhet vid dimensionering, så kan metoden anses lämplig för analysen och resultaten är därmed tillförlitliga.

Nyckelord: Gerbersystem, Trapetsprofilerad tunnplåt, Rotationsstyvhet, Kollapsade tak, Numeriska modeller, Abaqus

Contents

Preface

This master's thesis has been a working progress. We started off looking at the roof collapses in general, but with time we focused our attention more and more on the behavior of the splice.

We would like to thank Björn Mattsson at Boverket for encouraging us to have an open mind and to learn as much as possible. His help when interpreting the design codes and his knowledge on the subject of the roof collapses has been invaluable.

Our examiner Mohammad Al-Emrani has been priceless when it comes to the technical parts of this study; understanding the behavior of the sheet, as well as interpreting the results. When the original method changed and we were no longer able to test actual sheets, his help is what made the final results possible.

We would also like to give a warm thanks to Erik Andersson and Johan Andersson at Lindab who have helped us to understand the Gerber system, as well as for their openness and cooperation. And to Torsten Höglund for his expertise regarding thin steel sheets.

With regard to the numerical models we would finally like to thank Mohsen Heshmati. Without his help with Abaqus, we would have been lost.

Göteborg March 2016

Josefine Sjölander, Emy Tiderman

Notations

Roman upper case letters

C_e	Exposure coefficient
C_t	Thermal coefficient
C_b	Basic snow load factor, Canada
F_v	Vertical force on the connector
K_{rot}	Rotational stiffness
L	Length of sheet
M	Moment distribution along the sheet
$M_{c,Rd}$	Design moment resistance of a cross-section for bending
M_{Ed}	Applied moment
M_o	Moment in the joint
M_{ref}	Reference moment corresponding to applied moment
M_s	Moment at the support without considering support width
N	Normal force in the edge beam
$N_{c,Rd}$	Design resistance of a cross-section for compression
Q_{Rd}	Load-carrying resistance
Q_{Ed}	Applied load
R_A	Reaction force at left support
R_B	Reaction force at right support
R_{gable}	Reaction force acting on the bracing in the gables
$R_{w,Rd}$	The local transverse resistance of a web
S	Shear flow
V	Shear force
W_{el}	Elastic section modulus

Roman lower case letters

a	Length of cantilever
b	Width of the plate/sheet
b_{eff}	Effective width
b_p	Theoretical plane width for a plate
b_R	Width of divided profile
c_{beam}	Distance between primary beams
f_{ya}	Average yield strength

f_{yb}	Basic yielding strength
q	Load acting on the sheet
s	Snow load on the roof
$s_{eff,0}$	Basic effective width regard to effective fold
s_k	Characteristic value of snow load on the ground at the relevant site
t	Plate/sheet thickness
t_{red}	Reduced thickness
z	Vertical distance

Greek lower case letters

α_{tot}	Total change of angle at the support
γ_{M0}	Partial factor
γ_{M1}	Partial factor
γ_d	Partial factor regarding different reliability classes
δ	Deflection
ε_p	Plastic strain
λ_d	Slenderness parameter with regard to distortional buckling
λ_p	Slenderness parameter
μ	Snow load shape coefficient
v	Poisson's ratio in elastic stage
ξ	
ρ	Reduction factor
$\sigma_{com,Ed}$	Compressive stress at the centreline of the stiffener
σ_{cr}	Critical buckling stress
$\sigma_{cr,mod}$	Modified elastic critical stress
σ_x	Longitudinal stress
τ_{Ed}	Shear stress
φ	Angle of the web
φ_{rot}	Rotation in the joint
χ_{d}	Reduction factor with regard to distortional buckling
ψ	Stress ratio

1 Introduction

The first chapter in this report aims to introduce the subject of this master's thesis and its relevance in the building industry today. The overall intention is defined and the method of achieving this is clarified.

1.1 Background

In Sweden during the winters of 2009/2010 and 2010/2011, several roofs collapsed all around the country. The reason at first seemed to be the heavy snow fall. However, further analysis showed that the size of the snow loads did not exceed the design values and the roofs were actually built to hold for even larger loads.

The majority of the collapsed roofs were of thin steel sheeting over continuous spans and with a design called the Gerber system, see Figure 1. This design utilises the sheets in an optimal manner, both in the spans and over the supports, by having joints located where the moment, in theory, is zero. The Gerber system is used for its economic benefits, mostly as a result of better material utilisation.

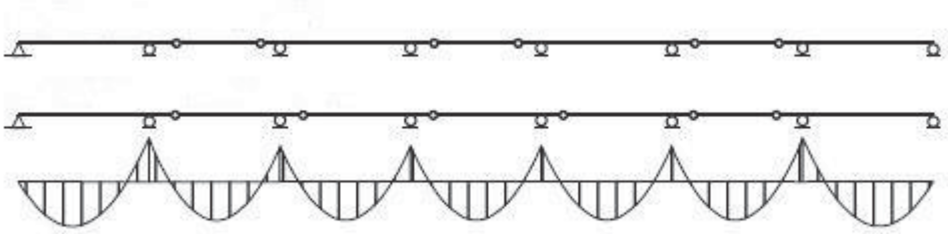

Figure 1: Illustration of the moment distribution and placement of joints in a Gerber system. (Höglund, 2015)

The investigations conducted in conjunction with the roof collapses indicated that because of unevenly distributed snow the Gerber system did not perform as expected, resulting in severe damages in the roof structures.

The National Board of Housing, Building and Planning (Boverket) has previously performed studies concerning what could have been the reasons for the collapses as well as mapping which certain roof types were mostly affected. Boverket is an administrative authority that handles questions on the built environment, construction, management of buildings et cetera. Their conclusions with regard to the Gerber system will be described in chapter 2.

This master's thesis continues the research of the collapsing roofs but will concentrate on the roofs with thin steel sheeting and Gerber system design, trying in such a way to answer the question of how the sheeting actually behaves.

The investigation is performed in collaboration with Boverket, and the thin steel sheeting which is studied is a profile produced by Lindab, a manufacturer of these kinds of structural elements.

1.2 Purpose

The aim of this study is to investigate and analyse the performance of roofs designed with thin steel sheeting and jointed according to the Gerber system. Focus lies on the moment distribution and the design of the joints. The purpose of the study is to analyse the behaviour of the sheets' splicing in detail.

An overall goal is to understand the behaviour of the Gerber system and present an answer to what may have caused these specific roof collapses.

1.3 Limitations

This master's thesis only investigates the roofs with trapezoidal steel sheeting, see Figure 4 on page 15, and Gerber system design. It is the unexpected or unforeseen behaviour of the continuous sheeting that is of specific interest. Many types of buildings with different design and materials choices were damaged during the two winters in question. However, previous research shows that many were due to a wide range of different design and construction errors not related to the behaviour of the design. Therefore, these are not analysed further.

In general, the conclusions presented by Boverket with regard to the roof collapses are considered valid and are therefore not examined in this report.

The focus is on evaluating the moment distribution and not the magnitude of snow load. This limitation is based on the fact that Boverket previously has stated that the amount of snow was never the issue, it was rather the unexpected distribution of the load (Boverket, 2011).

1.4 Method

The content in this master's thesis is divided into two separate parts. The first part is an extensive literature study, which aims to give a more profound understanding and aid in identifying appropriate delimitations for the work. It includes different case studies of collapsed roofs, previous research on the subject as well as recommendations by Boverket regarding the use of the Gerber systems.

The final part consists of numerical studies of the thin steel sheeting, using the FE-programme ABAQUS/CAE 6.13. The computed models are; shell element, solid element, and beam element models. These are analysed and verified by the comparison with analytical results.

A more detailed description of the methodology and process of this work can be found in chapter 7.

2 Previous Investigations of the Collapsed Roofs

The National Board of Housing, Building and Planning (Boverket) was commissioned by the Swedish government to investigate the roof collapses linked to the snowy winters of 2009/2010 and 2010/2011. This was made in collaboration with the Technical Research Institute of Sweden (SP), Faculty of Engineering at Lund University (LTH), Skanska and the Swedish University of Agricultural Sciences (SLU). The aim of these studies was to get a better understanding of the causes of failure and how this could be avoided in the future. The results and conclusions are presented in this chapter.

2.1 Cause of Failure According to Boverket

During the winters of 2009/2010 and 2010/2011 roofs collapsed all around Sweden, see Figure 2. Most were found in the south-west part of the country as well as around the counties Östergötland and Småland, only a few cases were reported in the northern parts (Boverket, 2010).

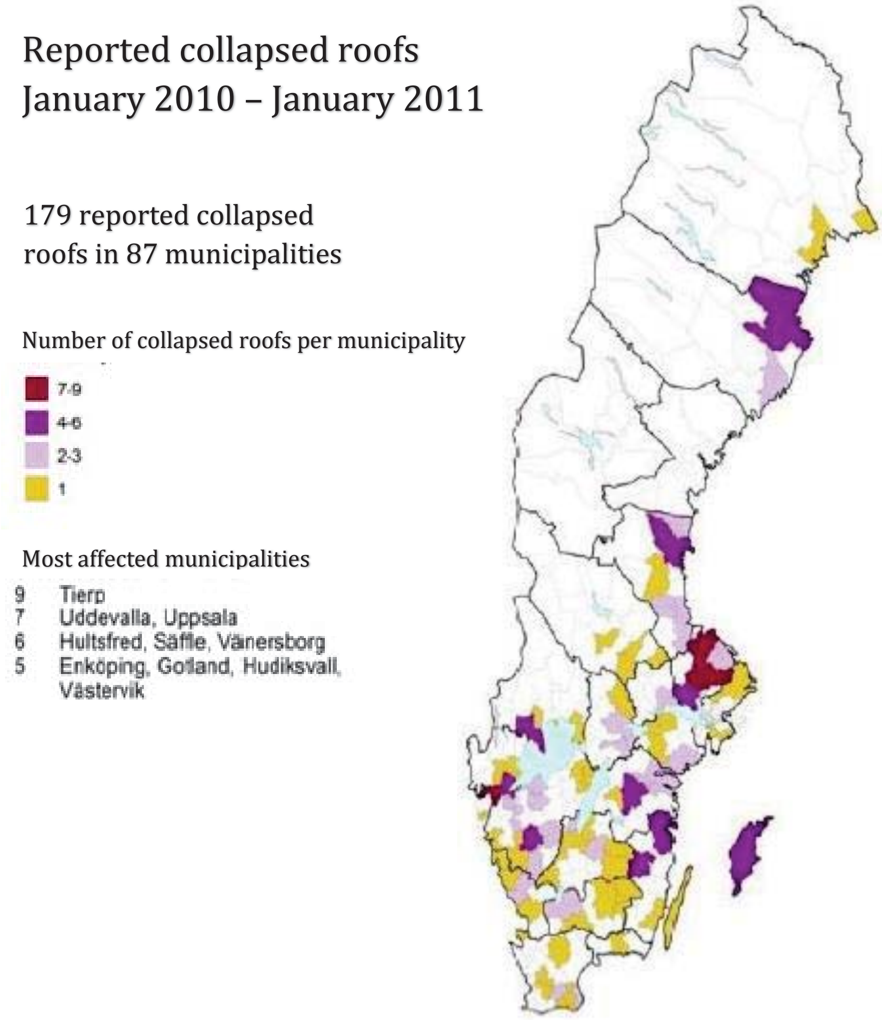

Figure 2: Location of roof -collapses in Sweden during the winters 2009/2010 and 2010/2011 according to SP. Most collapses were found in the southern part of the country. (Boverket, 2011)

Boverket concluded early on that even though the snowfall had been heavy during this time period, it was not the main reason for the roof collapses. The roofs were in most cases designed to carry the loads in question and had often even higher capacity (Boverket, 2010). Comparison between the calculated snow loads and the characteristic values around Sweden according to the present Eurocodes showed only a few places where the load was higher than anticipated. However, there was nothing indicating that the codes were incorrect (Johansson, Lidgren, Nilsson, & Crocetti, 2011). Instead, Boverket believes that the large loads exposed faults of the structures that were in fact made in design, during construction, or due to lack of maintenance.

In general, there was a certain type of building that was found damaged more often than others in these investigations. Typically the structures were very slender with long spans, 50 % of the cases had spans over 20 m, and had low-pitched roofs with the ridge of the roof in a north-east to east direction (Johansson et al., 2011). Common material choices were steel, timber, and glulam. Only a few cases with concrete have been mentioned in the media (Boverket, 2010).

With regard to the snow fall, SP made some observations concerning the load distribution on the roofs that collapsed. First of all the low-pitched roofs seem to have more snow on the leeward side compared to the windward side of the roofs (Boverket, 2011). Secondly the larger the roof area, the more variation of the load was detected along the roof. Finally, SP noticed that the snow amounts on the roofs depended on the topography of the area in which the building was erected. If the surrounding was open, the direction of the ridge in relation to the direction of the wind was of greater importance, as well as any extensions made to the building. (Boverket, 2010)

Boverket emphasises in their report the importance of reviewing the design and all changes made to it, saying that the risk of collapse can be reduced if the design errors are found at an earlier stage. The owner of the building, the client or the contractor in the case of design-build procurement, is responsible for making sure that all demands with regard to load-bearing capacity and stability are met throughout the full service life of the building (Boverket, 2010). This includes any extensions or changes made to the structure.

2.2 Statistics Regarding the Collapsed Roofs in Sweden

During the two winters in question a total of 180 roofs of larger buildings collapsed and the majority of the failures occurred during the end of February 2010 (Johansson et al., 2011). According to weather data this was when the snow amounts were the greatest. The temperatures were below 0 degrees Celsius and the wind direction was steady north to east during the whole specific time-period (Johansson et al., 2011).

The investigations show that the snow weight was in fact not the problem and that 30 % of the collapses can be traced back to design and construction errors (Crocetti, Johansson, & Wikström, 2011). The design loads in a large majority of the cases were not exceeded. According to the report only a few exceptions could be found.

Around 4000 failed or damaged farm buildings were also reported during this time-period (Boverket, 2011). These will not be considered further, mainly due to the fact that they can be built without applying for a building permit and that many of them were never designed by a competent structural designer.

Out of the 180 cases of collapse; only 37 could be studied in close enough detail for conclusions to be made about the actual causes of failure (Crocetti et al., 2011). For that reason these cases are used to analyse the statistics of the collapses, keeping in mind that the data gathered by SP during their documentation of the collapses varies in attention to detail when comparing case to case (Johansson et al., 2011). For example 11 out of the 37 cases have “too high snow load” as their recorded cause of failure, without giving any more details regarding why this conclusion was made (Crocetti et al., 2011).

First of all it can be stated that low-pitched roofs, up to 15 degrees angle, have been dominating among the roofs that collapsed (Boverket, 2011). In 89 % of these cases the snow amounts on top of the roofs were actually higher than the amounts on the ground. It should be added that a high degree of snow redistribution was also detected on the roofs. (Crocetti et al., 2011)

Secondly the choices made during design have influenced the vulnerability of the roof structures. Among the collapsed roofs the primary load-bearing systems were most commonly designed in steel (49 %) then timber (27 %) and glulam (24 %) (Johansson et al., 2011). The most common secondary systems found, according to the report, were trapezoidal steel sheeting (TRP) (30 %), steel purlins (22 %) and in a total of 43 % of the cases it was either: timber, glulam, or canvas. The reason of failure related to material of the primary load-bearing system can be seen in Table 1.

Table 1 *Material in the primary load-bearing system in relation to the reason why the roof in question collapsed.*[1]*It can be concluded that incorrect design was most common in cases with steel girders/frames/bows.* ***(Johansson et al., 2011)***

Material	Lack of or incorrect design	Material or component errors	Lack of maintenance	Construction errors	Other[2]
Steel	8	1	-	3	5
Timber	5	1	2	4	3
Glulam	3	2	-	4	3

Table 1 indicates that a high variety of design materials were found among the roofs that collapsed. Steel was the most common. Research showed that the roofs

[1] 37 cases have been studied but the total sum of the table is not 37 because one collapse can be related to multiple faults.
[2] The column refers to the reason of failure being too much snow on the roof.

designed in timber or glulam all had very few things in common and they were therefore difficult to analyse more closely (Crocetti et al., 2011). The statistics need to be further analysed before any certain conclusions can be drawn.

The *Lack of or incorrect design* in steel structures is the most common cause of failure, but there are still many uncertainties regarding these statistics. Whether or not the design itself was correct cannot be for certain, nor if the behaviour of the structure when the snow fell was different than expected (Crocetti et al., 2011).

SP has listed technical reasons for failure based on their studies of the damaged buildings. Different reason for collapse with regard to incorrect design are listed below (Johansson et al., 2011). These are examples taken from the investigated collapses:

- Snow drifting and the development of so-called snow pockets on the roof were not considered when new buildings were constructed in connection to the one in question.
- Incorrect safety factors used in design, especially in buildings with TRP sheeting.
- The effects of the deflections were not taken into consideration in design *i.e.* second order effects.
- Welded profiles were calculated incorrectly.
- Risk of lateral torsional buckling was not taken into consideration in the design.
- The bolted joints had too low capacity.
- Design based on the wrong snow zone according to the building code.
- The risk of snow drifting or snow falling down on the roof from other buildings was not considered.
- The stabilisation was designed incorrectly.

Some failures happened in the secondary load-bearing system. The roofs with TRP sheeting placed on girders or frames showed the highest numbers of collapses due to incorrect design. Out of the 37 cases studied, 10 were constructed with TRP sheeting. Which by itself does not sound like a lot but it is a common denominator worth highlighting. 7 out of these 10 failures were actually in the sheeting. All these 7 cases have in common that the TRP sheeting was designed with the joints placed according to the so-called Gerber system, see chapter 5. A total of 57 % of the roofs with this specific design actually failed after or during the removal of snow from the roofs. (Crocetti et al., 2011)

Finally, a comment on the age of the structures; even though some of the buildings were in fact built before 1910, the age was not believed to influence the risk of collapse. In fact, 60 % of the buildings were built in the year 1980 or later. (Crocetti et al., 2011)

In conclusion; the statistics show a wide range of faults leading to the roofs collapsing. The common denominators seem to be the low pitch of the roofs, the rather large roof area with a high degree of snow redistribution and the type of material in the load-bearing system. Regarding incorrect design, the TRP sheeting with the Gerber system design should not be considered among those. However, the investigations show that collapses occurred frequently in roofs with this design. The load-bearing capacity should in theory have been sufficient, but still a large number of collapses were seen. That leaves the question of why they collapsed, unanswered.

2.3 Problems Linked to TRP Sheeting

Three specific problems could be identified with regard to the roofs with TRP sheeting as the secondary system; the formation of snow pockets, the sensitivity to unevenly distributed load, and the choice of reliability class with regard to the sheeting acting like a stabilizing system.

In their investigations SP found that the engineer designing the TRP sheeting often did not get enough information regarding obstacles on the roof. These affect the drifting of snow and need to be considered in the design in order to make proper assumptions regarding the formation of snow pockets (Johansson et al., 2011).

In all the 7 cases where the TRP sheeting failed, the Gerber system was used in the design. If the sheets are made continuous, the structure will have a higher robustness if the loads were to be larger than anticipated (Johansson et al., 2011). However, using the Gerber system and placing the hinges at their most optimal location makes the system very sensitive to unevenly distributed loads, see chapter 5.

The reliability class used in design is in practice often RC3 for diaphragm action and RC2 for transversal loading, see Table 2 on page 31, but these need to be reconsidered when looking at steel sheeting as a secondary system. Most often the primary load-bearing system is designed in RC3 and the secondary in RC2 (Johansson et al., 2011). The TRP sheeting is not just a secondary system, it also acts to stabilise the primary load-bearing members. Designing it in RC2 is a design error that might cause failure (Johansson et al., 2011).

2.4 Boverket's Conclusions from the Collapses

Based on their research Boverket drew some conclusions with regard to the roof collapses and their cause of failure. The most common failures were due to construction mistakes or incorrect design, in some cases both. These faults are represented in a total of 75 % of the studied cases according to SP. TRP sheets placed according to the Gerber system were found in many of the collapsed roofs. (Boverket, 2011)

Failure in thin steel sheeting was also mentioned in SP's report on the roof collapses. It was concluded that roofs become sensitive to unevenly distributed load when the Gerber system was applied. It also seems that the designs have been made with the incorrect reliability factors, since failure of the sheeting itself was not considered (Johansson et al., 2011).

According to SP's investigations progressive collapse should be taken into consideration more often in structural design (Johansson et al., 2011). A building is considered to fail when the design value of the effect of actions is higher than design resistance. There is however a difference between a building that collapses in a span and one where progressive collapse occurs. The latter can lead to much more devastating consequences since multiple spans are failing.

The drifting of snow due to steady winds combined with heavy snowfall caused many problems, but the size of the snow load was actually not a problem with regard to calculated design loads. Revision of the characteristic snow loads in Sweden according to the Swedish codes, EKS, was therefore not considered relevant (Boverket, 2011). This can also be confirmed by research made after the snowy winter in 1976/1977 (Johansson et al., 2011). Nevertheless it can be concluded that the weather did in fact lead to a high degree of snow drifting, which essentially caused problems (Johansson et al., 2011).

Furthermore, Boverket noticed that due to the media cover of the collapses, the public became concerned and worried. Many people started to remove snow from their roofs to prevent collapse and damage. What the investigations show, however, is that moving snow off the roofs may actually have been a contributing reason for failure (Boverket, 2011). If one removes snow it is important to make sure that the snow load is still evenly distributed or that a proper snow removal plan, recommended by a structural engineer, is being followed (Johansson et al., 2011).

Finally, when it comes to large roof areas with a lower pitch than 15 degrees, the shape coefficients presented in SS-EN 1991-1-3 might need more modification. SP concludes that the shape factors used in design, at the time of the investigation, might not be representative for the actual snow drift. Especially since the investigations showed that, in some cases, the snow on the roofs were equal to the amounts on the ground (Johansson et al., 2011). Worth mentioning is that previous building codes used higher shape factor for pitched roofs compared to Eurocode. Boverket therefore suggested further research regarding snow loads sizing, calculations, and wind tunnel simulations (Boverket, 2011).

As a final recommendation Boverket suggests that proper information regarding snow density and amount of water in the snow should be made available for property owners via the Swedish Metrological and Hydrological Institute (SMHI) (Boverket, 2011). The snow depth data is not sufficient information, when one is checking snow loads it is more correct to base it on hydrological models of calculating (Johansson et al., 2011). According to SP's report on the collapses, SMHI multiplied the depth of the snow with a constant density of 280 kg/m^2. The value is unusually high for February, and thereby SMHI trusts themselves to be on the safe side (Johansson et al., 2011). Also the density is related to a maximum snow depth occurring once in 50 year, on average.

3 The Effects of the Snow Distribution

Boverket has concluded that the characteristic snow loads are correct and do not need to be altered with regard to the collapsed roofs during the two snowy winters (Boverket, 2011). This master's thesis will not question this or the regulations regarding snow load on the ground. Still, it is evident from the investigations that the load distribution did in fact cause problems when it comes to the trapezoidal steel sheeting constructed according to a Gerber system design. It is thought relevant to elaborate on the factors that might have played a part in the failures, for example the exposure and shape coefficients.

Snow load is a form of natural load and as everything in nature; it can be difficult to predict how it will act. Variations and accumulations are common and unfortunately they can cause a static load-bearing system to collapse in a progressive matter (Johansson et al., 2011). This must be considered in design.

The total snow load acting on a roof is based on a characteristic value combined with shape coefficients (Johansson et al., 2011). This means that it is not only the amount of snow fallen that decides the design load; the shape and pitch of the roof, wind speed and wind direction, as well as drifting of snow, all influence the total load that should be decisive when designing a roof structure. The design load for the roof can become up to four times as high as the snow load on the ground when all factors are considered (Boverket, 2010).

3.1 Calculating Snow Loads

The snow distribution on a roof depends highly on the shape of the roof (Johansson et al., 2011). Other factors that influence the distribution according to SS-EN 1991-1-3, section 5.1.(2) are as follows:

- Thermal properties
- Roughness of the surface of the roof
- Heat transfer through the roof
- Closeness to other buildings
- The terrain in which the building lies
- Climate and weather

The effect of this is that the snow can be evenly distributed or it can have drifted thus giving an unevenly distributed design load. This is in fact a big problem found in conjunction with the roof collapses of 2009/2010 and 2010/2011 (Boverket, 2011).

3.1.1 Snow Load on a Roof

In order to analyse the behaviour of the trapezoidal steel sheeting that suffered from the effects of the unevenly distributed snow load, one calculates the design load based on Eurocode SS-EN 1993-1-3 and EKS 10.

The design snow load on a roof is calculated in the following order according to SS-EN 1991-1-3, section 5.2 (3)P :

$$s = \mu_i C_e C_t s_k \quad [kN/m^2] \tag{3.1}$$

μ Snow load shape coefficient
C_e Exposure coefficient
C_t Thermal coefficient
s Snow load on the roof [kN/m^2]
s_k Characteristic value of snow load on the ground at the relevant site [kN/m^2]

3.1.2 Load Combination

The load-bearing capacity should be larger or equal to the applied load, $Q_{Rd} \geq Q_{Ed}$. To regulate the capacity the Swedish codes, EKS 10, includes the coefficient $\xi = 0.89$ for unfavourable load, to improve the partial coefficient (Johansson et al., 2011).

When designing the roof sheeting there are four primary load combinations which need to be considered according to SS-EN 1990 (6.10a), (Höglund, 2015):

- Load case 1 (ULS): Self-weight, wind (main), snow.
- Load case 2 (ULS): Self-weight (favourable), wind suction.
- Load case 3 (ULS): Self-weight, wind, snow (main).
- Load case 4 (SLS): Self-weight, wind, snow (main).

These load cases are used in different design situations. For designing the sheet based on diaphragm action (load case 1), the connections (load case 2), the sheet with regard to bending moment (load case 3) and the deflection of the sheet (load case 4).

The collapsed roofs studied in this report are all considered light-weight. Arguably the snow load should then be considered as the main load when looking at the capacity of the sheet.

Snow loads higher than the capacity of the roof does not for certain mean failure. Boverket points out that the design capacity is not only a function of the annual snow load distribution based on a 2 % probability per year on average, but also on the distribution of strength of materials according to design methods (Boverket, 2011). The probability of failure per year is 1/1000 000 for a structural element in Reliability class 3.

3.1.3 Characteristic Snow Load

Sweden is divided in to different snow zones representing the characteristic snow loads on ground in different parts of the country. It is calculated based on EKS.

The characteristic snow loads are defined based on measurements of snow amounts and snow densities, made by SMHI (Boverket, 2010). These densities are assumed to vary in Sweden according to the following measurements: 230 kg/m^2 in the south of Sweden, 240 kg/m^2 in the middle of Sweden, and 280 kg/m^2 in the north[3]. Snow density is the product of snow load and snow depth. However combining the highest density with the deepest snow measured is too much on the safe side considering the fact that these two do not occur during the same time-period (Johansson et al., 2011).

When designing based on Eurocode the calculations with regard to snow load often state the density that is required in each specific calculation (SS-EN 1991-1-3, 2003). The fact that the snow density might have played a part in the roof collapses is considered small and unlikely (Johansson et al., 2011).

3.1.4 Snow Load Shape Coefficient, μ

When the characteristic snow load on the ground has been defined; this value is multiplied with a shape factor, μ, to give the actual snow load acting on the roof.

The geometry of the roof can lead to an uneven distribution of snow load and therefore these shape coefficients are crucial in design. Different types of roofs are considered in the Eurocodes; mono-pitched, pitched, multi-span, and cylindrical roofs. As well as roofs abutting and roofs close to taller structures (SS-EN 1991-1-3, 2003). Factors that include the effect of snow falling from a close by higher structure and that of wind are also considered in the codes.

Snow shape coefficients with regard to exceptional snow drift are somewhat different and should be decided according to SS-EN 1991-1-3, ANNEX B. Obstacles on a roof will have an impact on the drifting of the snow during windy conditions. When calculating the shape coefficients this will have to be taken in to consideration according to SS-EN 1991-1-3, section 6.2.

The Swedish handbook BSV 97, now replaced by Eurocode, has an addition to the calculation of duo-pitched roof's shape coefficients. Certain shape coefficient are used when the load distribution is uneven; however it is only valid for roof pitches between 15 and 60 degrees (Johansson et al., 2011). The new codes however take the distribution in consideration also for lower pitched roofs (SS-EN 1991-1-3, 2003).

3.1.5 Exposure Coefficients, C_e

The exposure coefficient, C_e, is used to determine the load acting on the roof with regard to wind exposure (SS-EN 1991-1-3, 2003). The recommended values depend on the topography in which the structure is situated. According to SS-EN 1991-1-3, section 5.2 (7) future development around the site should be considered when choosing this coefficient from Figure 3.

[3] Mail conversation with Björn Mattsson, Boverket, 2016-05-25

Table 5.1 Recommended values of C_e for different topographies

Topography	C_e
Windswept [a]	0,8
Normal [b]	1,0
Sheltered [c]	1,2

[a] *Windswept topography*: flat unobstructed areas exposed on all sides without, or little shelter afforded by terrain, higher construction works or trees.

[b] *Normal topography*: areas where there is no significant removal of snow by wind on construction work, because of terrain, other construction works or trees.

[c] *Sheltered topography*: areas in which the construction work being considered is considerably lower than the surrounding terrain or surrounded by high trees and/or surrounded by higher construction works.

Figure 3: Recommended national values for the exposure coefficient depending on topography according to ***(SS-EN 1991-1-3, 2003)***

Boverket stresses the importance of this further, saying that the value 0.8 should be used very carefully. In order for it to be applied; the temperature must stay below 0 degrees and the structure should be constantly exposed to wind (from all directions), as well as no heating radiating from inside the building (Boverket, 2011). On parts of the roof where snow can gather in larger amounts, *e.g.* on a distinct leeward side, the factor 0.8 must not be used (Johansson et al., 2011). Actually, according to the new building code EKS 10 from 2016, it is no longer possible to use a lower value than 1.0.

3.1.6 Thermal coefficient, C_t

When it comes to the thermal coefficient, C_t, it should according to SS-EN 1991-1-3, section 5.2 (8) be put to 1.0. Only if melting due to heat loss and high thermal transmittance of the roof occurs may the load be reduced.

3.2 Investigations in Other Nordic Countries

Other Nordic countries have also experienced roof collapses during past winters with harsh weather conditions. Their investigations and conclusions help in understanding the problems with the snow distributions on the roofs.

During the winter of 2009/2010 Denmark experienced many roof collapses, mostly in the northern parts of Jylland. Most affected were the light-weight structures in steel or timber, with long spans (Johansson et al., 2011). The conclusions that were made from the investigations showed that design and construction errors, as well as poor maintenance and large snow amounts, were the main reasons of failure. Interesting is, however, that it was confirmed that the characteristic snow loads on the ground were exceeded and that the Danish Standard actually recommended a revision of the values (Johansson et al., 2011).

Meetings between Swedish and Danish authorities, regarding the outcome of the heavy snow falls, resulted in some defined areas in need of further research

(Tolstoy, 2011). Especially exposure coefficients and shape factors needed to be reconsidered for larger one-storey buildings with low-pitched roofs. Snow drifting, uneven distribution of snow, and the formation of snow pockets, were all of particular interest.

In Norway special attention was given to structures with larger roof areas. The conclusion was that the snow load on a longer building is not as likely to be reduced all over the roof; in the middle part some of the snow might not have drifted off the roof. The Norwegian national annexes to the Eurocodes express that the exposure factor when the roof structure is longer than 50 m, must not be reduced to 0.8 but the factor should instead be calculated as 1.0 (Boverket, 2011). This can be compared with the Swedish values in Figure 3.

3.3 Canadian Weather Simulations

Similar conclusions can be found in Canada where the basic snow load factor, C_b, depends on the size of the roof. Thereby the designer takes in consideration that larger roof areas tend to be less affected by wind blowing snow of the roof (Tolstoy, 2011). This means that the coefficient should be larger for a larger roof area.

Wind tunnel tests have previously been performed in Canada, however the problem is more complex then testing a wind acting on a building from one direction over a specific time period (Irwin, Gamble, & Taylor, 1995). The complexity of all the following factors acting together had hardly been analysed: wind changing direction, wind speed, snow fall, snow melting, rain, and heat loss through the roof. In regard to this the Finite Area Element method, the FAE-method, was developed in Canada 1986 (Irwin et al., 1995). The method consists of a combination of wind tunnel tests and metrological data to be used as inputs in an FE-analysis. In this way the snow quality will be more realistic and the change of weather conditions more accurately portrayed.

The simulations that were made showed that $C_b = 0.8$ is conservative when it comes to unsheltered terrain, but actually too low when it comes to large rectangular roofs in sheltered terrain (Irwin et al., 1995). This correlates with the Swedish exposure coefficient and the Norwegian exposure factor. The conclusion was that snow on the roof should not be reduced compared to the snow load on the ground in these situations, mostly due to the size of the roof.

4 Thin Steel Sheeting

Based on the investigations regarding the roof collapses described in chapter 2, it is evident that roofs designed with trapezoidal steel sheeting as the secondary load-bearing system, show a different behaviour than what is assumed in design. To fully understand the reason for this, it is important to first and foremost look at the steel sheeting and how it is designed to function. This chapter will present information about how sheet functions, the designing steps of the trapezoidal profile sheeting, and the capacity of the sheeting.

4.1 Cold-Formed Profiled Sheet

The building industry can today, after years of improvements, offer several well-developed steel products. One of these products is cold-formed profiles that in its turn have many different options of shapes and thicknesses. Within the construction of buildings, the trapezoidal profile sheeting is the most widely used design, especially regarding roof and wall sheeting.

The method of producing cold-formed profiles has its origin in the USA. The aeronautical division has a big influence on the development of the production industry regarding thin steel sheets, and a dedicated standard was created for the technology. During the 1960s this standard came to Europe and Sweden, and in the end of the 1970s it was developed into the Swedish thin sheet standard 79, StBK-N5. This standard is the basis for the current Eurocode 3, SS-EN 1993-1-3, which is a standard for design of steel structures, especially regarding cold-formed members and sheeting. (Höglund & Strömberg, 2006)

Cold-formed steel products; trapezoidal sheet, panels, cassettes, profiles, and composites products are the organised groups in the construction industry. As mentioned previously, when it comes to constructing roofs and walls the trapezoidal profile is the most widely used one. The profiled sheet has characteristics adopted from the three generations previously developed throughout the years (Höglund & Strömberg, 2006), see Figure 4.

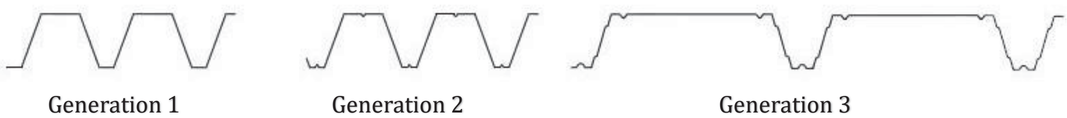

Figure 4: Three generations of profiled profiles.

- Generation 1: Trapezoidal sheet with plane sections parts, height 45-100 mm, spans 3-6 m.
- Generation 2: Trapezoidal sheet with stiffened (grooved) sections parts, height 50-120 mm, spans 4-8 m.
- Generation 3: Trapezoidal cassettes with both longitudinal and transversal grooves (embossing), height 210 mm, spans 6-12 m.

The cold-formed technology has a great capacity to form different profiles of thin steel sheets. The yield strength of the sheet material before any processes to form the profile is presented as f_{yb} in SS-EN 1993-1-3. In Eurocodes there is also an increased value of the yield strength as an average value denoted as f_{ya}. The elevated value is achieved through strain hardening after cold-working the steel sheet. This value can only be used for profiles in cross-section class 1 and 2 which do not buckle. Steel sheeting is often galvanized and has a thickness between 0.4 – 2.5 mm in Sweden. (Höglund & Strömberg, 2006)

In the book Cold-formed profiles by T Höglund and J Strömberg, the advantages of the thin sheet technology are mentioned, some of them are listed below:

- Standard products can be manufactured with high productivity, thus at low cost.
- The coating can be performed when the material is still flat, *i.e.* before the sheeting is formed, which increases the productivity considerably and provides better quality and lower cost compared to the case where coating is done after the sheet is formed.
- The profiles can be made stackable, which facilitates the storage and transportation of the sheets.
- The fasteners that are used, *e.g.* the stainless steel tapping screws, are developed to give a simple and quick installation and good life-span with low maintenances costs.

As mentioned before the trapezoidal sheeting is very useful in the building industry. In order for this profile to sustain larger amount of stresses it is provided with longitudinal stiffeners; grooves in the flanges and folds in the webs. A profile can have either both of the stiffeners or just one of them (Höglund & Strömberg, 2006). In order to utilise the full potential of the stiffeners it is important that the stiffeners do not buckle themselves (SS-EN 1993-1-3, 2006). The shape of the stiffeners is shown in the Figure 5.

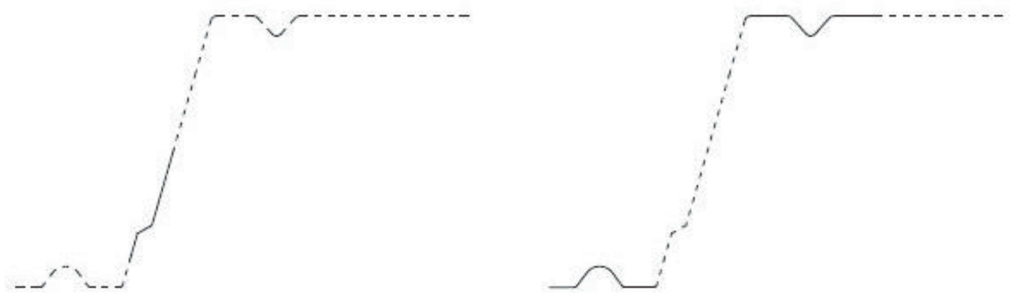

Figure 5: On the left-hand side illustration showing the folds in the webs and on the right-hand side illustration showing the grooves in the flanges.

4.2 Design of Thin Steel Sheeting with Trapezoidal Profile

Trapezoidal profiles are designed with regard to bending moment in the spans and bending moment combined with shear force at the supports. Other concerns that have to be taken into account when choosing which kind of sheeting profile is needed are the restrictions with regard to the deflection as well as the possibility to walk on the steel sheets. (Höglund & Strömberg, 2006)

The steps of calculations that are used for conventional steel profiles are the basis for the cold-formed profiles as well, but the substantial difference in the design is the estimation of the effective cross-section, which will be more described in subchapter 4.2.3. These calculations are more complicated, particularly for thin cold-formed trapezoidal profiles with longitudinal stiffeners in both the flanges and the webs. This is because of the impact of distortional buckling, which requires additional cross-section constants and more variables to consider. (Höglund & Strömberg, 2006)

4.2.1 Buckling

In the calculation of the load-carrying capacity of trapezoidal sheeting it is important to consider three types of buckling, which are: local buckling, distortional buckling, and global buckling. Specifically local buckling and distortional buckling have a tendency to occur for cold-formed profiles and are usually the cause of failure with regard to the compressed parts of the cross-section. There are two ways of handling these occurrences of buckling, either to reduce the stresses, or to determine the load-carrying capacity by calculating the effective cross-section (Höglund & Strömberg, 2006). The three types of buckling are shown in Figure 6, the local buckling and distortional buckling will be further described below.

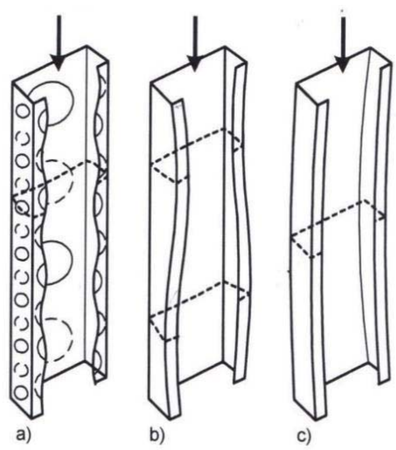

Figure 6: Different types of buckling a) local buckling, b) distortional buckling, c) global buckling (flexural buckling) (Höglund & Strömberg, 2006)

The use of cold-formed profiles with free edges leads to distortional buckling. The distortional buckling appears in the form of long waves and does not have one particular area which would be more critical than the others. When considering distortional buckling of trapezoidal sheeting with stiffeners, it is a flexural buckling of the stiffener themselves. Due to this the buckling of the stiffeners should also constitute a concern. (Höglund & Strömberg, 2006)

The local buckling will be seen as small buckles. In contrary to the distortional buckling, this buckling type is known for its distinctly critical areas where the sheet will buckle locally. As a result of this the load can still increase until its ultimate breach. (Höglund & Strömberg, 2006)

As mentioned before, local buckling and distortional buckling are almost always the cause of the ultimate breach in the compressed sheet. If there is a risk for a distortional buckling mode, this will in fact be the reason for the total collapse. The final failure can occur at different stress levels depending on the slenderness of the cross-section which is divided into four cross-section classes; these indicate when either local or distortional buckling occurs. (Höglund & Strömberg, 2006)

Also important with reference to local or distortional buckling is the critical buckling stress, σ_{cr}, for when buckling is initiated. It is proportional to $(t/b)^2$, where t and b stands for the plate thickness and width respectively (Höglund & Strömberg, 2006). In SS-EN 1993-1-3 there are many different critical buckling stress equations, and the choice of which equations that should be used depends on many factors. For example whether the profile is with or without stiffeners, the type of stiffeners, and which shape the sheet has; *i.e.* plane or trapezoidal profile.

The buckling's impact on both the load-carrying capacity and the stiffness of the profile is considered by using the effective cross-section, which will be explained in subchapter 4.2.3.

4.2.2 Trapezoidal Sheeting Profiles with Intermediate Stiffeners

As mentioned; a trapezoidal profile can be produced with stiffeners in many different ways, the options are listed below:

- Flange with one or several grooves
- Webs with one or several folds
- Both flanges with grooves and folds in the webs

The effective area is calculated in different ways depending on the cross-section and type of stiffener. In SS-EN 1993-1-3, section 5.5.3.4, the different designs are specified.

When a profiled sheeting is created with stiffeners, for example grooves in the flanges, the distortional buckling needs to be considered, which is the flexural buckling of a stiffener. The impact of the distortional buckling in the calculations is taken into account by the reduction factor, χ_d, which is obtained by different value of the slenderness parameter, $\overline{\lambda}_d$. The index d refers to distortional buckling. The slenderness parameter is calculated according to equation (4.1).

$$\bar{\lambda}_d = \sqrt{\frac{f_{yb}}{\sigma_{cr}}} \tag{4.1}$$

$\bar{\lambda}_d$ Slenderness parameter with regard to distortional buckling
f_{yb} Yield strength [MPa]
σ_{cr} Critical buckling stress [MPa]

The stiffeners, grooves and folds, have a big impact, not just when calculate the load-carrying capacity. For example the stress distribution in the flange will differ comparing a flange with grooves and one without. If the flange is formed with a groove, the distribution changes and the groove itself takes care of some of the stresses (Höglund & Strömberg, 2006). The stress distribution with a groove in the flange is illustrated in Figure 7.

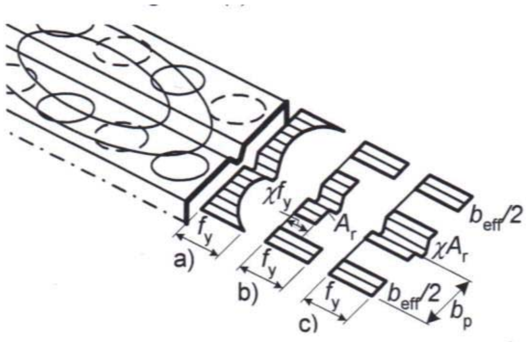

Figure 7: *Flange with a groove. a) actual stress distribution b) idealised stress distribution c) stress distribution over effective cross-section* (Höglund & Strömberg, 2006).

4.2.3 Effective Cross-Section

There is a difference in how to calculate the effective cross-section and it depends on whether or not the profile is plane, or with stiffeners. If the profile, like the trapezoidal sheet, has stiffeners; the stiffeners have their own effective parts (SS-EN 1993-1-3, 2006).

When the steel sheet is plane and without stiffeners the traditional calculation for the effective cross-section is made according to the steps in SS-EN 1993-1-5 with some alterations of the terms. The theoretical plane width, b_p, corresponds to $\bar{b}$ in SS-EN 1993-1-5. Further the effective width is calculated through the equation (4.2):

$$b_{eff} = \rho b_p \qquad (4.2)$$

ρ Reduction factor
b_p Theoretical plane width for a plate [mm]
b_{eff} Effective width [mm]

The reduction factor, ρ, for steel sheet buckling is calculated with the help of the steel sheet slenderness parameter, $\bar{\lambda}_p$, which in its turn is calculated through the yield strength, f_{yb}, and the critical buckling stress, σ_{cr}.

$$\bar{\lambda}_p = \sqrt{\frac{f_{yb}}{\sigma_{cr}}} \qquad (4.3)$$

$$\rho = \frac{1-0.055(3+\psi)/\lambda_p}{\lambda_p} \qquad \rho \leq 1 \qquad (4.4)$$

$\bar{\lambda}_p$ Slenderness parameter
ψ Stress ratio

Both the slenderness parameter and the reduction factor can be defined using other equations due to *e.g.* the impact of distortional buckling, see equation (4.1).

When it comes to TRP sheets, the effective width of the compressed flange is calculated according to equations (4.2) to (4.4). However, if the sheeting is produced with grooves in the flange, it is important to remember that the cross-section is dependent on both the stiffeners and the effective parts of the flange according to section 5.5.3.3 in SS-EN 1993-1-3. The actual width of the plane parts will differ, see Figure 8. Without a groove the width is the width of the whole flange, compared to the width of the flange with a groove, which will be separate in two parts, one on each side of the groove.

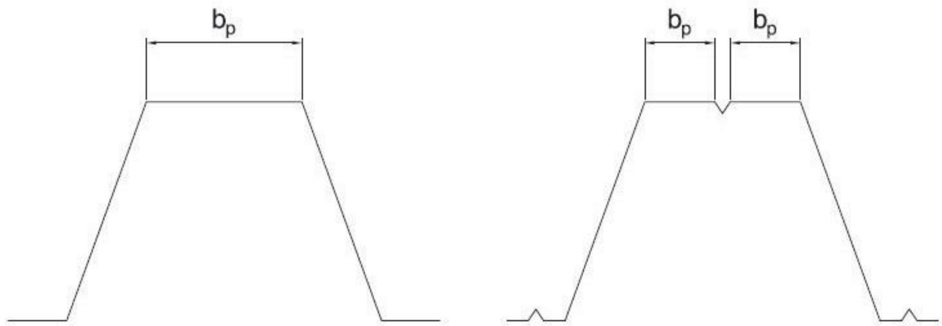

Figure 8: To the left, illustration of the width b_p without a groove in the flange and to the right an illustration of the width b_p with a groove in the flange.

The effective area of the folds in the webs is first calculated according to Eurocode, SS-EN 1993-1-3, section 5.5.3.4.3(5) and then revised if the plane elements are fully effective.

The initial location of the centroidal axis is based on the effective area of the compressed flange but the gross area of the webs, this gives the value e_c in Figure 9. Considering the fact that both the flanges and the webs have stiffeners; the reduction factor for the distorional buckling, χ_d, is obtained from a relative slenderness that depends on the elastic critical stress for the stiffeners, equation (4.5), where the modified elastic critical stress regards both types of stiffeners.

$$\bar{\lambda}_d = \sqrt{\frac{f_{yb}}{\sigma_{cr.mod}}} \tag{4.5}$$

$\sigma_{cr,mod}$ Modified elastic critical stress [MPa]

The bottom fold of a trapezoidal sheet is in tension, but the top fold will be in compression and therefore have an effective cross-section area, A_{sa}. The widths, $s_{eff.1}$ to $s_{eff.n}$ in Figure 9, are all a function of the basic effective width $s_{eff.0}$ calculated according to equation (4.6), where $\sigma_{com.Ed}$ is the stress in the compressed flange when the cross-section resistance is reached.

$$s_{eff.0} = 0.76t\sqrt{\frac{E}{\gamma_{M0}\,\sigma_{com.Ed}}} \tag{4.6}$$

$s_{eff.0}$	Basic effective width [mm]
t	Thickness of the sheet [mm]
E	Modulus of elasticity [N/mm²]
γ_{M0}	Partial factor
$\sigma_{com,Ed}$	Compressive stress at the centreline of the stiffener [MPa]

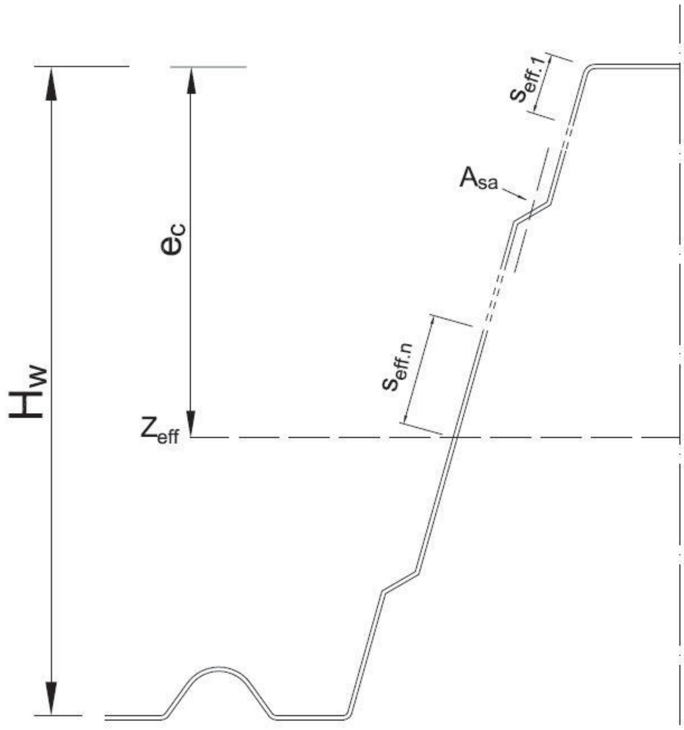

Figure 9: Effective width calculated for webs with fold.

The reduced effective area is then represented by a reduced thickness according to equation (4.7), for all elements included in A_{sa}.

$$t_{red} = \chi_d t \tag{4.7}$$

t_{red}	Reduced thickness
χ_d	Reduction factor for distorsional buckling

4.2.4 Load-Carrying Capacity

Local buckling is the cause for reduced load-carrying capacity. It is often occurring because of the slenderness of the profile's tops, bottoms, and webs. To identify the actual slenderness of a cold-formed profile is difficult but if the gross cross-section is larger than the effective cross-section, the profile can be classified in class 4 (Höglund & Strömberg, 2006).

In design the impact of buckling is decided by the effective cross-section properties according to SS-EN 1993-1-3, section 6.1. When it comes to the load-carrying capacity of a profile, whether it is exposed to; compressive forces, bending moment, or both, the effective and the gross properties should be considered when choosing design method. If the effective area is less or equal to the gross area there are appropriate equation *e.g.* when calculating the compressive reaction force, $N_{c,Rd}$. In the same manner the design moment reaction, $M_{c.Rd}$, can be decided depending on if the effective sectional modulus is less or equal to the gross elastic sectional modulus (SS-EN 1993-1-3, 2006).

Shear and concentrated forces, like support reactions and concentrated loads, are considered in the design of the webs with regard to slenderness and load-carrying capacity. Different rules of design apply depending on the cross-section of the sheet, *e.g*. the specific shape of the cross-section and whether the webs are formed with folds or without. In SS-EN 1993-1-3 *e.g.* it is considered if the web is stiffened or unstiffened when it comes to calculating the load-carrying capacity for the support reaction, $R_{w,Rd}$. See the two options in Figure 10.

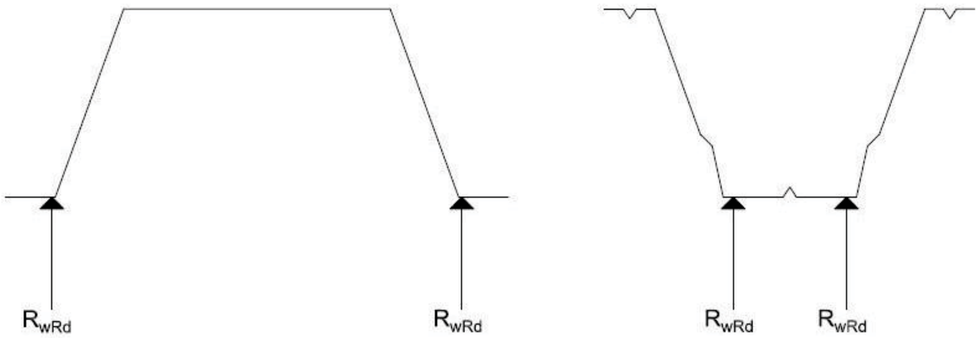

Figure 10: Support reaction for an unstiffened web and support reaction for a stiffened web.

Decisive in design of a trapezoidal sheeting profile is most often the interaction between the bending moment and the support reaction force (Höglund & Strömberg, 2006). This equation can be found in SS-EN 1993-1-3, section 6.1.11.

4.2.4.1 Changes of Codes from Boverket's Consequence Investigation, EKS 10

Design calculations of standardized profiled steel sheet products are often based on and verified by testing. When this kind of testing is made it should be performed with equipment that can simulate the real supports and loads in a stabilising system (SS-EN 1993-1-3, 2006).

Boverket issued new design rules in 2016, EKS 10, which is the Swedish building code regarding mechanical strength and stability. General requirements and national choices to the Eurocodes are given. One of the changes is of particular interest to this project and can be found in chapter 3.1.3, §12a in EKS 10. It presents a new regulation regarding how the capacity of thin steel sheet profiles should be determined on the basis of testing. More specifically it is the change of material parameters when using test methods which only include a few test samples.

The change from earlier codes concerns the design coefficients from the test values. The characteristic fractile factor, k_n, from table D.1 in SS-EN 1990 must no longer be used according to Boverket. The factor to be used instead can be retrieved from table B-5 in BFS 2015:6. This is because the design based on testing does not match the capacity in reality. The safety against failure will be too low if the method from SS-EN 1993-1-3 is applied, which is thought to potentially be the cause of the collapsed roofs (Boverket, 2015).

This change of regulations concerns the collapsed roofs during the past winters in question. In fact the model in SS-EN 1993-1-3 is incorrect with regard to probability theory and that is the actual cause of the change. Hopefully fewer collapses will be reported in the future after this alteration is applied. (Boverket, 2015)

4.3 Connectors

The screws that are used when constructing roofs with thin steel sheeting are most often a type of self-tapping screw. Meaning a clamping force will be generated from joining the two plates together in a splice. An illustration of the clamping effect is shown in Figure 11. The tip of the screw has a reduced diameter and a so-called shank between the thread and the head, see Figure 12. The sheets will be clamped together in the shank part which has a length corresponding to the thickness of the two joined sheets. If the shank is too large the sheets will not be pressed together properly and the capacity with regard to bearing failure is lost. (Höglund, 2015)

These types of clamping connectors are very practical to use when it comes to simplicity during construction (Höglund, 2015); the screws are fully drilled through the sheets. This however puts pressure on the engineer and the way of communicating the importance of following the design drawings very thoroughly.

In SS-EN 1993-1-3 it is prescribed that screws in the top flange must be drilled in a matter to avoid the formation of buckles. In joints which are located in the spans; the screws should be placed in the webs in order to keep the continuous system intact (Höglund, 2015). Remaining screws are only used for practical reasons during mounting and these do not transfer shear. For example the screws that are placed in the longitudinal grooves, see Figure 30 on page 38, these are not important for the capacity in the design. Their location is only chosen for practical reasons.[4]

The design capacity of the screws should be made with regard to bearing failure and some restrictions apply concerning minimum distances (Höglund, 2015). These depend on the type of connection and the profile of sheeting.

[4] Mail conversation with Erik Andersson, structural engineer Lindab, 2016-05-30

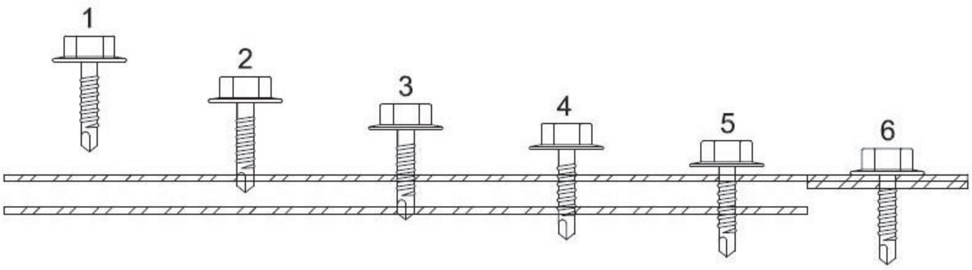

Figure 11: *Clamping effect when the connector is being attached.*

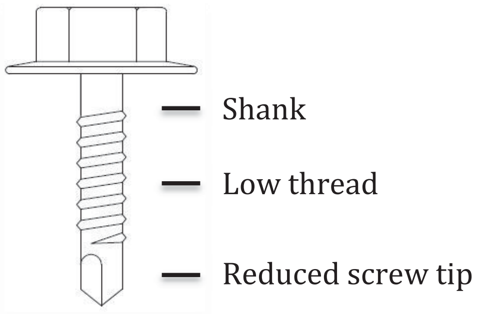

Figure 12: *The screw used for assembly of thin steel sheets.*

5 Gerber System

The sheets described in chapter 4 can be used in design of different components. This master's thesis will, based on the previous investigations described in chapter 2, look more closely at the sheeting when it is designed with the so-called Gerber system. Boverket's studies exposed the flaws and vulnerabilities of this specific type of roof structure, this chapter therefore aims to describe how the Gerber system actually works. In doing so it also tries to answer the question of why the collapses occurred.

5.1 Gerber System in Theory

In the year 1866 the German engineer Heinrich Gerber got the patent for a system called Gerber beam. In Sweden it is called Gerber system (Fernández Troyano, 2003). It is also called: the cantilever, suspended span system, and compound beams (Bill Jr, 2000). The system can be used in the design of for example floors, but to gain its full potential the designer should use it when designing roof structures. This according to Herbert L. Bill Jr who fully explains the function of the system in his article: Cantilever and Suspended Span Roof Framing System. The reason for this, explains the author, is because when designing floors with the system a designer needs to consider imposed loads which the roof system is not subjected to. Preferably the system should be used when the actions are rather constant.

The Gerber system can be used with different materials, but is most commonly designed with timber or steel. In this study, only the Gerber system concerning roof designs with steel sheet material will be described.

For larger buildings like industrial buildings, sports centres, commercial buildings, and others, the roof's steel sheeting can be designed in many different ways. By using the steel sheeting as a secondary load-bearing system above the primary girders, purlins are not needed in the design. Trapezoidal profiles are one of the most common shapes for this kind of roofing. Some other roof designs used in Sweden are the so-called: "2-Span" system, the "Simple Overlapping" system, and the "Double Overlapping" system.[5]

In the construction of multiple-span buildings, the 2-Span system is the most commonly used. This system is continuous over two spans and above every third support – a hinge is used, see Figure 13. The sheet will handle the moment and the shear force is handled at the support[5].

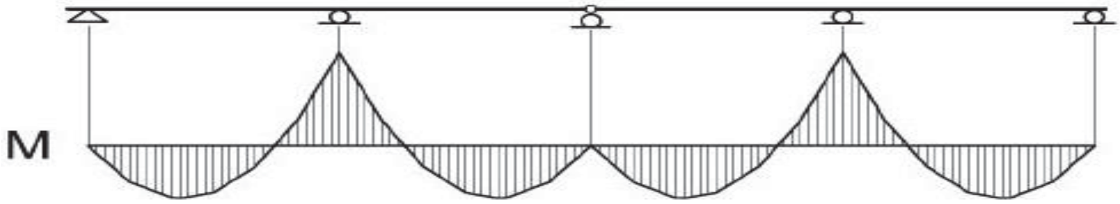

Figure 13: *2-span system with a hinge at the third support. (Erik Andersson, 2016)*

[5] Dialog with Erik Andersson, structural engineer Lindab 2016-02-15

If the Overlapping system is used instead, the steel sheeting is spliced above the support, either single or double splice, see Figure 14 and Figure 15. The benefit of using the Double Overlapping system is that the sheeting can handle twice as much moment and support reactions. An alternative to the Overlapping system, is to place the joints in the spans instead of over the supports. This is the so-called Gerber system[6].

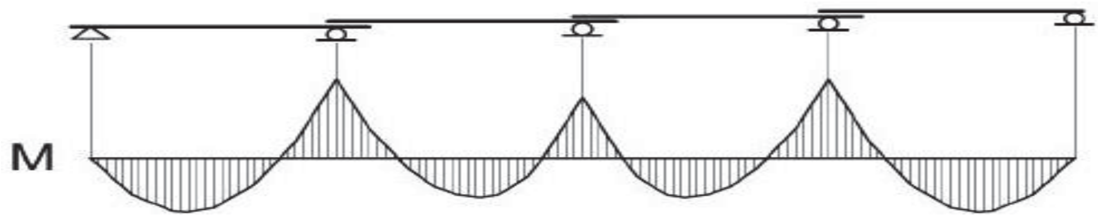

Figure 14: *Single Overlapping system; the sheeting is spliced on right side of the supports with a certain length. (Erik Andersson, 2016)*

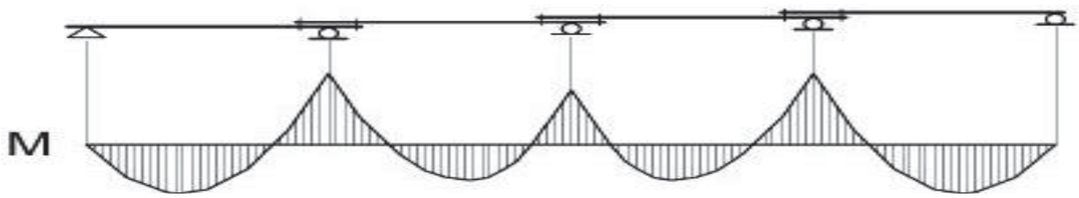

Figure 15: *Double Overlapping system; the sheeting is spliced on both sides of the supports, with a certain length at each side. (Erik Andersson, 2016)*

In a Gerber system the moment distribution on the roof is decided by the location of the joints in the spans. The sheets are connected with hinges at the points where the moment is theoretically zero; these hinges are supposedly not transferring any moment and it makes the system statically determined. Because of the location of the hinges the material is used in a more optimised manner. The sheet is equally utilised in the spans as over the supports. (Höglund, 2015)

Like the 2-Span system the Gerber system with splicing makes a continuous system. Because of the continuity it can: handle larger loads, smaller deflections arise, and the mounting process becomes easier (Höglund, 2015).

The main advantage and reason to use this system is the opportunity to optimise the material use by the location of the hinges, the use of the material can be reduced with 50 % (Bill Jr, 2000). This gives an economic and competitive value for the system. The Gerber system is designed for a uniformly distributed load, if the load pattern changes compared to the designed one, the risk of a collapse increases due to the unforeseen higher local loads. If the design takes into account the different load cases, the material efficiency is no longer economically justified[6].

[6] Dialog with Erik Andersson, structural engineer Lindab 2016-02-15

Another economical advantage is the simplicity during construction. To build a roof framing with this system usually goes faster[7], more about this in subchapter 5.2.

There are two different design options with regard to this system – “Real” and “Fake” Gerber systems. (Höglund, 2015) See Figure 16.

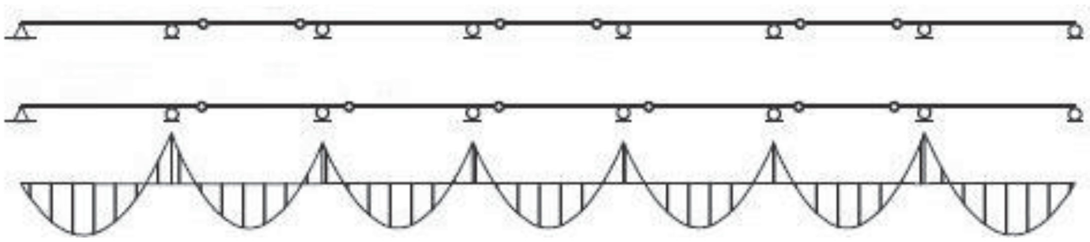

Figure 16: Illustration of the two alternative Gerber systems. The uppermost line is the Real Gerber system and the bottom one illustrates the Fake Gerber system. (Höglund, 2015)

The Real Gerber system is made with two hinges in every other span. Having a hinge in every span instead and two hinges in the penultimate span makes it the so-called Fake Gerber system. In each of these design options the outer spans are always without hinges. Generally, these edge-spans are designed to handle the loads as simply supported because of the possible occurrence of collapse in another span – resulting in lost continuity[7]. This correlates with the new design codes, EKS 10, mentioned in subchapter 4.2.4.1.

The Real Gerber system has two different options, either symmetrical or asymmetrical (Hoesch, 2007). The symmetrical one is used with an odd number of spans and the asymmetrical one is used with an even number of spans. This is shown in Figure 17. The asymmetrical option needs, due to the even number of spans, to place a single hinge in the penultimate span; this results in a difference in the calculations. The symmetrical option often tolerates larger permissible distributed load than the asymmetrical alternative. The longer the span, the greater the difference between the permissible distributed loads becomes to the

[7] Dialog with Erik Andersson, structural engineer Lindab 2016-02-15

symmetrical option's advantage. (Hoesch, 2007)

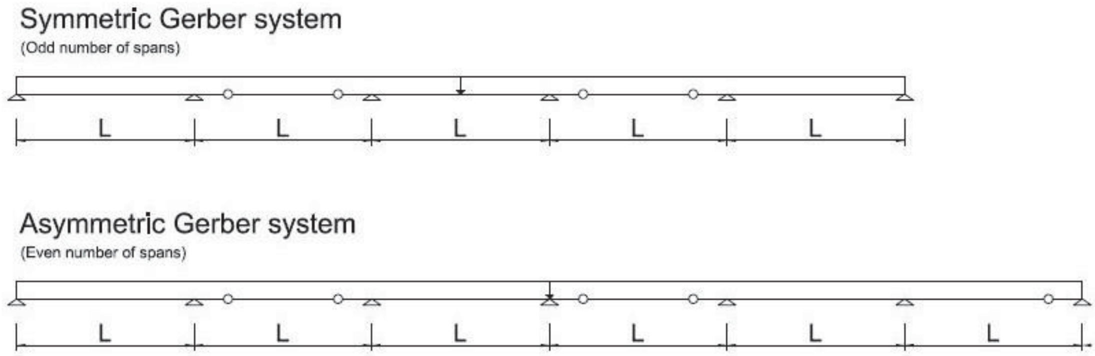

Figure 17: Symmetrical and Asymmetrical Gerber system.

5.2 Gerber System in Practice

During construction there are a few things that need to be considered and carefully executed with regard to the Gerber system. It performs well with evenly distributed loads, but is very vulnerable if the moment distribution changes. It is important that the workers follow the drawings thoroughly, even small alterations can result in severe consequences. For example, the location of the hinges in the spans must be very precisely located in accordance with the drawings. The sheeting is usually spliced with 200 mm – with the right-hand sheet above the left-hand sheet[8], see Figure 18. Another example is that the sheeting must be fastened to the girders directly after mounting to prevent the risk of sheets falling down. (Hoesch, 2007)

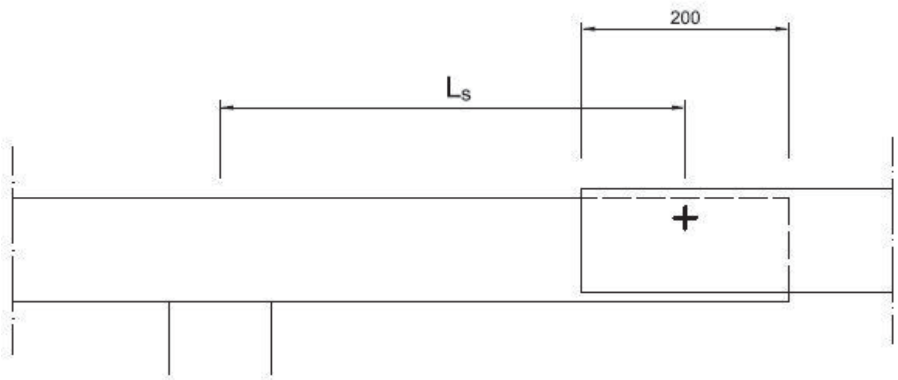

Figure 18: Illustration of the splice in a Gerber system.

The sheeting is assembled in the joints with the help of screws, a more detailed description of the screws is found in the previous subchapter 4.3 on page 22.

For the Real Gerber system, construction methods vary depending on framework supplier. At Lindab the roofing is constructed through a two girders lift, the Swedish term is "Parlyft". The roofing is formed in several pieces and then assembled together.

[8] Dialog with Erik Andersson, structure engineer Lindab 2016-02-15

Firstly, the primary girders are mounted on the ground in pairs with fastened sheets up on the girders creating assembled parts. Secondly, these assembled parts are one by one lifted up on the columns and attached, which is shown in the left picture in Figure 19. Finally, the spaces between these parts are covered by a single sheet which gives two hinges in every second field[8]. See the illustration on the right picture in Figure 19.

Figure 19: *Construction method by Lindab; the so-called two girders lift. (Erik Andersson, 2016)*

The two options of Gerber systems, Real and Fake, have different approaches of instalment during the construction of the building. The Fake Gerber system is the most common one to use but also the least safe one since it has a higher risk of progressive collapse. A recurring event is when a collapse first occurs in one span due to a breach of the local moment capacity, the equilibrium condition is violated and the structure cannot stabilise the other remaining sheeting. The collapse then continues to other spans[9]. This behaviour is not found in the Real Gerber system; progressive collapses do occur but not in the same matter or to the same extent.

The placing of the sheeting of the Fake Gerber system is shown in Figure 20 and the continuity of the collapse is shown in Figure 21. In Figure 22 is the Real Gerber system shown with distributed snow.

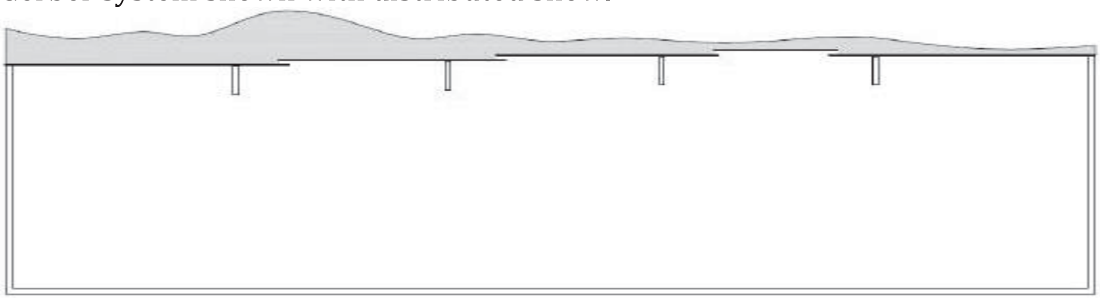

Figure 20: *Fake Gerber system, the placement of the sheeting. (Erik Andersson, 2016)*

[9] Dialog with Erik Andersson, structure engineer Lindab 2016-02-15

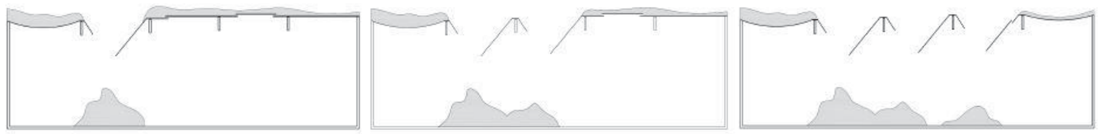

Figure 21: Illustration of the progressive collapse for the Fake Gerber system. (Erik Andersson, 2016)

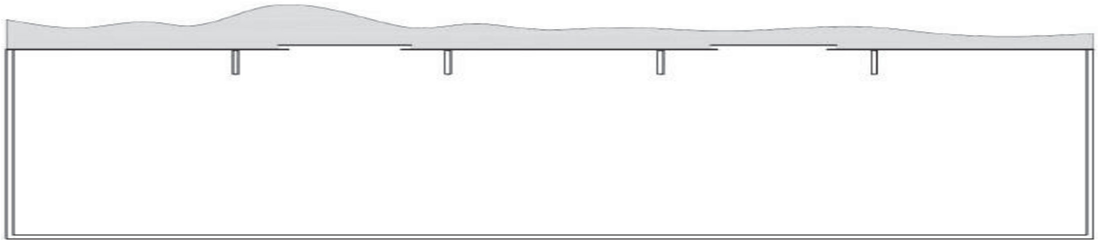

Figure 22: Real Gerber system. (Erik Andersson, 2016)

It is important that the structures are correctly designed with regard to handling the catenary action, which is the effect when the first collapse occurs in one field and the remaining fields compensate for that collapse. The Real Gerber system can get partial collapses and major deflection of different parts of the roof, resulting from the effect of the unevenly distributed load that gives change in the local moment capacity[10]. This however does not necessarily lead to total collapse as long as the design is correct. These collapses and deflection are shown in Figure 23 and Figure 24.

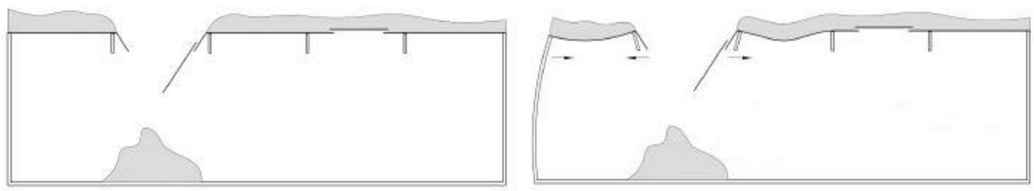

Figure 23: Illustrating one alternative collapse for the Real Gerber system. (Erik Andersson, 2016)

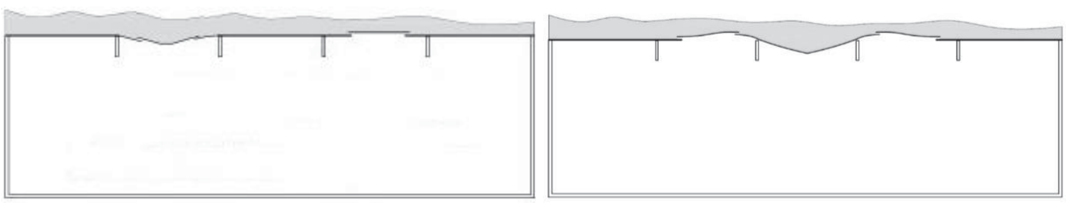

Figure 24: Illustration of different deflection of parts of the sheeting, with Real Gerber system. (Erik Andersson, 2016)

To conclude the comparison of the Real and Fake Gerber system it can be said that the Real by far handles progressive collapse better, making the consequences of a collapse not as severe as in the case of the Fake Gerber system. In fact, after the many collapsed Gerber systems during the winters of

[10] Dialog with Erik Andersson, structure engineer Lindab 2016-02-15

2009/2010 and 2010/2011 the building industry deemed the Fake Gerber system inappropriate to use. The industry simply wants to discontinue this system due to the possibility of the severe damages of the buildings and the potential injuries of individuals that can follow[10].

5.2.1 Consequence Class and Reliability Class

When designing roofs for larger buildings consequence classes, CC, are used to define what type of checks and documentations that are specified for the building. The reliability classes, RC, on the other hand defines the probability and consequence of failure. The degree of severity of the consequences from a potential collapse decides the class of the construction part.

The reliability classes are divided into three parts: RC1, RC2, and RC3. The Table 2 shows what each class is considered for. All reliability classes have different partial factors, γ_d, which are multiplied with the characteristic loads in the load combinations. (Höglund & Strömberg, 2006)

Table 2: Definition of consequences class and equivalent reliability class (Höglund & Strömberg, 2006), table 8.1

Consequences class	**Reliability class**	**Description**	**Ex. of building and civil engineering works**
CC3	RC3 $\gamma_d = 1.0$	**Large** risk for serious injury or huge economic, social or environmental consequences.	Grandstand, public buildings where consequences of failure are large
CC2	RC2 $\gamma_d = 0.91$	**Middle** risk for serious injury or major economic, social of environmental consequences.	House- and office buildings, public buildings where consequences of failure are moderate
CC1	RC1 $\gamma_d = 0.83$	**Small** risk for serious injury and small economic, social and environmental consequences.	Land use buildings where people rarely staying (*e.g.* warehouses, glasshouses)

5.2.2 Gerber System Related to Previous Collapsed Roofs

As mentioned in Chapter 2, the Gerber system was a recurring roof design found among the roofs that collapsed. The system can be considered to work well in accordance with the design as long as the load is evenly distributed. The question is what would happen when this is not the case. Boverket stated in their report of the roof collapses that formations of snow-pockets and unevenly distributed snow load was a problem relating to the failure of the roofs. It is therefore important to consider the consequences of a change in moment distribution. Since the hinges are placed at the theoretical location of the zero moment, a change in distribution will result in the hinges being placed unfavourably[11]. The moments then risk exceeding the design values causing failure of the sheeting. This needs to be analysed more thoroughly in order to verify how it actually happens and what the consequences could be.

A closer examination of the collapsed roofs designed with the Gerber system can help clarify the actual behaviour of the system. A collapse that happened in Saltsjöbaden outside of Stockholm is used as an example to visualise this.

The collapse was first initiated by localised deformation of the sheets above the supports, which can be seen in Figure 25. This deformation leads to a change of moment distribution and consequently the curvature of the sheet increased, shown in Figure 26. This was assumed to be the cause of failure, and the beginning of a progressive collapse causing severe damages to the structure, see Figure 27. (Höglund, 2013)

Figure 25: *Deformation of the steel sheet above the support.* (Höglund, 2013)

Figure 26: *Deformation above the support and increased deflection at the hinge.* (Höglund, 2013)

[11] Dialog with Erik Andersson, structural engineer Lindab 2016-02-15

Figure 27: A collapsed roof. (Erik Andersson)

Boverket also stated that these issues often seem to occur in conjunction with snow being removed from the roofs (Johansson et al., 2011), an action that would alter the moment distribution. For example; in two buildings in the northern parts of Sweden, Luleå and Skellefteå respectively, the roofs collapsed while snow was being shovelled (Strömberg & Veljkovic, 2010b) (Strömberg & Veljkovic, 2010a). The basis of the problem is that when snow is removed from only one span, the moment distribution changes. Meaning that the other spans risk higher moments than what the roof was actually designed to handle. This is an issue that the design cannot compensate for since the Gerber system is sensitive to unevenly distributed load. It is important that the removing of snow from the roof is bay for bay, in the same order as it was mounted during construction. If this is made accordingly the field or support moments will not increase (Boverket, 2011).

The question of most concern when it comes to Gerber splicing is that the theory of the Gerber system does not seem to reflect the real behaviour in practice. One important factor is the splice itself and if the joint really acts like a hinge that does not transfer moments.

As mentioned previously, the splice is 200 mm and the hinge is in theory assumed to be located in the middle of this distance, *i.e.* the location is 100 mm from the sheet-edges (Strömberg & Veljkovic, 2010b). After a collapsed roof in Luleå, the University of Luleå started investigating the behaviour of the splices with regard to the actual localisation of the hinges. As illustrated in Figure 28, the right sheet is placed on top of the left sheet with a + marking the hinge, its displacement is showing in the bottom illustration. The report states that when the deformation increases the location of the theoretical hinge between the sheets is moved towards the edge of the bottom sheet (Strömberg & Veljkovic, 2010b).

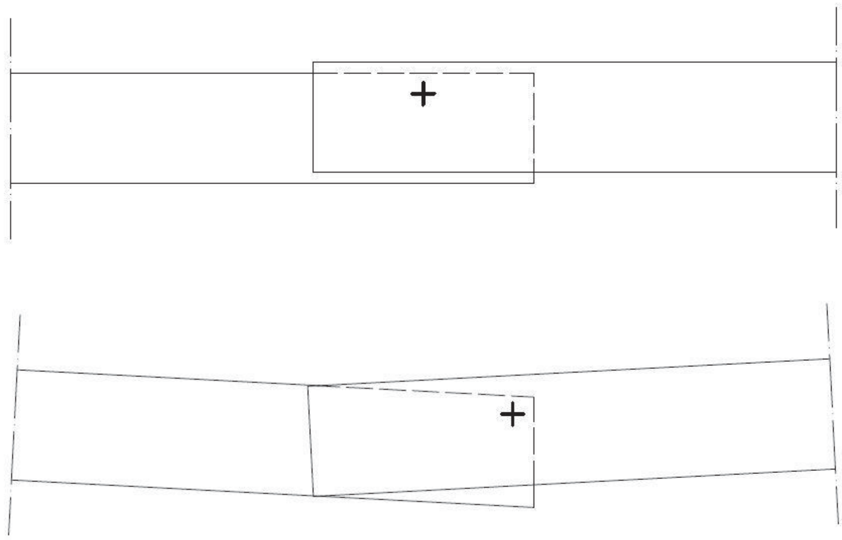

Figure 28: *Illustration of how the inclination of the sheeting changes the location of the zero-moment (marked with a +) towards the edge of the splice when the deflection increases.*

In the investigation, calculations were made regarding the consequences of moving the hinge more towards the right of the splice, compared to it being supposedly located in the middle of the splice. The analysis showed that when the hinges were moved closer to the supports; the support moments increased. As a result of this the filed moment decreased and the steel in the spans was no longer utilised as efficiently. This correlates with the observations made at the collapsed building in Luleå and it confirms the assumptions made regarding the theoretical move of the hinge and the risk it brings regarding the capacity of the roof (Strömberg & Veljkovic, 2010b).

Further on the report highlights the screws used to connect the separate sheets in the splice, which can be seen in Figure 30 on page 38. Even though the screws are designed to transfer shear, they were found to also contribute in carrying some small moments. Estimating how much moment would be difficult to calculate and the original assumption makes an easier design. However, this master's thesis aims to analyse the presumed stiffness more closely in order to explain the behaviour of the sheeting even better.

6 Stabilising Systems

If a structure is slender it is important to analyse the global stability especially when considering buildings with longer spans which normally need additional bracing. Stabilisation can be achieved either by; utilising diaphragm action, wind bracing, or by having columns with stiff connections. Stiffness can be achieved both by full restraints to the foundation or by frame action (Höglund, 2015). Without proper bracing the load-bearing capacity will suffer. It is not just that the system should take care of horizontal loads, also transversal loads can cause instabilities and lateral torsional buckling of the primary system must be prevented.

With regard to the Gerber system and the failure of it, described in chapters 2 and 5, the use of continuous roof sheeting creates a secondary stabilising system that helps in carrying the loads. If this is to work correctly it is important that the bracing function of the sheet is considered in the design.

One example of the stabilising system not working correctly is if a structure has purlins as the secondary system but with the wind bracings placed too far apart. The roof sheet between wind bracing trusses will succumb to the horizontal load thus moving the purlins in the direction of the load *i.e.* parallel to the length of the purlins, meaning that the purlins no longer support the primary system against lateral torsional buckling (Johansson et al., 2011). In the end this will affect the load-carrying capacity of the system.

If instead roof sheeting is used to stabilise the primary system high in-plane stiffness will provide adequate support to the main load-carrying system. Keeping in mind that the slender sheets are rather flexible in the out-of-plane direction, resulting in instability in the form of distortional buckling (Höglund, 2015). Trapezoidal sheeting has a good in-plane capacity providing that the load is static (Höglund, 2015). This static load includes self-weight, snow load and wind load.

6.1 Diaphragm Action

The type of building most commonly effected during the two snowy winters of 2009/2010 and 2010/2011 can be defined based on the investigations performed by Boverket, see subchapter 2.2. It is one-storey buildings with long spans and rather flat pitched roofs. The most common and economical way of constructing these type of buildings is by utilising the diaphragm action of the roof sheeting. Horizontal loads will be transferred to the roof and then through the vertical wind bracing down to the foundation. If the stabilising action of the sheeting is not utilised, the horizontal loads acting on the base of the columns become much higher (Höglund, 2015).

This system gives a very efficient design, provided that the connections to the primary load-bearing system have been designed properly and constructed accordingly. This can be done either by mechanical fasteners or welding (Höglund, 2015).

For sheeting placed directly on the primary structure; the stresses in the edge beams consist of a force couple, meaning that the shear flow along the sheet is evenly distributed. This is calculated according to equation (6.1).

$$S = V/b \tag{6.1}$$

S Shear flow per unit width [kN/m]
V Shear force [kN]
b Width of sheet [m]

Without edge beams the moments would be handled directly by the sheet. Using purlins will not give an even flow due to the fact that the moment is not just handled by the edge beams but also by all the purlins (Höglund, 2015).

The angle of the roof also plays an important part regarding the in-plane capacity. A very high pitch will give the vertical load a force component in the direction of the pitched roof, in-plane forces (Höglund, 2015). Meaning that the capacity to carry horizontal loads will be less for a high pitched roof than for a low pitched one. A problem that can be linked to this is when a roof is highly deflected due to high snow loads (Höglund, 2015). The roof might then also take vertical loads in the plane of the roof, causing problems for the connectors in the sheet. This can be disregarded in the case of the specific roof collapses since the angle of the roof was very low.

6.1.1 Designing with Regard to Diaphragm Action

Design of the sheet includes calculating the moment, M, and shear force, V, distributions along the sheet, checking the shear flow, S, in the sheet, the normal force, N, in the edge beams, and the reaction forces in the gables, R_{gable}. These flows and forces are calculated according to the equations (6.2), (6.3), and (6.4).

The moment is calculated as for an evenly distributed load. However, the moment distribution would look somewhat different if the force from the top of the columns acting on the sheet were considered point loads.

$$S = \frac{V}{b} = \frac{qL}{2b} - \frac{qc_{beam}}{2b} \tag{6.2}$$

$$N = \frac{M}{b} = \frac{qL^2}{8b} \tag{6.3}$$

$$R_{gable} = \frac{qL}{2} \tag{6.4}$$

S Shear flow per unit width [kN/m]
V Shear force distribution along the sheet [kN]
b Width of sheet [m]
q Load acting on the sheet, assuming equal distance between columns [kN/m]
L Length of sheet [m]
c_{beam} Distance between primary beams [m]
N Normal force in the edge beams [kN]
M Moment distribution along the sheet [kNm]
R_{gable} Reaction force acting on the bracing in the gables [kN]

Based on this the deformations can be calculated and buckling considered in order to finally make sure that the forces between the sheeting and the primary system are within limits.

Holes in the sheeting will interrupt the shear flow in the way that it increases elsewhere and decreases around the holes. This must be regarded in design, *e.g.* beams can be mounted around the opening to relive the stresses and carry the self-weights and snow loads (Höglund, 2015). Depending on the placement of the hole, special shear flow calculations need to be adapted in design.

Deflection of the sheet depend mostly on the shear deformation of the sheet (Höglund, 2015). The biggest concern is the deformations in the connections to the primary load-bearing system and the connections between two sheets. Localised buckling at the support or lost capacity of the connectors in the splices will result in a change of the moment distribution that the system might not be able to compensate for. The deformation at the ends of the sheet has the largest impact. This deformation depends on the thickness of the sheet, the height of the profile, and if the sheet is connected to the beam at every profile bottom or every other one.

According to SS-EN 1993-1-3, section 16. The influence of transversal loading and shear flow do not need to be combined in design. However, the shear stress, τ_{Ed}, due to diaphragm action needs to fulfil the following condition of equation (6.5).

$$\tau_{Ed} \leq 0.25 f_{yb}/\gamma_{M1} \tag{6.5}$$

τ_{Ed} Shear [MPa]
γ_{M1} Partial factor

6.1.2 Connections with Regard to Stabilisation

Wind load on the walls of a building, is transferred through the columns to the top where it acts on the edge beam which spreads the load to the sheet. The connectors are therefore very important when transferring the loads, trough shear, to the sheeting (Höglund, 2015). The sheeting also needs to transfer the shear flow between the separate sheets in order for the roof to fulfil its stabilising function. The use of load insertion rods can help give a more even distribution within the sheet (Höglund, 2015).

In the splice the screws should not be attached in the bottom of the profile, but in the web. This is to make sure that the sheet acts as continuous (Höglund, 2015). A detailed drawing of the splice is shown in Figure 29 and the placement of the screws can be seen in Figure 30.

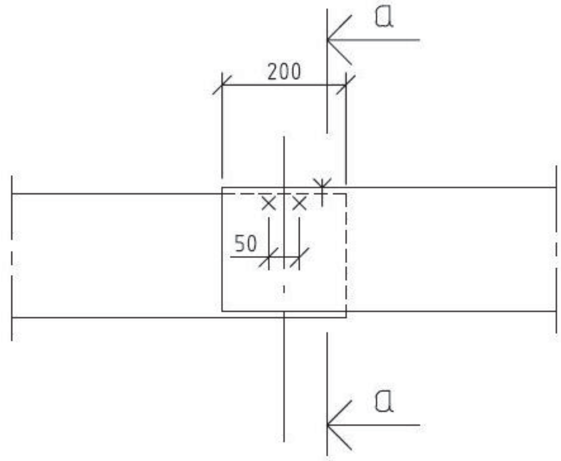

Figure 29: Detailed drawing of the splice. (Erik Andersson 2016)

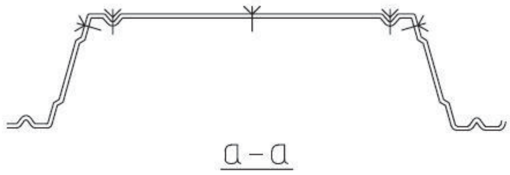

Figure 30: Detailed drawing of the placement of the screw in the sheet. (Erik Andersson 2016)

According to Torsten Höglund, the joint should be designed with regard to moment, shear force and support reactions.

The forces acting on the connection can be decided according to equation (6.6).

$$F_v = \frac{|M_s|}{2\text{a}\sin(\varphi)} \cdot b_R \tag{6.6}$$

F_v Vertical force on the connectors [N]
M_s Moment at the support without considering support width [Nm]
a Length of cantilever [mm]
φ Angle of the web [°]
b_R Width of divided profile [mm]

If the connectors are only in every other bottom; the deformations will be even larger (Höglund, 2015). However, if the end of the sheeting is placed beyond the beam to make the connections further from the end of the sheet, the deformations and stresses will be smaller (Höglund, 2015), about 30 % smaller. Furthermore if the connection is both in the top and bottom of the profile the deformations are noticeably smaller (Höglund, 2015).

6.2 Reliability Class for a Stabilising System

Designing based on Eurocode means that the design method is based on probability. Reliability classes are representing the probability of a load-bearing system failing over a period of time (Johansson et al., 2011), these classes are found in SS-EN 1990, see Table 2 on page 31 of this report. When calculating according to Eurocode it is apparent that this risk exists but that it is rather small. The values are used for adapting the calculations to specific buildings of different classes.

When designing the sheet in ultimate limit state based on the partial coefficient method; the design load is the product of the partial coefficient based on reliability class, γ_d, and the characteristic load.

Normally a secondary load-carrying system is considered as being of reliability class 2 according to Eurocode. But when it comes to secondary systems that are also used to stabilise the structures then a higher reliability class is needed, both the primary and secondary system will then be considered in class 3. (Crocetti et al., 2011)

This thesis considers a typical one-storey high building with spans over 15 m, where many people dwell, the primary load-bearing system should therefore be designed in reliability class 3 (Höglund, 2015). The secondary system acts stabilising and with high consequences of failure the coefficient becomes the same as for the primary system: $\gamma_d = 1.0$. Meaning that the sheet must be designed in class 3 for diaphragm action but for transversal loading it can still be of the lower classes 1 or 2; making the coefficient smaller.

6.3 Preventing Progressive Collapse

The new design codes, EKS 10, state that the continuous system considered in this thesis must be designed to fulfil its function even after the collapse of one span *i.e.* progressive collapse must be prevented. Meaning that for buildings in reliability class 2 and 3, there is a maximum limit for the size of the collapsed area (Boverket, 2015). It is further described how the stiffness of the joint effects the moment distribution, causing higher moments than anticipated in the area surrounding the first collapse. This would lead to buckling of the sheet and the area losing its capacity; the collapse would thereby progress.

In design one must assume that the sheet will collapse in one span. The size is half the distance between the ridge and the eave, but with 10 m as a maximum length[12].

Progressive collapse from failure of the sheeting can be studied in SS-EN 1991-1-7. The design loads should be taken as exceptional which gives a tension capacity large enough to handle the connection, no matter what load-bearing system the sheeting is defined as (Höglund, 2015).

[12] Björn Mattsson, Boverket 2016-02-09

Secondary systems like purlins and sheets are most often designed as continuous over multiple spans. The connections are thoroughly detailed to optimise the use of material and the capacity. If yielding occurs the moment will redistribute and allow for the system to still carry higher loads. If snow was to accumulate to an area of the roof, it would cause an uneven load distribution and more than just the specific area would be affected (Johansson et al., 2011).

In an area where there is a risk of snow accumulation the designer can choose to make the specific part of the roof into a separate section, no longer continuous. This will limit the affected area. It might be a more expensive way of design and to construct, but still safer with regard to progressive collapse (Johansson et al., 2011). Another advantage listed regarding not having continuous spans is that the deflection will be larger. This contradicts what has mentioned before in chapter 5 about the advantages with continuous spans, but it makes it easier to detect the deformation if it is larger. Thereby measures can be taken earlier to avoid failure due to heavier loads than anticipated. The static system however needs to be design with the loss of the stabilising secondary system in mind (Johansson et al., 2011).

7 Process of the Analytical and Numerical Modelling

Based on the literature study presented in the previous chapters of this thesis, the work was delimited to focusing on the splice of the sheeting. According to the theoretical design model the splice behaves like a hinge, *i.e.* it does not transfer moments. When considering the way, the sheets are actually connected to each other, in order to make a continuous roof sheeting, it would be unlikely that the splice shows no stiffness. It is therefore assumed that the splice does not behave like a hinge but that it will have a moment capacity.

This chapter describe the simplifications, assumptions and design steps made in the master's thesis.

7.1 Purpose of the Method

The method used in this study aims to describe the behaviour of a continuous sheet designed according to the Gerber system.

Looking at a general continuous beam over multiple spans; the moment distribution differs depending on if the load is evenly or unevenly distributed. The location of the zero-moment changes, see the mid-span of Figure 31. When, on the other hand, splices are included in the design the system is made statically determined, this is the advantage of the Gerber system in theory. Hinges in the mid-span will not transfer any moment but joints with stiffness will.

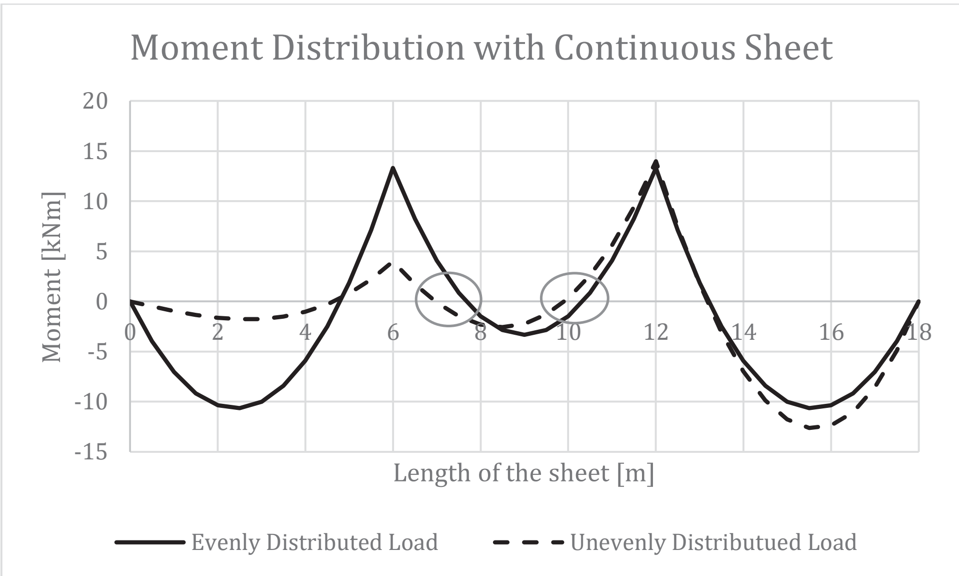

Figure 31: The circles illustrate the theoretical movement of zero-moment with evenly- and unevenly distributed load for a continuous sheet.

Numerical models were computed in order to capture the real behaviour of the splice. Then the rotational stiffness of joint was derived, and finally the behaviour of a continuous steel sheet designed according to the Gerber system could be analysed. This final analysis is made to illustrate the effects of including a rotational stiffness in the splice when the snow load is no longer evenly distributed.

7.2 The TRP Sheet Used in the Analysis

The profile analysed in this work is the LHP 200 seen in Figure 32. From the literature study it was evident that this profile was found in many of the cases of collapsed roofs constructed with steel sheeting and the Gerber system. An AutoCAD-drawing given by Lindab was used for the more specific geometries when calculating and modelling the behaviour of the sheet, see APPENDIX A.

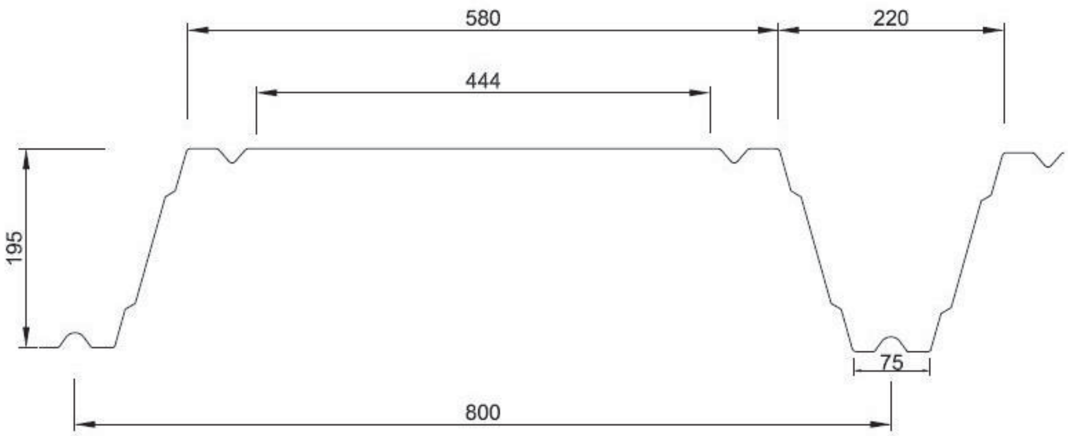

Figure 32: LHP 200 profile received from Lindab [mm]. (Authors, 2016)

The material data is defined in Table 3 and the full geometry is found in APPENDIX B, chapter 1.

Table 3: Steel properties used in the analysis. (Authors, 2016)

Steel properties	Value/Unit
Yield strength, f_{yb}	420 MPa
Modulus of elasticity, E	210 000 N/mm^2
Poisson's ratio in elastic stage, v	0.3
Plastic strain, $\boldsymbol{\varepsilon_p}$	0.086
Thickness of the sheet, t	1.25 mm

7.3 Numerical Modelling of the Sheet

In order to fully understand the joint's effect on the behaviour, the sheet is analysed using the FE-program Abaqus/CAE 6.13-3. Creating an advanced FE-model requires simplifications and in order to confirm the credibility of the results these simplifications need to be verified.

In this study three different numerical models were created in order to validate the results:

- Shell element models
- Solid element models
- Beam element models

The first one was a simplified model with 3D shell elements, see Figure 33 . It was used to run an elastic analysis and to verify specific simplifications. The second one was a more detailed solid element model. This one was used for both elastic and plastic analysis, see Figure 34, and a stiffness in the joint could be calculated based on these results. The final model was a beam element model used to analyse the global behaviour of the continuous sheeting over multiple spans, when the stiffness of the joint is included in the design, see Figure 35. The final model is designed as a Real Gerber system.

Figure 33: Shell element model, 3D (Authors, 2016)

Figure 34: Solid element model, 3D (Authors, 2016)

Figure 35: Beam element model, 3D (Authors, 2016)

7.3.1 Parts and Their Interaction

The geometries used in the numerical models correlate with subchapter 7.2. The in-data was however adapted to make more efficient models.

The most important simplifications are with regard to:

- The transversal grooves of the top flange
- The connectors
- The interaction of the two sheets in the splice

Here follows a more detailed description of these simplifications and how they were confirmed to be reasonable.

The top flange of the profile has transversal grooves all along the length of the sheet, but in Abaqus the flanges are modelled as flat with only longitudinal grooves. The difference can be seen in Figure 36. Including the transversal grooves made the splice difficult to compute and to mesh. The simplification was confirmed by modelling a single sheet with transversal grooves and one without, and comparing the results, see Figure 37 and Figure 38. It is evident that the transversal grooves help in handling the stresses in a way that the flat flange does not, it instead resulted in a distorted flange, visualised by comparing the sheets in Figure 39 and Figure 40. The moment distribution along the two single sheets did, however, correlate well. This can be seen in APPENDIX B, chapter 3.

All numerical models were therefore computed without transversal grooves. With regard to this, the stress distributions studied in this report are taken from the edge of the top flange. At this location the effect of disregarding the transversal grooves is less evident in the stress distribution.

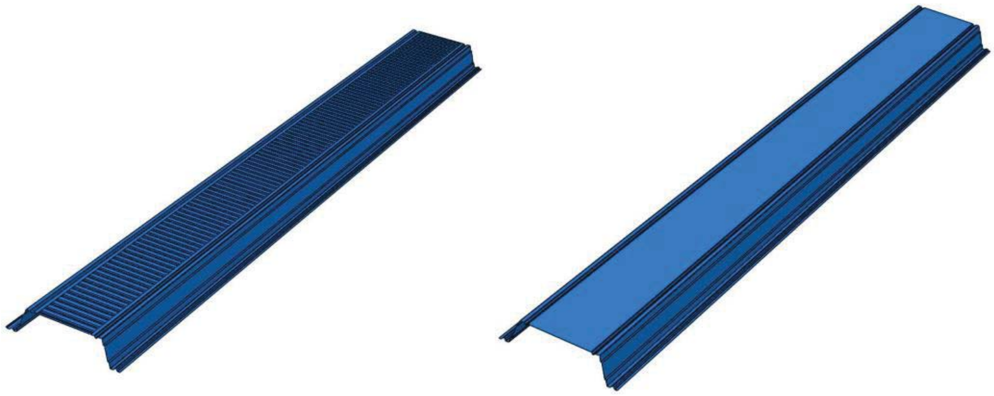

Figure 36: Models of the sheet. To the left is the model with transversal grooves and to the right is the model with a flat top flange (Authors, 2016)

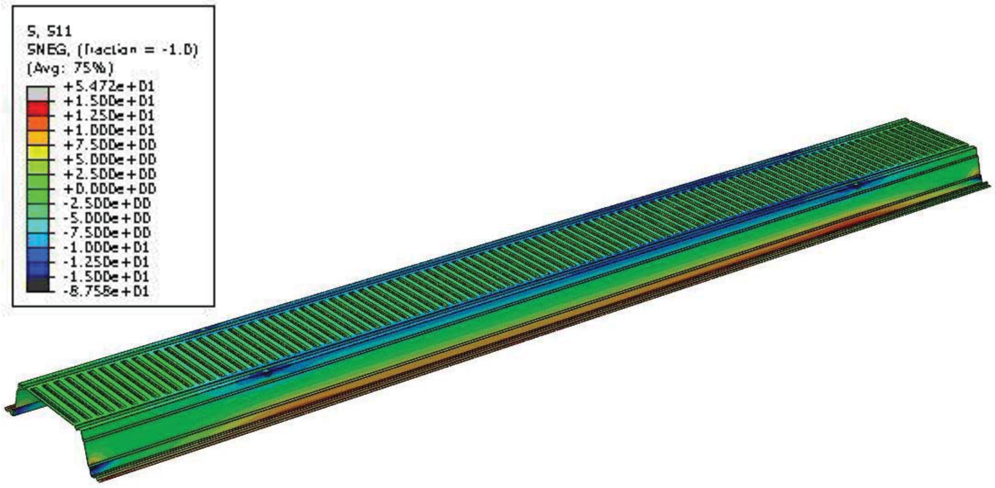

Figure 37: *Stress distribution, σ_x, for a sheet including transversal grooves in the top flange. The result differs from a sheet without transversal grooves. (Authors, 2016)*

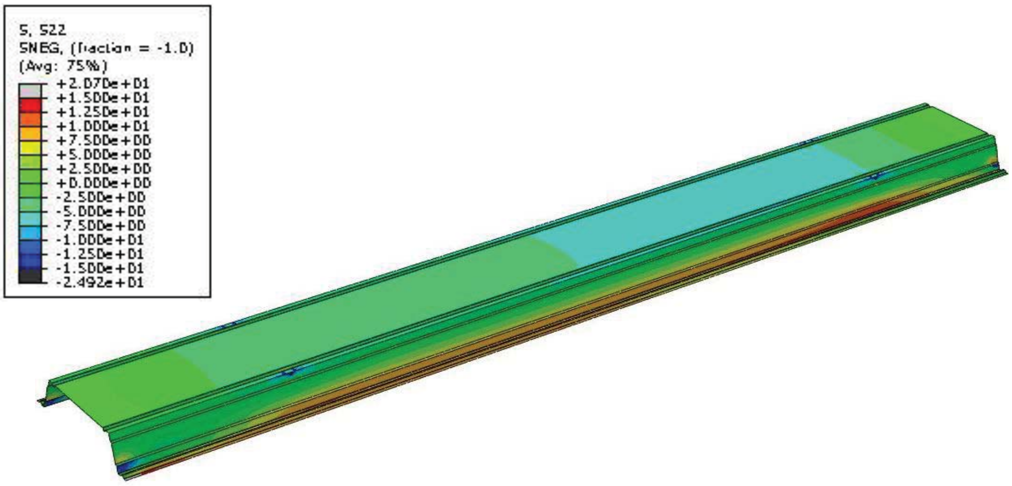

Figure 38: *Stress distribution, σ_x, for a sheet without transversal grooves in the top flange. The result differs from a sheet including transversal grooves. (Authors, 2016)*

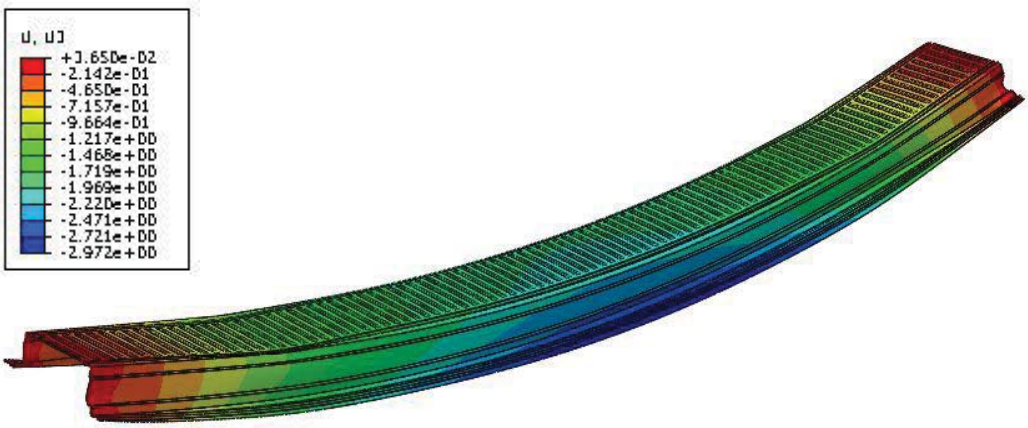

Figure 39: *Deformation in z-direction of a sheet including transversal grooves. (Authors, 2016)*

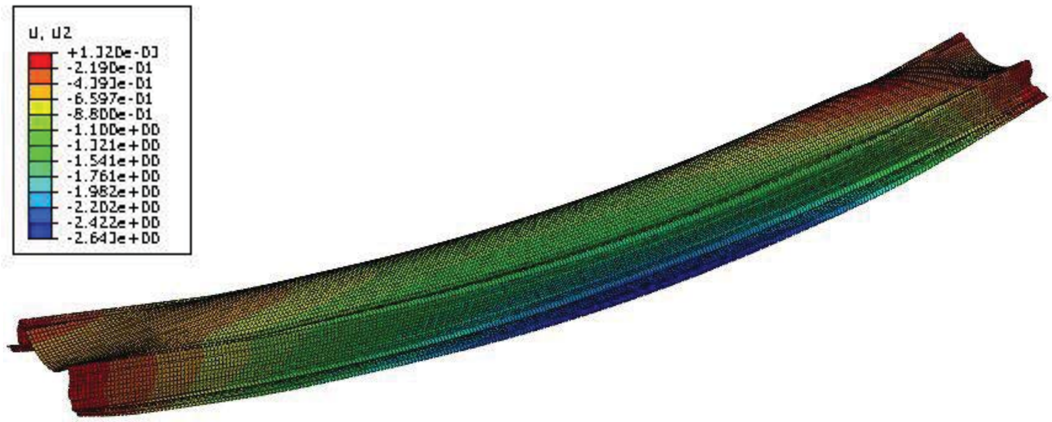

Figure 40: *Deformation in z-direction of a sheet without transversal grooves. The distortion of the top flange differs from that of a flange including transversal grooves. (Authors, 2016)*

In order to model the behaviour of the splice, the connectors need to be considered. In reality these are screws with a 6.3 mm diameter, see subchapter 4.3.

The first simplified shell element model was made with ties in-between the holes in the top and the bottom sheets of the splice. These restrains were created in order to simulate the clamping effect of the screws. This however, resulted in stress concentrations that were thought to affect the results in a negative matter. By building a more advanced solid element model, including solid screws, the analysis and the stress distribution was considered more consistent with real connectors used in the roof structures. The model of the screws can be seen in Figure 41. The placement of the connectors, according to Lindab, can be seen in Figure 30 on page 38.

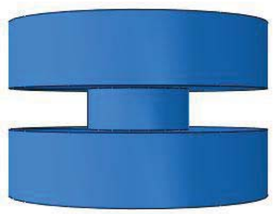

Figure 41: *Solid screw model in Abaqus to simulate clamping effect. (Authors, 2016)*

The function of the screws is that they transfer shear and help avoid peeling. The problem with using solid screws is evident when looking at the connectors placed in the grooves of the top flange. The faces of the screws need to be connected to the faces of the sheet in order for them to interact. In the grooves this is problematic due to the radius of the grooves. When Abaqus is running it will only find nodes that are interacting, but it needs to find elements that can interact. The solid screws would have to be of a different size and shape for them to fit in the grooves and this is complicated to model and as well does not correlate with the screws used according to Lindab.

Considering the fact that the analysis of the sheet itself is elastic, the capacity of the sheet is not considered in the solid element model and therefore the grooves are less important at this stage. Moving the screws to the top flange, see Figure 42, is a simplification that will help Abaqus in analysing the model and it means no difference in the screws' function.

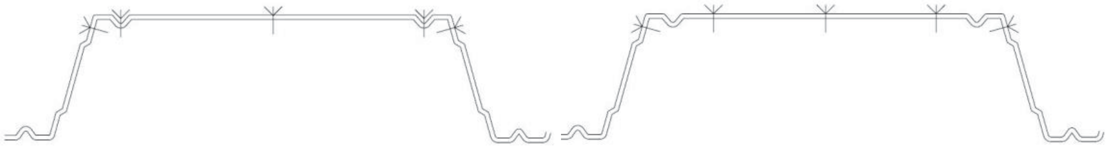

Figure 42: *Changing the placement of the screws from the grooves to the top flange. (Authors, 2016)*

See Figure 43 and Figure 44 for the shell element model and solid element model respectively.

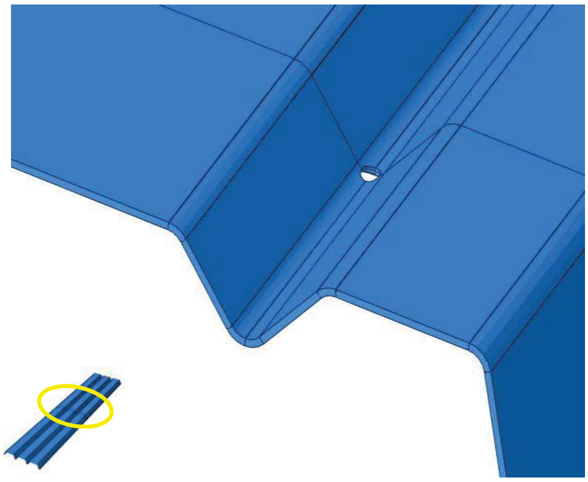

Figure 43: *Location of the holes in the grooves in the top flange, shell element model. The edge of the hole is where the tie is created. (Authors, 2016)*

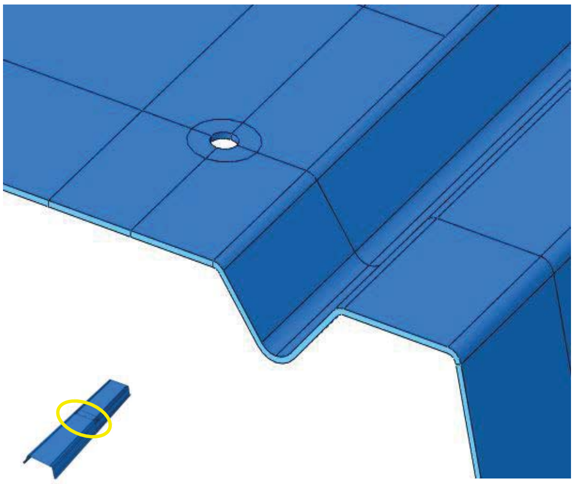

Figure 44: *Location of the holes in the top flange, solid element model. The circle around the hole is the surface that the screw is interacted to. (Authors, 2016)*

The models also include interactions in-between the faces of the splice, which constrains the degrees of freedom between the two separate sheets. In the simplified shell element model, the interaction has the properties of Frictionless in the tangential direction and Hard Contact in the normal direction. The first means that the parts are permitted to slide along each other without friction. The second property makes each part dependent on the other's deformations *i.e.* it eliminates the risk of the geometries intersecting.

For the solid element model on the other hand, the property of Frictionless made the analysis difficult to converge. Instead a friction coefficient, $\mu_s = 0.3$, was used in the tangential direction. The value is for static friction in-between two steel material surfaces when a movement of parts would occur. Considering the actual sheets with transversal grooves that lock to each other when connected, a friction is reasonable.

These simplifications were thereby confirmed and the stiffness of the joint could be derived. It was then used in the analysis of the behaviour of the sheeting designed with the Gerber system.

The beam element model, compared to the shell element and the solid element models, was not computed with an overlap. Instead, the interaction was made with couplings in-between the edges of the sheets. These prevented translations in the x-, y-, and z-direction as well as rotation around the x- and z-axis. The modelled splice was thereby free to rotate around the y-axis, but with a stiffness of the joint in the form of added spring features. The rotational stiffness, $K_{rot} = 415500\ Nmm/rad$, was used based on the results from the analysis of the solid element model.

The final beam element model was made with 3D beam elements and an arbitrary profile giving the model its cross-sectional properties and material orientation. Nevertheless, this model also required some simplifications. The intended 2D analysis cannot be performed on arbitrary profiles in Abaqus. The boundary conditions were therefore chosen to give 2D results from a 3D analysis, meaning deflections in the y-direction and stresses in the x-direction. More about the boundary conditions can be read in subchapter 7.3.2.

7.3.2 Boundary Conditions

When it comes to the boundary conditions some assumptions have been made to simulate the real behaviour of the sheet. The actual roof sheeting is continuous over multiple spans and it is extended in the transvers direction by the connection of multiple sections. In the FE-models this is represented in different ways depending on the model.

In the simplified shell element model, the analysis was made on a sheet with three sections in the transversal direction, see Figure 33. The results show that the behaviour of each section differs depending on if the longitudinal edges are free or not, see Figure 45. It can be assumed that the centre section behaves the most similar to the multiple-sheeting used in construction.

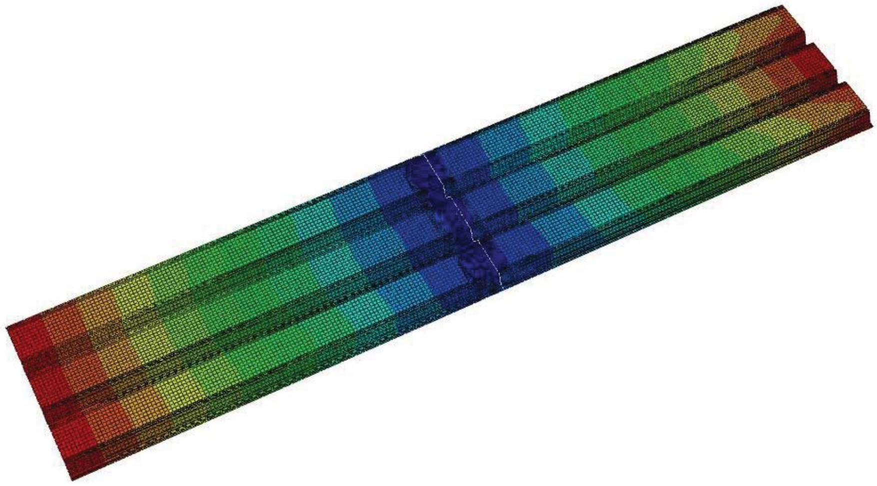

Figure 45: *Deformation in z-direction in the shell element model illustrates the different behaviour of each section. The section in the middle is considered the most appropriate for the analysis. (Authors, 2016)*

With this in mind, the solid element model was made with only one section but with a symmetry condition applied along both longitudinal edges of the sheet; in order to better simulate the real continuity along the width of the sheeting. This boundary condition did not allow for translation in the y-direction nor rotation around the x- and z-axis, according to Figure 46.

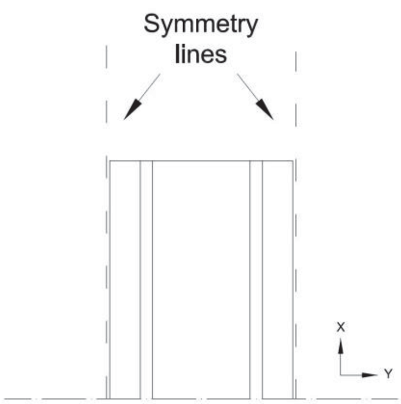

Figure 46: *Y-axis symmetry lines at each longitudinal edge of the solid element model. (Authors, 2016)*

Regarding the supports, the sheet is considered simply supported. This is simulated in shell element and solid element models by creating a pinned and a rolling boundary condition respectively. As it can be seen in Figure 47, the pinned support on the left-hand side is modelled as locked in the x-, y-, and z-direction, but free to rotate around all axes. The rolling support on the right-hand side is only locked in the z-direction.

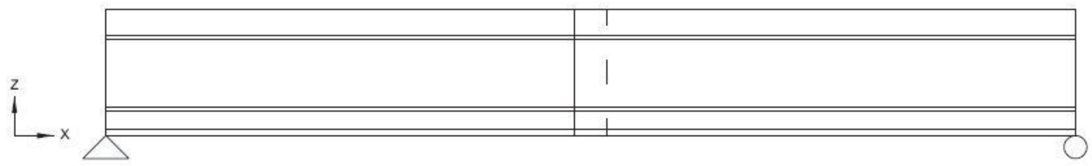

Figure 47: *Illustration of the type of boundary condition at the supports for the shell element and the solid element models. (Authors, 2016)*

The same goes for the beam element model, but concerning three spans instead of one, see Figure 48. The splices were placed in the mid-span. Symmetry was implemented but here with the intention of making the 3D model behave like a 2D beam. The symmetry line only allowed for translation in the x- and z-direction as well as rotation around the y-axis.

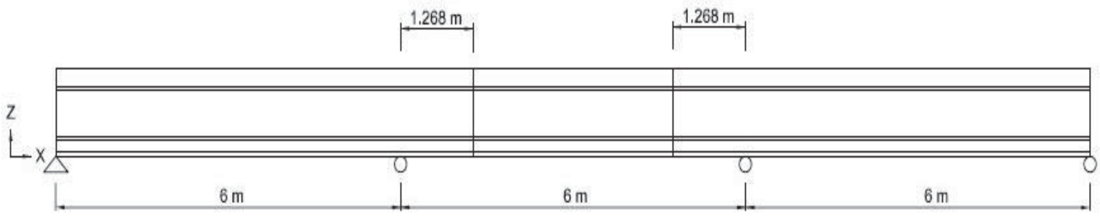

Figure 48: *Illustration of the type of boundary condition at the supports for the beam element models. (Authors, 2016)*

7.3.3 Loads

This subchapter will present how the loads are applied in the different numerical models.

One load case was used for the analysis of the shell element model and in the comparison with the analytical stress distributions. The application of the load can be seen in Figure 49. The figure includes the placement of the supports and the loads. This specific load case was chosen in order for the splice, in the centre of the span, to experience moment but no shear forces.

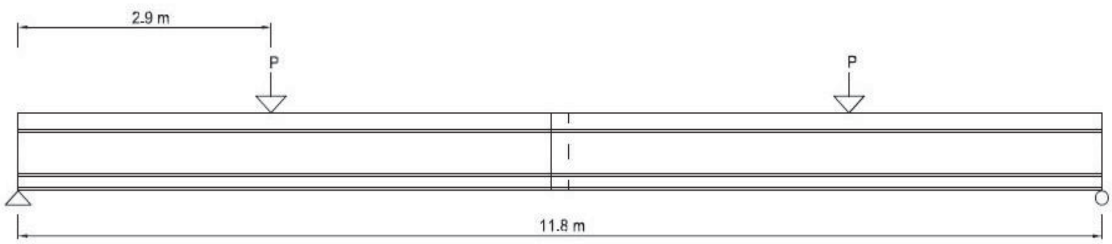

Figure 49 *Illustration of the locations for the boundary conditions and loads in the shell element model. (Authors, 2016)*

To get as similar loading principle in Abaqus, the loads are modelled as concentrated loads across the width of the sheet and applied with small increments at a time.

In the simplified shell element model, the loads are placed at the edges of the outer parts of the upper flange, see Figure 50. Having them act on the middle part of the top flange gave an unreasonable behaviour of the sheet due to the fact that the model was made with a flat top flange. The transversal grooves in the actual sheet would take care of the imposed stresses, but the simplification can still be considered valid as long as the loads are applied closer to the webs that handle the shear. The assumption is then considered reasonable and the loads in the solid element model are therefore applied in the same manner as for the simplified shell element model but with a different length of the sheets, see Figure 51. This change of length does not affect the analysis.

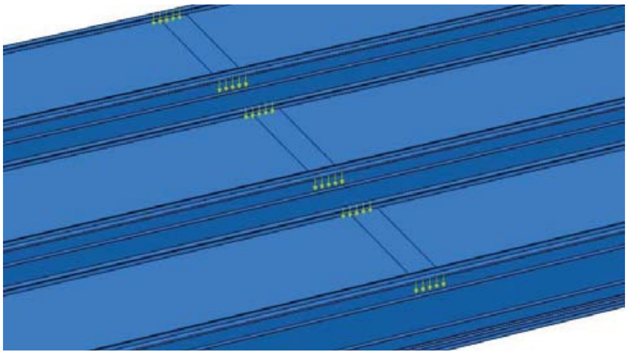

Figure 50 *The concentrated loads in a row across the section in Abaqus (Authors, 2016)*

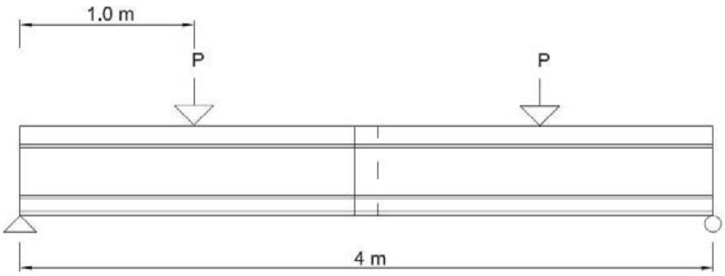

Figure 51: *Load case for the solid element model. (Authors, 2016)*

The beam element model was analysed with two different load cases, see Figure 52. The first load was evenly distributed and the second was unevenly distributed, starting from zero at the left edge and increasing linearly towards the right edge. These two options were developed in order to illustrate the difference in the sheet's behaviour with regard to the moment distribution when a stiffness of the splice is included in the model. The length of the sheet is different due to the fact that it should resemble the roof sheeting used in practice.

The same load cases were also applied on a continuous sheet with altered stiffness in the connections. The aim was to show the changes in moment distribution when the splices are acting like hinges compared to stiffer joints.

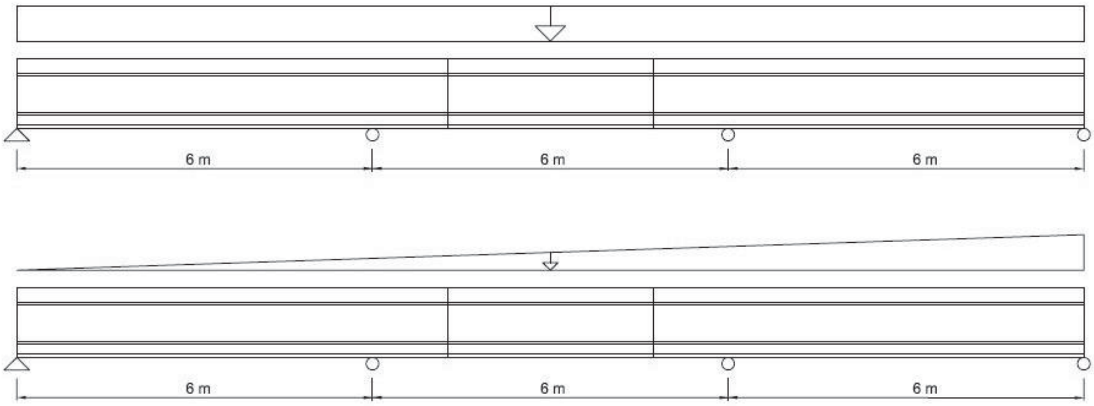

Figure 52: The two different load cases for the beam element model. First one, evenly distributed load and the second one with unevenly distributed load. (Authors, 2016)

7.3.4 Meshing of the Models

Refined meshes have been created for all models and their quality was validated by a convergence study. An optimal mesh is fine enough to generate good result without taking too long to complete the analysis.

Due to the geometry of the TRP sheet the meshing was rather complicated, especially around the holes and in the grooves. The method varied a bit depending on the model.

7.3.4.1 Mesh of the Shell Element Model

To establish an approved mesh; both face partitions and edge seeds have been customary applied on the model.

Each of the two connected sheets was partitioned into three part instances. The first defining the splice, which was in need of a finer mesh with regard to the holes. The second, outer part was meshed with larger global seeds. The mesh of the part instance in-between the two previously mentioned was made to translate the outer mesh size of 50 to the splice mesh size of 10. The partitions can be seen in Figure 53.

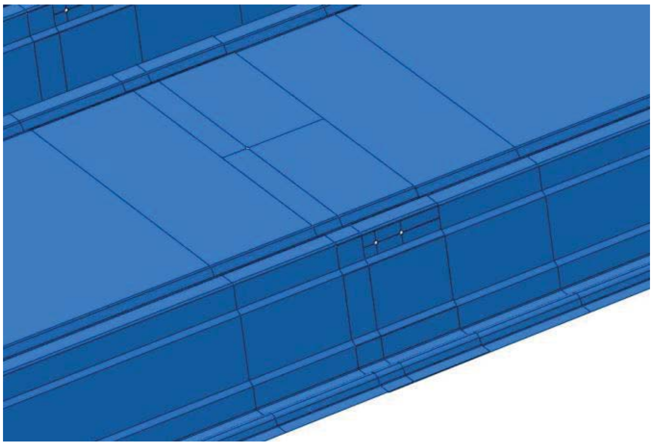

Figure 53: Shell element model including partitions of the part instances. (Authors, 2016)

To avoid stress concentrations around the holes, the meshing needed to be made more detailed in these areas. Square face partitions were constructed around the holes in order to achieve this. Local edge seeds were applied to create a better quality of the mesh.

In the grooves, where the mesh was the most difficult to compute, the local edge seeding was important in order to avoid distorted elements.

The element shape was quad for the entire model, but the technique to mesh was different depending on the partitioned part. Most of the meshes in the model were made structured but some critical faces needed a free mesh. Free elements are created more flexibly and do not work with a pre-established mesh pattern. In critical parts, like the ones in the splice, the model cannot create a mesh based on strict patterns.

7.3.4.2 Mesh of the Solid Element Model

In the solid element model, the properties of the elements demand that the partitions are swept through the whole thickness of the sheets, making the model more complicated to mesh. In general; the solid element model needed more cells partitioned in order to create a high quality mesh without distorted elements.

This model was only partitioned into two part instances with a global element size of 10. See Figure 54. Local edge seeding was also applied where it was necessary.

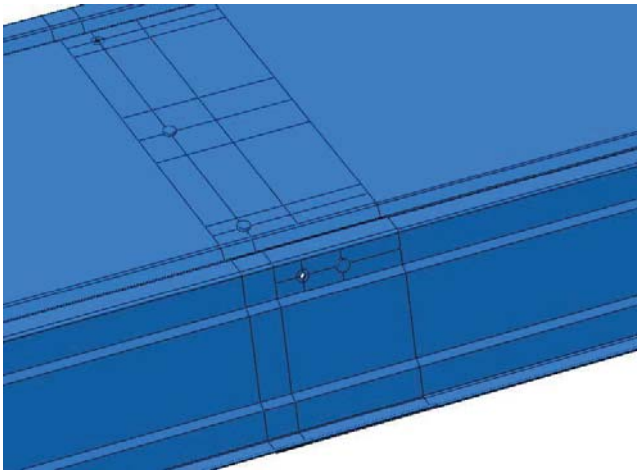

Figure 54: Solid element model including partitions of the part instances (Authors, 2016)

Due to the placement of the screws, the holes in the grooves needed to be moved onto the upper flange, as previously mentioned. This was not a change with regard to the quality of the mesh but rather to create better surfaces for the screw-to-sheet interactions. A partitioned circle around the hole helped to connect the surfaces by restricting the areas of interaction.

The element shape in this model was 3D hex, which correlates with the 2D quad shape used in the shell element model. Tetra shaped elements could have been a suitable option since these are created more freely, but they require a finer mesh, which would extend the time needed to complete the analysis.

The meshing technique used was mostly sweep, but in the critical parts of the splice it was structured. The sweeping technic implies that Abaqus chooses a face to mesh which becomes the source-side; this mesh is then swept all through the model. If a region is too complicated to be swept, Abaqus will request these elements to be structured.

7.3.4.3 Mesh of the Beam Element Model

The meshing of a beam element model is very simple. The beam is constructed with only a length in the x-direction and then given cross-sectional properties. All the difficulties regarding the geometry are therefore avoided. This is one of the advantages with performing the analysis on a beam element model.

7.3.4.4 Convergence Study to Verify the Meshes

To verify the quality of the mesh a convergence study was performed on the solid element model with plastic material property, three different element sizes were compared.

The three meshes were of element size: 10, 15, and 30 mm. See Figure 55, Figure 56, and Figure 57. The first model was uniformly meshed with a global element size of 10 and with a more detailed local edge seeding around the holes. The other two mesh sizes were modelled in a somewhat different manner. More cell partition along the width were created as well as the utilisation of part instance in order to translate the outer mesh sizes of 15 or 30 to the splice mesh size of 10.

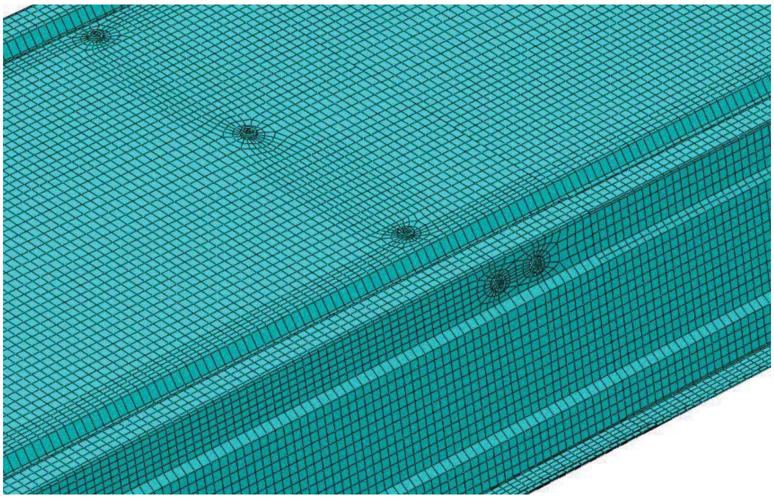

Figure 55: *The element mesh size of 10. (Authors, 2016)*

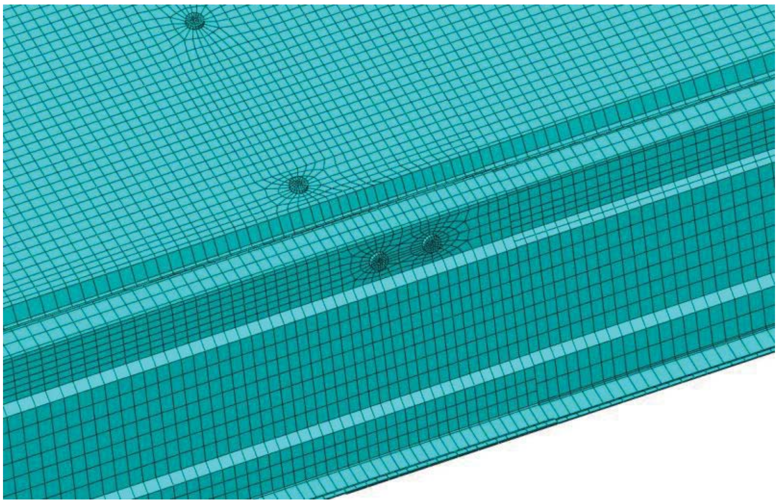

Figure 56: *The element mesh size of 15. (Authors, 2016)*

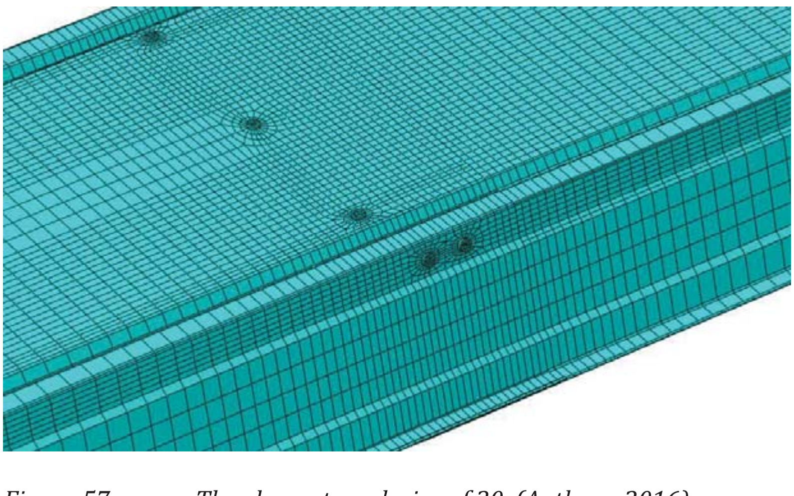

Figure 57: *The element mesh size of 30. (Authors, 2016)*

The different mesh element sizes were plotted in a graph to illustrate the change in deflection when the applied load increased. This helped to analysis the quality of the meshes further, see Figure 58.

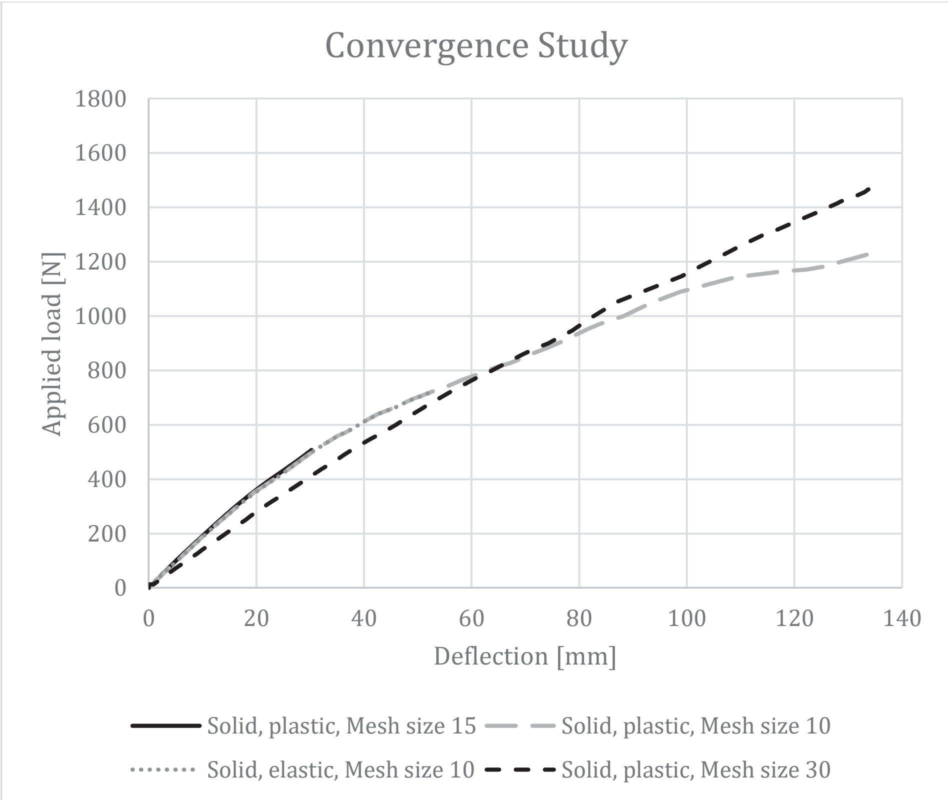

Figure 58: *Convergence study illustrated in a graph of the different mesh element sizes and also compared to the shell element model with elastic material property. (Authors, 2016)*

It can be seen in Figure 58 that the curves have different shapes and end at different deflections and applied loads. This can be explained by the total applied load being different for the three meshes. Nevertheless, this does not matter for the convergence study since it is the shape of the curves that is important.

Looking closer at the curves, Figure 59 illustrates how the solid element models with plastic material properties display the same behaviour. The shape of the curves for the models with element size 10 and 15 follow the same curving. The model with an element size of 30 displays a different behaviour. The latter mesh is for that reason considered poor quality.

It was also observed that the element sizes of 10 and 15 from the solid plastic element models follow the same curved shape as the solid element model with elastic material properties. This further confirms the quality of the meshes and validates the choice of mesh size 10.

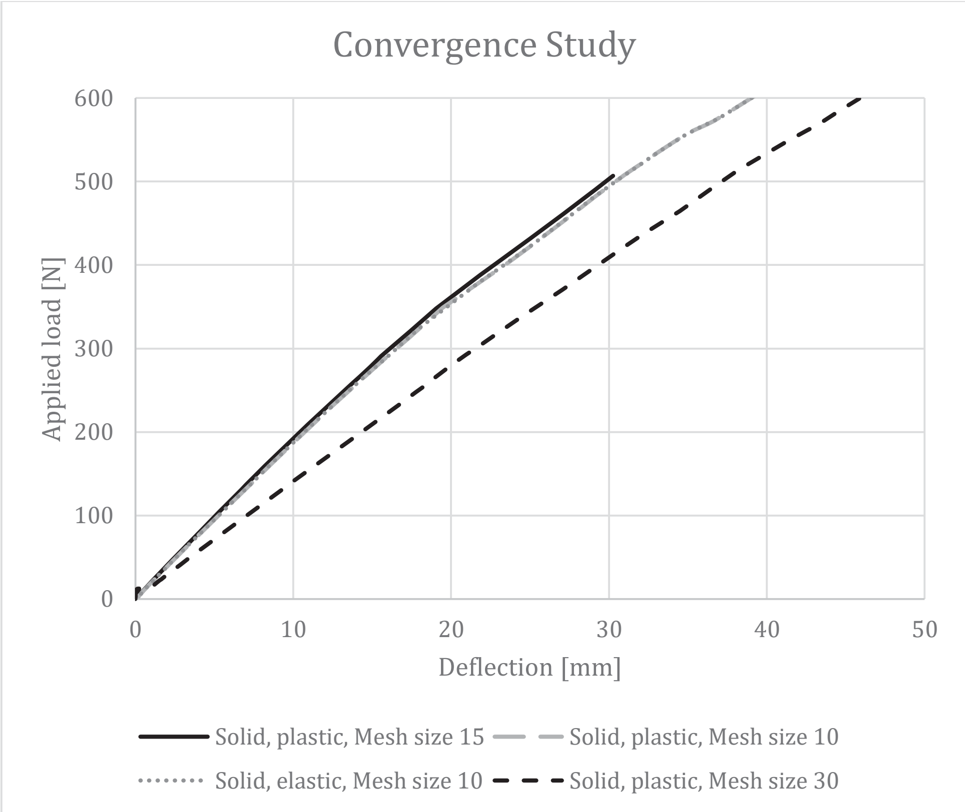

Figure 59: *Convergence study in a more detailed view. (Authors, 2016)*

To show that the convergence study is valid no matter the location of the point chosen for the measured deflection; different points along the width of the sheet were analysed. A similar shape of the curve could be observed for all points analysed, Figure 60, thus confirming the study.

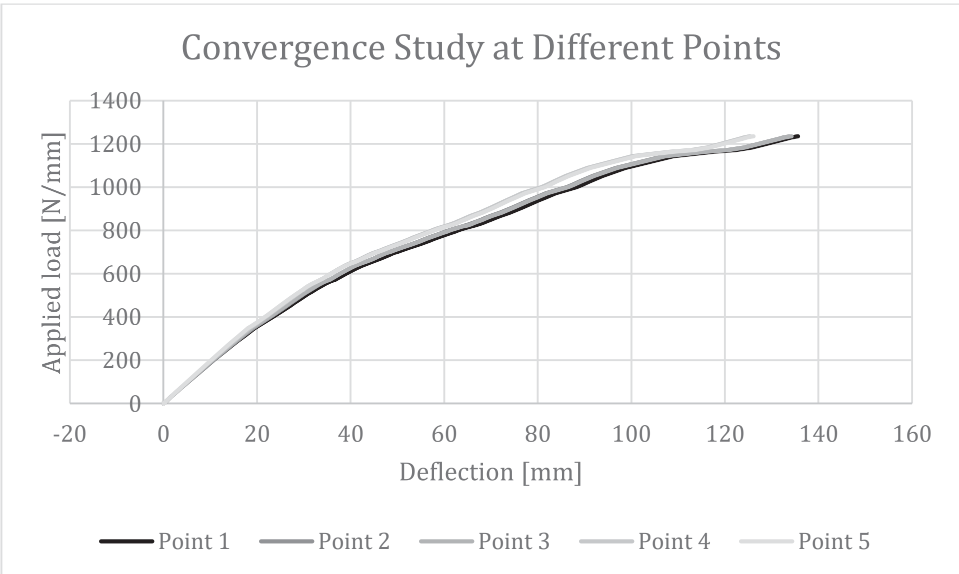

Figure 60: *Convergence study at different points in the solid element model with plastic material property with the element size of 10. (Authors, 2016)*

7.4 Analytical Modelling of the Sheet

In order to analyse the roof system one first needs to understand what happens when a TRP sheet is loaded, more specifically how the splice behaves. Analytical calculations help in describing this behaviour but the method also aims to validate the numerical models.

The geometry of the sheet was based on measurements given by Lindab and the calculation methods were based on Eurocodes together with EKS 10. Separate calculations for the shell element model, the solid element models and the beam element model were performed. The calculations were used to validate the FE-models described in subchapter 7.3 and the results are found in chapter 8. Comparisons were also made with regard to the cross-sectional data presented by Lindab.

First of all, the shape of the sheet must be considered with regard to the rounded corners of the cross-section, according to SS-EN 1993-1-3. The condition applied to the corners at the grooves and in-between the web and the flanges.

In order to analyse the behaviour of the splice, it was important to look at the deflections and the stresses in the loaded sheet. The grooves and folds are critical for the capacity of the sheet according to the literature study. This does however not concern the splice. This study was meant to derive a rotational stiffness from the deflection of the sheet and therefore the analysis of the cross-section was elastic while the splice still needed to be considered for its plastic behaviour.

The shell element model and the solid element models are of one span and were calculated as simply supported. The joint placed in the centre of the span was not considered. Due to the fact that these types of numerical models better show results of stresses than moment distribution, stress distributions were presented as the analytical results.

The solid element model includes solid screws. The design resistance for self-tapping screws was calculated according to SS-EN 1993-1-3 Table 8.2.

The stiffness of the sheet was calculated as a function of each load increment and the corresponding deflection it gave. When increasing the load, each measured deflection equals a certain change in rotation.

$$M_0 = K_{rot} \cdot \varphi \tag{7.1}$$

$$M_{ref} = M_{Ed}(x) \tag{7.2}$$

M_0 Moment in the joint [kNm]
K_{rot} Rotational stiffness [kNm/rad]
φ Angle of the sheet [rad]
M_{ref} Reference moment corresponding to the applied moment [kNm]

The plastic stiffness of the joint describes its full behaviour. The analysis was made under the assumption that it is the joint that fails and that the sheet itself still behaved elastically.

The beam element model was calculated for three spans with two joints placed in the mid-span. It was considered statically determined in accordance with the theory of the Gerber system. Meaning that the support moments were defined based on the location of the joints. The stiffness is not included in the analytical model. Two different cases were calculated; one assuming continuity and the other assuming the behaviour of a hinge. To clarify the support moments were in both cases defined based on a statically determined system.

The resulting deflection and moment distribution are presented and analysed in chapter 9.

8 Verification and Analysis of Analytical and Numerical Models

From the literature study it can be concluded that a Gerber system, in theory, is made by placing hinges at the location of the zero-moment. The hinges will not transfer any moments and the whole system then becomes statically determined (Höglund & Johansson, 2015).

It is clear from the investigations performed by Boverket with regard to the collapsed roof, that the joints actually will carry small moments. The behaviour of the sheet in reality is not correlating with assumptions made in the design. When the load is no longer evenly distributed the applied moment should no longer be zero at the location of the splice. The consequence of the moment being transferred is that it can cause a moment redistribution which might exceed the capacity of the sheet.

Based on this analyse; the capacity of a thin steel sheet roof constructed using the Gerber system should consider the rotational stiffness of the joint. In order to describe this stiffness, the numerical and analytical models have been analysed and verified. The results and comparison can be found in the following sub-chapters.

8.1 Stresses in a Thin Steel Sheet

The stresses in the sheeting have been analysed according to the longitudinal distribution as well as the cross-sectional. All models have been validated by comparing the retrieved results from Abaqus with calculated stresses based on the applied load.

First of all, the applied load is compared to the reaction forces and the reaction moments, see Table 4 and Table 5. The correspondence is considered very well.

Table 4: Reaction forces at the left (A) and right (B) support, calculated values compared to values retrieved from Abaqus. (Authors, 2016)

Model	R_A [kN]			R_B [kN]		
	Calc.	Abaqus	Ratio	Calc.	Abaqus	Ratio
Shell	0.6	0.6	1.0	0.6	0.6	1.0
Solid Elastic	0.72	0.72	1.0	0.72	0.72	1.0
Solid Plastic	1.236	1.234	1.002	1.236	1.234	1.002

Table 5: Moment applied compare to the section moment retrieved from Abaqus models at the same x-coordinate. (Authors, 2016)

Model	M_{Ed} **[kNm]**	M_{Abaqus} **[kNm]**	**Ratio**
Shell	1.74	1.741	0.999
Solid Elastic	0.72	0.728	0.989
Solid Plastic	1.236	1.259	0.982

When comparing the reaction forces it was evident that the models behave according to the design. The moments are affected by the splice and this affects the distribution and ratio.

To verify the credibility of the numerical models the stress and moment distributions have been compiled. The stress distribution in the longitudinal x-direction can be seen in Figure 61 and Figure 62 and the calculated values are included in the graph.

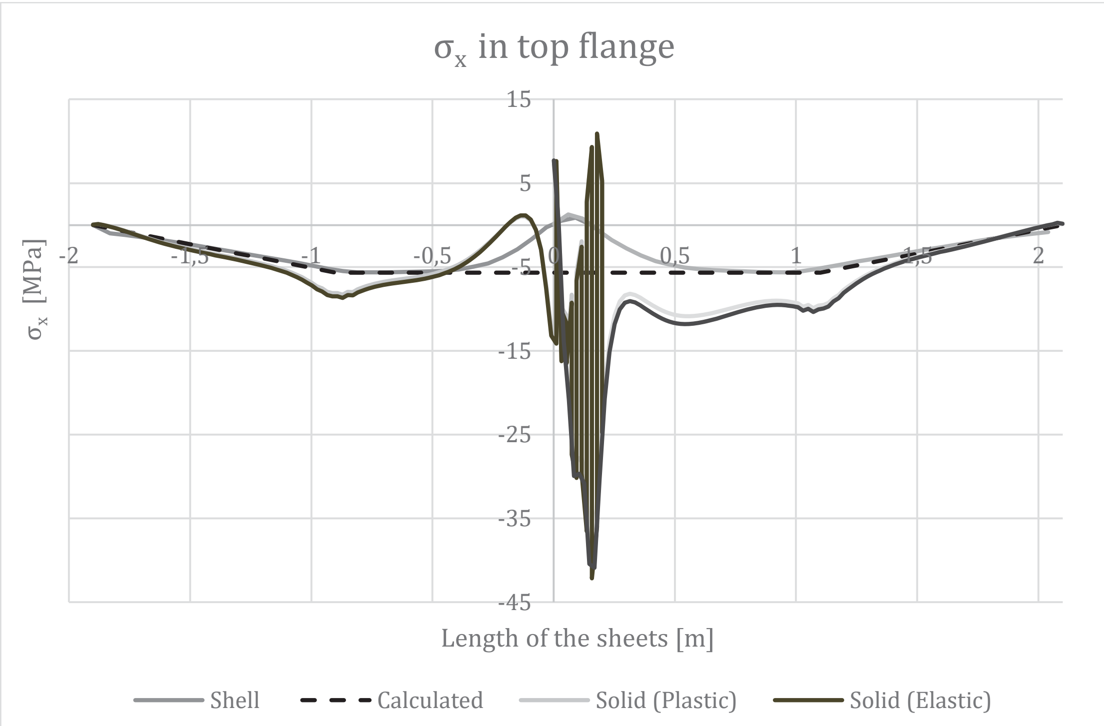

Figure 61: Longitudinal stresses, σ_x, in the smaller upper flange compared between different models and calculated values. (Authors, 2016)

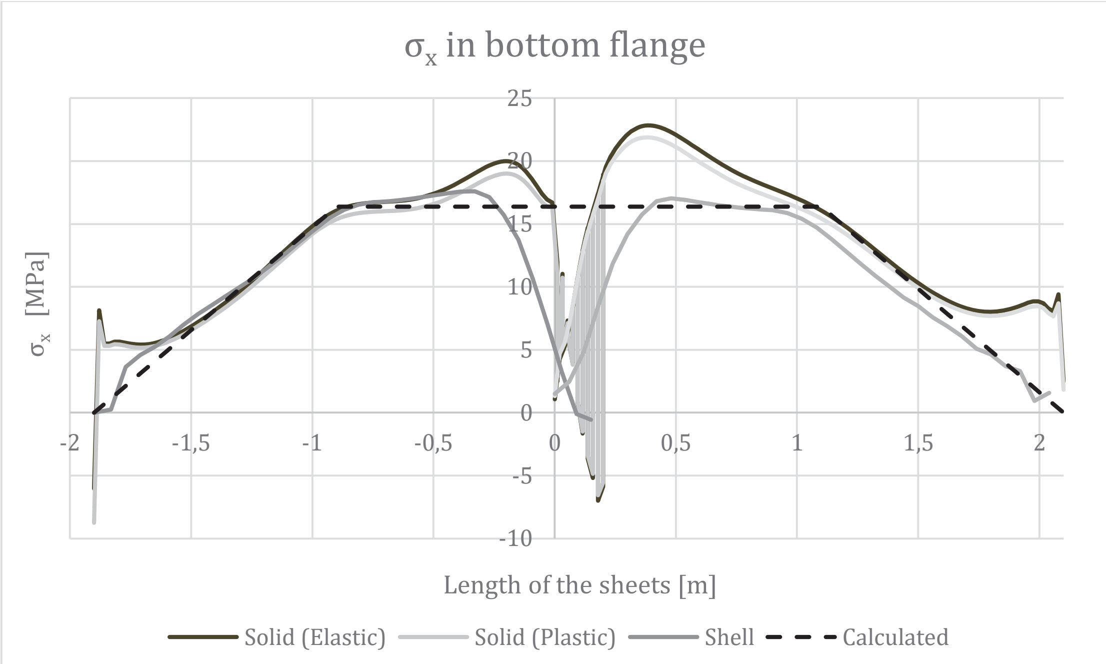

Figure 62: Longitudinal stresses, σ_x, in the bottom flange compared between different models and calculated values. (Authors, 2016)

The stresses in the cross-section correlate better in the left sheet than in the right sheet. APPENDIX B includes the comparison. In the splice however, the left sheet displays a stress distribution that is very irregular, seen in Figure 61 and Figure 62. The splice was assembled with the left sheet underneath the right sheet.

In order to compare the stress distribution of the cross-section the analytical and numerical models are compared in Table 6. A contributing factor for the difference in results was the moment of inertia. The calculations were based on the reduction of entities with regard to rounded corners; the values Abaqus calculates were larger, see Table 7.

Table 6: Stresses in the cross-section of the sheet [MPa]. The z-coordinates are taken at: the top of the top flange, $z_{fo.o.}$; the bottom of the top flange, $z_{fo.u}$; the top of the bottom flange, $z_{fu.o}$; and at the bottom of the bottom flange, $z_{fu.u}$. (Authors, 2016)

	Shell			Solid Elastic			Solid Plastic		
	σ_{calc}	σ_{Ab}	Ratio	σ_{calc}	σ_{Ab}	Ratio	σ_{calc}	σ_{Ab}	Ratio
$z_{fo.o}$	-4.44	-4.77	0.93	-5.68	-4.88	1.16	-9.75	-9.43	1.03
$z_{fo.u}$	-4.34	-4.43	0.98	-5.54	-4.98	1.11	-9.51	-6.63	1.43
$z_{fu.o}$	11.50	12.72	0.90	16.24	16.67	0.97	27.88	30.57	0.91
$z_{fu.u}$	11.60	12.31	0.94	16.38	16.49	0.99	28.12	28.20	1.00

Table 7: Section modulus for the different models; calculated with regard to rounded corners, calculated with sharp corners, and values retrieved from Abaqus based on the moment and stress in that specific cross-section. (Authors, 2016)

Model	W_{el} [mm^3]	$W_{el.sc}$ [mm^3]	W_{Ab} [mm^3]	Ratio W_{el}/W_{Ab}	Ratio $W_{el.sc}/W_{Ab}$
Shell	$3.918e^5$	$4.093e^5$	$3.652e^5$	1.073	1.121
Solid Elastic	$1.267e^5$	$1.324e^5$	$1.497e^5$	0.846	0.884
Solid Plastic	$1.267e^5$	$1.324e^5$	$1.336e^5$	0.948	0.991

The section modulus of the plastic solid element model correlates the best with the calculated values. Disregarding the rounded corners makes it even better. The values are compared in APPENDIX B, chapter 13. The beam element model was therefore calculated for entities with sharp corners, in order to better compare the numerical and the analytical models. These calculations are found in APPENDIX B, chapter 10 and 11.

8.1.1 Stress in the Solid Element Model

The solid element model was the basis of the stiffness in the joint and validating it was fundamental if any conclusion regarding the joint was to be made. Therefore, the stresses in the model were studied more thoroughly.

The capacity of the splice could be analysed with regard to von Mises stresses, see Figure 63. When yielding in the splice first occurs; the stresses in the rest of the sheet were in fact very much smaller than the capacity of the sheet according to Lindab, see chapter 2 in APPENDIX B. It was the sheet around the holes in the top flange and the webs that experienced the highest stresses. The grey areas in Figure 64 represent the breached capacity. The stresses in the grooves were also larger than the f_{yb}.

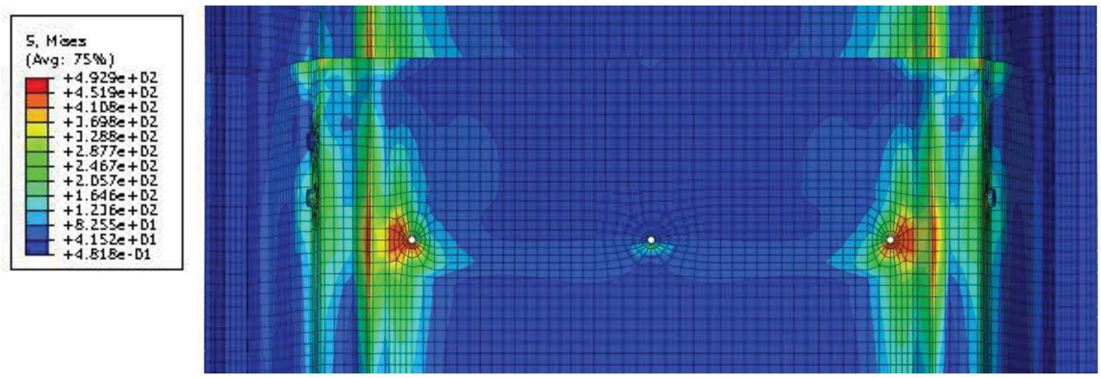

Figure 63: Von Mises stresses in the plastic solid element model (Authors, 2016)

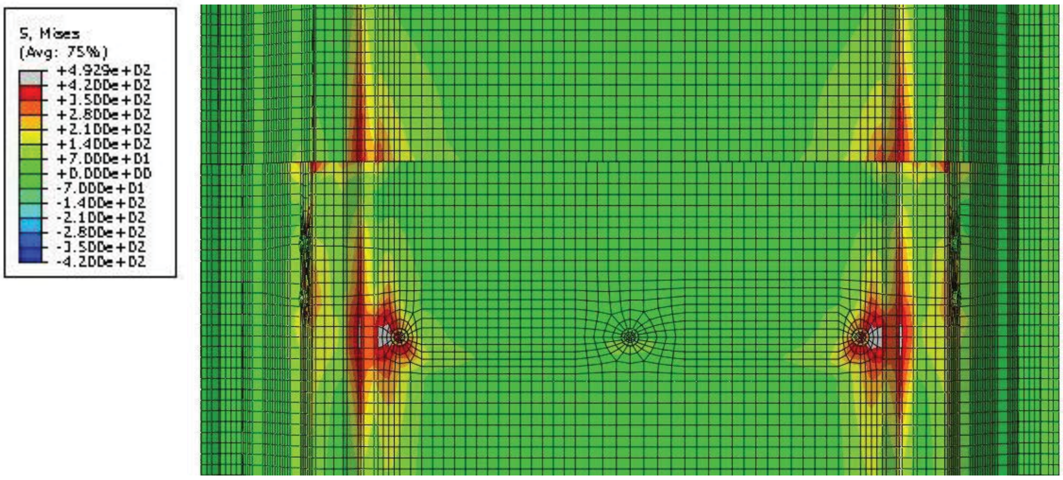

Figure 64: *Von Mises stresses in the splice in the plastic solid element model. The gray areas around the holes and in the grooves indicate yielding. (Authors, 2016)*

The grooves in the top flange displayed tension, which does not correlate with the assumed stress distribution of the cross-section. The moments however correlated. The literature study refers to the capacity of the stiffeners being the decisive factor in design. The stress distribution in the grooves along the length of the sheeting is shown in Figure 65. Considering the fact that the top sheet of the splice pressed down on a flat top flange where the transversal grooves were disregarded, the pressure was not handled by the flange in the same manner as it realistically would have been. The grooves helped in compensating for this. The graph displays the previously mentioned stress concentrations caused by the interaction applied to the surfaces of the two sheets, which in similar manner affected the grooves.

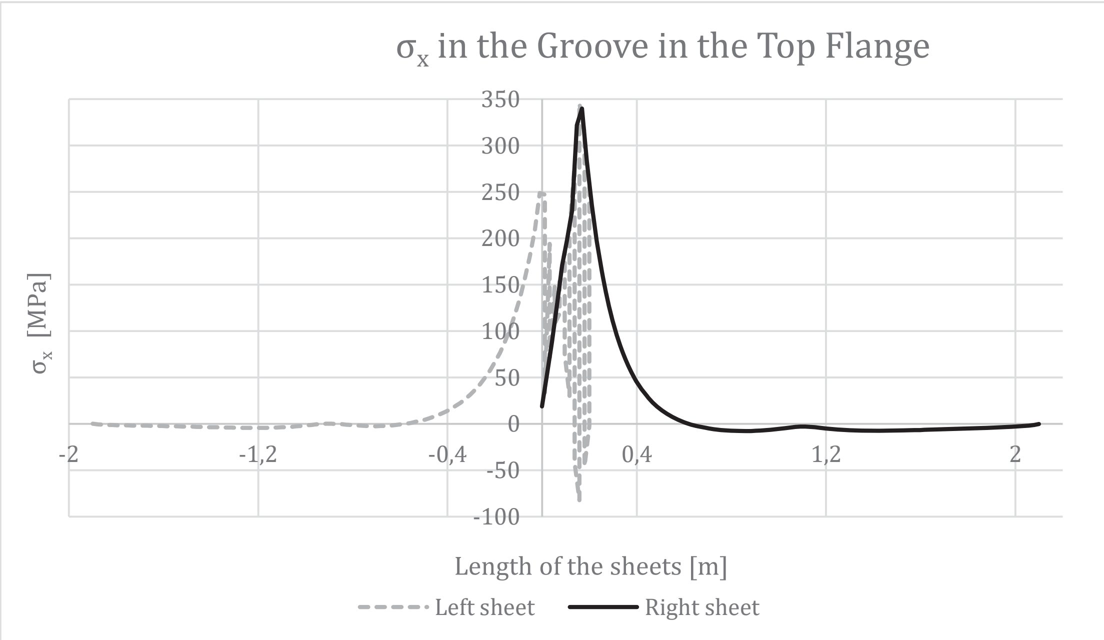

Figure 65: *Graph of the longitudinal stress, σ_x, in the groove of the top flange in the solid element model with plastic material property. (Authors, 2016)*

The stresses in the longitudinal x-direction were close to zero at the edges of the sheets. This correlates with the design. The stress in the longitudinal direction of the sheet should be zero at the locations where the moment is zero, *i.e.* the edges of the sheeting and in the hinge, in accordance with the theory of the Gerber system in chapter 5.

The stresses in the vertical z-direction in Figure 66, affected the sheet around the areas of the reaction forces at the supports and the applied load. These stresses were however very small. In the splice, on the other hand, the stresses were much higher. The screws in the web are transferring shear, according to subchapter 6.1.2 on page 36.

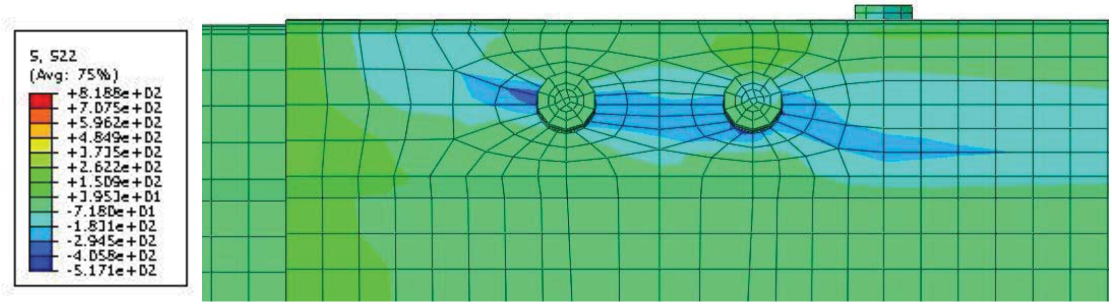

Figure 66: Vertical stresses around the holes in the web in the plastic solid element model. The darkest blue indicates the highest compressional stress of 405.8 MPa. (Authors, 2016)

Stresses in the transversal y-direction, Figure 67, were most noticeable around the connectors in the flange. These are the screws that were moved from their original location in the grooves according to subchapter 7.3.1 on page 43.

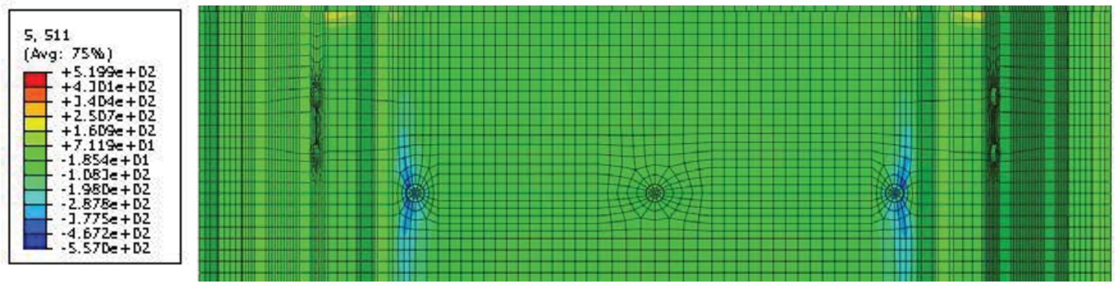

Figure 67: Transversal stresses around the holes in the top flange in the plastic solid element model. The darkest blue indicates the highest compressional stress of 557 MPa. (Authors, 2016)

The connectors, in both cases, created compression on the sheet where the surfaces were constrained. While in-between the sheets in the splice, where there was no constraint, tension was observed. This correlates well with the clamping effect the screws were made to generate.

8.2 Deformation of a Thin Steel Sheet

The way the solid element and shell element models have been computed with interaction in-between the surfaces of the splice and with screws and ties respectively, the behaviour of the splice was not that of a hinge. If it on the other hand had been; the deflection would instantly be very large as soon as the load was applied, considering the load cases in Figure 49 and Figure 51. There was evidently a stiffness in the joint.

The measured deflections in the FE-analysis differed depending on what type of model is considered, see Figure 68. The shell element model displayed an elastic behaviour; the deflection increases linearly with the increased load. This model did not capture the behaviour of the joint very well.

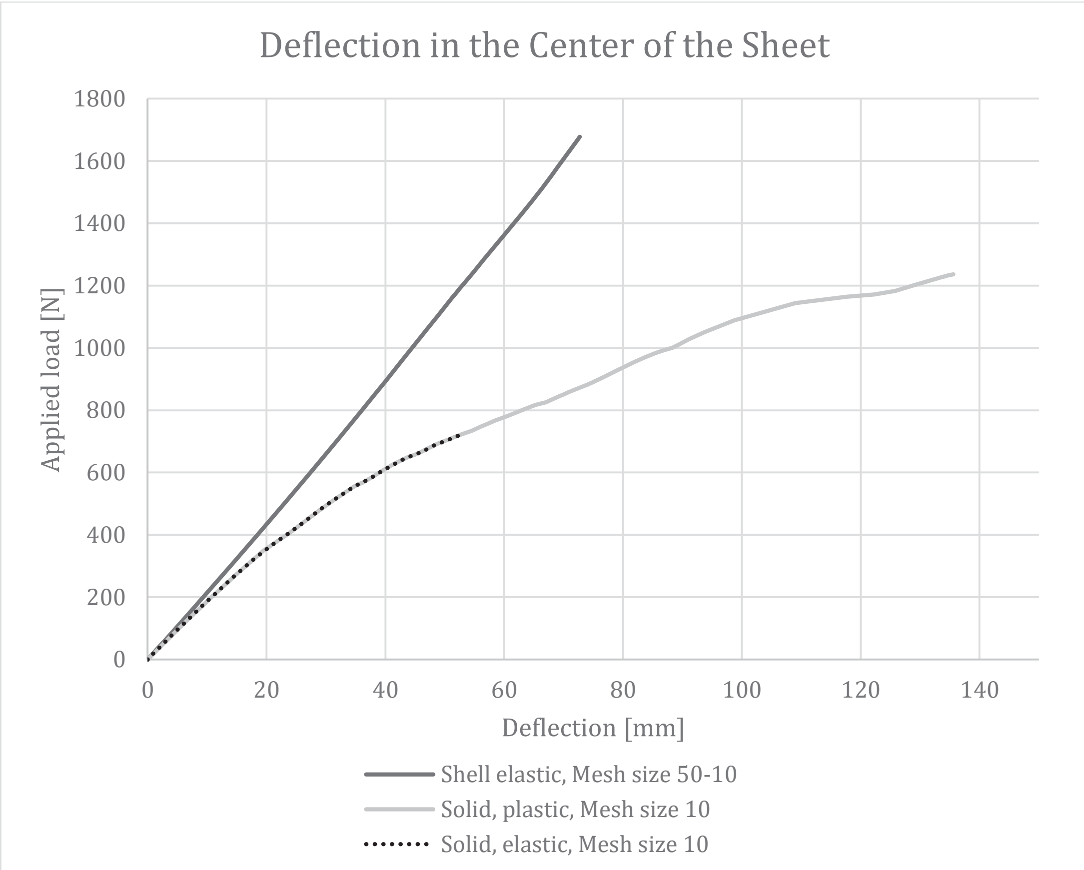

Figure 68: *Comparing the deflection in order to visualize the linear and non-linear behaviour of the different numerical models. (Authors, 2016)*

Considering the solid element model and its elastic analysis; it was apparent that the deformation of the sheet displayed a non-linear behaviour. Therefore, the solid element model was also analysed based on its plastic behaviour by including the yield strength of the material. The fact that the curves for the elastic and plastic analyses correlate indicates that the non-linear behaviour of the sheet was not due to plasticity but rather due to friction, yielding, or bearing failure in the splice. The conclusion is that an elastic analysis of the sheet was sufficient when performing the analysis. The stiffness of the joint, on the other hand, should be modelled with plastic behaviour in order to better describe the splice and the connectors.

An analysis of the screws was made in order to see if these may have caused the non-linear behaviour. Figure 69 shows the location of the screws on the left-hand side and on the right-hand side the black line indicates where the forces were retrieved.

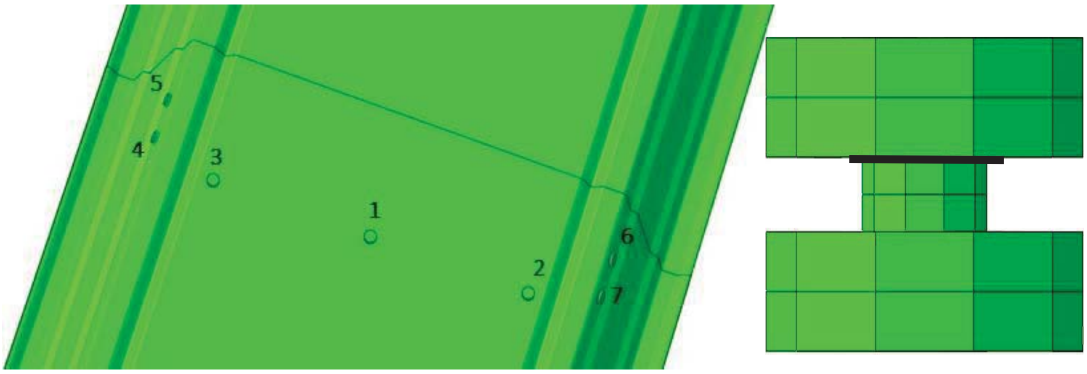

Figure 69: On the left-hand side: The location of the screws. On the right-hand side: The location where the forces are retrieved. (Authors, 2016)

In Table 8 the capacity of the screws is presented and in Table 9 the forces in the screws and the comparison with the capacities are presented. These values are based on APPENDIX B, chapter 8 and 12.

Table 8: The calculated capacity of the screws. (Authors, 2016)

Shear capacity [kN]	***Tension resistance [kN]***	***Bearing resistance [kN]***	**Pull-through resistance [kN]**
7.84	9.8	3.772	6.72

As can be seen in Table 9 the normal forces in screw 2 and 3 exceeds the tension and pull-through resistances. Since this only occurs in these two screws the impact of this is not considered crucial for the analysis. Even though, it set the limit for the allowed percentage of the applied load causing failure in the numerical model, it was in fact only notice in the screws that where moved from their original locations.

Table 9: Forces in the screws and compared to the calculated capacity. (Authors, 2016)

Screw	**Shear force [kN]**	**Utilisation Shear Capacity**	**Utilisation Bearing Resistance**	**Normal force [kN]**	**Utilisation Tension Resistance**	**Utilisation Pull-through Resistance**
1	$0.344e^3$	0.04	0.035	$2.412e^3$	0.64	0.36
2	$-0.472e^3$	0.06	0.048	$12.45e^3$	3.30	1.85
3	$-0.511e^3$	0.07	0.052	$12.36e^3$	3.28	1.84
4	$0.101e^3$	0.01	0.010	$-1.941e^3$	0.52	0.29
5	$0.178e^3$	0.02	0.018	$-1.758e^3$	0.47	0.26
6	$0.168e^3$	0.02	0.017	$1.832e^3$	0.49	0.27
7	$0.886e^3$	0.11	0.090	$1.746e^3$	0.46	0.26

9 Rotational Stiffness in the Joint

This thesis aims to describe the behaviour of the joint in a trapezoidal steel sheeting, TRP, constructed according to the Gerber system design. By inserting the plastic behaviour of the rotational stiffness into a numerical study of a continuous sheet, the behaviour of the system can be described more accurately.

This chapter presents the calculated rotational stiffness in the joint as well as the results from the FE-analysis of the beam element model with the specific stiffness applied at the location of the splices in the mid-span.

9.1 Calculated Rotational Stiffness

The stiffness of a joint varies according to whether it acts like a hinge that cannot transfer moments, or like a rigid joint where the behaviour is as if there was no joint present at all. Then the joint would carry the full applied moment, M_{ref}.

The stiffness in this study was calculated from the plastic solid element model. The total change of angle at the support, α_{tot}, was calculated based on the deflection with regard to the applied load, meaning that the increased load gave an increased angle. The rotation in the joint due to the stiffness, φ_{rot}, was retrieved by subtracting the deformation caused by the bending moment from the total deformation. These calculations are found in APPENDIX B, chapter 9.

The maximum moment applied to the plastic analysis of the solid element model gave the maximum rotational stiffness of the joint, K_{rot}.

$M_{ref} = 1.236$ kNm
$K_{rot} = 4.155 * 10^5$ Nmm/rad

The non-linear relation between increased load and deflection was captured in the non-linear increment of the rotational angle of the joint, Figure 70.

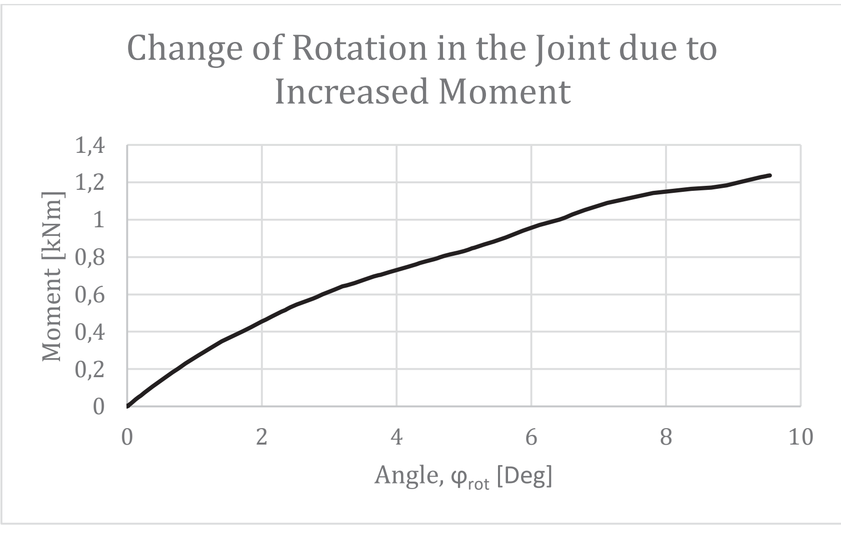

Figure 70: The graph illustrating the non-linear behaviour between increased applied moment and the increased angel in deflection. (Authors, 2016)

9.2 Rotational Stiffness Included in the Design

With regard to the aim of this master's thesis, the behaviour of a continuous TRP sheet constructed with the Gerber system design was studied in a beam element model computed with a rotational stiffness at the location of the joints. The analysis showed a moment distribution which correlates well with the calculated values. The same goes for the deformations when an evenly distributed load was applied. The effects of the unevenly distributed load are presented in the subchapters below.

From the literature study it was evident that an evenly distributed load causes no problem to the sheet as long as the design of the sheeting meets the requirements of the specific location where the building will be constructed. Analysing the effect of unevenly distributed load and the behaviour with and without splices gave a clear view of the effect of the stiffness in the joint.

9.2.1 Deformation in the Beam Element Model

The deformation of the TRP sheet was included in this analysis in order to highlight the effects of unevenly distributed load on continuous sheeting with splices. The magnitudes were calculated, and a comparison with the FE-models gave the crucial differences in results that dictate the actual behaviour of the joint.

With regard to the evenly distributed load, the behaviour of the sheet was affected by the joints. The deflection according to the calculations and according to the FE-analysis can be seen in Figure 71. The effects of including the rotational stiffness in the numerical model showed that the behaviour correlated better with the analytical model that assumed a hinge than with the numerical model without splices. The latter is similar to a sheet with splices that act like rigid joints. The difference between the analytical and numerical deformations with regard to the sheets without splices can be explained by the fact that the analytical values were calculated as statically determined and the numerical graph acted statically indeterminate.

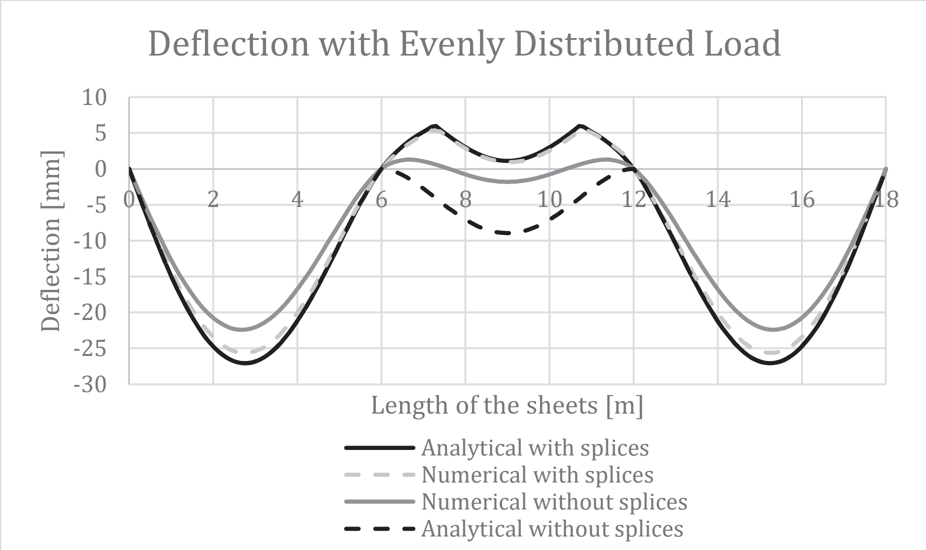

Figure 71: Deflection in the beam element model for evenly distributed load including rotational stiffness in the splices and without compared to the calculated values. (Authors, 2016)

The differences between evenly distributed load and unevenly distributed load with splices can be seen in Figure 72. The graph shows that the numerical values with evenly distributed load correlate well with the analytical ones, which is also shown in Figure 71. The graph illustrates even further that the left and right sheets act like independent cantilevers while the sheet placed in the middle part behaves like a simply supported beam. The shape of the deflection curve of the numerical analysis with unevenly distributed load is affected by both the rotational stiffness and the unevenly distributed load according to previous assumptions.

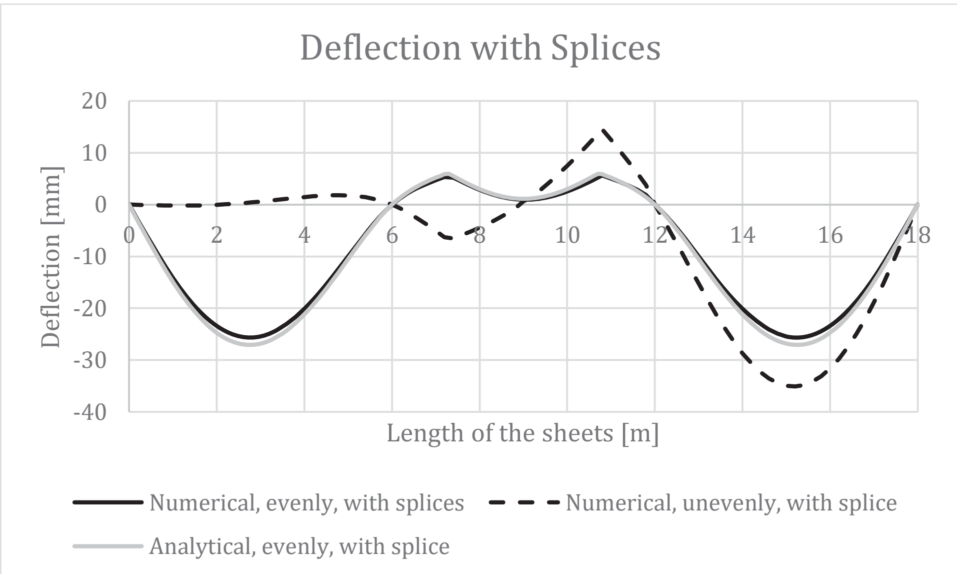

Figure 72: Deflections with numerical and analytical values. (Authors, 2016)

Besides, the numerical model including splices, see Figure 73, also shows the numerical and analytical values when the splices are not included. Ones again it can be seen that the splices with rotational stiffness changes the behaviour of the sheet.

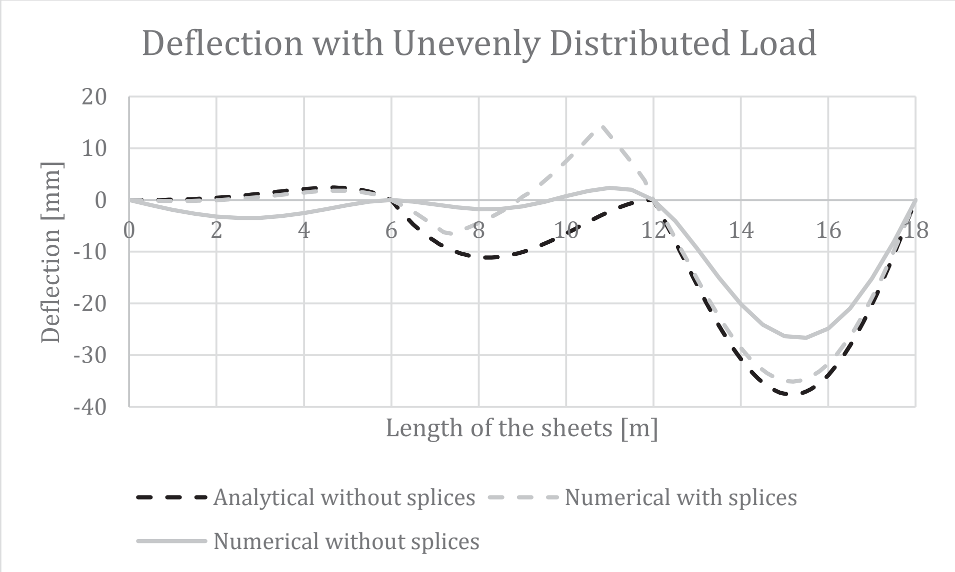

Figure 73: *Deflection in the beam element model with unevenly distributed load including rotational stiffness in the splices and without compared to the analytical value without splices. (Authors, 2016)*

9.2.2 Moment Distribution in the Beam Element Model

The results of the moment distribution for the evenly distributed load are shown in Figure 74. The unevenly distributed load is shown in Figure 75. Both graphs are compared to the analytical values and show good correlation.

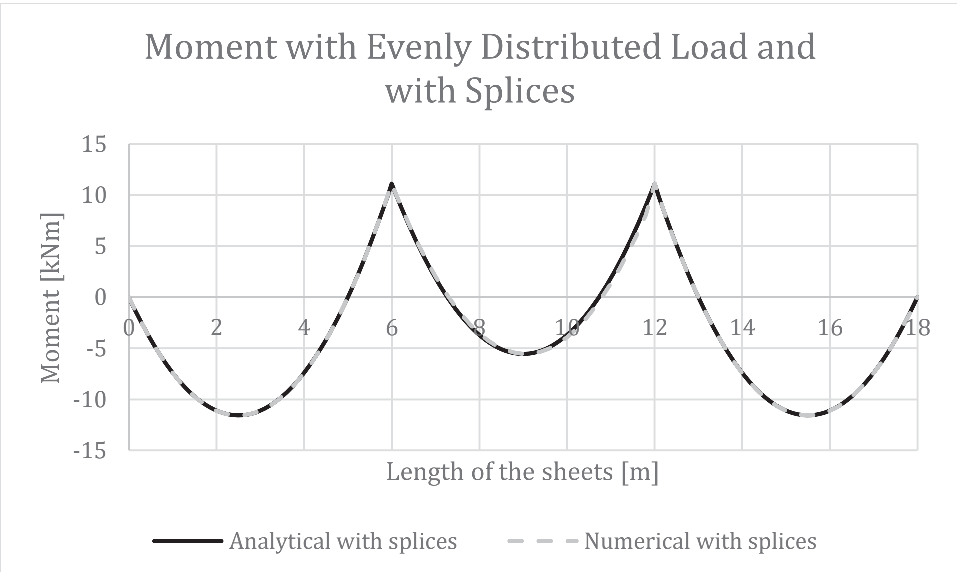

Figure 74: *Moment distribution in the beam element model with evenly distributed load and with splices compared to analytical values. (Authors, 2016)*

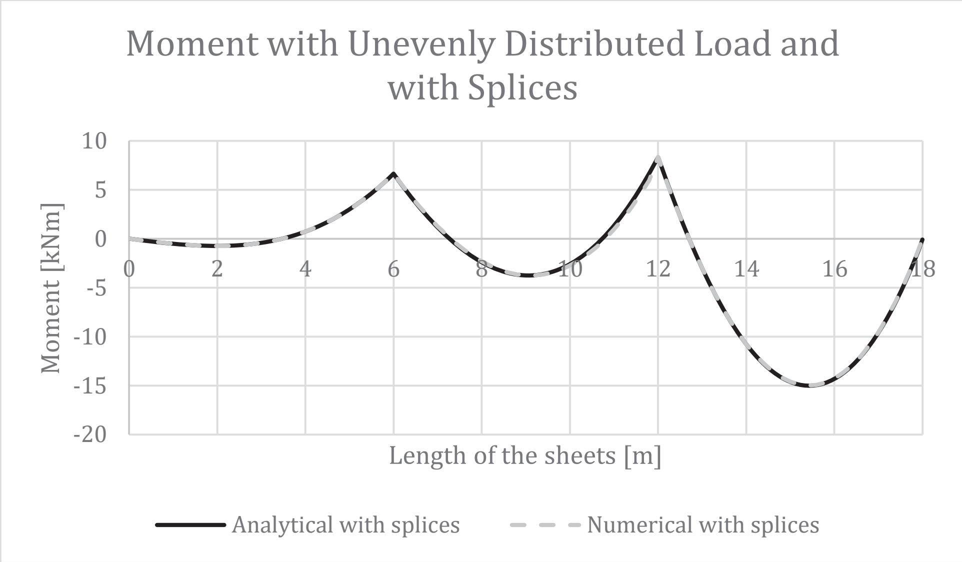

Figure 75: *Moment distribution in the beam element model with unevenly distribution load and with splices compared to analytical values. (Authors, 2016)*

As mentioned in the literature study the Gerber system has no problem with evenly distributed load. Because of that, the model with unevenly distributed load was analysed more thoroughly. Figure 76 shows that the numerical analysis with splices correlates well with both of the analytical values for unevenly distributed load. However, the numerical values for the model without splices differed from the calculated value. The reason for this was that the analytical was calculated as a statically determined system and the numerical as a statically indeterminate one.

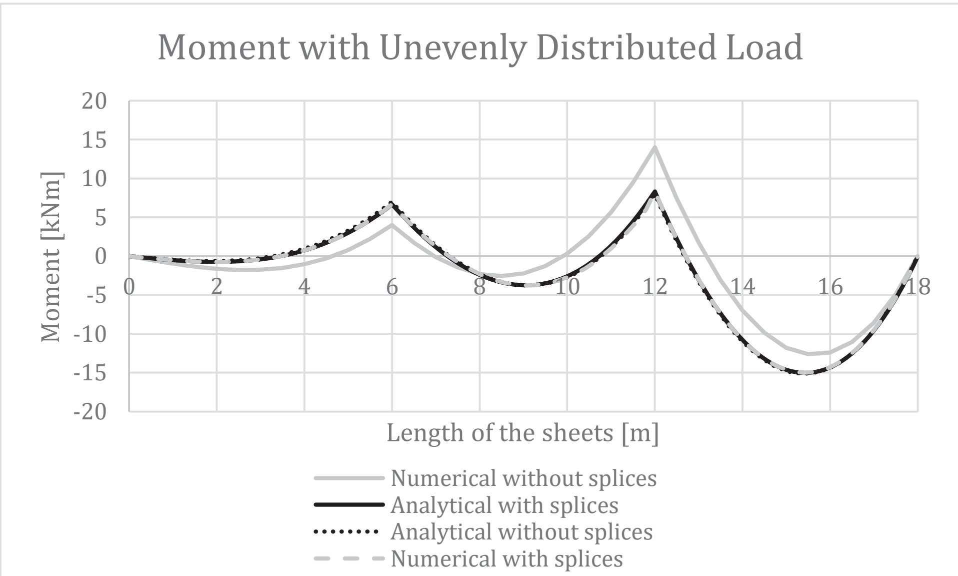

Figure 76: *Moment distribution in the beam element model with unevenly distributed load, both with and without splices. (Authors, 2016)*

The results that can be seen in Figure 77 illustrate that the moment was zero at the locations of the splices, no matter if the load was evenly or unevenly distributed. Thus indicating that the splices behave like hinges that do not transfer moments. When analysing the graph more closely small differences were detected, see Figure 78. Looking at the curves of the numerical models the results indicate that the splice acts like a hinge. However, the location is not that of the actual splice, indicated by the vertical line where the analytical model crosses the x-axis. The joint was given a rotational stiffness and as a result it transferred moments but the splice in the graph will still act like a hinge when comparing evenly and unevenly distributed loading.

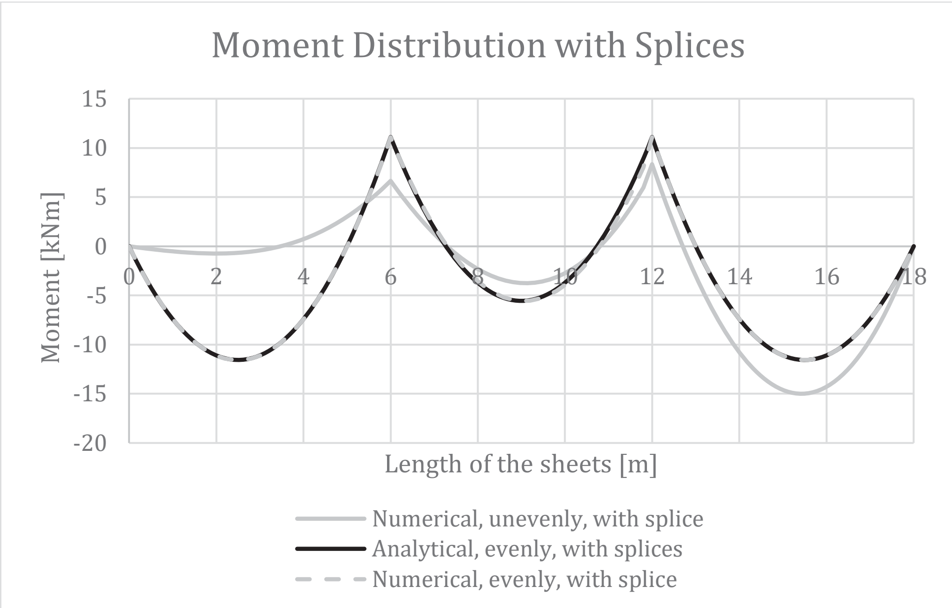

Figure 77: Moment distributions with the numerical and analytical models with splices. (Authors, 2016)

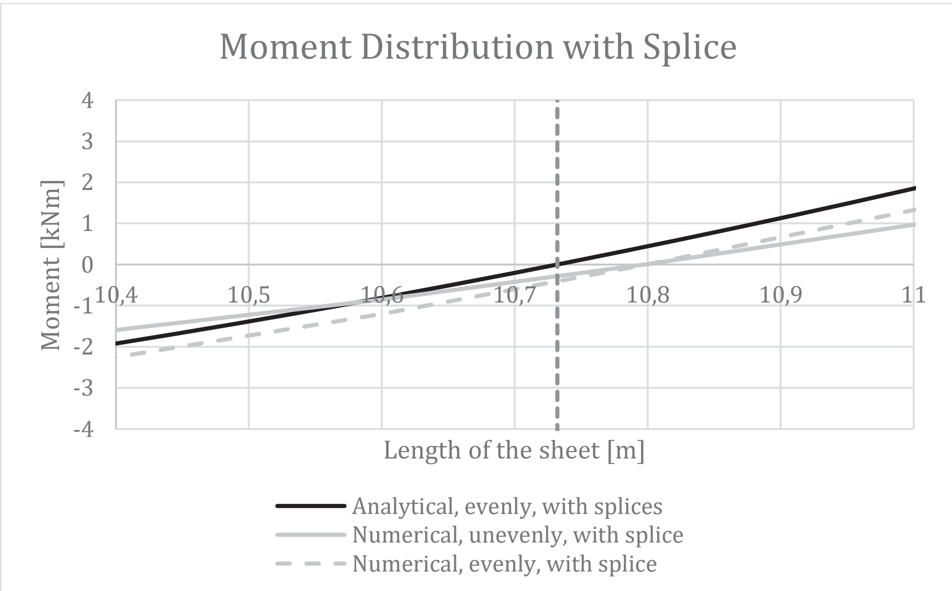

Figure 78: The zoomed in graph illustrate the displacement of the joint between the numerical models and the analytical one. The dotted vertical line indicates the location of the joint in the analytical model. (Authors, 2016)

The results from comparing the numerical model with no stiffness in the joint and the numerical model with the calculated rotational stiffness, see Table 10, showed very small deviations. The reason for the difference in the analytical values is the way they were calculated based on a statically determined system.

Table 10: Maximum moment in fields and over supports compared between analytical and numerical models. (Authors, 2016)

Model	M_{AB} [kNm]	M_B [kNm]	M_{BC} [kNm]	M_C [kNm]	M_{CD} [kNm]
Analytical Model with Hinge	0.741	6.667	5.554	8.428	11.554
Capacity According to Lindab	15.160	20.768	15.160	20.768	15.160
Numerical Model with Rotational Stiffness	0.742	6.660	3.749	8.330	14.999
Numerical Model with Hinge	0.741	6.664	3.750	8.324	15.002

The size of the moment is almost constant when comparing the joint acting with a rotational stiffness compared to it being modelled as a hinge. The moment distribution in general changes very little and the rotational stiffness can therefore be assumed to not contribute significantly to changing the moment distribution.

However, a stiffness higher than the value derived from the plastic analysis of the solid element model would in fact change the moment distribution, see Figure 79. The increased moment at support C, x=12 m, illustrates the effect of increasing the rotational stiffness.

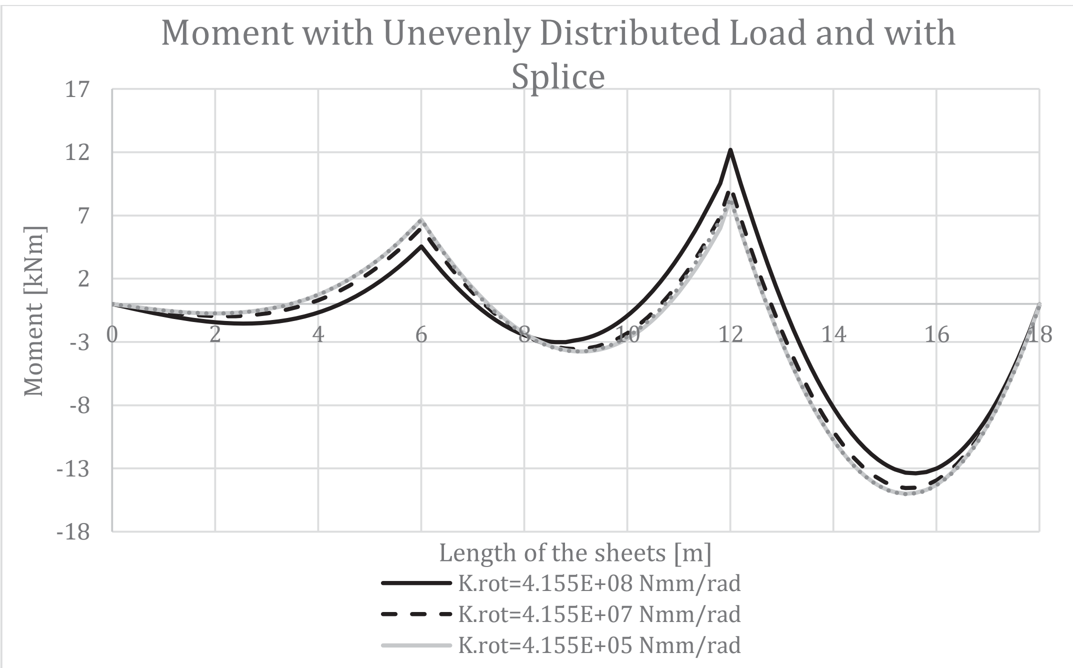

Figure 79: Moment redistribution with increased rotational stiffness, unevenly distributed load. (Authors, 2016)

10 Discussion

The results of this master's thesis illustrates how a rotational stiffness can be derived from numerical and analytical models, and the effects of including this specific stiffness in an analysis of the behaviour of the Gerber system.

This chapter aims to compare and discuss the study, the results, and the limitations that come with the chosen methodology. It is also meant to put the analysis back into the context from which it originated. Roofs collapsed and a common denominator was the trapezoidal steel sheets designed using the Gerber system. Whether or not a rotational stiffness in the joint can help in explaining why the collapses occurred was the main goal of this thesis.

From the literature study it was evident that the unevenly distributed load was a contributing factor to the collapses. The support moments became higher than the design values and the sheeting failed. The question is if this was solely due to the change in loads or if the moments were redistributed. The latter should not be possible if the splices in the system were actually acting like hinges. However, it was initially considered that this could not be the case due to the construction of the splice.

The method of this study was chosen with this in mind, and focused upon capturing the real behaviour of the sheet and more specifically the splice. The resulting stiffness of the joint was validated but in the end it was considered too low to effect the moment distribution noticeably.

10.1 The Choice of Method

Whether the method in question was the most suitable alternative to achieve the purpose of the study is difficult to say. Assumptions were made but also verified in order to create a realistic simplified model that could generate results. In chapter 8 and 9 all results from the numerical study are compared to the analytical results. The correlation is very good and therefore the numerical methods were considered valid.

Numerical models were computed in order to first explain the behaviour of the splice; shell and solid element models. The results showed that the solid element model was able to capture the non-linearity in a better way than the shell element model. The ties in the shell model locked the nodes in the holes while the solid screws rather acted according to the clamping effect. Its constraints and interactions were created in order to simulate the real behaviour of the splice, including friction between the sheets and with connectors transferring shear, making it a better choice of model.

Using constraints in-between the sheets could have given the joint a higher stiffness then it would have had in reality. More likely however, is that it simulated the actual interaction of the two sheets very well. For example, the transversal grooves locking in-between the two sheets and the clamping effect of the screws both act to constrain the splice in reality.

The geometry of the sheet was simplified; a flat top flange and rounded corners calculated according to Eurocode. The reason was to get better performing numerical models when running the analysis in the program Abaqus. Making the models too advanced would result in too long runtimes.

The effects of disregarding the transversal grooves in the top flange might result in a change in the stability of the sheet, but with regard to the comparison of the stresses in subchapter 7.3.1 and APPENDIX B chapter 3, the simplification was considered valid. Since the analysis was made in the service state and the rotational stiffness was derived from the deflection of the loaded sheet, it was considered unaffected by the simplification.

The analytical models were used to verify the shell element and solid element models. The calculations were based on entities that take into account the rounded corners of the cross-section, according to Eurocode. Since the sharp corner geometry gave a stress distribution that correlated better with Abaqus; the calculations for the beam element model were made with assumed sharp corners. However, by comparing the moments instead of the stresses, the effects of the difference in entities could be disregarded.

The final numerical models were the beam element models. The advantage of using beam elements was the simplicity of the model. The meshing was very simple compared to the other models and the moment distribution could easily be compared with the analytical model. By basing the stiffness in the joint on the more advanced plastic analysis of the solid element model, the behaviour can still be considered to capture the detailed behaviour of the splice.

In order to further verify the numerical models, it is suggested that the study should be complemented with tests of LHP 200 sheets. The solid element model is made to simulate two steel sheets joined together by a splice in the centre of the span. An alternative to this would have been to compare the shell element models with actual laboratory tests. Deformation controlled continuous loading would better show the actual stiffness of the joint and more accurate values could be derived. This was a limitation in the thesis and could be considered in future studies.

10.2 The Credibility of the Results

The expected result was a rotational stiffness in the joint, which in some extent would account for the moment redistribution that caused the roof collapses of the investigated building. The analyses instead suggested that even though the joint did transfer moment the derived rotational stiffness was not high enough to be considered as anything but a hinge.

Since the method was believed to be relevant and appropriate for the type of analysis this thesis aimed to perform; the results can, in general, be considered valid.

Depending on the type of element model, different outputs were compared in order to validate the results. For the shell element model and the solid element models the longitudinal stress distribution, σ_x, was compared to calculated values based on beam theory. The analytical model did not consider the effects of placing a hinge in the centre of the span, resulting in the differences in stress distribution.

The beam element model was instead analysed based on its moment distribution. This was thought as more relevant with regard to the aim of the thesis. Comparing the moments instead of the stresses gave a better correlation since the effect of the different sectional modulus used in the numerical and analytical models could be disregarded.

When comparing the elastic and plastic analysis it was evident that the non-linear behaviour did not depend on the plasticity in the sheet. The convergence study showed that the two analyses gave the same behaviour with regard to deformation of the sheet. It was therefore reasonable to assume that the sheet does not display a plastic behaviour and that an elastic analysis of the beam element model would be sufficient in order to capture the behaviour of the loaded sheet.

Due to the yielding around the holes in the splice and in the grooves it was, however, considered reasonable to assume that the splice behaves plastically. With this in mind the rotational stiffness of the joint was derived from the plastic analysis of the solid element model as a function of the deformation. Since it was concluded that the non-linearity of the solid element model did not depend on the plasticity of the model, it could have been reasonable to use elastic stiffness instead. The difference was however small enough to be neglected.

The grooves of the upper flange set the limit for the capacity of the sheet, according to the literature study. This was illustrated by the von Mises stresses in the splice. The capacity of the sheet was reached in the splice and this was presumed to be an effect of the stress concentrations due to the interaction of the faces in the splice. The yielding around the holes indicated bearing failure and this was believed to be the reason for failure of the numerical model.

In reality the connectors in the splice were assumed to only experience very small or no moments. Therefore, the failure would be with regard to the capacity of the sheet and not of the splice. This can be compared with the failures of the examined roof collapses which were assumed to be caused by too high moments at the support causing the formation of a mechanism.

The results from the solid element model showed that it was actually the tension capacity of the screws that set the limit for this analysis. Since this model was based on two applied point loads, there was no shear force in the middle of the span. Having an evenly distributed load and placing the screws in the grooves instead of the top flange would probably have given the expected result of shear capacity breach in the form of bearing failure.

The capacity of the screws was calculated analytically and compared to the numerical values. The two screws that breached their capacity were the ones moved from the grooves to the top flange. This change should, in theory, not affect the behaviour of the sheet. They are only placed in the grooves in order to make construction easier. The results from the numerical beam element model showed very high von Mises stress at the location of these screws. This needs to be further investigated in order to better describe the reason for the high stresses. Because of the high stress in the y-direction, which was earlier determined to be caused by the constraint of the surfaces, the numerical models display yielding where a real sheet would not.

Also worth mentioning is the stresses in the splice. The numerical analysis showed that the stresses in the top of the left sheet, which is placed underneath the right sheet in the splice, are very much affected by the stress concentrations. These are thought to be caused by the restraints of the splice due to the applied interaction. This regards the solid element model but not the shell element model. The latter displayed a more even distribution which is thought to be a consequence of the shell element model only behaving linearly. The same stress concentration was also found in the bottom of the sheet in the splice, which confirms the theory.

The final results showed that the splice does behave like a joint that transfers small moments in the centre of the splice. The rotational stiffness did however not noticeably change the moment distribution of the sheeting. What was disregarded in this study was the translational stiffness of the joint. The load cases studied only gave the effect of the moment acting on the splice. This was the basis of what was used as in-data in the beam element model and the results of this thesis might have been more general if translational stiffness had also been included. This indeed is suggested as further need of investigation in order to improve the results of the analysis.

11 Conclusion

The collapses during the winters of 2009/2010 and 2010/2011 lead to the Gerber system design in roofs with trapezoidal steel sheeting being questioned. It was deemed unsuitable for further usage. Based on a literature study, as well as analytical and numerical models, this thesis aimed to contribute to the explanation of why the behaviour of the sheeting differed from the design. The focus of the analysis was on the moment distribution and the behaviour of the sheets' splicing in detail.

This chapter highlights the conclusions that could be made with regard to the previously presented analysis. The results presented leave room for improvements, not necessarily concerning the method itself but rather complementing the study with further research and testing.

- The splices in continuous roof sheeting designed according to the Gerber system do behave like a joint that transfers moment. However, the rotational stiffness derived according to the chosen numerical method is too small to affect the moment distribution noticeably. The conclusion is therefore that the splices, in this case, act like a hinges.
- The method is relevant for the type of analysis performed. Numerical models were compared and all assumptions have been validated. However, simplifications were made in order to run the analysis, and this is the weakness of the chosen method. Still the presented results do correlate with the theory of the literature study and this indicates that the models actually do help in describing the behaviour of the joint more realistically. Thus, confirming the method.
- Looking at a higher rotational stiffness in the joint, see Figure 79 on page 75, it would correlate with the assumptions made in accordance with the literature study. It states that unevenly distributed load acting on a sheet with rotational stiffness in the joints would cause a moment redistribution, resulting in higher support moments. This might be a contributing factor to the roof collapses but further research is needed before any final conclusions can be made about its effects.

The result of this thesis might still help in understanding the behaviour of the continuous Gerber system designed sheeting. A better understanding might be the key to proceeding with the specific design of trapezoidal steel sheeting in the future. It is a cost efficient system that utilises the material in a cost efficient way and continuing to build with it is therefore desirable.

11.1 Suggested Further Investigations

The calculated stiffness should be updated with a translational stiffness and then adapted to the analysis of the specific case of roof collapse in order to better describe the behaviour of the sheet. This can be done with more advanced numerical models or by tests of actual steel sheets in a laboratory.

A more advanced numerical model could include transversal grooves in the top flange and screws placed according to the construction plans.

New design codes have been adapted since the roofs were constructed and the effects of these have not been studied in this thesis. Progressive collapse must be avoided in the design phase and new restrictions with regard to the exposure factor have been added. Also new recommendations when testing the capacity of the sheets have been issued. This will help in avoiding the type of roof collapses that happened during the snowy winters of 2009/2010 and 2010/2011. It would therefore be interesting to compare the studied collapses with the regulations of the current design code.

12 References

Bill Jr, H. L. (2000). Cantilever and Suspended Span Roof Framing System. *Journal of Architectural Engineering*, *6*(1), 35–38.

Boverket. (2010). *Erfarenheter från takras i Sverige vintern 2009/2010 En delredovisning av Boverkets regeringsuppdrag M2010/2276/H*. Karlskrona.

Boverket. (2011). *Erfarenheter från takras i Sverige vintrarna 2009/10 och 2010/11 En slutredovisning av Boverkets regeringsuppdrag M2010/2276/H*. Karlskrona.

Boverket. (2015). *Konsekvensutredning EKS 10*. Karlskrona: Boverket.

Crocetti, R., Johansson, C.-J., & Wikström, J. (2011). Takras avslöjar allvarliga brister. *Samhällsbyggaren*, *5*, 22–27.

Fernández Troyano, L. (2003). *Bridge engineering - A global perspective*. London: Thomas Telford Publishing.

Hoesch. (2007). HOESCH ROOF SYSTEM 2000. Retrieved February 22, 2015, from http://www.hoesch-bau.com/uploads/tx_downloads/381GB_Dachsys2000_0907.pdf

Höglund, T. (2013). *Takskada Saltsjöbaden Ishall*. Stockholm.

Höglund, T. (2015). *Stabilisering genom skivverkan* (2nd ed.). Stockholm: Stålbyggnadsinstitutet.

Höglund, T., & Johansson, B. (2015, November). Skivverkan allt vanligare. *Nyheter Om Stålbyggnad*, *4*, 30–32.

Höglund, T., & Strömberg, J. (2006). *Kallformade profiler, Modul 7* (2nd ed.). Stockholm: Stålbyggnadsinstitutet, Luleå tekniska universitet, Kungliga tekniska högskolan.

Irwin, P. ., Gamble, S. ., & Taylor, D. . (1995). Effect of roof size, heat transfer, and climate on snow loads: studies for the 1995 NBC. *Canadian Jounal of Civil Engineering*, *22*(4), 770–784.

Johansson, C.-J., Lidgren, C., Nilsson, C., & Crocetti, R. (2011). *Takras vintrarna 2009/2010 och 2010/2011 Orsaker och förslag till åtgärder*. Borås.

SS-EN 1991-1-3. (2003). *Eurocode 1 - Actions on structures - Part 1-3: General actions - Snowloads*. Stockholm: SIS Förlag AB.

SS-EN 1993-1-3. (2006). *Eurocode 3 - Design of steel structures - Part 1-3: General rules - Supplementary rules for cold-formed members and sheeting*. Stockholm: SIS Förlag AB.

Strömberg, J., & Veljkovic, M. (2010a). *Utredning av skador på Fotbollshall i Skellefteå*. Luleå: Luleå Tekniska Högskola.

Strömberg, J., & Veljkovic, M. (2010b). *Utredning av takras B-hall, Luleå*. Luleå: Luleå Tekniska Högskola.

Tolstoy, N. (2011). Bygg & Teknik, *4*, 12–26. Retrieved from https://issuu.com/byggteknikforlaget/docs/4-11?e=0

APPENDIX A

Drawings

Retrieved from Lindab

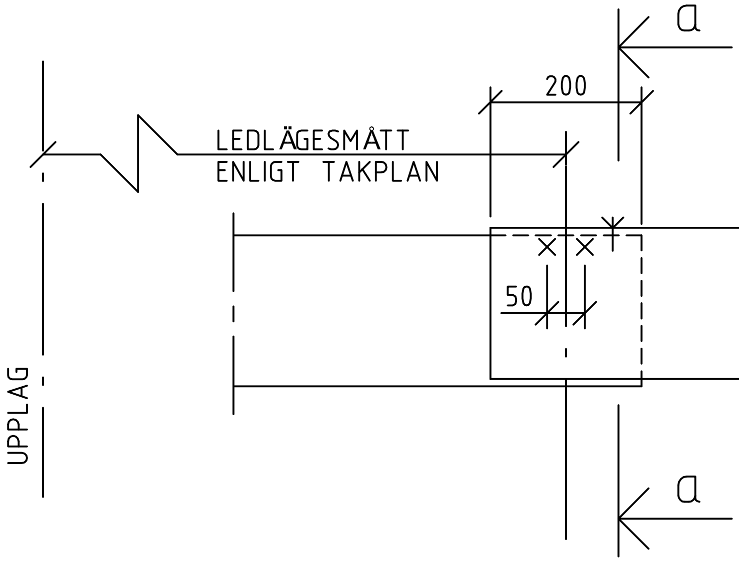

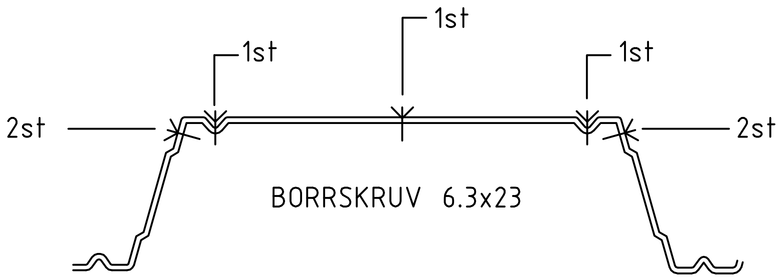

a – a

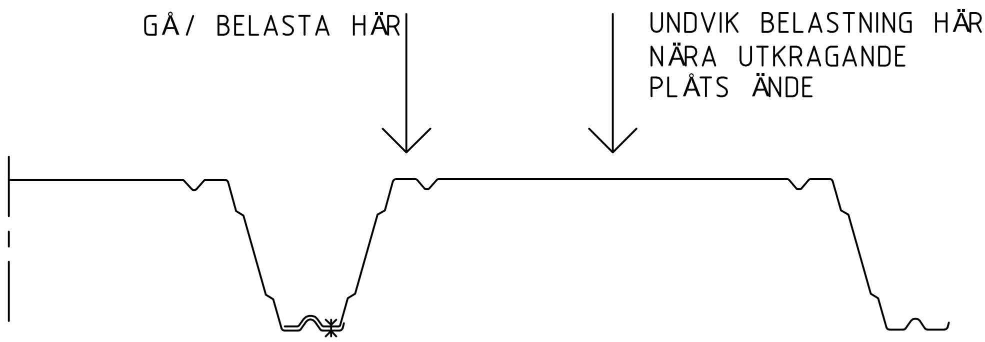

NÄR ETT FACK MONTERATS MÅSTE SIDSKARVARNA
HOPFOGAS MED NIT VID DEN FRIA PLÅTÄNDEN
FÖRE PLÅTARNA I NÄSTA FACK LÄGGS UT.

C. ÄNDSKARV LTP 200 –1:10

APPENDIX B

Analytical Models

Content for the Appendix B – Analytical Models

Gerber Splicing in Thin Steel Sheeting of Roofs

A Study of the Rotational Stiffness in the Joint

B 1 Trapezoidal Steel Sheet - Indata

B 1.1 Cross-sectional data:

The length of parts that end in rounded corners here includes to the center of the bend according to SS-EN 1993-1-3.

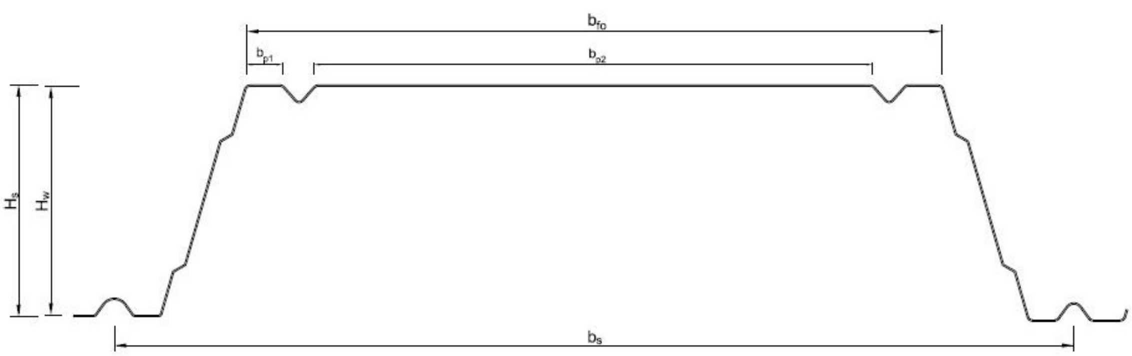

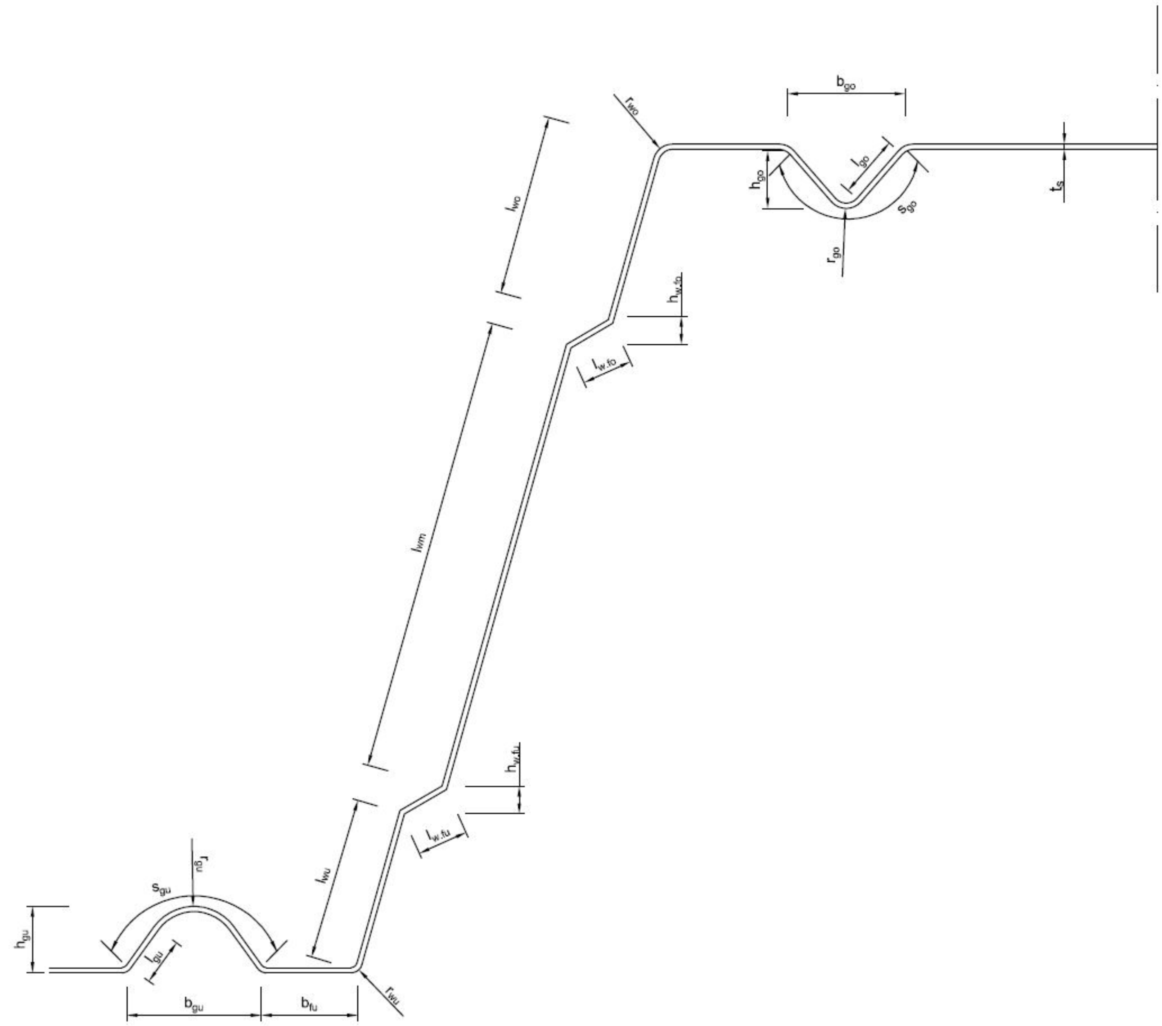

Lengths and heights of the cross-section:

$h_s := 195mm$	Total height of the sheet
$t_{nom} := 1.25mm$	Thickness of the sheet
$t_s := t_{nom}$	Thickness of the steel
$h_w := h_s - t_s = 193.75 \cdot mm$	Height of the web
$b_s := 800mm$	Width of one section (symmetry)

$b_{fo} := 578.33mm$ Total width of the top flange

$b_{p1} := 29.23mm$ Width of the top flange, on each outer side of the grooves

$b_{p2} := 463.67mm$ Width of the middle part of the top flange

$b_{fu} := 22.15mm$ Width of the bottom flange, on each side of the groove

$l_{wu} := 38.54mm$ Length of the bottom part of the web

$l_{wm} := 108.65mm$ Length of the middle part of the web

$l_{wo} := 42.4mm$ Length of the upper part of the web

$l_{w.fu} := 11.51mm$ Length of the bottom web fold

$h_{w.fu} := 5.8mm$ Height of the bottom web fold

$l_{w.fo} := 11.45mm$ Length of the top web fold

$h_{w.fo} := 5.8mm$ Height of the top web fold

$b_{go} := 28.33mm$ Width of the groove in the top flange

$s_{go} := 2 \cdot 19.66mm$ Length of the grooves in the upper flange

$h_{go} := 13.64mm$ Height of the groove in the top flange

$l_{go} := 14.9mm$ The plane part's length of the top groove

$b_{gu} := 32.08mm$ Width of the groove in the bottom flange

$s_{gu} := 12.09mm \cdot 2 + 10.04mm \cdot 2$ Length of the groove in the bottom flange

$h_{gu} := 14.27mm$ Height of the groove in the bottom flange

$l_{gu} := 11.17mm$ The plane part's length of the bottom groove

Radius of the rounded corners in the cross-section:

$r_{gu} := 11mm$ Radius of the groove in the bottom flange

$r_{go} := 4mm$ Radius of the groove in the top flange

$r_{wo} := 4mm$ Radius of the top corner between web and top flange

$r_{wu} := 2mm$ Radius of the bottom corner between the web and the bottom flange

Angles in the cross-section:

$\phi_w := 74deg$ Angle between the flange and the web

$\phi_f := (180 - 136)deg$ Angle between the fold and its center axis

$\phi_{wf.u} := 106deg$ Angle between web and bottom flange

$\phi_{wf.o} := 106deg$ Angle between web and top flange

$\phi_{fg.u} := 126deg$ Angle between bottom flange and bottom groove

$\phi_{fg.o} := 131deg$ Angle between top flange and top groove

B 1.2 Material Data for the Steel Sheet

$f_{yb} := 420MPa$ Yielding of the sheet

$f_u := 420MPa$ Ultimate capacity of the sheet

$E_s := 210GPa$ Modulus of elasticity

$\nu := 0.3$ Poisons ratio

$G_s := \dfrac{E_s}{2\cdot(1+\nu)} = 80.769\cdot GPa$ Shear modulus

$\gamma_{M0} := 1.0$ For cross-sectional checks

$\gamma_{M1} := 1.0$ For instability checks

$\gamma_{M2} := 1.25$ For welds

$skt := 2$ Safety class

$$\gamma_d := \frac{1}{1 + (3 - skt)\cdot 0.1} = 0.909$$ Partial factor

$$\varepsilon := \sqrt{\frac{235\cdot MPa}{f_{yb}}}$$ Buckling strain

$$\rho_{sheet} := \begin{array}{|l} 10.2\,\frac{kg}{m^2} \text{ if } t_{nom} = 0.85mm \\ 12\,\frac{kg}{m^2} \text{ if } t_{nom} = 1.0mm \\ 15\,\frac{kg}{m^2} \text{ if } t_{nom} = 1.25mm \\ 18\,\frac{kg}{m^2} \text{ if } t_{nom} = 1.5mm \end{array}$$

Plastic strain:

$$\varepsilon_e := \frac{f_{yb}}{E_s} = 2 \times 10^{-3}$$ Calculated elastic strain

$$\varepsilon_p := \frac{600MPa - f_{yb}}{\frac{E_s}{100}} = 0.086$$ Calculated plastic strain to be incerted in the plastic analysis

$$\varepsilon_{steel} := 0, 0.001 .. 0.085$$

$$f_{steel}(\varepsilon_{steel}) := \begin{array}{|l} (E_s\cdot\varepsilon_{steel}) \text{ if } (\varepsilon_{steel}) \le \frac{f_{yb}}{E_s} \\ \left(\frac{E_s}{100}\cdot\varepsilon_{steel} + f_{yb}\right) \text{ if } (\varepsilon_{steel}) > \frac{f_{yb}}{E_s} \end{array}$$

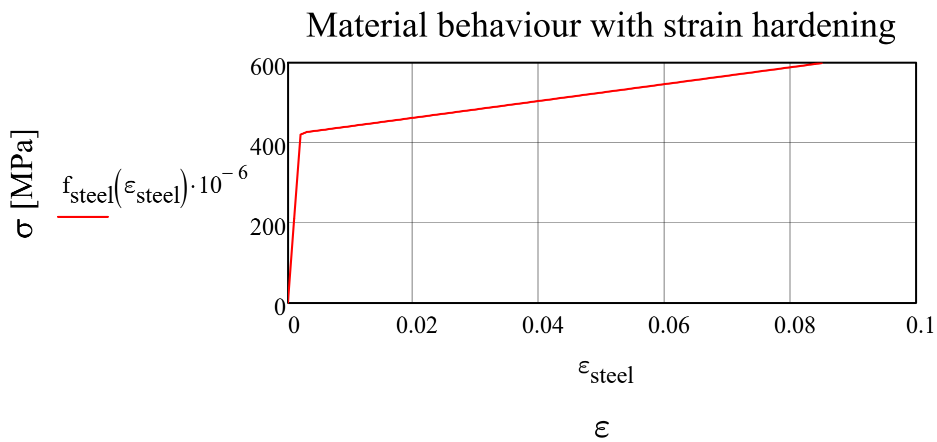

B 1.3 Updated Lengths and Heights with regard to Sharp Corners

Correction for the corner between the top flange and the web:

$r_{wo} \le 5 \cdot t_{nom} = 1$ $\quad r_{wo} \le 0.1 \cdot b_{p1} = 0$ Rounded corners must be regarded

Correction for the corner between the bottom flange and the web:

$r_{wu} \le 5 \cdot t_{nom} = 1$ $\quad r_{wu} \le 0.1 \cdot b_{fu} = 1$ Assume sharp corners

$$r_m := r_{wu} + \frac{t_{nom}}{2}$$

$$g_r := r_m \cdot \left(\tan\left(\frac{\phi_{wf.u}}{2}\right) - \sin\left(\frac{\phi_{wf.u}}{2}\right)\right) = 1.387 \cdot mm$$

$b_{fu} := b_{fu} + g_r = 23.537 \cdot mm$ Width of the bottom flange, on each side of the groove

$l_{wu} := l_{wu} + g_r = 39.927 \cdot mm$ Length of the bottom part of the web

Correction for the corner of the groove in the top flange:

$r_{go} \le 5 \cdot t_{nom} = 1$ $\quad r_{go} \le 0.1 \cdot b_{p1} = 0$ Rounded corners must be regarded

Correction for the corner of the groove in the bottom flange:

$r_{gu} \le 5 \cdot t_{nom} = 0$ $\quad r_{gu} \le 0.1 \cdot b_{fu} = 0$ Rounded corners must be regarded

Correction factor when considering the rounded corner between the top flange and the web:

$$\delta_{sc} := 0.43\cdot\frac{\left(r_{gu}\cdot\frac{\phi_{fg.u}}{90deg}+r_{go}\cdot\frac{\phi_{fg.o}}{90deg}+r_{wo}\cdot\frac{\phi_{wf.o}}{90deg}\right)\cdot 2}{\left(2\cdot b_{fu}+l_{wu}+l_{w.fu}+l_{wm}+l_{w.fo}+l_{wo}+b_{p1}\right)\cdot 2+b_{p2}} = 0.021$$

B 1.4 Calculated Areas and Distances

$A_{fu} := t_s\cdot b_{fu} = 2.942\times 10^{-5}\,m^2$

$A_{gu} := t_s\cdot s_{gu} = 5.532\times 10^{-5}\,m^2$

$A_{fo} := t_s\cdot\left(2b_{p1}+b_{p2}\right) = 6.527\times 10^{-4}\,m^2$

$A_{go} := t_s\cdot s_{go} = 4.915\times 10^{-5}\,m^2$

$A_{wu} := t_s\cdot l_{wu} = 4.991\times 10^{-5}\,m^2$

$A_{wm} := t_s\cdot l_{wm} = 1.358\times 10^{-4}\,m^2$

$A_{wo} := t_s\cdot l_{wo} = 5.3\times 10^{-5}\,m^2$

$A_{w.fu} := t_s\cdot l_{w.fu} = 1.439\times 10^{-5}\,m^2$

$A_{w.fo} := t_s\cdot l_{w.fo} = 1.431\times 10^{-5}\,m^2$

$z_{fu} := \frac{t_s}{2}$

$z_{gu} := \frac{h_{gu}}{3}$

$z_{fo} := h_s - \frac{t_s}{2}$

$z_{go} := h_s - \frac{t_s}{2} - \frac{h_{go}}{3}$

$z_{wu} := t_s + \sin\left(\phi_w\right)\cdot\frac{l_{wu}}{2}$

$z_{wm} := t_s + \sin\left(\phi_w\right)\cdot l_{wu} + h_{w.fu} + \sin\left(\phi_w\right)\cdot\frac{l_{wm}}{2}$

$z_{wo} := h_s - t_s - \sin\left(\phi_w\right)\cdot\frac{l_{wo}}{2}$

$z_{w.fu} := t_s + \sin\left(\phi_w\right)\cdot l_{wu} + \frac{h_{w.fu}}{2}$

$z_{w.fo} := t_s + \sin\left(\phi_w\right)\cdot l_{wu} + h_{w.fu} + \sin\left(\phi_w\right)\cdot l_{wm} + \frac{h_{w.fo}}{2}$

B 2 LHP Sheet from Lindab

A trapezoidal steel sheet is analysed numerically to fully understand the behaviour of the joints connecting the sheets in the longitudinal direction.

B 2.1 Geometry of Tested Sheet:

$L_s := 6\mathrm{m}$	Length of one sheet
$L_{ol} := 200\mathrm{mm}$	Length of the overlap
$L_{tot} := L_s \cdot 2 - L_{ol} = 11.8\,\mathrm{m}$	Total length of the two connected sheets
$a := \dfrac{L_s - L_{ol}}{2} = 2.9\,\mathrm{m}$	Location of point load, measured from the sheet edge
$a_{load} := 100\mathrm{mm}$	Width of the applied load
$b_{tot} := b_s \cdot 3$	Width of the tested sheet

B 2.2 Capacity of a Sheet

Second moment of area based on values from Lindab, decisive when upper and lower flange respectively are compressed:

$$I := \left| \begin{array}{l} 4460 \dfrac{\mathrm{mm}^4}{\mathrm{mm}} \ \text{ if } t_{nom} = 0.85\mathrm{mm} \\ 5410 \cdot \dfrac{\mathrm{mm}^4}{\mathrm{mm}} \ \text{ if } t_{nom} = 1.00\mathrm{mm} \\ 6760 \cdot \dfrac{\mathrm{mm}^4}{\mathrm{mm}} \ \text{ if } t_{nom} = 1.25\mathrm{mm} \\ 8330 \cdot \dfrac{\mathrm{mm}^4}{\mathrm{mm}} \ \text{ if } t_{nom} = 1.50\mathrm{mm} \end{array} \right.$$

$$I = 6.76 \times 10^3 \cdot \frac{\mathrm{mm}^4}{\mathrm{mm}}$$

When looking at a multi span roof; I.tot is a function of the support vs. field second moment of area. In our case they are the same.

Values from Lindab, field moment and support moment:

$$M_{k.f} := \begin{cases} \left[9.67\cdot\left(kN\cdot\frac{m}{m}\right)\right] & \text{if } t_{nom} = 0.85mm \\ \left[13.61\cdot\left(kN\cdot\frac{m}{m}\right)\right] & \text{if } t_{nom} = 1.00mm \\ \left[18.95\cdot\left(kN\cdot\frac{m}{m}\right)\right] & \text{if } t_{nom} = 1.25mm \\ \left[22.04\cdot\left(kN\cdot\frac{m}{m}\right)\right] & \text{if } t_{nom} = 1.50mm \end{cases} \qquad M_{k.s} := \begin{cases} \left[13.26\cdot\left(kN\cdot\frac{m}{m}\right)\right] & \text{if } t_{nom} = 0.85mm \\ \left[18.33\cdot\left(kN\cdot\frac{m}{m}\right)\right] & \text{if } t_{nom} = 1.00mm \\ \left[25.96\cdot\left(kN\cdot\frac{m}{m}\right)\right] & \text{if } t_{nom} = 1.25mm \\ \left[31.02\cdot\left(kN\cdot\frac{m}{m}\right)\right] & \text{if } t_{nom} = 1.50mm \end{cases}$$

$$M_{k.f} = 18.95\cdot\frac{kN\cdot m}{m} \qquad M_{k.s} = 25.96\cdot\frac{kN\cdot m}{m}$$

$$M_{d.f} := M_{k.f}\cdot b_s = 15.16\,m\cdot kN \qquad M_{d.s} := M_{k.s}\cdot b_s = 20.768\,m\cdot kN$$

Values from Lindab, shear force:

$$V_k := \begin{cases} \left[10.62\cdot\left(\frac{kN}{m}\right)\right] & \text{if } t_{nom} = 0.85mm \\ \left[17.93\cdot\left(\frac{kN}{m}\right)\right] & \text{if } t_{nom} = 1.00mm \\ \left[32.83\cdot\left(\frac{kN}{m}\right)\right] & \text{if } t_{nom} = 1.25mm \\ \left[59.39\cdot\left(\frac{kN}{m}\right)\right] & \text{if } t_{nom} = 1.50mm \end{cases}$$

$$V_k = 32.83\cdot\frac{kN}{m}$$

Values from Lindab, reaction force:

$$R_k := \begin{cases} \left[5.30\cdot\left(\frac{kN}{m}\right)\right] & \text{if } t_{nom} = 0.85mm \\ \left[7.30\cdot\left(\frac{kN}{m}\right)\right] & \text{if } t_{nom} = 1.00mm \\ \left[11.60\cdot\left(\frac{kN}{m}\right)\right] & \text{if } t_{nom} = 1.25mm \\ \left[17.10\cdot\left(\frac{kN}{m}\right)\right] & \text{if } t_{nom} = 1.50mm \end{cases}$$

$$R_k = 11.6 \cdot \frac{kN}{m}$$

Values from Lindab, Shear buckling in flange and web respectively:

$$V_{f.k} := \begin{vmatrix} \left[14.2 \cdot \left(\frac{kN}{m}\right)\right] \text{ if } t_{nom} = 0.85mm \\ \left[18.6 \cdot \left(\frac{kN}{m}\right)\right] \text{ if } t_{nom} = 1.00mm \\ \left[27.2 \cdot \left(\frac{kN}{m}\right)\right] \text{ if } t_{nom} = 1.25mm \\ \left[37.1 \cdot \left(\frac{kN}{m}\right)\right] \text{ if } t_{nom} = 1.50mm \end{vmatrix} \qquad V_{w.k} := \begin{vmatrix} \left[18.9 \cdot \left(\frac{kN}{m}\right)\right] \text{ if } t_{nom} = 0.85mm \\ \left[26 \cdot \left(\frac{kN}{m}\right)\right] \text{ if } t_{nom} = 1.00mm \\ \left[40.7 \cdot \left(\frac{kN}{m}\right)\right] \text{ if } t_{nom} = 1.25mm \\ \left[58.3 \cdot \left(\frac{kN}{m}\right)\right] \text{ if } t_{nom} = 1.50mm \end{vmatrix}$$

$$V_{f.k} = 27.2 \cdot \frac{kN}{m} \qquad V_{w.k} = 40.7 \cdot \frac{kN}{m}$$

Values from Lindab, global shear buckling:

$$V_{gl.k} := \begin{vmatrix} \left[1534 \cdot \left(\frac{kN}{m} \cdot m^2\right)\right] \text{ if } t_{nom} = 0.85mm \\ \left[1998 \cdot \left(\frac{kN}{m} \cdot m^2\right)\right] \text{ if } t_{nom} = 1.00mm \\ \left[2876 \cdot \left(\frac{kN}{m} \cdot m^2\right)\right] \text{ if } t_{nom} = 1.25mm \\ \left[3850 \cdot \left(\frac{kN}{m} \cdot m^2\right)\right] \text{ if } t_{nom} = 1.50mm \end{vmatrix}$$

$$V_{gl.k} = 2.876 \times 10^3 \, m^2 \cdot \frac{kN}{m}$$

Values to Compare with Hand Calculations:

These values are calculated for the capacity of the sheet and the deflection of the sheet respectively
This can be compare with the elastic and plastic analyses which are performed.

$$W_{Lindab.f} := \frac{M_{k.f}}{f_{yb}} \qquad W_{Lindab.s} := \frac{M_{k.s}}{f_{yb}}$$

$$z_{Lindab.f} := \frac{I}{W_{Lindab.f}} = 149.826 \cdot mm \qquad z_{Lindab.s} := \frac{I}{W_{Lindab.s}} = 109.368 \cdot mm$$

Since I is the same for the deflection and the ultimate capacity, as is the σ, we assume the capacity is based on the elastic analysis i.e. the full cross-section is active?

B 3 Validating the Shell Element Model without Hinges

A simplification is made in the Abaqus models with regard to the transversal grooves in the top flange. Assuming that the top flange is flat in the analysis needs to be verified, this is the aim of this chapter.

B 3.1 Cross-section of the Sheet

Area of the gross cross-section with sharp corners:

$$A_{g.sc} := 4A_{fu} + 2A_{gu} + 2A_{wu} + 2\cdot A_{w.fu} + 2\cdot A_{wm} \ldots + 2\cdot A_{w.fo} + 2\cdot A_{wo} + 1\cdot A_{fo} + 2\cdot A_{go} = 1.514 \times 10^3 \cdot mm^2$$

Area of the gross cross-section considering the rounded corners:

$$A_g := A_{g.sc}\cdot\left(1 - \delta_{sc}\right) = 1.482 \times 10^3 \cdot mm^2$$

$$z_{tp} := \frac{4A_{fu}\cdot\left(z_{fu}\right) + 2A_{gu}\cdot\left(z_{gu}\right) + 1\cdot A_{fo}\cdot\left(z_{fo}\right) + 2\cdot A_{go}\cdot\left(z_{go}\right) + 2A_{wu}\cdot\left(z_{wu}\right) \ldots + 2A_{wm}\cdot\left(z_{wm}\right) + 2\cdot A_{wo}\cdot\left(z_{wo}\right) + 2A_{w.fu}\cdot\left(z_{w.fu}\right) + 2\cdot A_{w.fo}\cdot\left(z_{w.fo}\right)}{A_g} = 134.067 \cdot mm$$

$$\begin{aligned} I_{g.sc} := {} & 4\left[\frac{b_{fu}\cdot\left(t_s\right)^3}{12} + A_{fu}\cdot\left(z_{tp} - z_{fu}\right)^2\right] + 2A_{gu}\cdot\left(z_{tp} - z_{gu}\right)^2 \ldots \\ & + 1\cdot\left[\frac{\left(2\cdot b_{p2} + b_{p1}\right)\cdot\left(t_s\right)^3}{12} + A_{fo}\cdot\left(z_{fo} - z_{tp}\right)^2\right] + 2\cdot A_{go}\cdot\left(z_{go} - z_{tp}\right)^2 \ldots \\ & + 2\left[\frac{t_s\cdot\left(l_{wu}\cdot\sin\left(\phi_w\right)\right)^3}{12} + A_{wu}\cdot\left(z_{tp} - z_{wu}\right)^2\right] + 2\left[\frac{t_s\cdot\left(l_{wm}\cdot\sin\left(\phi_w\right)\right)^3}{12} + A_{wm}\cdot\left(z_{tp} - z_{wm}\right)^2\right] \ldots \\ & + 2\cdot\left[\frac{t_s\cdot\left(l_{wo}\cdot\sin\left(\phi_w\right)\right)^3}{12} + A_{wo}\cdot\left(z_{wo} - z_{tp}\right)^2\right] \ldots \\ & + 2\left[\frac{t_s\cdot\left(h_{w.fu}\right)^3}{12} + A_{w.fu}\cdot\left(z_{tp} - z_{w.fu}\right)^2\right] + 2\cdot\left[\frac{t_s\cdot\left(h_{w.fo}\right)^3}{12} + A_{w.fo}\cdot\left(z_{w.fo} - z_{tp}\right)^2\right] \end{aligned}$$

$$I_{g.sc} = 8.953 \times 10^6 \cdot mm^4$$

$$I_g := I_{g.sc}\cdot\left(1 - 2\delta_{sc}\right) = 8.57 \times 10^6 \cdot mm^4$$

$$W_{el} := \frac{I_g}{\left(h_s - z_{tp}\right)} = 1.406 \times 10^5 \cdot mm^3$$

Sectional modulus at the top of the sheet

$$W_{el.sc} := \frac{I_{g.sc}}{\left(h_s - z_{tp}\right)} = 1.469 \times 10^5 \cdot mm^3$$

Sectional modulus with regard to sharp corners

$$z := -z_{tp}, \left(-z_{tp} + 0.1 \cdot mm\right) .. \left(h_s - z_{tp}\right)$$

$$W_{el.dist}(z) := \frac{I_g}{z}$$

Sectional modulus along the height

B 3.2 Calculated Stresses in the Sheet

The stresses in the sheet based on a chosen applied load, not the critical value since elastic analysis.

$P := 600N$ Chosen point load to act on the sheet for an elastic analysis

$P := P \cdot 1$ Time step in Abaqus

$a_{test} := 1000mm$ Distance from support to applied load in the test-sheet

$L_{test} := 6m$ Length of the tested sheet

$M_{Ed.test} := P \cdot a_{test} = 0.6 \cdot kN \cdot m$ Moment acting on the sheet inbetween the applied point loads

$\sigma_{dist.test}(z) := \frac{M_{Ed.test}}{W_{el.dist}(z)}$ Cross-sectional stresses in the center of the sheet according to beam-theory.

Stresses in the elastic cross-section (calculated)

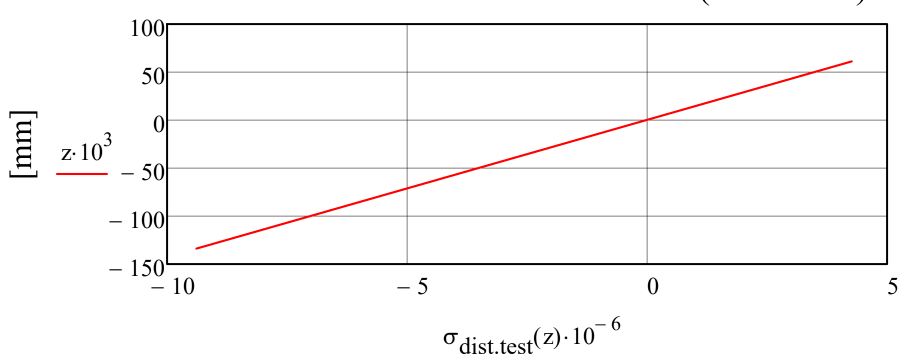

Compression at the top of the cross-section:

$$\sigma_{fo.o.test} := \frac{-M_{Ed.test}}{W_{el.dist}\left(h_s - z_{tp}\right)} = -4.266 \cdot MPa$$

Compression at the bottom of the top flange:

$$\sigma_{fo.u.test} := \frac{-M_{Ed.test}}{W_{el.dist}(h_s - z_{tp} - t_s)} = -4.178 \cdot MPa$$

Tension at the top of the bottom flange:

$$\sigma_{fu.o.test} := \frac{-M_{Ed.test}}{W_{el.dist}(-z_{tp} + t_s)} = 9.299 \cdot MPa$$

Tension at the bottom of the cross-section:

$$\sigma_{fu.u.test} := \frac{-M_{Ed.test}}{W_{el.dist}(-z_{tp})} = 9.386 \cdot MPa$$

B 3.3 Abaqus Results

Sheet with transversal grooves:

Measured moments from Abaqus model inbetween point loads:

$$M_{Ab.tg} := 5.836 \cdot 10^5 N \cdot mm = 0.584 \cdot kN \cdot m$$

$$M_{Ed.test} \cdot 1 = 0.6 \cdot kN \cdot m$$

Ratio of the moment applied and moment measured in Abaqus:

$$\frac{M_{Ed.test}}{M_{Ab.tg}} = 1.028$$

Stress measured at the middle of the top flange, longitudinal direction:

$$\sigma_{Ab.tg} := -4.71426 \cdot MPa$$

Average value from Abaqus

$$M_{Ab.tg.Max} := -\sigma_{Ab.tg} \cdot W_{el} = 0.663 \cdot kN \cdot m$$

$$\sigma_{dist.tg}(z) := \frac{M_{Ab.tg.Max}}{W_{el.dist}(z)}$$

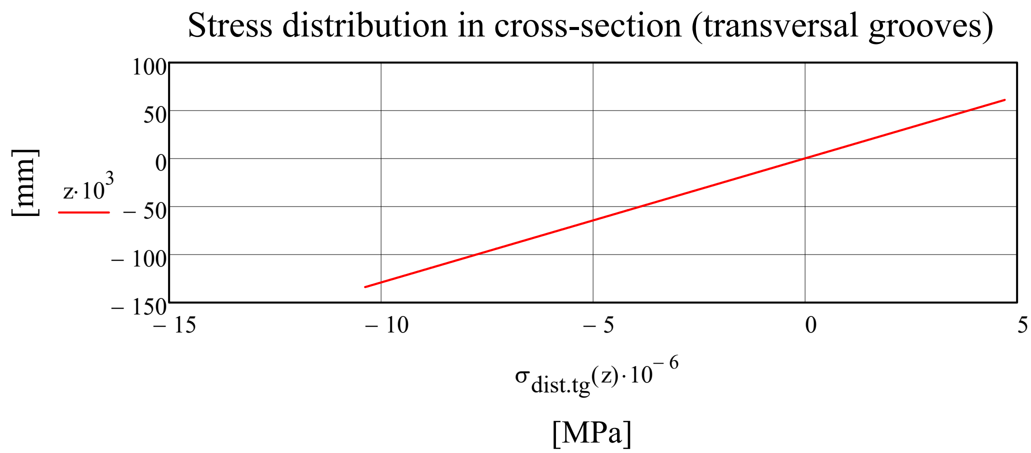

Stresses in the cross-section (node 85079), compared to calculated values

$\sigma_{Ab.fo.o.tg} := 2.85638 MPa$ $\quad -\sigma_{dist.tg}(h_s - z_{tp}) = -4.714 \cdot MPa$ $\quad \sigma_{fo.o.test} = -4.266 \cdot MPa$

$\sigma_{Ab.fo.u.tg} := -3.92799 MPa$ $\quad -\sigma_{dist.tg}(h_s - z_{tp} - t_s) = -4.618 \cdot MPa$ $\quad \sigma_{fo.u.test} = -4.178 \cdot MPa$

$\sigma_{Ab.fu.o.tg} := 10.375 MPa$ $\quad -\sigma_{dist.tg}(-z_{tp} + t_s) = 10.276 \cdot MPa$ $\quad \sigma_{fu.o.test} = 9.299 \cdot MPa$

$\sigma_{Ab.fu.u.tg} := 10.6098 MPa$ $\quad -\sigma_{dist.tg}(-z_{tp}) = 10.372 \cdot MPa$ $\quad \sigma_{fu.u.test} = 9.386 \cdot MPa$

Calculated sectional modulus that Abaqus uses:

$$W_{Ab.tg} := \frac{M_{Ab.tg}}{\sigma_{Ab.fo.o.tg}} = 2.043 \times 10^5 \cdot mm^3$$

$$W_{el.tg} := W_{el} = 1.406 \times 10^5 \cdot mm^3$$

Sheet with flat flange, without transversal grooves:

Measured moment inbetween the point loads:

$M_{Ab.flat} := -5.970 \cdot 10^5 N \cdot mm = -0.597 \cdot kN \cdot m$ $\qquad M_{Ed.test} \cdot 1 = 0.6 \cdot kN \cdot m$

Ratio of the moment applied and moment measured in Abaqus:

$$\frac{-M_{Ed.test}}{M_{Ab.flat}} = 1.005$$

Stress measured at the middle of the top flange, longitudinal direction:

$\sigma_{Ab.flat} := -5.01766 \cdot MPa$

Average value from Abaqus

$M_{Ab.flat.Max} := \sigma_{Ab.flat} \cdot W_{el} = -0.706 \cdot kN \cdot m$

$$\sigma_{dist.flat}(z) := \frac{-M_{Ab.flat.Max}}{W_{el.dist}(z)}$$

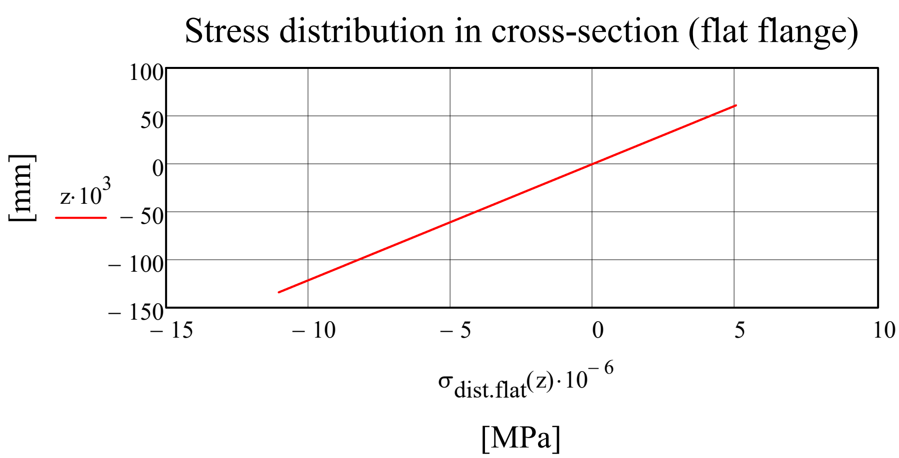

Stresses in the cross-section (node 19775), compared to calculated values

$\sigma_{Ab.fo.o.flat} := -3.75968 MPa$ $\quad -\sigma_{dist.flat}(h_s - z_{tp}) = -5.018 \cdot MPa$ $\quad \sigma_{fo.o.test} = -4.266 \cdot MPa$

$\sigma_{Ab.fo.u.flat} := -4.99458 MPa$ $\quad -\sigma_{dist.flat}(h_s - z_{tp} - t_s) = -4.915 \cdot MPa$ $\quad \sigma_{fo.u.test} = -4.178 \cdot MPa$

$\sigma_{Ab.fu.o.flat} := 9.54267 MPa$ $\quad -\sigma_{dist.flat}(-z_{tp} + t_s) = 10.937 \cdot MPa$ $\quad \sigma_{fu.o.test} = 9.299 \cdot MPa$

$\sigma_{Ab.fu.u.flat} := 9.73692 MPa$ $\quad -\sigma_{dist.flat}(-z_{tp}) = 11.04 \cdot MPa$ $\quad \sigma_{fu.u.test} = 9.386 \cdot MPa$

Calculated sectional modulus that Abaqus uses:

$$W_{Ab.flat} := \frac{M_{Ab.flat}}{\sigma_{Ab.fo.o.flat}} = 1.588 \times 10^5 \cdot mm^3$$

$$W_{el.flat} := W_{el} = 1.406 \times 10^5 \cdot mm^3$$

B 4 Validating the Solid Element Model without Hinges

A short span solid element model is constructed in Abaqus in order to analyse the method of computing the model. The calculated values bellow are used as a comparison.

B 4.1 Cross-sectional Data for one Section

Area of the gross cross-section with sharp corners:

$$A_{g.sc.1} := 2A_{fu} + 1A_{gu} + 2A_{wu} + 2\cdot A_{w.fu} + 2\cdot A_{wm} \dots + 2\cdot A_{w.fo} + 2\cdot A_{wo} + 1\cdot A_{fo} + 2\cdot A_{go} = 1.4\times 10^{3}\cdot mm^{2}$$

Area of the gross cross-section considering the rounded corners:

$$A_{g.1} := A_{g.sc.1}\cdot\left(1-\delta_{sc}\right) = 1.37\times 10^{3}\cdot mm^{2}$$

$$z_{tp.1} := \frac{2A_{fu}\cdot\left(z_{fu}\right) + 1A_{gu}\cdot\left(z_{gu}\right) + 1\cdot A_{fo}\cdot\left(z_{fo}\right) + 2\cdot A_{go}\cdot\left(z_{go}\right) + 2A_{wu}\cdot\left(z_{wu}\right) \dots + 2A_{wm}\cdot\left(z_{wm}\right) + 2\cdot A_{wo}\cdot\left(z_{wo}\right) + 2A_{w.fu}\cdot\left(z_{w.fu}\right) + 2\cdot A_{w.fo}\cdot\left(z_{w.fo}\right)}{A_{g.1}} = 144.781\cdot mm$$

$$\begin{aligned}I_{y.sc.1} := {} & 2A_{fu}\cdot\left(z_{tp.1}-z_{fu}\right)^{2} + 1A_{gu}\cdot\left(z_{tp.1}-z_{gu}\right)^{2} + 1\cdot A_{fo}\cdot\left(z_{fo}-z_{tp.1}\right)^{2} + 2\cdot A_{go}\cdot\left(z_{go}-z_{tp.1}\right)^{2} \dots \\ & + 2A_{wu}\cdot\left(z_{tp.1}-z_{wu}\right)^{2} + 2A_{wm}\cdot\left(z_{tp.1}-z_{wm}\right)^{2} + 2\cdot A_{wo}\cdot\left(z_{wo}-z_{tp.1}\right)^{2} \dots \\ & + 2A_{w.fu}\cdot\left(z_{tp.1}-z_{w.fu}\right)^{2} + 2\cdot A_{w.fo}\cdot\left(z_{w.fo}-z_{tp.1}\right)^{2}\end{aligned}$$

$$I_{y.1} := I_{y.sc.1}\cdot\left(1-2\delta_{sc}\right) = 6.364\times 10^{6}\cdot mm^{4}$$

$$W_{el.1} := \frac{I_{y.1}}{\left(h_{s}-z_{tp.1}\right)} = 1.267\times 10^{5}\cdot mm^{3}$$ Sectional modulus at the top of the sheet

$$W_{el.s.sc} := \frac{I_{y.sc.1}}{\left(h_{s}-z_{tp.1}\right)} = 1.324\times 10^{5}\cdot mm^{3}$$ Sectional modulus with regard to sharp corners

$$z_{1} := -z_{tp.1}, \left(-z_{tp.1}+0.1\cdot mm\right) .. \left(h_{s}-z_{tp.1}\right)$$

$$W_{el.dist.1}\left(z_{1}\right) := \frac{I_{y.1}}{z_{1}}$$ Sectional modulus along the height

B 4.2 Calculated Moments Compared to Abaqus

The stresses in the sheet based on a chosen applied load, smaller than the critical one.

$P := 720N$ Chosen point load to act on the sheet for an elastic analysis

$L_{2.solid} := 2.1m$ Total length of the model, including overlap

$l_s := 2.1m$ Length of one sheet

$a_{2.solid} := 1m$ Distance between edge and applied point load

$R_{A.s.s} := P \cdot \frac{(L_{2.solid} - a_{2.solid})}{L_{2.solid}} = 0.377 \cdot kN$ Reaction force at the left support

$R_{B.s.s} := P - R_{A.s.s} = 0.343 \cdot kN$ Reaction force at the right support

$x_{s.2} := 0m, 0.1m .. L_{2.solid}$

Moment acting on the short symmetrical sheet inbetween the applied point loads

$$M_{Ed.s.s}(x_{s.2}) := \begin{cases} -R_{A.s.s} \cdot x_{s.2} & \text{if } 0 \le x_{s.2} \le a_{2.solid} \\ -R_{A.s.s} \cdot x_{s.2} + P \cdot (x_{s.2} - a_{2.solid}) & \text{if } a_{2.solid} \le x_{s.2} \le L_{2.solid} \end{cases}$$

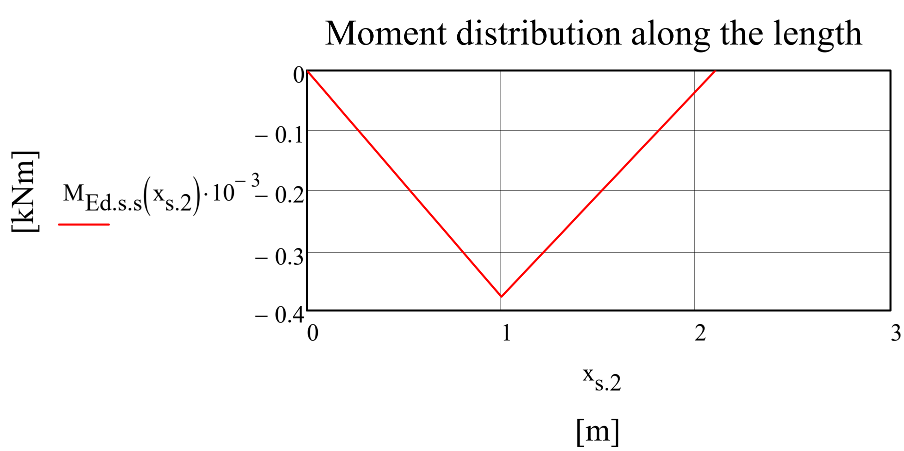

$dM_{Ed.s.s}(x_{s.2}) := \frac{d}{dx_{s.2}} M_{Ed.s.s}(x_{s.2})$ The derivates of the moment is the shear

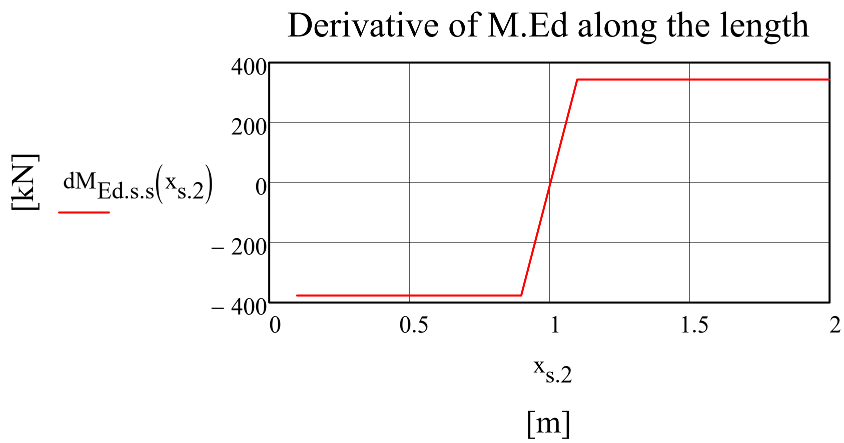

Comparing calculated moments and moments in Abaqus:

$x_1 := 1584.91\,mm \quad M_{1.Ab.s} := -1.667 \cdot 10^5 N \cdot mm \quad M_{Ed.s.s}(x_1) = -0.177 \cdot kN \cdot m \quad \dfrac{M_{Ed.s.s}(x_1)}{M_{1.Ab.s}} = 1.059$

$x_2 := 1624.53\,mm \quad M_{2.Ab.s} := -1.538 \cdot 10^5 N \cdot mm \quad M_{Ed.s.s}(x_2) = -0.163 \cdot kN \cdot m \quad \dfrac{M_{Ed.s.s}(x_2)}{M_{2.Ab.s}} = 1.06$

The moments correlate nicely, as do the reaction forces.

B 4.3 Calculated Stresses in the Sheet

Determining the location of the maximum moment:

$a_{2.solid} = 1\,m$

$M_{Ed.s.s}(x_2) = -0.163 \cdot kN \cdot m$

Critical moment according to LIndab, in the field and over support respectively:

$M_{k.f} = 18.95 \cdot kN \qquad M_{k.s} = 25.96 \cdot kN$ — Maximum values according to Lindab, per meter width

$P_{cr.solid.2} := \dfrac{M_{k.f} \cdot b_s}{x_2} = 9.332 \cdot kN$ — Maximum point load, with regard to the sheet's capacity

Stress distribution in the cross-section at maximum moment:

$\sigma_{dist.s.s}(z_1) := \dfrac{-M_{Ed.s.s}(a_{2.solid})}{W_{el.dist.1}(z_1)}$ — Cross-sectional stresses in the short symmetrical sheet at x=2m, according to beam-theory.

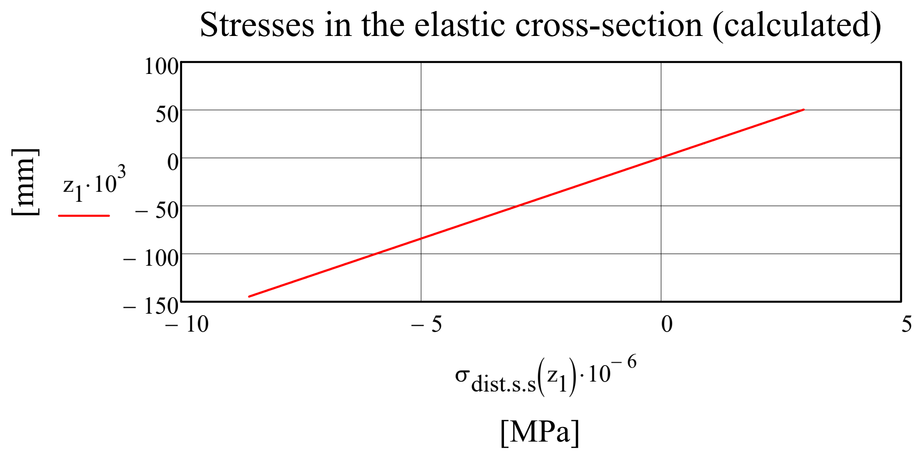

Stresses distribution in the cross-section at x=1584.91mm:

Compression at the top of the cross-section:

$$\sigma_{fo.o.s.s1} := \frac{M_{Ed.s.s}(x_1)}{W_{el.dist.1}(h_s - z_{tp.1})} = -1.394 \cdot MPa$$

Compression at the bottom of the top flange:

$$\sigma_{fo.u.s.s1} := \frac{M_{Ed.s.s}(x_1)}{W_{el.dist.1}(h_s - z_{tp.1} - t_s)} = -1.359 \cdot MPa$$

Tension at the top of the bottom flange:

$$\sigma_{fu.o.s.s1} := \frac{M_{Ed.s.s}(x_1)}{W_{el.dist.1}(-z_{tp.1} + t_s)} = 3.983 \cdot MPa$$

Tension at the bottom of the cross-section:

$$\sigma_{fu.u.s.s1} := \frac{M_{Ed.s.s}(x_1)}{W_{el.dist.1}(-z_{tp.1})} = 4.018 \cdot MPa$$

Stress distribution along the longitudinal x-direction (top):

$$I_{Lindab} := 6760 \frac{mm^4}{mm} \cdot b_s = 5.408 \times 10^6 \cdot mm^4$$

Second order of moment according to Lindab

$I_{11} := I_{y.1} = 6.364 \times 10^{6} \cdot mm^{4}$ Second order of moment according to calc.

$$\sigma_{11.Lindab.s}(x_s) := \frac{M_{Ed.s.s}(x_s)}{I_{Lindab}} \cdot (h_s - z_{tp.1})$$

$$\sigma_{11.calc.c.s}(x_s) := \frac{M_{Ed.s.s}(x_s)}{W_{el.1}}$$

Stress distribution at the top flange, S11

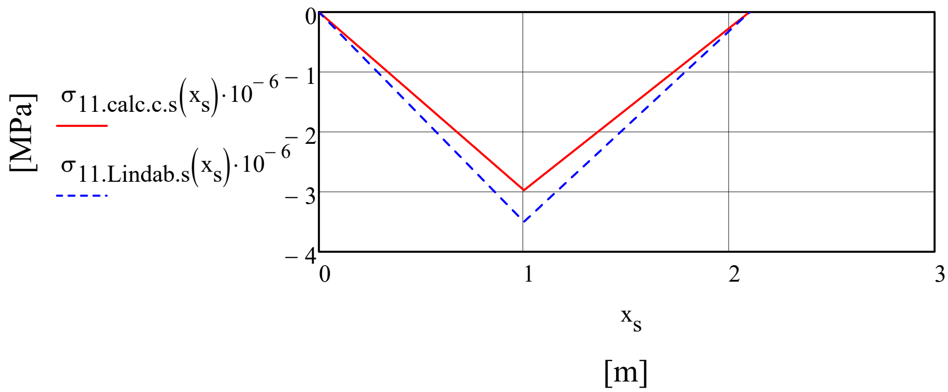

Stress distribution along the longitudinal x-direction (bottom):

$$\sigma_{11.calc.t.s}(x_s) := \frac{M_{Ed.s.s}(x_s)}{I_{11}} \cdot (-z_{tp.1})$$ Tension in the bottom flange

$$\sigma_{11.Lindab.t.s}(x_s) := \frac{M_{Ed.s.s}(x_s)}{I_{Lindab}} \cdot (-z_{tp.1})$$ Stress according to Lindab

Stress distribution at the bottom flange, S11

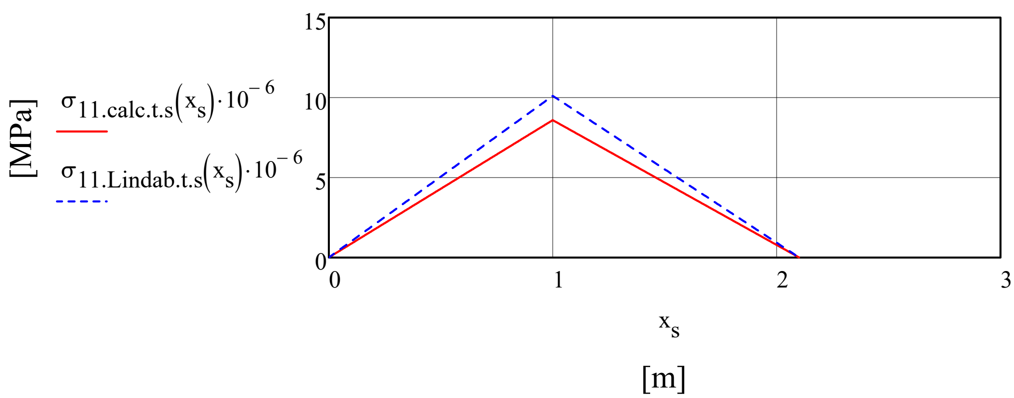

Determining the location of the maximum stresses:

$\sigma_{max.11.calc.c.s} := \sigma_{11.calc.c.s}\left(a_{2.solid}\right) = -2.976 \cdot MPa$ The maximum compression

$\sigma_{max.11.calc.t.s} := \sigma_{11.calc.t.s}\left(a_{2.solid}\right) = 8.58 \cdot MPa$ The maximum tension

B 4.4 Comparison with Results from Abaqus

Stresses in Abaqus compared to calculated values:

The stresses from Abaqus can be compared with the calculated ones in order to validate the results.

$R_{A.Ab.s.s} := 0.3771kN$ $R_{A.s.s} = 0.377 \cdot kN$

$R_{B.Ab.s.s} := 0.3429kN$ $R_{B.s.s} = 0.343 \cdot kN$

$M_{1.Ab.s} = -0.167 \cdot kN \cdot m$ $M_{Ed.s.s}\left(x_1\right) = -0.177 \cdot kN \cdot m$

$$\sigma_{dist.s.s}\left(z_1\right) := \frac{-M_{1.Ab.s}}{W_{el.dist.1}\left(z_1\right)}$$

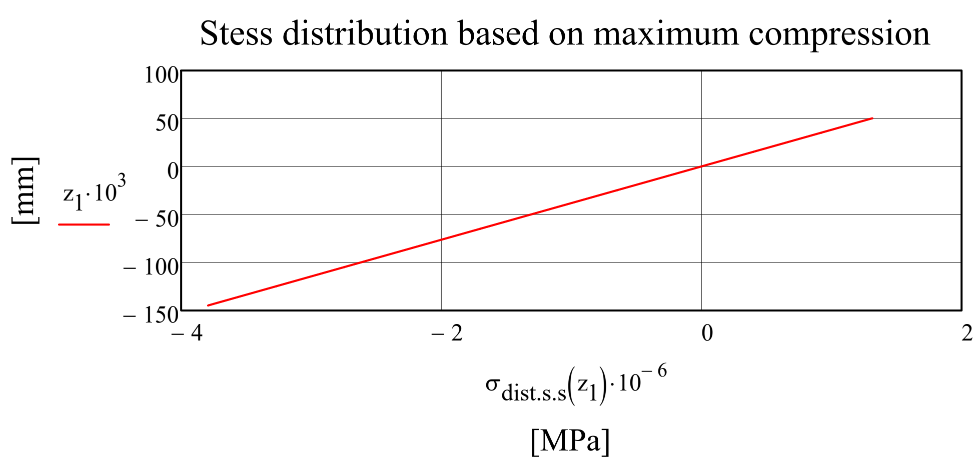

Stresses in the cross-section at x_1 compared to calculated values:

$\sigma_{Ab.fo.o.s} := -1.23594MPa$ $-\sigma_{dist.s.s}\left(h_s - z_{tp.1}\right) = -1.315 \cdot MPa$ $\sigma_{fo.o.s.s1} = -1.394 \cdot MPa$

$\sigma_{Ab.fo.u.s} := -1.23594MPa$ $-\sigma_{dist.s.s}\left(h_s - z_{tp.1} - t_s\right) = -1.283 \cdot MPa$ $\sigma_{fo.u.s.s1} = -1.359 \cdot MPa$

$\sigma_{Ab.fu.o.s} := 3.5709MPa$ $-\sigma_{dist.s.s}\left(-z_{tp.1} + t_s\right) = 3.76 \cdot MPa$ $\sigma_{fu.o.s.s1} = 3.983 \cdot MPa$

$\sigma_{Ab.fu.u.s} := 3.5709MPa$ $-\sigma_{dist.s.s}\left(-z_{tp.1}\right) = 3.792 \cdot MPa$ $\sigma_{fu.u.s.s1} = 4.018 \cdot MPa$

The reason for them not correlating as well might be that we calculate Ag, Ig and Wel with regard to rounded corners.

Calculated sectional modulus that Abaqus uses:

$$W_{Ab.s} := \frac{M_{1.Ab.s}}{\sigma_{Ab.fo.o.s}} = 1.349 \times 10^{5} \cdot mm^{3}$$

$$W_{el.s} := W_{el.1} = 1.267 \times 10^{5} \cdot mm^{3}$$

B 5 Calculations for the Shell Element Model

A shell element model was constructed in Abaqus in order to analyse the behaviour of a loaded LHP 200 sheet. The joint was placed in the middle of the span, in-between two point loads. This gave made the joint experience a moment but no shear. The analytical results are presented below as well as a comparison of the analytical and numerical values.

B 5.1 Elastic Cross-sectional Properties

An elastic analysis of the capacity of the sheet is made in order to define the maximum moment for cross-section. This value can then be compared with the model made in the FEM-program Abaqus.

Rounded corners will be considered by a simplification the area with sharp corners, according to SS-EN 1993-1-3 5.1(4)

Area of the gross cross-section with sharp corners:

$$A_{g.sc} := 8A_{fu} + 4A_{gu} + 6A_{wu} + 6\cdot A_{w.fu} + 6\cdot A_{wm} + 6\cdot A_{w.fo} \ldots + 6\cdot A_{wo} + 3\cdot A_{fo} + 6\cdot A_{go} = 4.314 \times 10^3\cdot mm^2$$

Area of the gross cross-section considering the rounded corners:

$$A_g := A_{g.sc}\cdot(1 - \delta_{sc}) = 4.222 \times 10^3\cdot mm^2$$

$$z_{tp} := \frac{8A_{fu}\cdot(z_{fu}) + 4A_{gu}\cdot(z_{gu}) + 3\cdot A_{fo}\cdot(z_{fo}) + 6\cdot A_{go}\cdot(z_{go}) + 6A_{wu}\cdot(z_{wu}) \ldots + 6A_{wm}\cdot(z_{wm}) + 6\cdot A_{wo}\cdot(z_{wo}) + 6A_{w.fu}\cdot(z_{w.fu}) + 6\cdot A_{w.fo}\cdot(z_{w.fo})}{A_g} = 141.021\cdot mm$$

$$I_{g.sc} := 8A_{fu}\cdot(z_{tp} - z_{fu})^2 + 4A_{gu}\cdot(z_{tp} - z_{gu})^2 + 3\cdot A_{fo}\cdot(z_{fo} - z_{tp})^2 + 6\cdot A_{go}\cdot(z_{go} - z_{tp})^2 \ldots + 6A_{wu}\cdot(z_{tp} - z_{wu})^2 + 6A_{wm}\cdot(z_{tp} - z_{wm})^2 + 6\cdot A_{wo}\cdot(z_{wo} - z_{tp})^2 \ldots + 6A_{w.fu}\cdot(z_{tp} - z_{w.fu})^2 + 6\cdot A_{w.fo}\cdot(z_{w.fo} - z_{tp})^2$$

$$I_g := I_{g.sc}\cdot(1 - 2\delta_{sc}) = 2.115 \times 10^7\cdot mm^4$$

$$W_{el} := \frac{I_g}{(h_s - z_{tp})} = 3.918 \times 10^5\cdot mm^3$$

Sectional modulus at the top of the sheet

$$W_{el.1.sc} := \frac{I_{g.sc}}{(h_s - z_{tp})} = 4.093 \times 10^5\cdot mm^3$$

Sectional modulus with regard to sharp corners

$$z := -z_{tp}, (-z_{tp} + 0.1\cdot mm) .. (h_s - z_{tp})$$

$W_{el.dist}(z) := \frac{I_g}{z}$ Sectional modulus along the height

B 5.2 Calculated Stresses in the Sheet

The stresses in the sheet based on a chosen applied load, smaller than the critical one.

$P := 0.6kN$ Chosen point load to act on the sheet for an elastic analysis

$P := P \cdot 1$ Time step in Abaqus

$a = 2.9\,m$ Distance between support and applied point load

$M_{Ed.1} := P \cdot a = 1.74 \cdot kN \cdot m$ Moment acting on the long sheet inbetween the applied point loads

$\sigma_{dist.1}(z) := \frac{M_{Ed.1}}{W_{el.dist}(z)}$ Cross-sectional stresses in the center of the sheet according to beam-theory.

$R_{A.1} := P$ Reaction force at left support, A

$R_{B.1} := P$ Reaction force at right support, B

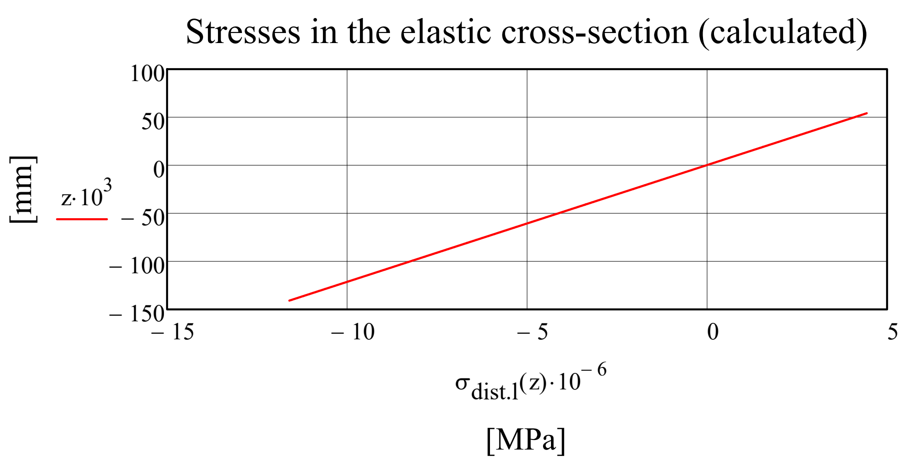

Stress distribution in the cross-section inbetween the point loads:

Compression at the top of the cross-section:

$$\sigma_{fo.o.1} := \frac{-M_{Ed.1}}{W_{el.dist}(h_s - z_{tp})} = -4.441 \cdot MPa$$

Compression at the bottom of the top flange:

$$\sigma_{fo.u.1} := \frac{-M_{Ed.1}}{W_{el.dist}(h_s - z_{tp} - t_s)} = -4.338 \cdot MPa$$

Tension at the top of the bottom flange:

$$\sigma_{fu.o.l} := \frac{-M_{Ed.l}}{W_{el.dist}(-z_{tp} + t_s)} = 11.499 \cdot MPa$$

Tension at the bottom of the cross-section:

$$\sigma_{fu.u.l} := \frac{-M_{Ed.l}}{W_{el.dist}(-z_{tp})} = 11.602 \cdot MPa$$

B 5.3 Comparison with Results from Abaqus

Stresses in Abaqus compared to calculated values:

The stresses from Abaqus can be compared with the calculated ones in order to validate the results.

$R_{A.Ab.l} := 0.6kN$ $\qquad R_{A.l} = 0.6 \cdot kN$

$R_{B.Ab.l} := 0.6kN$ $\qquad R_{B.l} = 0.6 \cdot kN$

$M_{Ab.l} := 1.741 \cdot 10^6 N \cdot mm = 1.741 \cdot kN \cdot m$ $\qquad M_{Ed.l} = 1.74 \cdot kN \cdot m$

$$\frac{M_{Ed.l}}{M_{Ab.l}} = 0.999$$

The stress at the edges of the overlap are zero and close to the overlap the stress is effected by the joint theoretically not carrying moment.

$x_1 := 4.99536m$ $\qquad x_2 := 6.957818m$ $\qquad l_{ol} := x_2 - x_1 = 1.962\ m$

Stresses inbetween the point loads. This does however not correlate with the stress within the l.ol distance of the hinge where the stresses decrease due to the hinge itself.

$\sigma_{Ab.max.l} := -4.46269MPa$

$M_{Ab.max.l} := \sigma_{Ab.max.l} \cdot W_{el} = -1.749 \cdot kN \cdot m$ $\qquad \sigma_{dist.l}(z) := \dfrac{-M_{Ab.max.l}}{W_{el.dist}(z)}$

Stess distribution in the cross-section (long sheet)

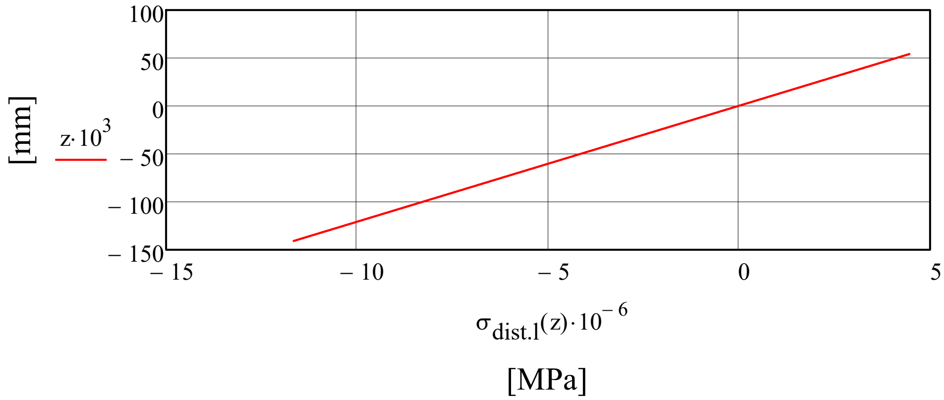

Stresses in the cross-section at x=3550mm compared to calculated values:

$\sigma_{Ab.fo.o.l} := -4.76663\,MPa$ $\quad -\sigma_{dist.l}\left(h_s - z_{tp}\right) = -4.463 \cdot MPa$ $\quad \sigma_{fo.o.l} = -4.441 \cdot MPa$

$\sigma_{Ab.fo.u.l} := -4.43723\,MPa$ $\quad -\sigma_{dist.l}\left(h_s - z_{tp} - t_s\right) = -4.359 \cdot MPa$ $\quad \sigma_{fo.u.l} = -4.338 \cdot MPa$

$\sigma_{Ab.fu.o.l} := 12.7161\,MPa$ $\quad -\sigma_{dist.l}\left(-z_{tp} + t_s\right) = 11.555 \cdot MPa$ $\quad \sigma_{fu.o.l} = 11.499 \cdot MPa$

$\sigma_{Ab.fu.u.l} := 12.3083\,MPa$ $\quad -\sigma_{dist.l}\left(-z_{tp}\right) = 11.659 \cdot MPa$ $\quad \sigma_{fu.u.l} = 11.602 \cdot MPa$

A local bending of the top flange is noticed due to the applied load. This does however not effect the bottom part of the cross section.

Calculated sectional modulus that Abaqus uses:

$$W_{Ab.l} := \frac{-M_{Ab.l}}{\sigma_{Ab.fo.o.l}} = 3.652 \times 10^5 \cdot mm^3$$

$$W_{el.l} := W_{el} = 3.918 \times 10^5 \cdot mm^3$$

B 6 Calculations for the Solid Model - Elastic

In order to capture the behaviour of the sheet when loaded and the more specific behaviour of the joint; a solid element model was constructed in Abaqus. This model was made similar to the shell element model with regard to loads and boundary conditions. However, it includes more details. The calculations were made with regard to the model being elastic.

B 6.1 Cross-sectional Data for one Section

Area of the gross cross-section with sharp corners:

$$A_{g.sc.1} := 2A_{fu} + 1A_{gu} + 2A_{wu} + 2\cdot A_{w.fu} + 2\cdot A_{wm} + 2\cdot A_{w.fo} \ldots + 2\cdot A_{wo} + 1\cdot A_{fo} + 2\cdot A_{go} = 1.4\times 10^{3}\cdot mm^{2}$$

Area of the gross cross-section considering the rounded corners:

$$A_{g.1} := A_{g.sc.1}\cdot\left(1-\delta_{sc}\right) = 1.37\times 10^{3}\cdot mm^{2}$$

$$z_{tp.1} := \frac{2A_{fu}\cdot\left(z_{fu}\right) + 1A_{gu}\cdot\left(z_{gu}\right) + 1\cdot A_{fo}\cdot\left(z_{fo}\right) + 2\cdot A_{go}\cdot\left(z_{go}\right) + 2A_{wu}\cdot\left(z_{wu}\right) \ldots + 2A_{wm}\cdot\left(z_{wm}\right) + 2\cdot A_{wo}\cdot\left(z_{wo}\right) + 2A_{w.fu}\cdot\left(z_{w.fu}\right) + 2\cdot A_{w.fo}\cdot\left(z_{w.fo}\right)}{A_{g.1}} = 144.781\cdot mm$$

$$z_{tp.sc.1} := \frac{2A_{fu}\cdot\left(z_{fu}\right) + 1A_{gu}\cdot\left(z_{gu}\right) + 1\cdot A_{fo}\cdot\left(z_{fo}\right) + 2\cdot A_{go}\cdot\left(z_{go}\right) + 2A_{wu}\cdot\left(z_{wu}\right) \ldots + 2A_{wm}\cdot\left(z_{wm}\right) + 2\cdot A_{wo}\cdot\left(z_{wo}\right) + 2A_{w.fu}\cdot\left(z_{w.fu}\right) + 2\cdot A_{w.fo}\cdot\left(z_{w.fo}\right)}{A_{g.sc.1}} = 141.689\cdot mm$$

$$I_{y.sc.1} := 2A_{fu}\cdot\left(z_{tp.1}-z_{fu}\right)^{2} + 1A_{gu}\cdot\left(z_{tp.1}-z_{gu}\right)^{2} + 1\cdot A_{fo}\cdot\left(z_{fo}-z_{tp.1}\right)^{2} + 2\cdot A_{go}\cdot\left(z_{go}-z_{tp.1}\right)^{2} \ldots + 2A_{wu}\cdot\left(z_{tp.1}-z_{wu}\right)^{2} + 2A_{wm}\cdot\left(z_{tp.1}-z_{wm}\right)^{2} + 2\cdot A_{wo}\cdot\left(z_{wo}-z_{tp.1}\right)^{2} \ldots + 2A_{w.fu}\cdot\left(z_{tp.1}-z_{w.fu}\right)^{2} + 2\cdot A_{w.fo}\cdot\left(z_{w.fo}-z_{tp.1}\right)^{2}$$

$$I_{y.1} := I_{y.sc.1}\cdot\left(1-2\delta_{sc}\right) = 6.364\times 10^{6}\cdot mm^{4}$$

$$I_{solid} := I_{y.1}$$

$$W_{el.1} := \frac{I_{y.1}}{\left(h_{s}-z_{tp.1}\right)} = 1.267\times 10^{5}\cdot mm^{3}$$

Sectional modulus at the top of the sheet

$$W_{el.s.l.sc} := \frac{I_{y.sc.1}}{\left(h_s - z_{tp.1}\right)} = 1.324 \times 10^5 \cdot mm^3$$ Sectional modulus with regard to sharp corners

$$z_1 := -z_{tp.1}, \left(-z_{tp.1} + 0.1 \cdot mm\right) .. \left(h_s - z_{tp.1}\right)$$

$$W_{el.dist.1}(z_1) := \frac{I_{y.1}}{z_1}$$ Sectional modulus along the height

$$y_{tp.1} := \frac{b_s}{2} = 0.4\,m$$

$$y_{gu} := b_s - \frac{b_{go}}{2}$$

$$y_{fu} := b_s - b_{go} - \frac{b_{fu}}{2}$$

$$y_{wu} := b_s - b_{go} - b_{fu} - \cos(\phi_w) \cdot \frac{l_{wu}}{2}$$

$$y_{w.fu} := b_s - b_{go} - b_{fu} - \cos(\phi_w) \cdot l_{wu} - \cos(\phi_{wf.u}) \cdot \frac{l_{w.fu}}{2}$$

$$y_{wm} := b_s - b_{go} - b_{fu} - \cos(\phi_w) \cdot l_{wu} - \cos(\phi_{wf.u}) \cdot l_{w.fu} - \cos(\phi_w) \cdot \frac{l_{wm}}{2}$$

$$y_{w.fo} := b_s - b_{go} - b_{fu} - \cos(\phi_w) \cdot l_{wu} - \cos(\phi_{wf.u}) \cdot l_{w.fu} - \cos(\phi_w) \cdot l_{wm} - \cos(\phi_{wf.o}) \cdot l_{w.fo}$$

$$y_{wo} := b_s - b_{go} - b_{fu} - \cos(\phi_w) \cdot l_{wu} - \cos(\phi_{wf.u}) \cdot l_{w.fu} - \cos(\phi_w) \cdot l_{wm} \cdots$$
$$+ \cos(\phi_{wf.o}) \cdot l_{w.fo} - \cos(\phi_w) \cdot \frac{l_{wo}}{2}$$

$$y_{bp1} := b_s - b_{go} - b_{fu} - \cos(\phi_w) \cdot l_{wu} - \cos(\phi_{wf.u}) \cdot l_{w.fu} - \cos(\phi_w) \cdot l_{wm} \cdots$$
$$+ \cos(\phi_{wf.o}) \cdot l_{w.fo} - \cos(\phi_w) \cdot l_{wo} - \frac{b_{p1}}{2}$$

$$y_{go} := b_s - b_{go} - b_{fu} - \cos(\phi_w) \cdot l_{wu} - \cos(\phi_{wf.u}) \cdot l_{w.fu} - \cos(\phi_w) \cdot l_{wm} \cdots$$
$$+ \cos(\phi_{wf.o}) \cdot l_{w.fo} - \cos(\phi_w) \cdot l_{wo} - b_{p1} - \frac{b_{go}}{2}$$

$$I_{z.sc.1} := 2A_{fu}\cdot(y_{tp.1} - y_{fu})^2 + 2\frac{A_{gu}}{2}\cdot(y_{tp.1} - y_{gu})^2 + 2\cdot t_s\cdot b_{p1}\cdot(y_{bp1} - y_{tp.1})^2 \ldots$$
$$+ 2\cdot A_{go}\cdot(y_{go} - y_{tp.1})^2 \ldots$$
$$+ 2A_{wu}\cdot(y_{tp.1} - y_{wu})^2 + 2A_{wm}\cdot(y_{tp.1} - y_{wm})^2 + 2\cdot A_{wo}\cdot(y_{wo} - y_{tp.1})^2 \ldots$$
$$+ 2A_{w.fu}\cdot(y_{tp.1} - y_{w.fu})^2 + 2\cdot A_{w.fo}\cdot(y_{w.fo} - y_{tp.1})^2 + \frac{t_s\cdot b_{p2}^{\,3}}{12}$$

$$I_{z.1} := I_{z.sc.1}\cdot(1 - 2\delta_{sc}) = 9.043 \times 10^7\cdot mm^4$$

Indata for the global model in Abaqus:

$I_{11} := I_{y.1} = 6.364 \times 10^6\cdot mm^4$ Second area of moment around y-axis

$I_{22} := I_{z.1} = 9.043 \times 10^7\cdot mm^4$ Second area of moment around z-axis

$I_{12} := \frac{I_{11} + I_{22}}{2} = 4.84 \times 10^7\cdot mm^4$ Cross bending

$J := 1$ Torsional constant

$\Gamma_O := 1$ Sectional moment

$\Gamma_W := 1$ Warping constant

B 6.2 Calculated Moments Compared to Abaqus

The stresses in the sheet based on a chosen applied load, smaller than the critical one.

$P := 720N$ Chosen point load to act on the sheet for an elastic analysis

$L_{solid} := 4m$ Total length of the model, including overlap

$l_s := 2.1m$ Length of one sheet

$a_{l.solid} := 1m$ Distance between edge and applied point load

$R_{A.s} := P = 0.72\cdot kN$ Reaction force at the left support

$R_{B.s} := R_{A.s} = 0.72\cdot kN$ Reaction force at the right support

$x_s := 0m, 0.1m .. L_{solid}$

Moment acting on the short symmetrical sheet inbetween the applied point loads

$$M_{Ed.s}(x_s) := \begin{cases} -R_{A.s} \cdot x_s & \text{if } 0 \le x_s \le a_{l.solid} \\ -R_{A.s} \cdot x_s + P \cdot (x_s - a_{l.solid}) & \text{if } a_{l.solid} \le x_s \le L_{solid} - a_{l.solid} \\ -R_{A.s} \cdot x_s + P \cdot (x_s - a_{l.solid}) \ldots & \text{if } L_{solid} - a_{l.solid} \le x_s \le L_{solid} \\ + P \cdot [x_s - (L_{solid} - a_{l.solid})] & \end{cases}$$

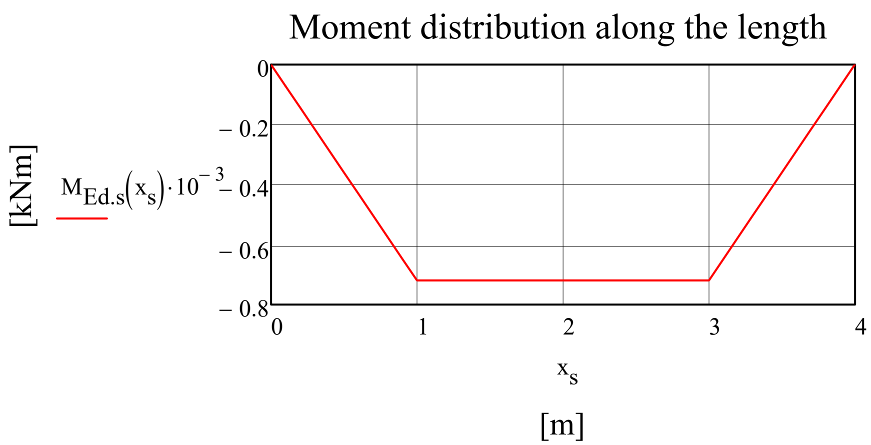

$dM_{Ed.s}(x_s) := \frac{d}{dx_s} M_{Ed.s}(x_s)$

The derivates of the moment is the shear

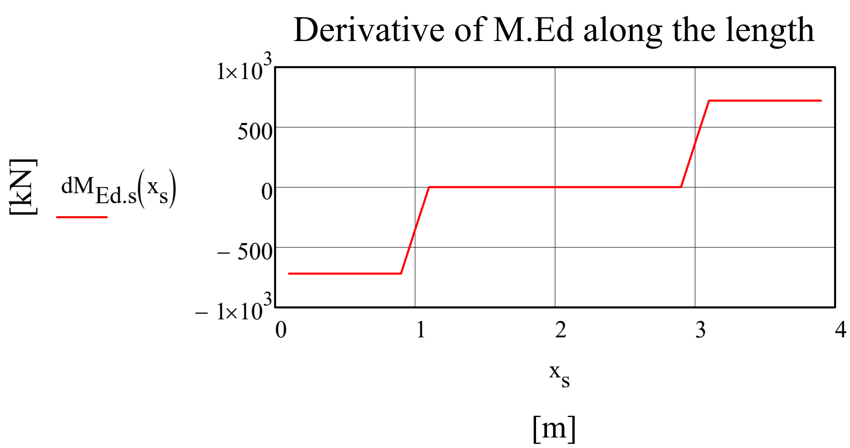

Comparing calculated moments and moments in Abaqus:

$x_1 := 1130mm \qquad M_{1.Ab} := -7.278 \cdot 10^5 N \cdot mm \qquad M_{Ed.s}(x_1) = -0.72 \cdot kN \cdot m \qquad \frac{M_{Ed.s}(x_1)}{M_{1.Ab}} = 0.989$

$x_2 := 2700mm \qquad M_{2.Ab} := -7.303 \cdot 10^5 N \cdot mm \qquad M_{Ed.s}(x_2) = -0.72 \cdot kN \cdot m \qquad \frac{M_{Ed.s}(x_2)}{M_{2.Ab}} = 0.986$

B 6.3 Calculated Stresses in the Sheet

Determining the location of the maximum moment:

$x := \frac{l_s}{2}$ — Approximate location of the maximum moment

Given

$(dM_{Ed.s}(x) = 0)$

$x_{root.s} := Find(x)$ — Find the location of zero derivates

$x_{root.s} = 1.05\,m$ — Location of maximum moment

$M_{max.s} := M_{Ed.s}(x_{root.s}) = -0.72 \cdot kN \cdot m$ — The maximum moment at the location

Stress distribution in the cross-section:

$\sigma_{dist.s}(z_1) := \frac{-M_{Ed.s}(2m)}{W_{el.dist.1}(z_1)}$ — Cross-sectional stresses in the short symmetrical sheet at x=2m, according to beam-theory.

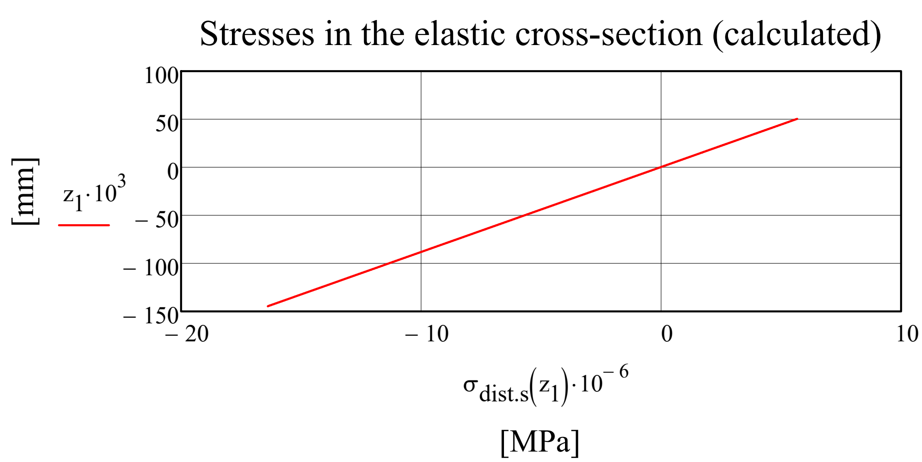

Stresses distribution in the cross-section at x=1130mm:

Compression at the top of the cross-section:

$$\sigma_{fo.o.s} := \frac{M_{Ed.s}(1130mm)}{W_{el.dist.1}(h_s - z_{tp.1})} = -5.681 \cdot MPa$$

Compression at the bottom of the top flange:

$$\sigma_{fo.u.s} := \frac{M_{Ed.s}(1130mm)}{W_{el.dist.1}\left(h_s - z_{tp.1} - t_s\right)} = -5.54 \cdot MPa$$

Tension at the top of the bottom flange:

$$\sigma_{fu.o.s} := \frac{M_{Ed.s}(1130mm)}{W_{el.dist.1}\left(-z_{tp.1} + t_s\right)} = 16.238 \cdot MPa$$

Tension at the bottom of the cross-section:

$$\sigma_{fu.u.s} := \frac{M_{Ed.s}(1130mm)}{W_{el.dist.1}\left(-z_{tp.1}\right)} = 16.379 \cdot MPa$$

Stress distribution along the longitudinal x-direction (top):

$$I_{Lindab} := 6760 \frac{mm^4}{mm} \cdot b_s = 5.408 \times 10^6 \cdot mm^4$$ Second order of moment according to Lindab

$$I_{11} = 6.364 \times 10^6 \cdot mm^4$$ Second order of moment according to calc.

$$\sigma_{11.Lindab}\left(x_s\right) := \frac{M_{Ed.s}\left(x_s\right)}{I_{Lindab}} \cdot \left(h_s - z_{tp.1}\right)$$ Stress distribution according to Lindabs capacity

$$\sigma_{11.calc.c}\left(x_s\right) := \frac{M_{Ed.s}\left(x_s\right)}{W_{el.1}}$$

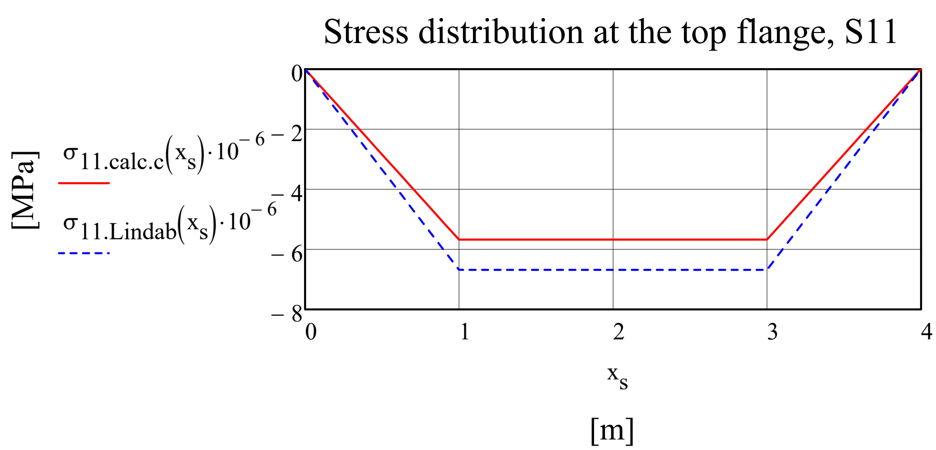

Determining the location of the maximum congressional stress:

$$d\sigma_{11.calc.c}\left(x_s\right) := \frac{d}{dx_s}\sigma_{11.calc.c}\left(x_s\right)$$ The derivates of the moment is the shear

$x := \frac{l_s}{2}$ — Approximate location of the maximum congressional stress

Given

$\left(d\sigma_{11.calc.c}(x) = 0\right)$

$x_{root.s} := \text{Find}(x)$ — Find the location of zero derivates

$x_{root.s} = 1.05\,\text{m}$ — Location of maximum stress

$\sigma_{max.11.calc.c} := \sigma_{11.calc.c}\left(x_{root.s}\right) = -5.681 \cdot \text{MPa}$ — The maximum stress at the location

Stress distribution along the longitudinal x-direction (bottom):

$\sigma_{11.calc.t}\left(x_s\right) := \frac{M_{Ed.s}\left(x_s\right)}{I_{11}} \cdot \left(-z_{tp.1}\right)$ — Tension in the bottom flange

$\sigma_{11.Lindab.t}\left(x_s\right) := \frac{M_{Ed.s}\left(x_s\right)}{I_{Lindab}} \cdot \left(-z_{tp.1}\right)$ — Stress according to Lindab

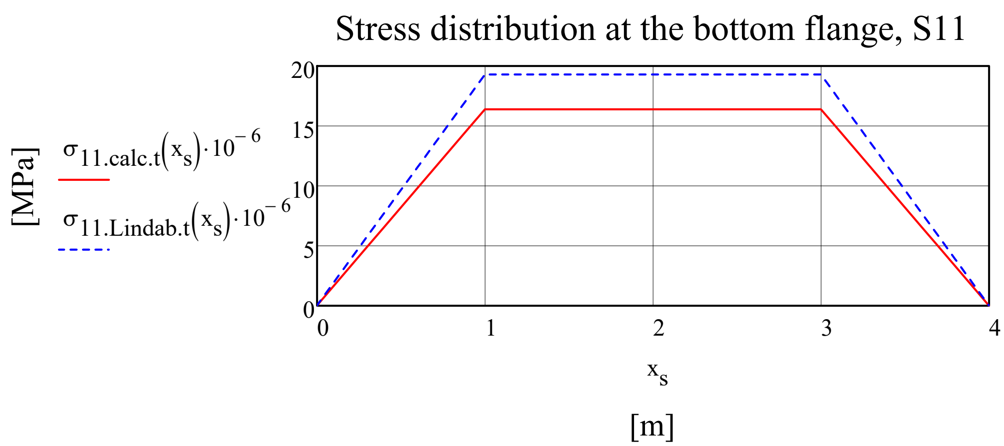

Determining the location of the maximum tension:

$d\sigma_{11.calc.t}\left(x_s\right) := \frac{d}{dx_s}\sigma_{11.calc.t}\left(x_s\right)$ — The derivates of the stress

$x := \frac{l_s}{2}$ — Approximate location of the maximum tension

Given

$\left(d\sigma_{11.calc.t}(x) = 0\right)$

$x_{root.s} := \text{Find}(x)$ — Find the location of zero derivates

$x_{root.s} = 1.05\,m$ Location of maximum stress

$\sigma_{max.11.calc.t} := \sigma_{11.calc.t}\left(x_{root.s}\right) = 16.379 \cdot MPa$ The maximum stress at the location

B 6.4 Comparison with Results from Abaqus

Stresses in Abaqus compared to calculated values:

The stresses from Abaqus can be compared with the calculated ones in order to validate the results.

Stresses in the cross-section at x=1130mm compared to calculated values:

$\sigma_{Ab.fo.o.s.l} := -4.87811MPa$ $\sigma_{fo.o.s} = -5.681 \cdot MPa$

$\sigma_{Ab.fo.u.s.l} := -4.98002MPa$ $\sigma_{fo.u.s} = -5.54 \cdot MPa$

$\sigma_{Ab.fu.o.s.l} := 16.6678MPa$ $\sigma_{fu.o.s} = 16.238 \cdot MPa$

$\sigma_{Ab.fu.u.s.l} := 16.4946MPa$ $\sigma_{fu.u.s} = 16.379 \cdot MPa$

Calculated sectional modulus that Abaqus uses:

$$W_{Ab.s.l} := \frac{M_{1.Ab}}{\sigma_{Ab.fo.o.s.l}} = 1.492 \times 10^{5} \cdot mm^{3}$$

$$W_{el.s.l} := W_{el.1} = 1.267 \times 10^{5} \cdot mm^{3}$$

B 7 Calculations for the Solid Model - Plastic

Due to the fact that the solid element model illustrates a non-linear behaviour, the model was analysed with an included plastic behaviour. The load in these calculations was made higher in order to capture the shape of the load vs. deflection curve.

B 7.1 Calculated Moments Compared to Abaqus

The stresses in the sheet based on a chosen applied load, smaller than the critical one.

$P := 2880 \cdot 0.4292N$ Chosen point load to act on the sheet for an elastic analysis

$L_{solid} = 4\,m$ Total length of the model, including overlap

$l_s = 2.1\,m$ Length of one sheet

$a_{l.solid} = 1\,m$ Distance between edge and applied point load

$R_{A.s.p} := P = 1.236 \cdot kN$ Reaction force at the left support

$R_{B.s.p} := R_{A.s.p} = 1.236 \cdot kN$ Reaction force at the right support

$x_s := 0m, 0.1m .. L_{solid}$

Moment acting on the short symmetrical sheet inbetween the applied point loads

$$M_{Ed.s.p}(x_s) := \begin{cases} -R_{A.s.p} \cdot x_s & \text{if } 0 \le x_s \le a_{l.solid} \\ -R_{A.s.p} \cdot x_s + P \cdot (x_s - a_{l.solid}) & \text{if } a_{l.solid} \le x_s \le L_{solid} - a_{l.solid} \\ -R_{A.s.p} \cdot x_s + P \cdot (x_s - a_{l.solid}) \ldots & \text{if } L_{solid} - a_{l.solid} \le x_s \le L_{solid} \\ + P \cdot \left[x_s - (L_{solid} - a_{l.solid})\right] & \end{cases}$$

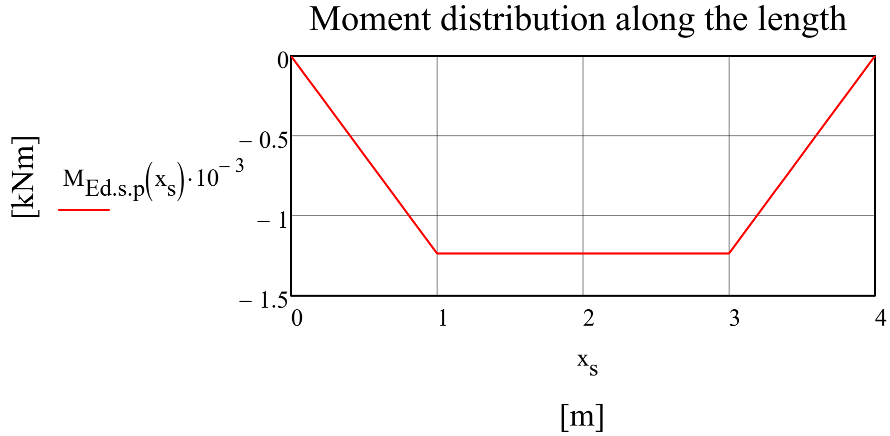

$$dM_{Ed.s.p}(x_s) := \frac{d}{dx_s} M_{Ed.s.p}(x_s)$$

The derivates of the moment is the shear

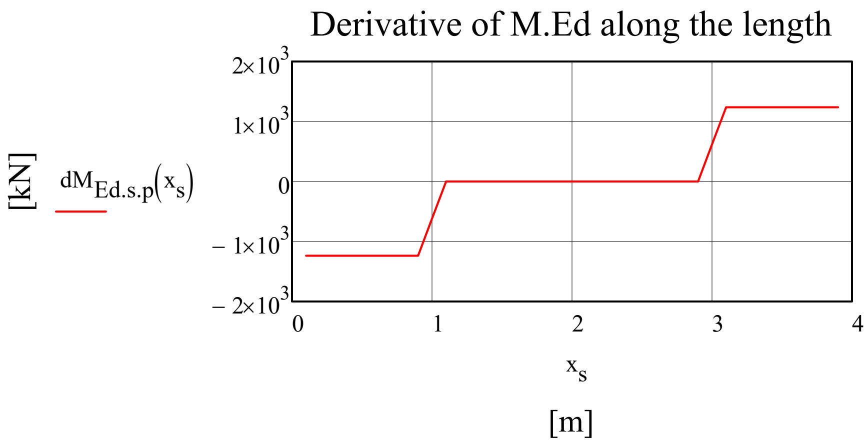

Comparing calculated moments and moments in Abaqus:

$x_1 := 2700\text{mm}$ $\quad M_{1.Ab.p} := -1.253 \cdot 10^6 \text{N} \cdot \text{mm}$ $\quad M_{Ed.s.p}(x_1) = -1.236 \cdot \text{kN} \cdot \text{m}$ $\quad \frac{M_{Ed.s.p}(x_1)}{M_{1.Ab.p}} = 0.987$

$x_2 := 1130\text{mm}$ $\quad M_{2.Ab.p} := -1.259 \cdot 10^6 \text{N} \cdot \text{mm}$ $\quad M_{Ed.s.p}(x_2) = -1.236 \cdot \text{kN} \cdot \text{m}$ $\quad \frac{M_{Ed.s.p}(x_2)}{M_{2.Ab.p}} = 0.982$

B 7.2 Calculated Stresses in the Sheet

Determining the location of the maximum moment:

$x := \frac{l_s}{2}$ — Approximate location of the maximum moment

Given

$(dM_{Ed.s.p}(x) = 0)$

$x_{root.s} := \text{Find}(x)$ — Find the location of zero derivates

$x_{root.s} = 1.05\,\text{m}$ — Location of maximum moment

$M_{max.s.p} := M_{Ed.s.p}(x_{root.s}) = -1.236 \cdot \text{kN} \cdot \text{m}$ — The maximum moment at the location

Critical moment according to LIndab, in the field and over support respectively:

$M_{k.f} = 18.95 \cdot \text{kN}$ $\quad M_{k.s} = 25.96 \cdot \text{kN}$ — Maximum values according to Lindab, per meter width

$$P_{cr.solid} := \frac{M_{k.f} \cdot b_s}{x_{root.s}} = 14.438 \cdot kN$$

Maximum point load, with regard to the sheet's capacity

Applied Load in the Abaqus model:

$$\frac{P_{cr.solid}}{6} = 2.406 \cdot kN$$

Applied point load in Abaqus if in 6 points representing each point load

Stress distribution in the cross-section:

$$\sigma_{dist.s.p}(z_1) := \frac{-M_{Ed.s.p}(2.7m)}{W_{el.dist.1}(z_1)}$$

Cross-sectional stresses in the sheet at x=2.7m, according to beam-theory.

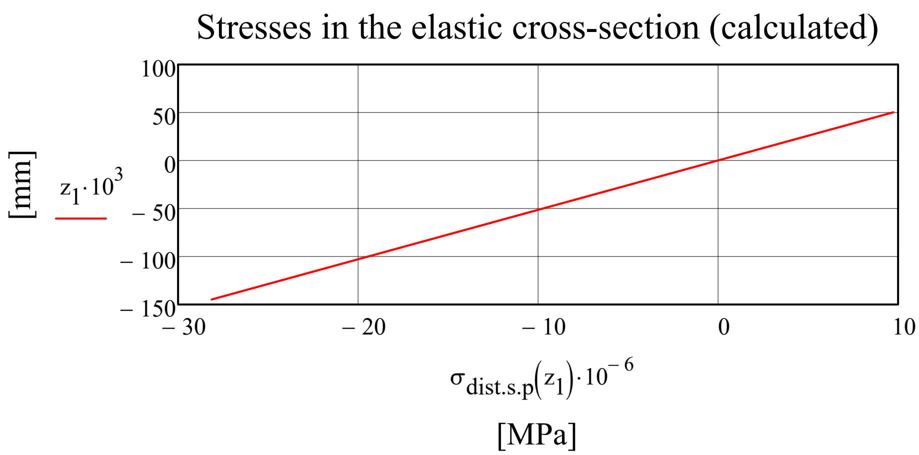

Stresses distribution in the cross-section at x=2700mm:

Compression at the top of the cross-section:

$$\sigma_{fo.o.s.p} := \frac{M_{Ed.s.p}(2700mm)}{W_{el.dist.1}(h_s - z_{tp.1})} = -9.754 \cdot MPa$$

Compression at the bottom of the top flange:

$$\sigma_{fo.u.s.p} := \frac{M_{Ed.s.p}(2700mm)}{W_{el.dist.1}(h_s - z_{tp.1} - t_s)} = -9.511 \cdot MPa$$

Tension at the top of the bottom flange:

$$\sigma_{fu.o.s.p} := \frac{M_{Ed.s.p}(2700mm)}{W_{el.dist.1}(-z_{tp.1} + t_s)} = 27.878 \cdot MPa$$

Tension at the bottom of the cross-section:

$$\sigma_{fu.u.s.p} := \frac{M_{Ed.s.p}(2700mm)}{W_{el.dist.1}(-z_{tp.1})} = 28.12 \cdot MPa$$

Stresses distribution in the cross-section at x=1130mm:

Compression at the top of the cross-section:

$$\sigma_{fo.o.s.p.2} := \frac{M_{Ed.s.p}(1130mm)}{W_{el.dist.1}(h_s - z_{tp.1})} = -9.754 \cdot MPa$$

Compression at the bottom of the top flange:

$$\sigma_{fo.u.s.p.2} := \frac{M_{Ed.s.p}(1130mm)}{W_{el.dist.1}(h_s - z_{tp.1} - t_s)} = -9.511 \cdot MPa$$

Tension at the top of the bottom flange:

$$\sigma_{fu.o.s.p.2} := \frac{M_{Ed.s.p}(1130mm)}{W_{el.dist.1}(-z_{tp.1} + t_s)} = 27.878 \cdot MPa$$

Tension at the bottom of the cross-section:

$$\sigma_{fu.u.s.p.2} := \frac{M_{Ed.s.p}(1130mm)}{W_{el.dist.1}(-z_{tp.1})} = 28.12 \cdot MPa$$

Stress distribution along the longitudinal x-direction (top):

$$I_{Lindab} := 6760 \frac{mm^4}{mm} \cdot b_s = 5.408 \times 10^6 \cdot mm^4$$ Second order of moment according to Lindab

$$I_{11} = 6.364 \times 10^6 \cdot mm^4$$ Second order of moment according to calc.

$$\sigma_{11.Lindab.p}(x_s) := \frac{M_{Ed.s.p}(x_s)}{I_{Lindab}} \cdot (h_s - z_{tp.1})$$ Stress distribution according to Lindab

$$\sigma_{11.calc.p.c}(x_s) := \frac{M_{Ed.s.p}(x_s)}{W_{el.1}}$$ Calculated stress distribution

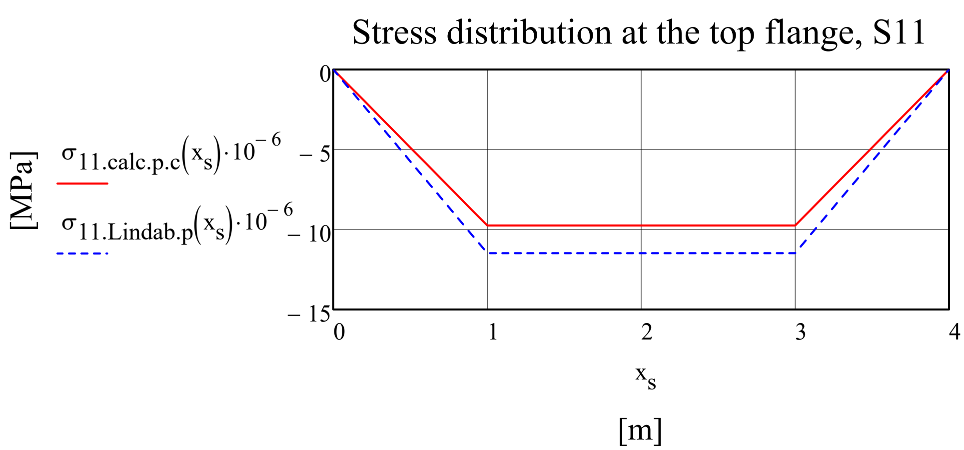

Determining the location of the maximum congressional stress:

$d\sigma_{11.calc.p.c}(x_s) := \frac{d}{dx_s}\sigma_{11.calc.p.c}(x_s)$ The derivates of the moment is the shear

$x := \frac{l_s}{2}$ Approximate location of the maximum stress

Given

$(d\sigma_{11.calc.c}(x) = 0)$

$x_{root.s} := \text{Find}(x)$ Find the location of zero derivates

$x_{root.s} = 1.05\,m$ Location of maximum compression

$\sigma_{max.11.calc.c.p} := \sigma_{11.calc.p.c}(x_{root.s}) = -9.754 \cdot MPa$ The maximum stress at the location

Stress distribution along the longitudinal x-direction (bottom):

$\sigma_{11.calc.p.t}(x_s) := \frac{M_{Ed.s.p}(x_s)}{I_{11}} \cdot (-z_{tp.1})$ Tension in the bottom flange

$\sigma_{11.Lindab.p.t}(x_s) := \frac{M_{Ed.s.p}(x_s)}{I_{Lindab}} \cdot (-z_{tp.1})$ Stress according to Lindab

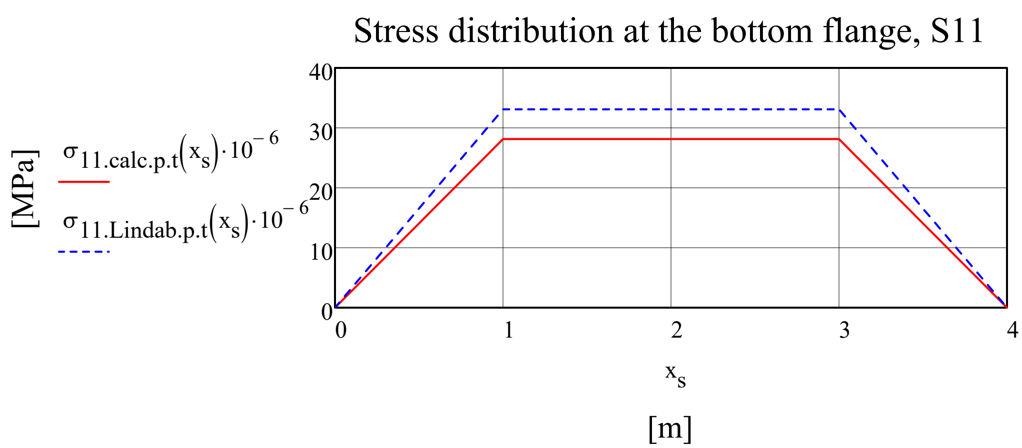

Determining the location of the maximum tension stress:

$d\sigma_{11.calc.p.t}(x_s) := \frac{d}{dx_s}\sigma_{11.calc.p.t}(x_s)$ The derivates of the stress

$x := \frac{l_s}{2}$ Approximate location of the maximum tension

Given

$(d\sigma_{11.calc.t}(x) = 0)$

$x_{root.s} := \mathrm{Find}(x)$ Find the location of zero derivates

$x_{root.s} = 1.05\,m$ Location of maximum tension

$\sigma_{max.11.calc.p.t} := \sigma_{11.calc.p.t}\left(x_{root.s}\right) = 28.12 \cdot MPa$ The maximum stress at the location

B 7.3 Comparison with Results from Abaqus

The stresses from Abaqus can be compared with the calculated ones in order to validate the results.

Reaction forces at the supports compared to calculated values:

$R_{Ab.A.s.p} := 1.234kN$ $\qquad R_{A.s.p} = 1.236 \cdot kN$

$R_{Ab.B.s.p} := 1.234kN$ $\qquad R_{B.s.p} = 1.236 \cdot kN$

Stresses in the cross-section at x=2700mm compared to calculated values:

$\sigma_{Ab.fo.o.s.l.p} := -11.4555MPa$ $\qquad \sigma_{fo.o.s.p} = -9.754 \cdot MPa$

$\sigma_{Ab.fo.u.s.l.p} := 6.50418MPa$ $\qquad \sigma_{fo.u.s.p} = -9.511 \cdot MPa$

$\sigma_{Ab.fu.o.s.l.p} := 35.5105MPa$ $\qquad \sigma_{fu.o.s.p} = 27.878 \cdot MPa$

$\sigma_{Ab.fu.u.s.l.p} := 35.5105MPa$ $\qquad \sigma_{fu.u.s.p} = 28.12 \cdot MPa$

Stresses in the cross-section at x=1130mm compared to calculated values:

$\sigma_{Ab.fo.o.s.l.p.2} := -9.42553MPa$ $\qquad \sigma_{fo.o.s.p.2} = -9.754 \cdot MPa$

$\sigma_{Ab.fo.u.s.l.p.2} := -6.62579MPa$ $\qquad \sigma_{fo.u.s.p.2} = -9.511 \cdot MPa$

$\sigma_{Ab.fu.o.s.l.p.2} := 30.5697MPa$ $\qquad \sigma_{fu.o.s.p.2} = 27.878 \cdot MPa$

$\sigma_{Ab.fu.u.s.l.p.2} := 28.2001MPa$ $\qquad \sigma_{fu.u.s.p.2} = 28.12 \cdot MPa$

Calculated sectional modulus that Abaqus uses:

$$W_{Ab.s.l.p} := \frac{M_{1.Ab.p}}{\sigma_{Ab.fo.o.s.l.p}} = 1.094 \times 10^{5} \cdot mm^{3}$$

$$W_{Ab.s.l.p.2} := \frac{M_{2.Ab.p}}{\sigma_{Ab.fo.o.s.l.p.2}} = 1.336 \times 10^{5} \cdot mm^{3}$$

$$W_{el.s.l.p} := W_{el.1} = 1.267 \times 10^{5} \cdot mm^{3}$$

B 8 Capacity of the Screws

Design of self-tapping screws according to Eurocode SS-EN 1993-1-3 table 8.2

The screws should be checked with regard to shear resistance and tension resistance.

B 8.1 Screws Loaded in Shear

Bearing resistance:

$t := t_s = 1.25 \cdot mm$ Thickness of thinner sheet

$t_1 := t_s = 1.25 \cdot mm$ Thickness of thicker sheet

$d := 6.3mm$ Diameter of the fastener

$t_1 = t = 1$

$\alpha := 3.2 \cdot \sqrt{\frac{t}{d}} = 1.425$

$F_{b.Rd} := \frac{\alpha \cdot f_u \cdot d \cdot t}{\gamma_{M2}} = 3.772 \cdot kN$ Bearing resistance

Shear resistance:

Shear capacity of the screw is determined by testing but with some conditions apply. The characteristic capacity is retrieved from EKS 10 table E-5.

$F_{v.Rk} := 9800N$

$F_{v.Rd} := \frac{F_{v.Rk}}{\gamma_{M2}} = 7.84 \cdot kN$

$F_{v.Rd} \geq 1.2 \cdot F_{b.Rd} = 1$

B 8.2 Screws Loaded in Tension

Pull-through resistance:

$d_w := 16mm$ Diameter of the head of the fastener

$F_{p.Rd} := \frac{d_w \cdot t \cdot f_u}{\gamma_{M2}} = 6.72 \cdot kN$ Pull-trough resistance for static load

Tension resistance:

Tension capacity of the screw is determined by testing but with some conditions apply. The characteristic capacity is retrieved from EKS 10 table E-5.

$F_{v.Rk} = 9.8 \cdot kN$

$$F_{t.Rd} := \frac{1.25 F_{v.Rk}}{\gamma_{M2}} = 9.8 \cdot kN$$

$F_{v.Rd} \geq F_{p.Rd} = 1$

B 9 Stiffness of the Joint in the Solid Model

The stiffness in the joint is derived from the solid element model and will depend on the rotation the joint in the model experiences. The rotation due to bending is subtracted from the total angle measured and the rotation due to stiffness is what remains.

First we do not consider a change in angle when load is increased from the Abaqus results, only the final value is used in the calculations for the elastic stiffness. Then the non-linear behaviour is described for the plastic stiffness. In the end a comparison is made with regard to deriving the stiffness from the deflection at the location of the joint.

B 9.1 Elastic Analysis of the Stiffness

The rotational stiffness of the joint is calculated based on the results from the deflection in Abaqus. The total Angle in Abaqus consist of the change in angle due to the bending moment and at the same time the effect of the mechanism in the hinge. The rotational stiffness can be derived from this.

$P_{Ab} := 720N$ Largest applied load in Abaqus

$P_{cr.solid} = 14.438 \cdot kN$ Critical load for the solid Abaqus model based on Lindabs capacity

$L_{tot} := 4m$ Total length of the tested sheet, including overlap

$a_l := 1m$ Distance between left support and left point load

$b_l := L_{tot} - a_l = 3\,m$ Distance between right support and left point load

$a_r := 1m$ Distance between right support and right point load

$b_r := L_{tot} - a_r = 3\,m$ Distance between left support and right point load

$a_{joint} := \dfrac{L_{tot}}{2}$ Theoretical location of the hinge

$M_{ref} := P_{Ab} \cdot a = 2.088 \cdot kN \cdot m$ Maximum moment if the joint is rigid is the applied load

$n := 0 .. 400$

$P_0 := 0 \cdot kN$

$$P_{n+1} := P_n + \left(\frac{P_{cr.solid}}{400}\right)$$

Angle at the left support after each increment due to bending moment:

$$\alpha_l(n) := \left[\frac{P_n \cdot b_l \cdot L_{tot}}{6 \cdot E_s \cdot I_{solid}} \cdot \left(1 - \frac{b_l^2}{L_{tot}^2}\right) + \frac{P_n \cdot a_r \cdot L_{tot}}{6 \cdot E_s \cdot I_{solid}} \cdot \left(1 - \frac{a_r^2}{L_{tot}^2}\right)\right]$$

Angle at the right support after each increment, due to bending moment:

$$\alpha_r(n) := \frac{P_n \cdot b_r \cdot L_{tot}}{6 \cdot E_s \cdot I_{solid}} \cdot \left(1 - \frac{b_r^2}{L_{tot}^2}\right) + \frac{P_n \cdot a_l \cdot L_{tot}}{6 \cdot E_s \cdot I_{solid}} \cdot \left(1 - \frac{a_l^2}{L_{tot}^2}\right)$$

Angle due to the formation of the mechanism, is calculated based on the angles measured in Abaqus:

$\alpha_{Ab.l} := 1.565494 \cdot deg$ $\quad$ $\alpha_{Ab.r} := 1.45419 \cdot deg$ $\quad$ Deflection angle, elastic model

$$\phi_l(n) := \alpha_{Ab.l} - \alpha_l(n)$$

$$\phi_r(n) := \alpha_{Ab.r} - \alpha_r(n)$$

Total angle if considering the load P:

$$\alpha_{P.l} := \left[\frac{P_{Ab} \cdot b_l \cdot L_{tot}}{6 \cdot E_s \cdot I_{solid}} \cdot \left(1 - \frac{b_l^2}{L_{tot}^2}\right) + \frac{P_{Ab} \cdot a_r \cdot L_{tot}}{6 \cdot E_s \cdot I_{solid}} \cdot \left(1 - \frac{a_r^2}{L_{tot}^2}\right)\right] = 0.046 \cdot deg$$

$$\phi_{P.l} := \alpha_{Ab.l} - \alpha_{P.l} = 1.519 \cdot deg$$

$$\alpha_{P.r} := \frac{P_{Ab} \cdot b_r \cdot L_{tot}}{6 \cdot E_s \cdot I_{solid}} \cdot \left(1 - \frac{b_r^2}{L_{tot}^2}\right) + \frac{P_{Ab} \cdot a_l \cdot L_{tot}}{6 \cdot E_s \cdot I_{solid}} \cdot \left(1 - \frac{a_l^2}{L_{tot}^2}\right) = 0.046 \cdot deg$$

$$\phi_{P.r} := \alpha_{Ab.r} - \alpha_{P.r} = 1.408 \cdot deg$$

Rotational stiffness of the joint in Abaqus:

$$K_{rot.e} := \frac{M_{ref}}{\left(\frac{\pi}{2} - \phi_{P.l}\right) + \left(\frac{\pi}{2} - \phi_{P.r}\right)} = 6.756 \times 10^5 \cdot \frac{N \cdot mm}{rad}$$

Rotational stiffness is for 2ϕ at the joint

B 9.2 Plastic Analysis of the Stiffness

The stiffness is calculated for the plastic analysis of the solid element model in Abaqus.

$P_{Ab.p} := 2880 \cdot 0.4292N = 1.236 \cdot kN$ $\quad$ Largest applied load in Abaqus

$M_{ref.p} := P_{Ab.p} \cdot a_l = 1.236 \cdot kN \cdot m$ $\quad$ Maximum moment if the joint is rigid is the applied load

$n := 0 .. 400$

$P_0 := 0 \cdot kN$

$P_{n+1} := P_n + \left(\frac{P_{cr.solid}}{400}\right)$

Angle at the left support after each increment due to bending moment:

$$\alpha_{l.p}(n) := \left[\frac{P_n \cdot b_l \cdot L_{tot}}{6 \cdot E_s \cdot I_{solid}} \cdot \left(1 - \frac{b_l^2}{L_{tot}^2}\right) + \frac{P_n \cdot a_r \cdot L_{tot}}{6 \cdot E_s \cdot I_{solid}} \cdot \left(1 - \frac{a_r^2}{L_{tot}^2}\right)\right]$$

Angle at the right support after each increment, due to bending moment:

$$\alpha_{r.p}(n) := \frac{P_n \cdot b_r \cdot L_{tot}}{6 \cdot E_s \cdot I_{solid}} \cdot \left(1 - \frac{b_r^2}{L_{tot}^2}\right) + \frac{P_n \cdot a_l \cdot L_{tot}}{6 \cdot E_s \cdot I_{solid}} \cdot \left(1 - \frac{a_l^2}{L_{tot}^2}\right)$$

Angle due to the formation of the mechanism, is calculated based on the angles measured in Abaqus:

$\alpha_{Ab.l.p} := 4.080849 \cdot deg$ $\qquad$ $\alpha_{Ab.r.p} := 3.798136 \cdot deg$ $\qquad$ Deflection angle, elastic model

$\phi_{l.p}(n) := \alpha_{Ab.l.p} - \alpha_{l.p}(n)$

$\phi_{r.p}(n) := \alpha_{Ab.r.p} - \alpha_{r.p}(n)$

Total angle if considering the load P:

$$\alpha_{P.l.p} := \left[\frac{P_{Ab.p} \cdot b_l \cdot L_{tot}}{6 \cdot E_s \cdot I_{solid}} \cdot \left(1 - \frac{b_l^2}{L_{tot}^2}\right) + \frac{P_{Ab.p} \cdot a_r \cdot L_{tot}}{6 \cdot E_s \cdot I_{solid}} \cdot \left(1 - \frac{a_r^2}{L_{tot}^2}\right)\right] = 0.079 \cdot deg$$

$\phi_{P.l.p} := \alpha_{Ab.l.p} - \alpha_{P.l.p} = 4.001 \cdot deg$

$$\alpha_{P.r.p} := \frac{P_{Ab.p} \cdot b_r \cdot L_{tot}}{6 \cdot E_s \cdot I_{solid}} \cdot \left(1 - \frac{b_r^2}{L_{tot}^2}\right) + \frac{P_{Ab} \cdot a_l \cdot L_{tot}}{6 \cdot E_s \cdot I_{solid}} \cdot \left(1 - \frac{a_l^2}{L_{tot}^2}\right) = 0.066 \cdot deg$$

$\phi_{P.r.p} := \alpha_{Ab.r.p} - \alpha_{P.r.p} = 3.732 \cdot deg$

Rotational stiffness of the joint in Abaqus:

$$K_{rot.p} := \frac{M_{ref.p}}{\left(\frac{\pi}{2} - \phi_{P.l.p}\right) + \left(\frac{\pi}{2} - \phi_{P.r.p}\right)} = 7.176 \times 10^{3} \cdot \frac{N \cdot mm}{deg}$$

Rotational stiffness is for 2ϕ

B 9.3 Comparing the Plastic and Elastic Stiffness

The stiffness increases linearly with the moment

$M_{ref.p} = 1.236 \cdot kN \cdot m$ $\quad K_{rot.p} = 4.111 \times 10^{5} \cdot N \cdot \frac{mm}{rad}$ $\quad K_{rot.p} = 7.176 \times 10^{-3} \cdot kN \cdot \frac{m}{deg}$

$M_{ref} = 2.088 \cdot kN \cdot m$ $\quad K_{rot.e} = 6.756 \times 10^{5} \cdot N \cdot \frac{mm}{rad}$ $\quad K_{rot.e} = 0.012 \cdot kN \cdot \frac{m}{deg}$

B 9.4 Non-linear Plastic Stiffness

The stiffness is calculated for the plastic analysis of the solid element model in Abaqus. The load increase gives a non-linear increase of deflection which is captured here.

Calculating with regard to change of angle:

$P_{Ab.p} = 1.236 \cdot kN$ Largest applied load in Abaqus

$x_d := 360mm$ Deflection measured at this point from the edge of the sheet

Measured load increments and increased deflection in the Abaqus solid element model with plastic analysis:

$\begin{pmatrix} P_p \\ \delta_p \end{pmatrix} :=$

1143,4234	25,0349
1163,9866	26,8298
1171,6992	27,7708
1183,2682	28,4999
1200,6202	29,1305

Values from excel are imported into P and δ

$P_p := P_p \cdot N$ $\quad \delta_p := \delta_p \cdot mm$

$M_{ref.p} = 1.236 \cdot kN \cdot m$ Maximum moment if the joint is rigid is the applied load

Angle at the support after each load increment due to bending moment:

$$\alpha_p := \left[\frac{P_p \cdot b_l \cdot L_{tot}}{6 \cdot E_s \cdot I_{solid}} \cdot \left(1 - \frac{b_l^{\,2}}{L_{tot}^{\,2}}\right) + \frac{P_p \cdot a_r \cdot L_{tot}}{6 \cdot E_s \cdot I_{solid}} \cdot \left(1 - \frac{a_r^{\,2}}{L_{tot}^{\,2}}\right)\right]$$

Moment for each load increment:

$$M_p := P_p \cdot a_1$$

Angle at the support due to stiffness is calculated based on the angles measured in Abaqus:

$$\alpha_{Ab.p} := \operatorname{atan}\left(\frac{\delta_p}{x_d}\right)$$

Total deflection angle from Abaqus model

$$\phi_p := \alpha_{Ab.p} - \alpha_p$$

Deflection due to stiffness

Rotational stiffness of the joint in Abaqus:

$$K_{rot.Ab} := \frac{M_p}{\left(\pi - 2\phi_p\right)}$$

Rotational stiffness is for 2ϕ at the joint

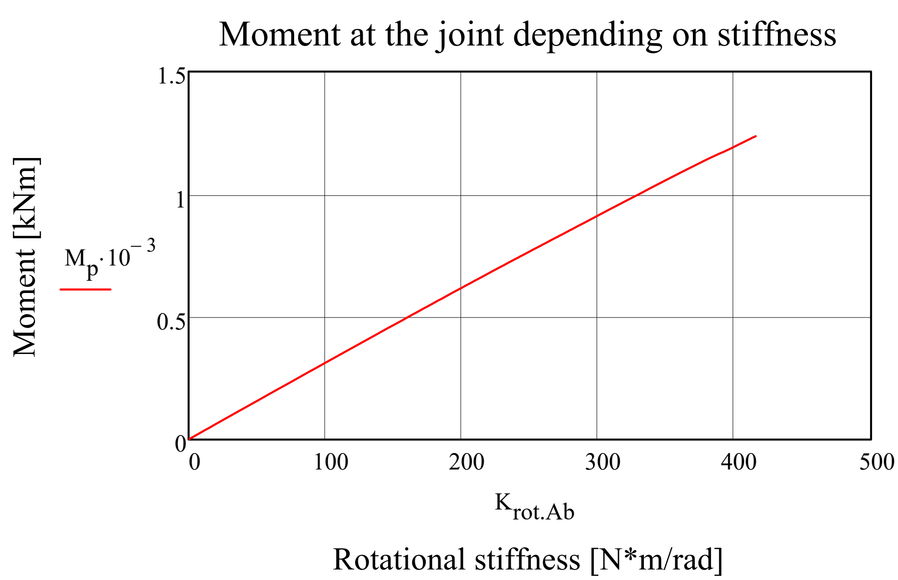

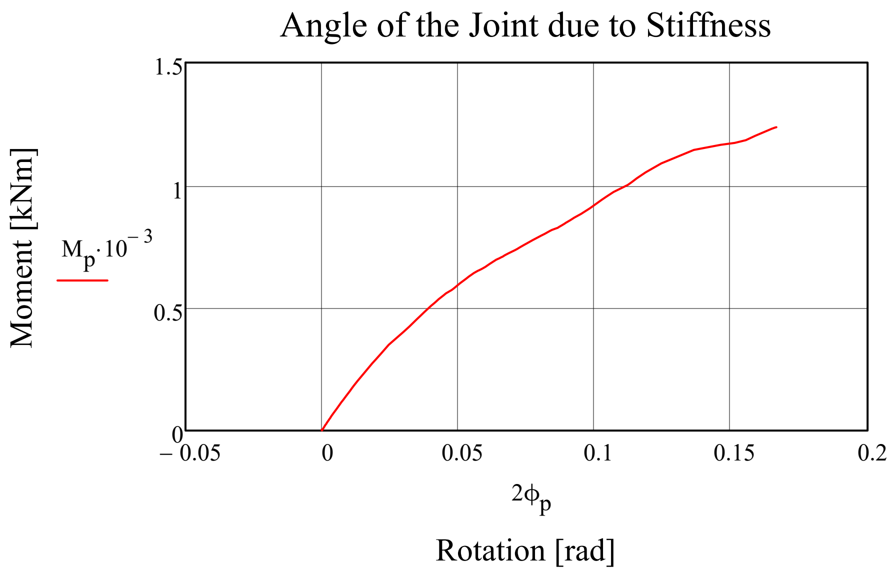

$K_{rot.Ab} =$ (values in $\cdot N \cdot \frac{mm}{rad}$)

	0
0	0
1	57.296
2	114.592
3	200.535
4	329.45
5	522.823
6	812.876
7	867.248
8	908.118
9	948.914
10	$1.01 \cdot 10^3$
11	$1.102 \cdot 10^3$
12	$1.24 \cdot 10^3$
13	$1.446 \cdot 10^3$
14	$1.756 \cdot 10^3$
15	...

Calculating with regard to deflection in the middle of the span:

$P_{Ab.d} := P_{Ab.p}$ Largest applied load in Abaqus

$x_d := \frac{L_{tot}}{2} = 2 \cdot m$ Deflection measured at this point from the edge of the sheet

Measured load increments and increased deflection in the Abaqus solid element model with plastic analysis:

$\begin{pmatrix} P_{Ab} \\ \delta_{Ab} \end{pmatrix} :=$

0	0
0,18	-2,4E-09
0,36	9,94E-10
0,63	1,64E-08
1,035	7,09E-08
1,642499	-1,8E-06
2,553751	0,000157
2,72461	0,008658
2,852755	0,184562

Values from excel are imported into P and δ

$P_{Ab} := P_{Ab} \cdot N$ $\delta_{Ab} := \delta_{Ab} \cdot mm$

$M_{ref.p} = 1.236 \cdot kN \cdot m$ Maximum moment if the joint is rigid is the applied load

Deflection in the center of the span after each load increment due to bending moment:

In order to derive the rotational stiffness of the joint; the deflection caused by load needs to be calculated on the sheet.

$$\delta_l := 2\left[\frac{P_p \cdot a_l \cdot L_{tot}^2}{48 \cdot E_s \cdot I_{solid}} \cdot \left(3 - \frac{4 \cdot a_l^2}{L_{tot}^2}\right)\right]$$

Moment for each load increment:

$M_p := P_p \cdot a_l$

Angle at the support due to stiffness is calculated based on the deflection:

$\delta_d := \delta_{Ab} - \delta_l$ Deflection due to rotational stiffness

$\alpha_d := \operatorname{atan}\left(\frac{\delta_d}{x_d}\right)$ Angle at the support due to rotational stiffness

$\phi_d := 2 \cdot \alpha_d$ Angle at the joint in the middle of the span

Rotational stiffness of the joint in Abaqus:

$K_{rot.d} := \frac{M_p}{\pi - \phi_d}$ Rotational stiffness is for 2ϕ at the joint

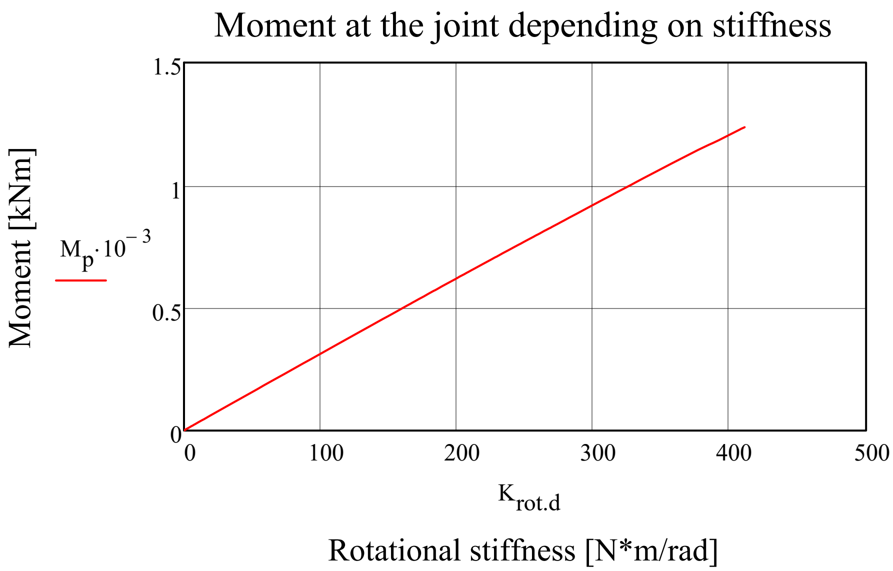

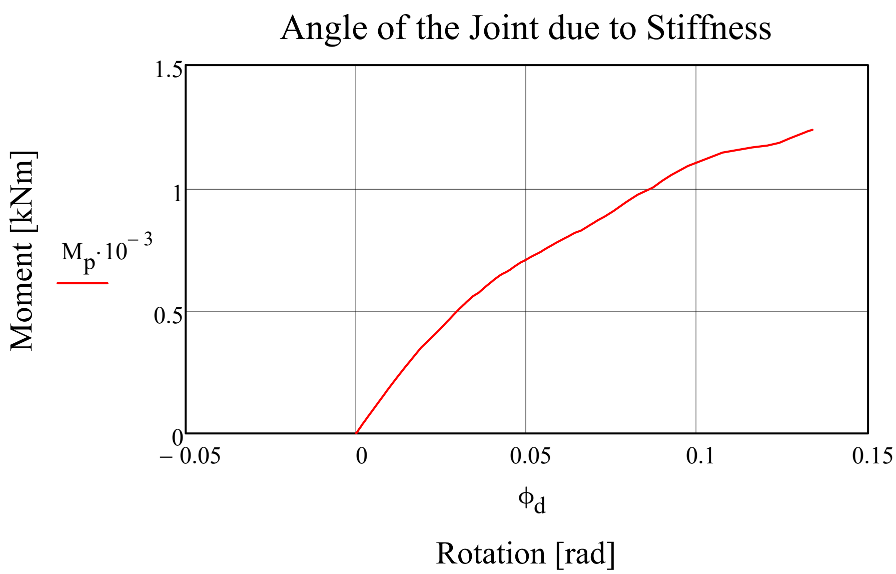

This is based on a constant moment applied inbetween the point loads. In the beam element model the moment applied is much smaller.

$$M_{joint.Ab} := 8.16 \cdot 10^3 N \cdot mm = 8.16 \times 10^{-3} \cdot kN \cdot m$$

This moment is very small compared to the curve above due to the fact that the joint is placed where the moment is teoretically zero.

Rotational stiffness based on deflection and change of angle respectively:

	0
0	0
1	57.296

	0
0	0
1	57.296

$K_{rot.d} =$

2	114.592
3	200.535
4	329.451
5	522.823
6	812.883
7	867.272
8	908.112
9	948.905
10	$1.01 \cdot 10^3$
11	$1.102 \cdot 10^3$
12	...

$\cdot N \cdot \frac{mm}{rad}$

$K_{rot.Ab} =$

2	114.592
3	200.535
4	329.45
5	522.823
6	812.876
7	867.248
8	908.118
9	948.914
10	$1.01 \cdot 10^3$
11	$1.102 \cdot 10^3$
12	...

$\cdot N \cdot \frac{mm}{rad}$

The calculated rotational stiffness is therefore confirmed in two different calculation methods.

$$K_{rot} := \max\left(K_{rot.Ab}\right) = 4.155 \times 10^5 \cdot \frac{N \cdot mm}{rad}$$

B 10 Global Analysis of a Gerber system - Continuous

The global analysis of the sheet is calculated and modeled in Abaqus. The system is a three span continuous Gerber system with two joints placed in the mid-span. First it is calculated as a continuous model exposed to an evenly distributed load, then an unevenly distributed load.

$L := 18m$

$l := 6m$

Critical moment according to LIndab, in the field and over support respectively:

$M_{k.f} = 18.95 \cdot kN$ $\qquad$ $M_{k.s} = 25.96 \cdot kN$

$M_{k.f} \cdot b_s = 15.16 \cdot kN \cdot m$ $\qquad$ $M_{k.s} \cdot b_s = 20.768 \cdot kN \cdot m$

B 10.1 Calculating the Moment Distribution for a 3-span Continuous Model:

$$q_d := 3.7 \frac{kN}{m} = 3.7 \cdot \frac{N}{mm}$$

$$q_{cr.f} := \frac{M_{k.f}}{l} = 3.158 \cdot \frac{kN}{m} \qquad q_{cr.s} := \frac{M_{k.s}}{l} = 4.327 \cdot \frac{kN}{m}$$

Calculating the support moment by simulating a fixed connection in the mid-span:

$$M_B := q_d \cdot \frac{l^2}{12} = 11.1 \cdot kN \cdot m$$

$$M_C := M_B$$

Calculating the reaction forces:

$$R_{Bh} := q_d \cdot \frac{l}{2} = 11.1 \cdot kN$$

$$R_{Cv} := R_{Bh}$$

Find the support moment which makes the the field moment zero at the joint:

$$x_{BC} := 0m, 0.1m .. l$$

$$M_{Ed.BC}(x_{BC}) := M_B - R_{Bh} \cdot x_{BC} + q_d \cdot \frac{x_{BC}^2}{2}$$

$$dM_{Ed.BC}(x_{BC}) := \frac{d}{dx_{BC}} M_{Ed.BC}(x_{BC})$$

The derivates of the moment is the shear

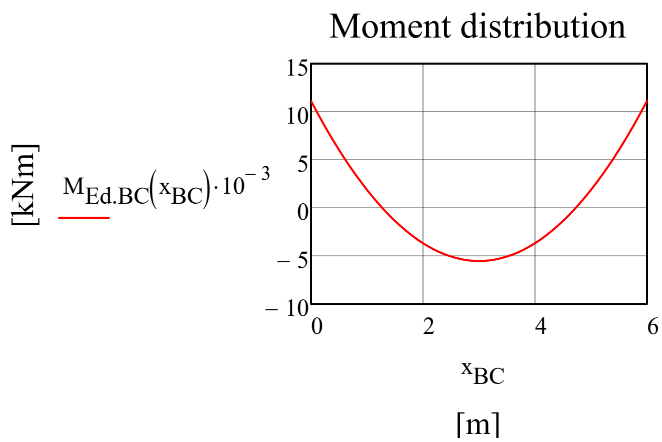

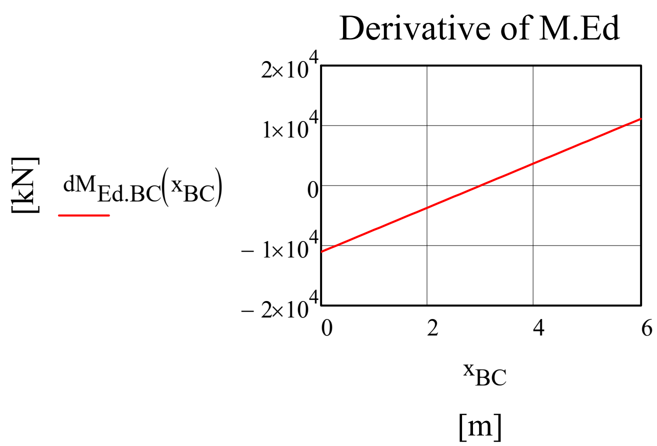

The joint is placed where the design moment is zero i.e. this will always be the location of the zero moment according to theory.

$x := \frac{1}{4}$

Approximate location where the derivates is zero

Given

$(M_{Ed.BC}(x) = 0)$

The joint is placed where the moment is zero

$x_{root} := \text{Find}(x)$

Find the location of the zero moment

$x_{root} = 1.268\ m$

$a_{joint} := x_{root}$

Distance from support to zero moment

$M_{Ed.BC}(a_{joint}) = 0 \cdot kN \cdot m$

Calculating the global moment distribution:

$R_A := -M_B \cdot \frac{1}{l} + q_d \cdot \frac{l}{2} = 9.25 \cdot kN$

$R_{Bv} := M_B \cdot \frac{1}{l} + q_d \cdot \frac{l}{2} = 12.95 \cdot kN$

$R_B := R_{Bv} + R_{Bh} = 24.05 \cdot kN$

$R_C := R_B$

$R_D := R_A$

$x := 0m, 0.1m .. L$

$$M_{Ed.g}(x) := \begin{vmatrix} -R_A \cdot x + q_d \cdot \frac{x^2}{2} & \text{if } 0 \le x \le l \\ -R_A \cdot x + q_d \cdot \frac{x^2}{2} - R_B \cdot (x - l) & \text{if } l \le x \le 2l \\ -R_A \cdot x + q_d \cdot \frac{x^2}{2} - R_B \cdot (x - l) - R_C \cdot (x - 2l) & \text{if } 2l \le x \le L \end{vmatrix}$$

$dM_{Ed.g}(x) := \frac{d}{dx} M_{Ed.g}(x)$

The derivates of the moment is the shear

$$V_{Ed.g}(x) := \begin{vmatrix} -R_A + q_d \cdot x & \text{if } 0 \le x \le l \\ -R_A + q_d \cdot x - R_B & \text{if } l \le x \le 2l \\ -R_A + q_d \cdot x - R_B - R_C & \text{if } 2l \le x \le L \end{vmatrix}$$

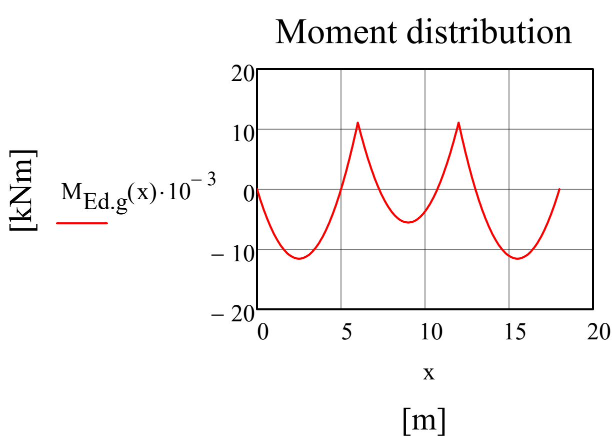

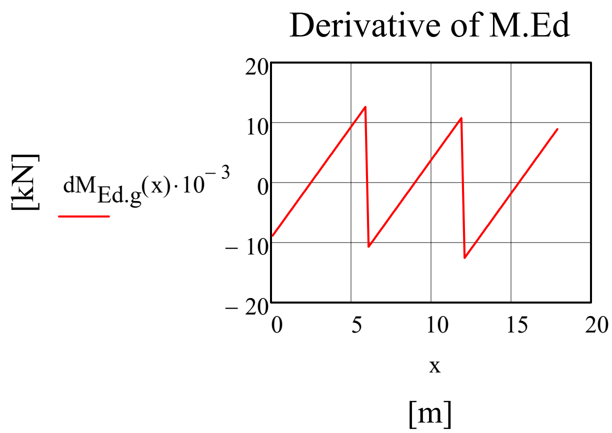

$x_{joint} := 1 + a_{joint}$

Approximate location where the moment is zero

Given

$(M_{Ed.g}(x_{joint}) = 0)$

The joint is placed where the moment is zero

$x_{root2} := Find(x_{joint})$

Find the location of the zero moment

$x_{root2} = 7.268\ m$

$M_{max} := M_{Ed.g}(x_{root2}) = 0\cdot kN\cdot m$

The moment at the calculated location

$x_{root2} - 1 = 1.268\ m$ $\quad a_{joint} = 1.268\ m$

They correlate!

Maximum field moment, first span:

$x_f := \frac{1}{2}$

Approximate location where the derivates is zero in the first span

Given

$(dM_{Ed.g}(x_f) = 0)$

The derivates is zero where the moment is its max or min

$x_{root.f} := Find(x_f)$

Find the location of the maximum moment

$x_{root.f} = 2.5\ m$

$M_{Ed.g.max.1} := M_{Ed.g}(x_{root.f}) = -11.563\cdot kN\cdot m$

The maximum moment in span 1 and 3

Maximum field moment, mid-span:

$x_f := 1.5l$

Approximate location where the derivates is zero in the second span

Given

$\left(dM_{Ed.g}\left(x_f\right) = 0\right)$

$x_{root.f} := \mathrm{Find}\left(x_f\right)$

$x_{root.f} = 9\,m$

$M_{Ed.g.max.mid} := M_{Ed.g}\left(x_{root.f}\right) = -5.55\cdot kN\cdot m$

The derivates is zero where the moment is its max or min
Find the location of the maximum moment

The maximum moment in mid-span

The ratio of the support and field moment in the mid-span needs to be kept in order for the location of the moment to be zero at the joints in the second span (mid-span).

$$r_M := \frac{M_B}{M_{Ed.g.max.mid}} = -2$$

The capacity of the sheet according to Lindab:

The moment which is decisive in design will dictate the moments in the sheet.

$-M_{k.f}\cdot b_s = -15.16\cdot kN\cdot m$

$-M_{k.s}\cdot b_s = -20.768\cdot kN\cdot m$

$M_{k.B} := r_M\cdot M_{k.f}\cdot b_s = -30.32\cdot kN\cdot m$

$M_{k.B} \geq -M_{k.s}\cdot b_s = 0$

$M_{k.BC} := \dfrac{M_{k.s}\cdot b_s}{r_M} = -10.384\cdot kN\cdot m$

$M_{k.BC} \geq -M_{k.f}\cdot b_s = 1$

This means that according to the capacity given by Lindab is critical at the support. A critical support moment gives an acceptable field moment, but a critical field moment gives a too high support moment. The support moment is decisive.

B 10.2 Stress Distribution Evenly Distributed Load

$z_{tp.1} = 144.781\cdot mm$ $z_{tp.sc.1} = 141.689\cdot mm$ $z_{g.Ab} := 141.54mm$

$A_{g.1} = 1.37\times 10^3\cdot mm^2$ $A_{g.sc.1} = 1.4\times 10^3\cdot mm^2$ $A_{g.Ab} := \dfrac{10214851mm^3}{7.268m} = 1.405\times 10^3\cdot mm^2$

The difference is assumed to be with regard to how the arbitrary 3D beam element model has be computed in Abaqus, with sharp corners. Therefore we assume a calculated sectional modulus based on the model with sharp corners.

$I_g := I_{y.sc.1} = 6.648\times 10^6\cdot mm^4$

$$I_{g.Ab} := 2A_{fu}\cdot(z_{g.Ab} - z_{fu})^2 + 1A_{gu}\cdot(z_{g.Ab} - z_{gu})^2 + 1\cdot A_{fo}\cdot(z_{fo} - z_{g.Ab})^2 + 2\cdot A_{go}\cdot(z_{go} - z_{g.Ab})^2 \dots$$
$$+ 2A_{wu}\cdot(z_{g.Ab} - z_{wu})^2 + 2A_{wm}\cdot(z_{g.Ab} - z_{wm})^2 + 2\cdot A_{wo}\cdot(z_{wo} - z_{g.Ab})^2 \dots$$
$$+ 2A_{w.fu}\cdot(z_{g.Ab} - z_{w.fu})^2 + 2\cdot A_{w.fo}\cdot(z_{w.fo} - z_{g.Ab})^2$$

$$W_{el.g} := \frac{I_g}{z_{tp.sc.1}} = 4.692 \times 10^4 \cdot mm^3$$

Sectional modulus according to calculations, considering sharp corners

$$W_{el.g.Ab} := \frac{I_{g.Ab}}{z_{g.Ab}} = 4.688 \times 10^4 \cdot mm^3$$

Sectional modulus according to Abaqus

The Stress Distribution Along the Sheet:

$$\sigma_{x.g}(x) := \frac{-M_{Ed.g}(x)}{W_{el.g}}$$

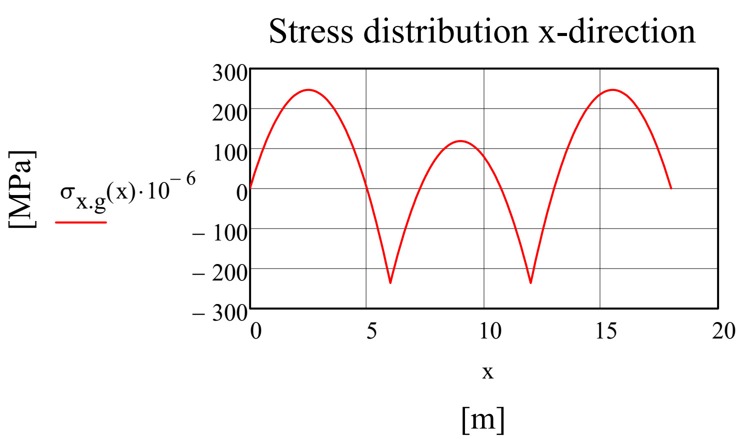

$$d\sigma_{x.g}(x) := \frac{d}{dx}\sigma_{x.g}(x)$$

The derivates of the moment is the shear

Stress in span 1:

$$x_{max.g1} := \frac{1}{2}$$

Approximate location where the derivates is zero

Given

$$\left(d\sigma_{x.g}(x_{max.g1}) = 0\right)$$

The max where the derivates is zero

$$x_{g.max.1} := Find(x_{max.g1})$$

Find the location of the zero derivates

$$x_{g.max.1} = 2.5\,m$$

$$\sigma_{x.g.max.1} := \sigma_{x.g}(x_{g.max.1}) = 246.424\cdot MPa$$

The maximum stress in span 1

Stress in mid-span:

$x_{max.gmid} := 1 + \frac{1}{2}$

Approximate location where the derivates is zero

Given

$\left(d\sigma_{x.g}\left(x_{max.gmid}\right) = 0\right)$

The max where the derivates is zero

$x_{g.max.mid} := \mathrm{Find}\left(x_{max.gmid}\right)$

Find the location of the zero derivates

$x_{g.max.mid} = 9\,\mathrm{m}$

$\sigma_{x.g.max.mid} := \sigma_{x.g}\left(x_{g.max.mid}\right) = 118.283 \cdot \mathrm{MPa}$

The maximum stress in mid-span

Stress at supports:

$\sigma_{x.g.B} := \sigma_{x.g}(l) = -236.567 \cdot \mathrm{MPa}$

$\sigma_{x.g.C} := \sigma_{x.g}(2 \cdot l) = -236.567 \cdot \mathrm{MPa}$

B 10.3 Comparing with Values from Abaqus

Comparing the reaction forces:

$R_{A.Ab} := 9256.98\mathrm{N} = 9.257 \cdot \mathrm{kN}$ $\qquad R_A = 9.25 \cdot \mathrm{kN}$

$R_{B.Ab} := 24054.8\mathrm{N} = 24.055 \cdot \mathrm{kN}$ $\qquad R_B = 24.05 \cdot \mathrm{kN}$

$R_{C.Ab} := 24054.8\mathrm{N} = 24.055 \cdot \mathrm{kN}$ $\qquad R_C = 24.05 \cdot \mathrm{kN}$

$R_{D.Ab} := 9256.98\mathrm{N} = 9.257 \cdot \mathrm{kN}$ $\qquad R_D = 9.25 \cdot \mathrm{kN}$

$2 \cdot R_{A.Ab} + 2 \cdot R_{B.Ab} = 66.624 \cdot \mathrm{kN}$ $\qquad 2 \cdot R_A + 2 \cdot R_B = 66.6 \cdot \mathrm{kN}$

$q_d \cdot L = 66.6 \cdot \mathrm{kN}$

Comparing the moments:

$M_{B.Ab} := 1.10954 \cdot 10^7 \mathrm{N} \cdot \mathrm{mm} = 11.095 \cdot \mathrm{kN} \cdot \mathrm{m}$ $\qquad M_B = 11.1 \cdot \mathrm{kN} \cdot \mathrm{m}$

$M_{AB.Ab} := -1.15637 \cdot 10^7 \mathrm{N} \cdot \mathrm{mm} = -11.564 \cdot \mathrm{kN} \cdot \mathrm{m}$ $\qquad M_{AB} := M_{Ed.g.max.1} = -11.563 \cdot \mathrm{kN} \cdot \mathrm{m}$

$M_{BC.Ab} := -5.54893 \cdot 10^6 \mathrm{N} \cdot \mathrm{mm} = -5.549 \cdot \mathrm{kN} \cdot \mathrm{m}$ $\qquad M_{BC} := M_{Ed.g.max.mid} = -5.55 \cdot \mathrm{kN} \cdot \mathrm{m}$

Comparing the stresses at the supports:

$\sigma_{B.Ab} := -205.4\mathrm{MPa}$ $\qquad \sigma_{B.Ab.calc} := \frac{-M_{B.Ab}}{W_{el.g.Ab}} = -236.696 \cdot \mathrm{MPa}$ $\qquad \sigma_{x.g.B} = -236.567 \cdot \mathrm{MPa}$

Comparing the stresses in the joint:

$\sigma_{joint.Ab} := 11.1434MPa$

$\sigma_{joint} := \sigma_{x.g}(2l - a_{joint}) = 3.101 \times 10^{-13} \cdot MPa$

Placement of joints vs. the location of the zero moment:

$a_{zero.l.Ab}$ $\quad$ $l + a_{joint} = 7.268\,m$

$a_{zero.r.Ab}$ $\quad$ $2 \cdot l - a_{joint} = 10.732\,m$

B 10.4 Deflection of the Sheet

Deflection of the 3-span continuous sheet, distributed loads:

$q_d = 3.7 \cdot \frac{kN}{m}$

$l = 6\,m$

$R_A = 9.25 \cdot kN$ $\quad$ $M_B = 11.1 \cdot kN \cdot m$

$R_B = 24.05 \cdot kN$ $\quad$ $M_C = 11.1 \cdot kN \cdot m$

$R_C = 24.05 \cdot kN$

$E_s = 2.1 \times 10^{5} \cdot MPa$

$I_g = 6.648 \times 10^{6} \cdot mm^{4}$

$a_m(x) := x - l$ $\quad$ $a_3(x) := x - 2l$

$$\delta_g(x) := \begin{cases} \left[\frac{q_d \cdot x \cdot l^3}{24 \cdot E_s \cdot I_g} \cdot \left(1 - \frac{2x^2}{l^2} + \frac{x^3}{l^3}\right) \ldots \right. \\ \left. + \frac{-M_B \cdot x \cdot l}{6 \cdot E_s \cdot I_g} \cdot \left(1 - \frac{x^2}{l^2}\right) \right] & \text{if } 0 \le x \le l \\ \left[\frac{q_d \cdot a_m(x) \cdot l^3}{24 \cdot E_s \cdot I_g} \cdot \left(1 - \frac{2\,a_m(x)^2}{l^2} + \frac{a_m(x)^3}{l^3}\right) + \frac{-M_B \cdot a_m(x) \cdot l}{6 \cdot E_s \cdot I_g} \cdot \left(1 - \frac{a_m(x)^2}{l^2}\right) \ldots \right. \\ \left. + \frac{-M_C \cdot \left(1 - a_m(x)\right) \cdot l}{6 \cdot E_s \cdot I_g} \cdot \left[1 - \frac{\left(1 - a_m(x)\right)^2}{l^2}\right] \right] & \text{if } l \le x < l \cdot 2 \\ \left[\frac{q_d \cdot a_3(x) \cdot l^3}{24 \cdot E_s \cdot I_g} \cdot \left(1 - \frac{2\,a_3(x)^2}{l^2} + \frac{a_3(x)^3}{l^3}\right) \ldots \right. \\ \left. + \frac{-M_C \cdot \left(1 - a_3(x)\right) \cdot l}{6 \cdot E_s \cdot I_g} \cdot \left[1 - \frac{\left(1 - a_3(x)\right)^2}{l^2}\right] \right] & \text{if } l \cdot 2 \le x \le L \end{cases}$$

$$d\delta_g(x) := \frac{d}{dx}\delta_g(x)$$

The derivates of the deflection

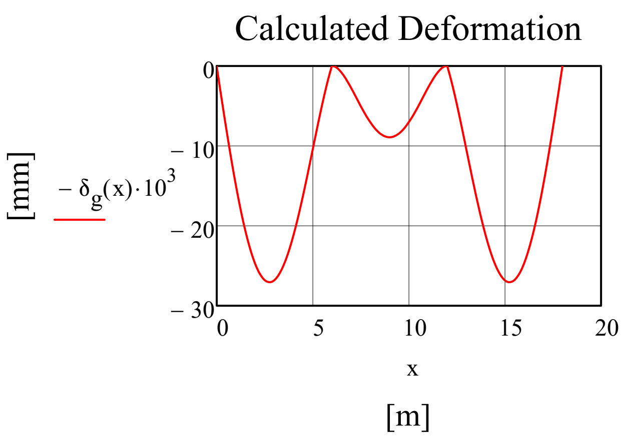

Maximum deflection first span:

$$x_f := \frac{l}{2}$$

Approximate location where the derivates is zero in the first span

Given

$$\left(d\delta_g\left(x_f\right) = 0\right)$$

The derivates is zero where the deflection is its max or min

$x_{root.1} := \mathrm{Find}(x_f)$

Find the location of the maximum deflection

$x_{root.1} = 2.754\,m$

$\delta_{g.1} := -\delta_g(x_{root.1}) = -27.079 \cdot mm$

The maximum deflection in span 1

Maximum deflection mid-span:

$x_f := \frac{L}{2}$

Approximate location where the derivates is zero in the first span

Given

$(d\delta_g(x_f) = 0)$

The derivates is zero where the deflection is its max or min

$x_{root.mid} := \mathrm{Find}(x_f)$

Find the location of the maximum deflection

$x_{root.mid} = 9\,m$

$\delta_{g.mid} := -\delta_g(x_{root.mid}) = -8.944 \cdot mm$

The maximum deflection in span 1

Maximum deflection third span:

$x_f := L - \frac{1}{2}$

Approximate location where the derivates is zero in the first span

Given

$(d\delta_g(x_f) = 0)$

The derivates is zero where the deflection is its max or min

$x_{root.3} := \mathrm{Find}(x_f)$

Find the location of the maximum deflection

$x_{root.3} = 15.246\,m$

$\delta_{g.3} := -\delta_g(x_{root.3}) = -27.079 \cdot mm$

The maximum deflection in span 3

Maximum calculated deflection in each span:

$\delta_{calc.g.1} := \delta_{g.1} = -27.079 \cdot mm$

$\delta_{calc.g.mid} := \delta_{g.mid} = -8.944 \cdot mm$

$\delta_{calc.g.3} := \delta_{g.3} = -27.079 \cdot mm$

B 10.5 Test with an Unevenly Distributed Load

The continuous sheet is now tested for a unevenly distributed load. The location of the hinge remains. This is done to show the effect of a change in load distribution.

A load is applied to simulate the effect of snow drifting. Span 3 has an evenly distributed load. span 1 starts with zero load and the load than increases over the first span and the mid span until it reaches its max at support C.

$$q_{test.A} := 0\frac{kN}{m}$$ Load at support A

$$q_{test.D} := 5\frac{kN}{m}$$ Load at support D

$$q_{test}(x) := \frac{q_{test.D}}{3\cdot l}\cdot x$$ Unevenly distributed load in span 1 and midspan

$$q_{test.B} := q_{test}(l) = 1.667\cdot\frac{kN}{m}$$ Load at support B

$$q_{test.C} := q_{test}(2l) = 3.333\cdot\frac{kN}{m}$$ Load at support C

$$q_{test.joint.c.l} := q_{test}(l + a_{joint}) = 2.019\cdot\frac{kN}{m}$$ Load at the left joint

$$q_{test.joint.c.r} := q_{test}(l\cdot 2 - a_{joint}) = 2.981\cdot\frac{kN}{m}$$ Load at the right joint

$$M_{B.test} := \frac{q_{test.B}\cdot l^2}{12} + \frac{(q_{test.C} - q_{test.B})\cdot l^2}{30} = 7\cdot kN\cdot m$$ Moment at support B

$$M_{C.test} := \frac{q_{test.B}\cdot l^2}{12} + \frac{(q_{test.C} - q_{test.B})\cdot l^2}{20} = 8\cdot kN\cdot m$$ Moment at support C

$$M_{f.mid.test} := \min\left(\frac{M_{B.test}}{r_M}, \frac{M_{C.test}}{r_M}\right) = -4\cdot kN\cdot m$$ Max moment in the mid-span in order to keep zero moment at the location of the joint

$$R_{Bh.test} := \frac{q_{test.B}\cdot l}{2} + \frac{(q_{test.C} - q_{test.B})\cdot 3\cdot l}{20} = 6.5\cdot kN$$ Reaction force

$$R_{Cv.test} := \frac{q_{test.B}\cdot l}{2} + \frac{(q_{test.C} - q_{test.B})\cdot 7\cdot l}{20} = 8.5\cdot kN$$ Reaction force

Find the support moment which makes the the field moment zero at the joint:

$$q_{test.B2}(x_{BC}) := \frac{q_{test.C} - q_{test.B}}{l}\cdot x_{BC}$$

$$M_{Ed.BC.test}(x_{BC}) := M_{B.test} - R_{Bh.test}\cdot x_{BC} + q_{test.B}\cdot\frac{x_{BC}^2}{2} + q_{test.B2}(x_{BC})\cdot\frac{x_{BC}^2}{2\cdot 3}$$

$$dM_{Ed.BC.test}(x_{BC}) := \frac{d}{dx_{BC}}M_{Ed.BC.test}(x_{BC})$$ The derivates of the moment is the shear

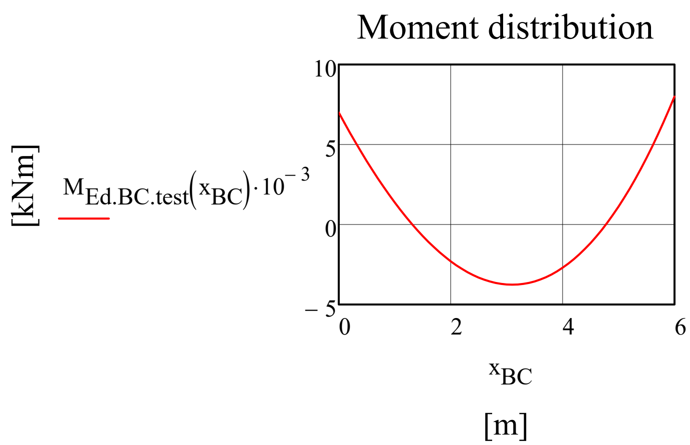

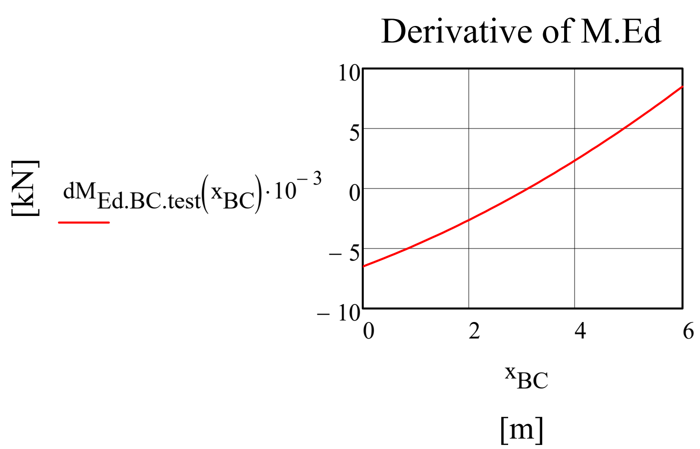

The joint is placed where the design moment is zero i.e. this will always be the location of the zero moment according to theory. First we check that the field moment correlates with the ratio.

$x_{max} := \frac{1}{2}$ — Approximate location where the derivates is zero

Given

$\left(dM_{Ed.BC.test}(x_{max}) = 0\right)$ — The derivates is zero where the moment is max

$x_{root} := \mathrm{Find}(x_{max})$ — Find the location of the zero derivates

$x_{root} = 3.099 \times 10^{3} \cdot mm$

$a_{max} := x_{root}$ — Distance from support B to max moment

$a_{joint} = 1.268 \times 10^{3} \cdot mm$ — Distance from support B to joint

comparing the moment from the evenly distributed and unevenly distributed load:

$M_{Ed.BC.test}(a_{max}) = -3.762 \cdot kN \cdot m$

$M_{Ed.BC}(a_{max}) = -5.532 \cdot kN \cdot m$

$M_{Ed.BC.test}(a_{joint}) = 0.192 \cdot kN \cdot m$

$M_{Ed.BC}(a_{joint}) = 0 \cdot kN \cdot m$

Moment at support needed in order to keep the moment zero at the joint, based on the relation between support moment and maximum moment in the middle of the span.:

$r_M \cdot M_{Ed.BC.test}(a_{max}) = 7.525 \cdot kN \cdot m$

$M_{B.test} = 7 \cdot kN \cdot m$ $\quad$ $M_{C.test} = 8 \cdot kN \cdot m$

Check the location of the zero moment:
Left side joint:

$x_{joint} := \frac{1}{4}$ — Approximate location where the derivates is zero

Given

$\left(M_{Ed.BC.test}(x_{joint}) = 0\right)$ — The joint is placed where the moment is zero

$x_{root} := \mathrm{Find}(x_{joint})$ — Find the location of the zero moment

$a_{test.l} := x_{root} = 1.315 \times 10^3 \cdot mm$ — Distance from support to left zero moment

$a_{joint} = 1.268 \times 10^3 \cdot mm$ — The distances do not correlates!

Right side joint:

$x_{joint} := \frac{31}{4}$ — Approximate location where the derivates is zero

Given

$\left(M_{Ed.BC.test}(x_{joint}) = 0\right)$ — The joint is placed where the moment is zero

$x_{root} := \mathrm{Find}(x_{joint})$ — Find the location of the zero moment

$a_{test.r} := x_{root} = 4.774 \times 10^3 \cdot mm$ — Distance from support to right zero moment

$l - a_{joint} = 4.732 \times 10^3 \cdot mm$ — The distances do not correlates!

Calculating the global moment distribution for the tested loads:

$$R_{A.test} := -M_{B.test} \cdot \frac{1}{1} + q_{test.B} \cdot \frac{1}{6} = 0.5 \cdot kN$$

$$R_{Bv.test} := M_{B.test} \cdot \frac{1}{1} + q_{test.B} \cdot \frac{1}{3} = 4.5 \cdot kN$$

$$R_{B.test} := R_{Bv.test} + R_{Bh.test} = 11 \cdot kN$$

$$R_{Ch.test} := M_{C.test} \cdot \frac{1}{1} + q_{test.C} \cdot \frac{1}{2} + \left(q_{test.D} - q_{test.C}\right) \cdot \frac{1}{6} = 13 \cdot kN$$

$$R_{C.test} := R_{Ch.test} + R_{Cv.test} = 21.5 \cdot kN$$

$$R_{D.test} := -M_{C.test} \cdot \frac{1}{1} + q_{test.C} \cdot \frac{1}{2} + \left(q_{test.D} - q_{test.C}\right) \cdot \frac{1}{3} = 12 \cdot kN$$

Check the reaction forces:

$$R_{A.test} + R_{B.test} + R_{C.test} + R_{D.test} = \frac{q_{test.D} \cdot 31}{2} = 1$$

$$x := 0m, 0.1m .. L$$

$$M_{Ed.g.test}(x) := \begin{cases} -R_{A.test} \cdot x + q_{test}(x) \cdot \dfrac{x^2}{3 \cdot 2} & \text{if } 0 \le x \le 1 \\ -R_{A.test} \cdot x + q_{test}(x) \cdot \dfrac{x^2}{3 \cdot 2} - R_{B.test} \cdot (x - 1) & \text{if } 1 \le x \le 21 \\ -R_{A.test} \cdot x + q_{test}(x) \cdot \dfrac{x^2}{3 \cdot 2} - R_{B.test} \cdot (x - 1) - R_{C.test} \cdot (x - 21) & \text{if } 21 \le x \le L \end{cases}$$

$$dM_{Ed.g.test}(x) := \frac{d}{dx} M_{Ed.g.test}(x)$$

The derivates of the moment is the shear

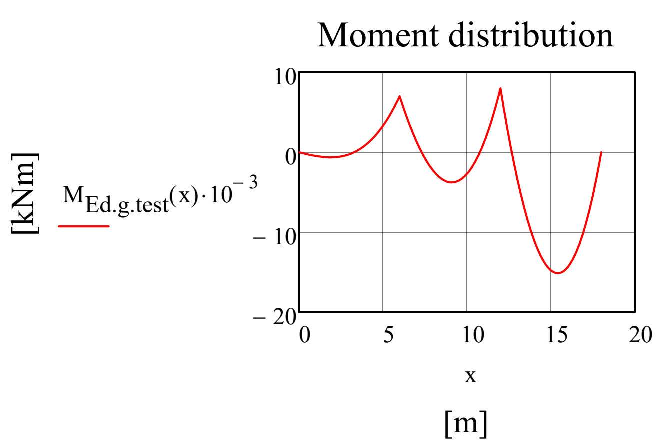

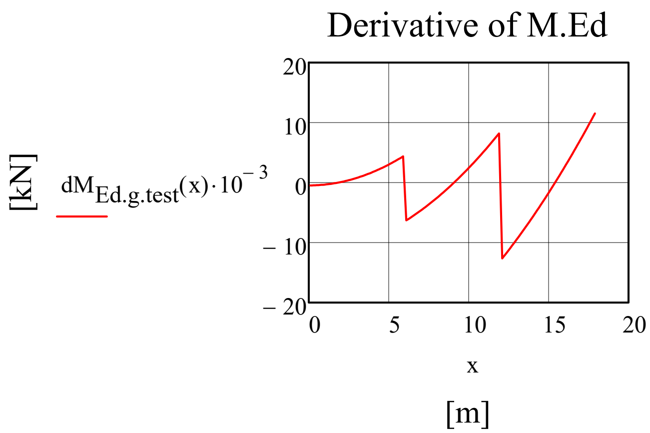

Location of the zero moment in the mid-span:

$x_{joint} := 1 + a_{joint}$ — Approximate location where the moment is zero

Given

$\left(M_{Ed.g.test}\left(x_{joint}\right) = 0\right)$ — The joint is placed where the moment is zero

$x_{root.test} := \text{Find}\left(x_{joint}\right)$ — Find the location of the zero moment

$x_{root.test} = 7.315\,\text{m}$

$M_{zero.test} := M_{Ed.g.test}\left(x_{root.test}\right) = -5.457 \times 10^{-15} \cdot \text{kN} \cdot \text{m}$ — The moment at the calculated location

$x_{root.test} = 7.315\,\text{m}$

$a_{joint} + 1 = 7.268\,\text{m}$ — They do not correlate!

Maximum field moment, first span:

$x_f := \frac{1}{2}$ — Approximate location where the derivates is zero in the first span

Given

$\left(dM_{Ed.g.test}\left(x_f\right) = 0\right)$ — The derivates is zero where the moment is its max or min

$x_{root.test.1} := \text{Find}\left(x_f\right)$ — Find the location of the maximum moment

$x_{root.test.1} = 1.897\,\text{m}$

$M_{Ed.g.max.test.1} := M_{Ed.g.test}\left(x_{root.test.1}\right) = -0.632 \cdot \text{kN} \cdot \text{m}$ — The maximum moment

Maximum field moment, mid-span:

$x_f := 1.5l$

Approximate location where the derivates is zero in the second span

Given

$\left(dM_{Ed.g.test}(x_f) = 0\right)$

The derivates is zero where the moment is its max or min

$x_{root.test.mid} := Find(x_f)$

Find the location of the maximum moment

$x_{root.test.mid} = 9.099\,m$

$M_{Ed.g.max.test.mid} := M_{Ed.g}(x_{root.test.mid}) = -5.532 \cdot kN \cdot m$

The maximum moment

Maximum field moment, third span:

$x_f := 2.5l$

Approximate location where the derivates is zero in the second span

Given

$\left(dM_{Ed.g.test}(x_f) = 0\right)$

The derivates is zero where the moment is its max or min

$x_{root.test.3} := Find(x_f)$

Find the location of the maximum moment

$x_{root.test.3} = 15.414\,m$

$M_{Ed.g.max.test.3} := M_{Ed.g}(x_{root.test.3}) = -11.549 \cdot kN \cdot m$

The maximum moment

Compare to the capacity according to Lindab:

$M_{Ed.g.max.test.1} \le M_{k.f} \cdot b_s = 1$ $\quad$ $M_{B.test} \le M_{k.s} \cdot b_s = 1$

$M_{Ed.g.max.test.mid} \le M_{k.f} \cdot b_s = 1$ $\quad$ $M_{C.test} \le M_{k.s} \cdot b_s = 1$

$M_{Ed.g.max.test.3} \le M_{k.f} \cdot b_s = 1$

10.6 Stress Distribution Unevenly Distributed Load

$$\sigma_{x.g.test}(x) := \frac{-M_{Ed.g.test}(x)}{W_{el.g}}$$

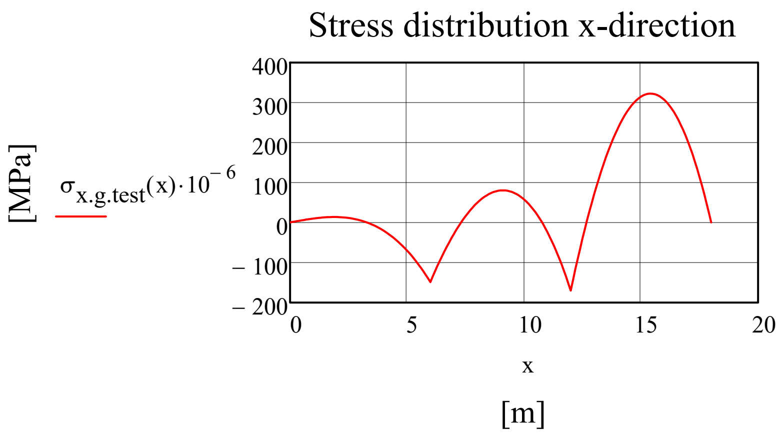

$d\sigma_{x.g.test}(x) := \frac{d}{dx}\sigma_{x.g.test}(x)$ — The derivates of the moment is the shear

Stress in span 1:

$x_{max.g1.test} := \frac{1}{2}$ — Approximate location where the derivates is zero

Given

$\left(d\sigma_{x.g.test}(x_{max.g1.test}) = 0\right)$ — The max where the derivates is zero

$x_{g.max.1.test} := \mathrm{Find}(x_{max.g1.test})$ — Find the location of the zero derivates

$x_{g.max.1.test} = 1.897\ \mathrm{m}$

$\sigma_{x.g.max.1.test} := \sigma_{x.g.test}(x_{g.max.1.test}) = 13.479\cdot\mathrm{MPa}$ — The maximum stress in span 1

Stress in mid-span:

$x_{max.gmid.test} := 1 + \frac{1}{2}$ — Approximate location where the derivates is zero

Given

$\left(d\sigma_{x.g.test}(x_{max.gmid.test}) = 0\right)$ — The max where the derivates is zero

$x_{g.max.mid.test} := \mathrm{Find}(x_{max.gmid.test})$ — Find the location of the zero derivates

$x_{g.max.mid.test} = 9.099\ \mathrm{m}$

$\sigma_{x.g.max.mid.test} := \sigma_{x.g}(x_{g.max.mid.test}) = 117.893\cdot\mathrm{MPa}$ — The maximum stress in mid-span

Stress in span 3:

$x_{max.g3.test} := 21 + \frac{1}{2}$ — Approximate location where the derivates is zero

Given

$\left(d\sigma_{x.g.test}\left(x_{max.g3.test}\right) = 0\right)$

The max where the derivates is zero

$x_{g.max.3.test} := \text{Find}\left(x_{max.g3.test}\right)$

Find the location of the zero derivates

$x_{g.max.3.test} = 15.414\,m$

$\sigma_{x.g.max.3.test} := \sigma_{x.g}\left(x_{g.max.3.test}\right) = 246.134 \cdot MPa$

The maximum stress in mid-span

Stress at supports:

$\sigma_{x.g.B.test} := \sigma_{x.g.test}(l) = -149.186 \cdot MPa$

$\sigma_{x.g.C.test} := \sigma_{x.g.test}(2 \cdot l) = -170.498 \cdot MPa$

B 10.7 Comparing with Values from Abaqus

Comparing the reaction forces:

$R_{A.Ab.test} := 556.957N = 0.557 \cdot kN$

$R_{A.test} = 0.5 \cdot kN$

$R_{B.Ab.test} := 10828.1N = 10.828 \cdot kN$

$R_{B.test} = 11 \cdot kN$

$R_{C.Ab.test} := 21680.3N = 21.68 \cdot kN$

$R_{C.test} = 21.5 \cdot kN$

$R_{D.Ab.test} := 11954.5N = 11.954 \cdot kN$

$R_{D.test} = 12 \cdot kN$

$R_{A.Ab.test} + R_{B.Ab.test} + R_{C.Ab.test} + R_{D.Ab.test} = 45.02 \cdot kN$

$R_{A.test} + R_{B.test} + R_{C.test} + R_{D.test} = 45 \cdot kN$

$$\frac{q_{test.D} \cdot 3l}{2} = 45 \cdot kN$$

Comparing the moments:

$M_{B.Ab.test} := 6.65537kN \cdot m$

$M_{B.test} = 7 \cdot kN \cdot m$

$M_{C.Ab.test} := 8.33612kN \cdot m$

$M_{C.test} = 8 \cdot kN \cdot m$

$M_{AB.Ab.test} := -0.743554kN \cdot m$

$M_{AB.test} := M_{Ed.g.max.test.1} = -0.632 \cdot kN \cdot m$

$M_{BC.Ab.test} := -3.74824kN \cdot m$

$M_{BC.test} := M_{Ed.g.max.test.mid} = -5.532 \cdot kN \cdot m$

$M_{CD.Ab.test} := -14.9966kN \cdot m$ $\qquad$ $M_{CD.test} := M_{Ed.g.max.test.3} = -11.549 \cdot kN \cdot m$

Comparing the stresses at support B and C:

$\sigma_{B.Ab.test} := -123.2MPa$ $\qquad$ $\sigma_{x.g.B.test} = -149.186 \cdot MPa$

$$\sigma_{B.Ab.calc.test} := \frac{-M_{B.Ab.test}}{W_{el.g.Ab}} = -141.978 \cdot MPa$$

$\sigma_{C.Ab.test} := -154.3MPa$ $\qquad$ $\sigma_{x.g.C.test} = -170.498 \cdot MPa$

$$\sigma_{C.Ab.calc.test} := \frac{-M_{C.Ab.test}}{W_{el.g.Ab}} = -177.833 \cdot MPa$$

Comparing the stresses at the location of the joint:

$\sigma_{joint.Ab.test.l} := -7.29816MPa$ $\qquad$ $\sigma_{joint.test.l} := \sigma_{x.g.test}(l + a_{joint}) = -4.102 \cdot MPa$

$\sigma_{joint.Ab.test.r} := 8.2048MPa$ $\qquad$ $\sigma_{joint.test.r} := \sigma_{x.g.test}(2l - a_{joint}) = 4.102 \cdot MPa$

Placement of joints vs. the location of the zero moment:

$l + a_{joint} = 7.268\,m$ $\qquad$ $a_{zero.l.Ab}$ $\qquad$ $l + a_{test.l} = 7.315\,m$

$2 \cdot l - a_{joint} = 10.732\,m$ $\qquad$ $a_{zero.r.Ab}$ $\qquad$ $l + a_{test.r} = 10.774\,m$

B 10.8 Deflection of the Tested Sheet

Deflection of the 3-span continuous sheet, distributed loads:

$q_{test.A} = 0 \cdot \frac{kN}{m}$ $\qquad$ $q_{test.B} = 1.667 \cdot \frac{kN}{m}$ $\qquad$ $q_{test.C} = 3.333 \cdot \frac{kN}{m}$ $\qquad$ $q_{test.D} = 5 \cdot \frac{kN}{m}$

$l = 6\,m$

$R_{A.test} = 0.5 \cdot kN$ $\qquad$ $M_{B.test} = 7 \cdot kN \cdot m$

$R_{B.test} = 11 \cdot kN$ $\qquad$ $M_{C.test} = 8 \cdot kN \cdot m$

$R_{C.test} = 21.5 \cdot kN$

$E_s = 2.1 \times 10^5 \cdot MPa$

$I_g = 6.648 \times 10^6 \cdot mm^4$

$x_{test} := 0m, 0.1m .. L$

$a_m(x_{test}) := x_{test} - l$ $\qquad$ $a_3(x_{test}) := x_{test} - l \cdot 2$

$$\delta_{test}(x_{test}) := \begin{cases} \left[\dfrac{q_{test.B}\cdot x_{test}\cdot l^3}{360\cdot E_s\cdot I_g}\cdot\left(7 - \dfrac{10x_{test}^{\ 2}}{l^2} + \dfrac{x_{test}^{\ 4}\cdot 3}{l^4}\right)\ldots + \dfrac{-M_{B.test}\cdot x_{test}\cdot l}{6\cdot E_s\cdot I_g}\cdot\left(1 - \dfrac{x_{test}^{\ 2}}{l^2}\right)\right] & \text{if } 0 \le x_{test} \le l \\ \left[\dfrac{q_{test.B}\cdot a_m(x_{test})\cdot l^3}{24\cdot E_s\cdot I_g}\cdot\left(1 - \dfrac{a_m(x_{test})}{l}\right)^2 \ldots + \dfrac{(q_{test.C} - q_{test.B})\cdot a_m(x_{test})\cdot l^3}{120\cdot E_s\cdot I_g}\cdot\left(\dfrac{2\cdot a_m(x_{test})}{l} - \dfrac{3\, a_m(x_{test})^2}{l^2} + \dfrac{a_m(x_{test})^4}{l^4}\right)\right] & \text{if } l \le \\ \left[\dfrac{q_{test.C}\cdot a_3(x_{test})\cdot l^3}{24\cdot E_s\cdot I_g}\cdot\left(1 - \dfrac{2\, a_3(x_{test})^2}{l^2} + \dfrac{a_3(x_{test})^3}{l^3}\right)\ldots + \dfrac{(q_{test.D} - q_{test.C})\cdot a_3(x_{test})\cdot l^3}{360\cdot E_s\cdot I_g}\cdot\left(7 - \dfrac{10\, a_3(x_{test})^2}{l^2} + \dfrac{a_3(x_{test})^4\cdot 3}{l^4}\right)\ldots + \dfrac{-M_{C.test}\cdot(1 - a_3(x_{test}))\cdot l}{6\cdot E_s\cdot I_g}\cdot\left[1 - \dfrac{(1 - a_3(x_{test}))^2}{l^2}\right]\right] & \text{if } 2l \le x_{test} \le \end{cases}$$

$$d\delta_{test}(x_{test}) := \frac{d}{dx_{test}}\delta_{test}(x_{test})$$

The derivates of the

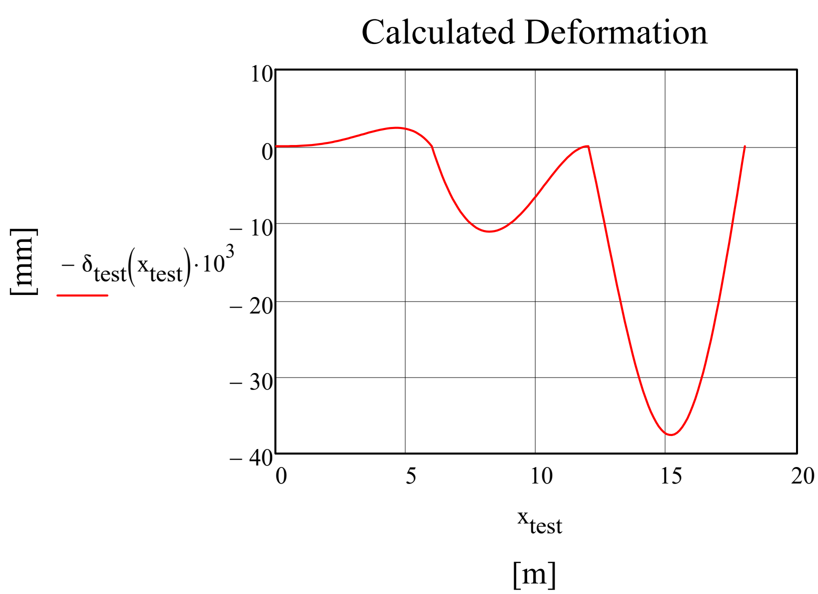

Maximum deflection first span:

$x_f := \frac{1}{2}$

Approximate location where the derivates is zero in the first span

Given

$\left(d\delta_{test}\left(x_f\right) = 0\right)$

The derivates is zero where the deflection is its max or min

$x_{root.test.1} := \mathrm{Find}\left(x_f\right)$

Find the location of the maximum deflection

$x_{root.test.1} = 1.806 \times 10^{-3}\,m$

$\delta_{test.1} := -\delta_{test}\left(x_{root.test.1}\right) = 3.514 \times 10^{-10}\cdot mm$

The maximum deflection in span 1

Maximum deflection first span:

$x_f := L - \frac{1}{2}$

Approximate location where the derivates is zero in the first span

Given

$\left(d\delta_{test}\left(x_f\right) = 0\right)$

The derivates is zero where the deflection is its max or min

$x_{root.test.3} := \mathrm{Find}\left(x_f\right)$

Find the location of the maximum deflection

$x_{root.test.3} = 15.164\,m$

$\delta_{test.3} := -\delta_{test}\left(x_{root.test.3}\right) = -37.613\cdot mm$

The maximum deflection in span 3

Maximum calculated deflection in each span:

$\delta_{calc.test.1} := -\delta_{test}\left(x_{root.test.1}\right) = 3.514 \times 10^{-10}\cdot mm$

$\delta_{calc.test.mid} := -\delta_{test}\left(x_{root.test.mid}\right) = -9.806\cdot mm$

$\delta_{calc.test.3} := -\delta_{test}\left(x_{root.test.3}\right) = -37.613\cdot mm$

B 11 Global Analysis of a Gerber system - Cantilever

The sheet is also analysed with regard to the splice acting like a hinge. This gives a more relevant stress distribution.

$L = 18\,m$	Total length, 3 spans
$l = 6\,m$	Length of span
$a_{joint} = 1.268\,m$	Location of joint in the mid-span

B 11.1 Calculating the Moment Distribution for a Cantilever Model:

$s_k := 2.4\frac{kN}{m}$ $\qquad g_s := \rho_{sheet} \cdot g \cdot b_s = 0.118 \cdot \frac{kN}{m}$

$q_d := 0.89 \cdot 1.35 \cdot g_s + 1.5 \cdot s_k = 3.741 \cdot \frac{kN}{m}$

$q_{d.c} := 3.7\frac{kN}{m} = 3.7 \cdot \frac{N}{mm}$

Calculating the support moment by including the hinges in the mid-span:

$P_1 := \frac{q_{d.c} \cdot (l - 2 \cdot a_{joint})}{2} = 6.409 \cdot kN$	Point load acting at the end of the cantilever due to mid sheet
$M_{B.c} := q_{d.c} \cdot \frac{a_{joint}^2}{2} + a_{joint} \cdot P_1 = 11.1 \cdot kN \cdot m$	Support moment B
$M_{C.c} := M_{B.c}$	Support moment C

Calculating the reaction forces:

$R_{Bh.c} := q_{d.c} \cdot a_{joint} + P_1 = 11.1 \cdot kN$	Partial reaction force support B
$R_{Cv.c} := R_{Bh.c}$	Partial reaction force support C
$R_{A.c} := -M_{B.c} \cdot \frac{1}{l} + q_{d.c} \cdot \frac{l}{2} = 9.25 \cdot kN$	Reaction force support A
$R_{Bv.c} := M_{B.c} \cdot \frac{1}{l} + q_{d.c} \cdot \frac{l}{2} = 12.95 \cdot kN$	Partial reaction force support B
$R_{B.c} := R_{Bv.c} + R_{Bh.c} = 24.05 \cdot kN$	Reaction force support B
$R_{C.c} := R_{B.c}$	Reaction force support C

$R_{D.c} := R_{A.c}$

Reaction force support D

$q_{d.c} \cdot L = 66.6 \cdot kN$

$R_{A.c} + R_{B.c} + R_{C.c} + R_{D.c} = 66.6 \cdot kN$

Angle of deflection:

$$m_2 := \frac{P_1 \cdot a_{joint}^2}{2 \cdot E_s \cdot I_g} + \frac{q_{d.c} \cdot a_{joint}^3}{6 \cdot E_s \cdot I_g} = 0.263 \cdot deg$$

Calculating the global moment distribution:

$x := 0m, 0.1m .. L$

$$M_{Ed.g.c}(x) := \begin{cases} -R_{A.c} \cdot x + q_{d.c} \cdot \frac{x^2}{2} & \text{if } 0 \le x \le 1 \\ -R_{A.c} \cdot x + q_{d.c} \cdot \frac{x^2}{2} - R_{B.c} \cdot (x - l) & \text{if } 1 \le x \le 1 + a_{joint} \\ q_{d.c} \cdot \frac{(x - 1 - a_{joint})^2}{2} - P_1 \cdot (x - 1 - a_{joint}) & \text{if } 1 + a_{joint} \le x \le 21 - a_{joint} \\ -R_{A.c} \cdot x + q_{d.c} \cdot \frac{x^2}{2} - R_{B.c} \cdot (x - l) & \text{if } 21 - a_{joint} \le x \le 21 \\ -R_{A.c} \cdot x + q_{d.c} \cdot \frac{x^2}{2} - R_{B.c} \cdot (x - l) - R_{C.c} \cdot (x - 2l) & \text{if } 21 \le x \le L \end{cases}$$

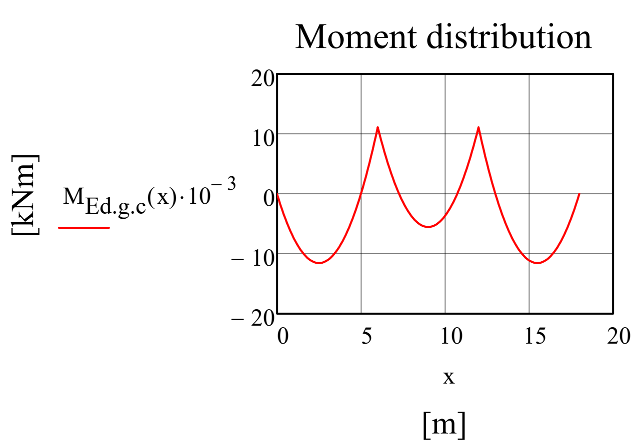

$dM_{Ed.g.c}(x) := \frac{d}{dx} M_{Ed.g}(x)$

The derivates of the moment is the shear

$V_{Ed.g.c}(x) := dM_{Ed.g}(x)$

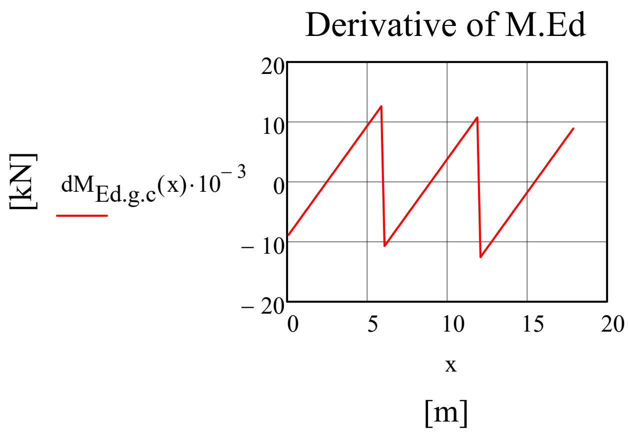

Check the moment at the joint:

$x_{joint.c} := 1 + a_{joint}$

Approximate location where the moment is zero

Given

$\left(M_{Ed.g.c}\left(x_{joint.c}\right) = 0\right)$

The joint is placed where the moment is zero

$x_{root2.c} := \text{Find}\left(x_{joint.c}\right)$

Find the location of the zero moment

$x_{root2.c} = 7.268\,m$

$M_{zero.c} := M_{Ed.g.c}\left(x_{root2.c}\right) = -2.846 \times 10^{-15} \cdot kN \cdot m$

The moment at the calculated location

$x_{root2.c} - 1 = 1.268\,m$ $\qquad a_{joint} = 1.268\,m$

They correlate!

Maximum field moment, first span:

$x_{f.c} := \frac{1}{2}$

Approximate location where the derivates is zero in the first span

Given

$\left(dM_{Ed.g.c}\left(x_{f.c}\right) = 0\right)$

The derivates is zero where the moment is its max or min

$x_{root.f.c} := \text{Find}\left(x_{f.c}\right)$

Find the location of the maximum moment

$x_{root.f.c} = 2.5\,m$

$M_{Ed.g.max.1.c} := M_{Ed.g.c}\left(x_{root.f.c}\right) = -11.563 \cdot kN \cdot m$

The maximum moment

$dx_{zero} := x_{root.f.c}$ The location of the zero derivates

Maximum field moment, mid-span:

$x_{f.c} := 1.5l$ Approximate location where the derivates is zero in the second span

Given

$\left(dM_{Ed.g.c}\left(x_{f.c}\right) = 0\right)$ The derivates is zero where the moment is its max or min

$x_{root.f.c} := Find\left(x_{f.c}\right)$ Find the location of the maximum moment

$x_{root.f.c} = 9\,m$

$M_{Ed.g.max.mid.c} := M_{Ed.g.c}\left(x_{root.f.c}\right) = -5.55 \cdot kN \cdot m$ The maximum moment

B 11.2 Stress Distribution Evenly Distributed Load

$z_{tp.1} = 144.781 \cdot mm$ $z_{tp.sc.1} = 141.689 \cdot mm$ $z_{g.Ab} := 141.54mm$

$A_{g.1} = 1.37 \times 10^{3} \cdot mm^{2}$ $A_{g.sc.1} = 1.4 \times 10^{3} \cdot mm^{2}$ $A_{g.Ab} := \dfrac{10214851mm^{3}}{7.268m} = 1.405 \times 10^{3} \cdot mm^{2}$

The difference is assumed to be with regard to how the arbitrary 3D beam element model has be computed in Abaqus, with sharp corners. Therefore we assume a calculated sectional modulus based on the model with sharp corners.

$I_{g} = 6.648 \times 10^{6} \cdot mm^{4}$

$W_{el.g} = 4.692 \times 10^{4} \cdot mm^{3}$

The Stress Distribution Along the Sheet:

$$\sigma_{x.g.c}(x) := \frac{-M_{Ed.g.c}(x)}{W_{el.g}}$$

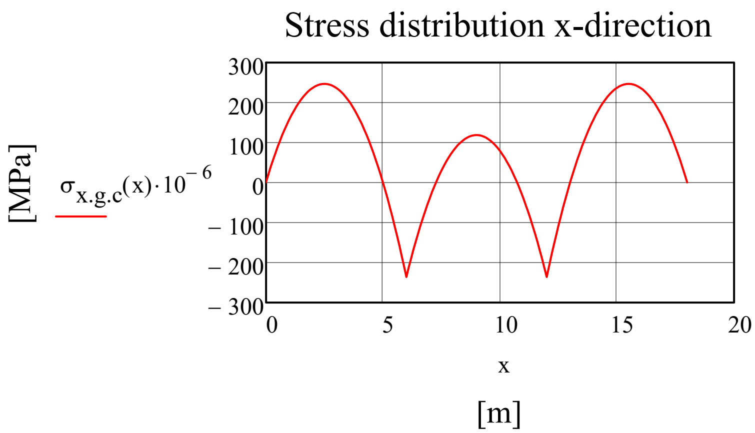

$d\sigma_{x.g.c}(x) := \frac{d}{dx}\sigma_{x.g.c}(x)$

The derivates of the moment is the shear

Stress in span 1:

$x_{max.g1.c} := \frac{1}{2}$

Approximate location where the derivates is zero

Given

$\left(d\sigma_{x.g.c}\left(x_{max.g1.c}\right) = 0\right)$

The max where the derivates is zero

$x_{g.max.1.c} := \mathrm{Find}\left(x_{max.g1.c}\right)$

Find the location of the zero derivates

$x_{g.max.1.c} = 2.5\,m$

$\sigma_{x.g.max.1.c} := \sigma_{x.g.c}\left(x_{g.max.1.c}\right) = 246.424 \cdot MPa$

The maximum stress in span 1

Stress in mid-span:

$x_{max.gmid.c} := 1 + \frac{1}{2}$

Approximate location where the derivates is zero

Given

$\left(d\sigma_{x.g.c}\left(x_{max.gmid.c}\right) = 0\right)$

The max where the derivates is zero

$x_{g.max.mid.c} := \mathrm{Find}\left(x_{max.gmid.c}\right)$

Find the location of the zero derivates

$x_{g.max.mid.c} = 9\,m$

$\sigma_{x.g.max.mid.c} := \sigma_{x.g.c}\left(x_{g.max.mid.c}\right) = 118.283 \cdot MPa$

The maximum stress in mid-span

Stress at supports:

$\sigma_{x.g.B.c} := \sigma_{x.g}(l) = -236.567 \cdot MPa$

$\sigma_{x.g.C.c} := \sigma_{x.g}(2 \cdot l) = -236.567 \cdot MPa$

B 11.3 Comparing with Values from Abaqus

Comparing the reaction forces:

$R_{A.Ab.c} := R_{A.Ab} = 9.257 \cdot kN$ $\quad R_{A.c} = 9.25 \cdot kN$

$R_{B.Ab.c} := R_{B.Ab} = 24.055 \cdot kN$ $\quad R_{B.c} = 24.05 \cdot kN$

$R_{C.Ab.c} := R_{C.Ab} = 24.055 \cdot kN$ $\quad R_{C.c} = 24.05 \cdot kN$

$R_{D.Ab.c} := R_{D.Ab} = 9.257 \cdot kN$ $\quad R_{D.c} = 9.25 \cdot kN$

$2 \cdot R_{A.Ab.c} + 2 \cdot R_{B.Ab.c} = 66.624 \cdot kN$

$2 \cdot R_{A.c} + 2 \cdot R_{B.c} = 66.6 \cdot kN$

$q_{d.c} \cdot L = 66.6 \cdot kN$

Comparing the moments:

$M_{B.c.Ab} := M_{B.Ab} = 11.095 \cdot kN \cdot m$ $\quad M_{B.c} = 11.1 \cdot kN \cdot m$

$M_{AB.c.Ab} := M_{AB.Ab} = -11.564 \cdot kN \cdot m$ $\quad M_{AB.c} := M_{Ed.g.max.1.c} = -11.563 \cdot kN \cdot m$

$M_{BC.c.Ab} := M_{BC.Ab} = -5.549 \cdot kN \cdot m$ $\quad M_{BC.c} := M_{Ed.g.max.mid.c} = -5.55 \cdot kN \cdot m$

Comparing the stresses at the supports:

$\sigma_{B.Ab} = -205.4 \cdot MPa$ $\quad \sigma_{x.g.B.c} = -236.567 \cdot MPa$

Comparing the stresses in the joint:

$\sigma_{joint.Ab} = 11.143 \cdot MPa$ $\quad l + a_{joint} = 7.268\,m$

$\sigma_{joint.c} := \sigma_{x.g.c}\left(l + a_{joint}\right) = 6.065 \times 10^{-14} \cdot MPa$

B 11.4 Deflection of the Sheet with Regard to Cantilever

Deflection of the 3-span continuous sheet, distributed loads:

$q_{d.c} = 3.7 \cdot \frac{kN}{m}$

$l = 6\,m$

$a_{joint} = 1.268 \times 10^{3} \cdot mm$

$R_{A.c} = 9.25 \cdot kN$ $\qquad M_{B.c} = 11.1 \cdot kN \cdot m$

$R_{B.c} = 24.05 \cdot kN$ $\qquad M_{C.c} = 11.1 \cdot kN \cdot m$

$R_{C.c} = 24.05 \cdot kN$

$E_s = 2.1 \times 10^5 \cdot MPa$

$I_g = 6.648 \times 10^6 \cdot mm^4$

Deflection of left part cantilever, based on two integrals of the moment:

$$EI \frac{d^2 y}{dx^2} = R_{A.c} \cdot x - \frac{q_{d.c} \cdot x^2}{2} + R_{B.c} \cdot (x - l)$$

$$EI \frac{d\,y}{dx} = R_{A.c} \cdot \frac{x^2}{2} - \frac{q_{d.c} \cdot x^3}{6} + \frac{R_{B.c} \cdot (x - l)^2}{2} + C_1$$

$$EI\,y(x) = R_{A.c} \cdot \frac{x^3}{6} - \frac{q_{d.c} \cdot x^4}{24} + \frac{R_{B.c} \cdot (x - l)^3}{6} + C_1 \cdot x + C_2$$

Boundary conditions y(0)=0 and y(l)=0 gives the valus for C1 and C2

$C_2 := 0$

$$C_1 := \frac{-C_2 - \left[R_{A.c} \cdot \frac{l^3}{6} - \frac{q_{d.c} \cdot l^4}{24} + \frac{R_{B.c} \cdot (l - l)^3}{6}\right]}{l} = -22.2 \cdot kN \cdot m^2$$

Global deformation:

The deflection of the beam is based on the two side sheet acting as cantilevers and the middle sheet as simply supported.

$a_m(x) := x - l$ $\qquad a_3(x) := x - 2l$ $\qquad a_c(x) := x - l - a_{joint}$

$x := 0m, 0.1m .. L$

$$\delta_{g.c}(x) := \begin{cases} \dfrac{\left(R_{A.c}\cdot\dfrac{x^3}{6} - \dfrac{q_{d.c}\cdot x^4}{24} + C_1\cdot x + C_2\right)}{E_s\cdot I_g} & \text{if } 0 \le x \le l \\[2ex] \dfrac{\left[R_{A.c}\cdot\dfrac{x^3}{6} - \dfrac{q_{d.c}\cdot x^4}{24} + \dfrac{R_{B.c}\cdot(x-l)^3}{6} + C_1\cdot x + C_2\right]}{E_s\cdot I_g} & \text{if } l \le x \le l + a_{joint} \\[2ex] \left[\dfrac{R_{A.c}\cdot\dfrac{\left(l+a_{joint}\right)^3}{6} - \dfrac{q_{d.c}\cdot\left(l+a_{joint}\right)^4}{24} \ldots + \dfrac{R_{B.c}\cdot\left(l+a_{joint}-l\right)^3}{6} + C_1\cdot\left(l+a_{joint}\right) + C_2}{E_s\cdot I_g} \ldots + \dfrac{-q_{d.c}\cdot a_c(x)\cdot\left(l-2\cdot a_{joint}\right)^3}{24\cdot E_s\cdot I_g}\cdot\left[1 - \dfrac{2\cdot a_c(x)^2}{\left(l-2a_{joint}\right)^2} + \dfrac{a_c(x)^3}{\left(l-2a_{joint}\right)^3}\right]\right] & \text{if } l + a_{joint} \le x \le 2l \\[2ex] \dfrac{\left[R_{D.c}\cdot\dfrac{(L-x)^3}{6} - \dfrac{q_{d.c}\cdot(L-x)^4}{24} + \dfrac{R_{C.c}\cdot[(L-x)-l]^3}{6} + C_1\cdot(L-x) + C_2\right]}{E_s\cdot I_g} & \text{if } 2l - a_{joint} \\[2ex] \dfrac{\left[R_{D.c}\cdot\dfrac{(L-x)^3}{6} - \dfrac{q_{d.c}\cdot(L-x)^4}{24} + C_1\cdot(L-x) + C_2\right]}{E_s\cdot I_g} & \text{if } 2l \le x \le L \end{cases}$$

Deformation of Sheet Considering Cantilever

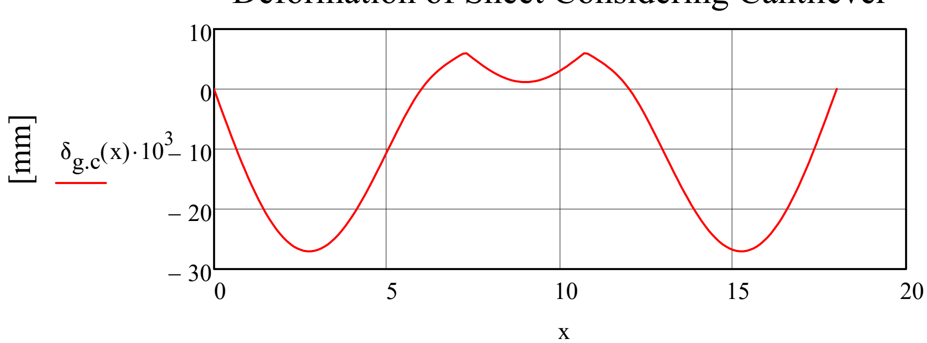

[m]

$$d\delta_{g.c}(x) := \frac{d}{dx}\delta_{g.c}(x)$$

The derivates of the deflection

Maximum deflection first span:

$x_{f.c} := \frac{1}{2}$

Approximate location where the derivates is zero in the first span

Given

The derivates is zero where the deflection is its max or min

$\left(d\delta_{g.c}\left(x_{f.c}\right) = 0\right)$

$x_{root.1.c} := \text{Find}\left(x_{f.c}\right)$

Find the location of the maximum deflection

$x_{root.1.c} = 2.754\ \text{m}$

$\delta_{g.1.c} := \delta_{g.c}\left(x_{root.1.c}\right) = -27.079 \cdot \text{mm}$

The maximum deflection in span 1

Maximum deflection mid-span:

$x_{f.c} := \frac{L}{2}$

Approximate location where the derivates is zero in the first span

Given

The derivates is zero where the deflection is its max or min

$\left(d\delta_{g.c}\left(x_{f.c}\right) = 0\right)$

$x_{root.mid.c} := \text{Find}\left(x_{f.c}\right)$

Find the location of the maximum deflection

$x_{root.mid.c} = 9\ \text{m}$

$\delta_{g.mid.c} := \delta_{g.c}\left(x_{root.mid.c}\right) = 1.137 \cdot \text{mm}$

The maximum deflection in span 1

Maximum deflection third span:

$x_{f.c} := L - \frac{1}{2}$

Approximate location where the derivates is zero in the first span

Given

The derivates is zero where the deflection is its max or min

$\left(d\delta_{g.c}\left(x_{f.c}\right) = 0\right)$

$x_{root.3.c} := \text{Find}\left(x_{f.c}\right)$

Find the location of the maximum deflection

$x_{root.3.c} = 15.246\ \text{m}$

$\delta_{g.3.c} := \delta_{g.c}\left(x_{root.3.c}\right) = -27.079 \cdot \text{mm}$

The maximum deflection in span 3

Maximum calculated deflection in each span:

$\delta_{calc.g.1.c} := \delta_{g.1} = -27.079 \cdot \text{mm}$

$\delta_{calc.g.mid.c} := \delta_{g.mid} = -8.944 \cdot mm$

$\delta_{calc.g.3.c} := \delta_{g.3} = -27.079 \cdot mm$

B 11.5 Test with an Unevenly Distributed Load on Cantilever

The continuous sheet is now tested for a unevenly distributed load. The location of the hinge remains. This is done to show the effect of a change in load distribution.

A load is applied to simulate the effect of snow drifting. Span 3 has an evenly distributed load. span 1 starts with zero load and the load than increases over the first span and the mid span until it reaches its max at support C.

$q_{test.A.c} := 0 \frac{kN}{m}$ Load at support A

$q_{test.D.c} := 5 \frac{kN}{m}$ Load at support D

$q_{test.c}(x) := \frac{q_{test.D.c}}{3 \cdot l} \cdot x$ Unevenly distributed load in span 1 and midspan

$q_{test.B.c} := q_{test.c}(l) = 1.667 \cdot \frac{kN}{m}$ Load at support B

$q_{test.C.c} := q_{test.c}(2l) = 3.333 \cdot \frac{kN}{m}$ Load at support C

$q_{test.joint.c.l} := q_{test.c}\left(l + a_{joint}\right) = 2.019 \cdot \frac{kN}{m}$ Load at the left joint

$q_{test.joint.c.r} := q_{test.c}\left(l \cdot 2 - a_{joint}\right) = 2.981 \cdot \frac{kN}{m}$ Load at the left joint

Point load on the joint:

$$P_{test.l} := \frac{q_{test.joint.c.l} \cdot \left(l - 2 \cdot a_{joint}\right)}{2} + \frac{\left(q_{test.joint.c.r} - q_{test.joint.c.l}\right) \cdot \left(l - 2 \cdot a_{joint}\right)}{6} = 4.052 \cdot kN$$

$$P_{test.r} := \frac{q_{test.joint.c.l} \cdot \left(l - 2 \cdot a_{joint}\right)}{2} + \frac{\left(q_{test.joint.c.r} - q_{test.joint.c.l}\right) \cdot \left(l - 2 \cdot a_{joint}\right)}{3} = 4.608 \cdot kN$$

$$M_{B.test.c} := P_{test.l} \cdot a_{joint} + \frac{q_{test.B.c} \cdot a_{joint}^{2}}{2} + \frac{2\left(q_{test.joint.c.l} - q_{test.B.c}\right) \cdot a_{joint}^{2}}{6} = 6.667 \cdot kN \cdot m$$

$$M_{C.test.c} := P_{test.r} \cdot a_{joint} + \frac{q_{test.joint.c.r} \cdot a_{joint}^{2}}{2} + \frac{2\left(q_{test.C.c} - q_{test.joint.c.r}\right) \cdot a_{joint}^{2}}{6} = 8.428 \cdot kN \cdot m$$

$$M_{f.mid.test.c} := \min\left(\frac{M_{B.test.c}}{r_M}, \frac{M_{C.test.c}}{r_M}\right) = -4.214 \cdot kN \cdot m$$

Max moment in the mid-span in order to keep zero moment at the location of the joint

$$R_{Bh.test.c} := P_{test.l} + q_{test.B.c} \cdot a_{joint} + \frac{\left(q_{test.joint.c.l} - q_{test.B.c}\right) \cdot a_{joint}}{2} = 6.389 \cdot kN$$

$$R_{Cv.test.c} := P_{test.r} + q_{test.joint.c.r} \cdot a_{joint} + \frac{\left(q_{test.C.c} - q_{test.joint.c.r}\right) \cdot a_{joint}}{2} = 8.611 \cdot kN$$

Check the reaction forces:

$$R_{A.test.c} := -M_{B.test.c} \cdot \frac{1}{l} + q_{test.B.c} \cdot \frac{l}{6} = 0.556 \cdot kN$$

Reaction force A

$$R_{Bv.test.c} := M_{B.test.c} \cdot \frac{1}{l} + q_{test.B.c} \cdot \frac{l}{3} = 4.444 \cdot kN$$

Partial reaction force

$$R_{B.test.c} := R_{Bv.test.c} + R_{Bh.test.c} = 10.833 \cdot kN$$

Reaction force B

$$R_{Ch.test.c} := M_{C.test.c} \cdot \frac{1}{l} + q_{test.C.c} \cdot \frac{l}{2} + \left(q_{test.D.c} - q_{test.C.c}\right) \cdot \frac{l}{6} = 13.071 \cdot kN$$

Partial reaction force

$$R_{C.test.c} := R_{Ch.test.c} + R_{Cv.test.c} = 21.682 \cdot kN$$

Reaction force C

$$R_{D.test.c} := -M_{C.test.c} \cdot \frac{1}{l} + \left(q_{test.D.c} - q_{test.C.c}\right) \cdot \frac{l}{3} + q_{test.C.c} \cdot \frac{l}{2} = 11.929 \cdot kN$$

Reaction force D

$$R_{A.test.c} + R_{B.test.c} + R_{C.test.c} + R_{D.test.c} = 45 \cdot kN$$

$$\frac{q_{test.D.c} \cdot 3l}{2} = 45 \cdot kN$$

$$x := 0m, 0.1m .. L$$

$$M_{Ed.g.test.c}(x) := \begin{cases} \left(-R_{A.test.c}\cdot x + q_{test.c}(x)\cdot\dfrac{x^2}{3\cdot 2}\right) & \text{if } 0 \le x \le l \\ \left[-R_{A.test.c}\cdot x + q_{test.c}(x)\cdot\dfrac{x^2}{3\cdot 2} - R_{B.test.c}\cdot(x-l)\right] & \text{if } l \le x \le l + a_{joint} \\ \left[\begin{array}{l} q_{test.joint.c.l}\cdot\dfrac{\left(x - l - a_{joint}\right)^2}{2} \ldots \\ + \left(q_{test.c}(x) - q_{test.joint.c.l}\right)\cdot\dfrac{\left(x - l - a_{joint}\right)^2}{6} \ldots \\ + -P_{test.l}\cdot\left(x - l - a_{joint}\right) \end{array}\right] & \text{if } l + a_{joint} \le x \le 2l - a_{joint} \\ \left[-R_{A.test.c}\cdot x + q_{test.c}(x)\cdot\dfrac{(x)^2}{2\cdot 3} - R_{B.test.c}\cdot(x-l)\right] & \text{if } 2l - a_{joint} \le x \le 2l \\ \left[-R_{A.test.c}\cdot x + q_{test.c}(x)\cdot\dfrac{(x)^2}{6} - R_{B.test.c}\cdot(x-l) - R_{C.test.c}\cdot(x-2l)\right] & \text{if } 2l \le x \le \end{cases}$$

$$dM_{Ed.g.test.c}(x) := \frac{d}{dx}M_{Ed.g.test.c}(x)$$

The derivates of the moment is the shear

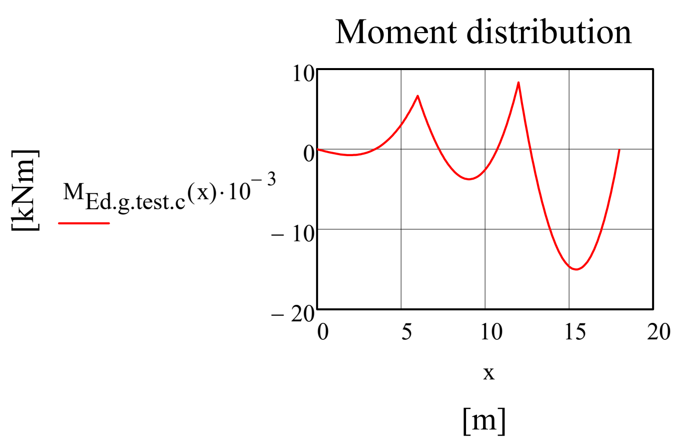

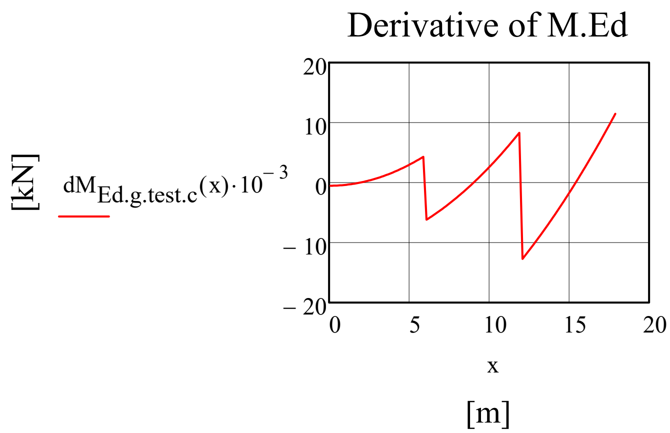

Location of the zero moment in the mid-span:

$x_{joint.c} := 1 + a_{joint}$ — Approximate location where the moment is zero

Given

$\left(M_{Ed.g.test.c}\left(x_{joint.c}\right) = 0\right)$ — The joint is placed where the moment is zero

$x_{root.test.c} := \mathrm{Find}\left(x_{joint.c}\right)$ — Find the location of the zero moment

$x_{root.test.c} = 7.268\ m$

$M_{zero.test.c} := M_{Ed.g.test.c}\left(x_{root.test.c}\right) = 0 \cdot kN \cdot m$ — The moment at the calculated location

$x_{root.test.c} = 7.268\ m$ $\qquad a_{joint} + 1 = 7.268\ m$ — They correlate since the cantilever is made with regard to the joint

Maximum field moment, first span:

$x_{f.c} := \frac{1}{2}$ — Approximate location where the derivates is zero in the first span

Given

$\left(dM_{Ed.g.test.c}\left(x_{f.c}\right) = 0\right)$ — The derivates is zero where the moment is its max or min

$x_{root.test.1.c} := \mathrm{Find}\left(x_{f.c}\right)$ — Find the location of the maximum moment

$x_{root.test.1.c} = 2\ m$

$M_{Ed.g.max.test.1.c} := M_{Ed.g.test.c}\left(x_{root.test.1.c}\right) = -0.741 \cdot kN \cdot m$ — The maximum moment span 1

Maximum field moment, mid-span:

$x_{f.c} := 1.5l$ Approximate location where the derivates is zero in the second span

Given

$\left(dM_{Ed.g.test.c}\left(x_{f.c}\right) = 0\right)$ The derivates is zero where the moment is its max or min

$x_{root.test.mid.c} := \text{Find}\left(x_{f.c}\right)$ Find the location of the maximum moment

$x_{root.test.mid.c} = 9.055\ \text{m}$

$M_{Ed.g.max.test.mid.c} := M_{Ed.g.c}\left(x_{root.test.mid.c}\right) = -5.544 \cdot \text{kN} \cdot \text{m}$ The maximum moment

Maximum field moment, third span:

$x_{f.c} := 2.5l$ Approximate location where the derivates is zero in the second span

Given

$\left(dM_{Ed.g.test.c}\left(x_{f.c}\right) = 0\right)$ The derivates is zero where the moment is its max or min

$x_{root.test.3.c} := \text{Find}\left(x_{f.c}\right)$ Find the location of the maximum moment

$x_{root.test.3.c} = 15.431\ \text{m}$

$M_{Ed.g.max.test.3.c} := M_{Ed.g.c}\left(x_{root.test.3.c}\right) = -11.554 \cdot \text{kN} \cdot \text{m}$ The maximum moment

Compare to the capacity according to Lindab:

$M_{Ed.g.max.test.1.c} \le M_{k.f} \cdot b_s = 1$ $M_{B.test.c} \le M_{k.s} \cdot b_s = 1$

$M_{Ed.g.max.test.mid.c} \le M_{k.f} \cdot b_s = 1$ $M_{C.test.c} \le M_{k.s} \cdot b_s = 1$

$M_{Ed.g.max.test.3.c} \le M_{k.f} \cdot b_s = 1$

B 11.6 Stress Distribution Unevenly Distributed Load

$$\sigma_{x.g.test.c}(x) := \frac{-M_{Ed.g.test.c}(x)}{W_{el.g}}$$

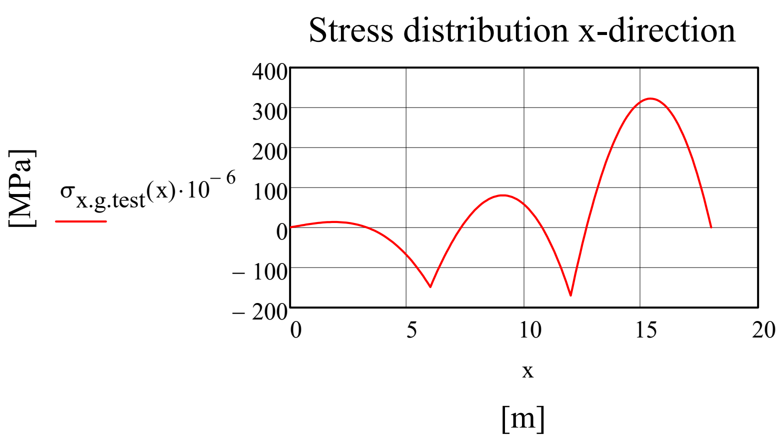

$d\sigma_{x.g.test.c}(x) := \frac{d}{dx}\sigma_{x.g.test.c}(x)$

The derivates of the moment is the shear

Stress in span 1:

$x_{max.g1.test.c} := \frac{1}{2}$

Approximate location where the derivates is zero

Given

$\left(d\sigma_{x.g.test.c}\left(x_{max.g1.test.c}\right) = 0\right)$

The max where the derivates is zero

$x_{g.max.1.test.c} := \text{Find}\left(x_{max.g1.test.c}\right)$

Find the location of the zero derivates

$x_{g.max.1.test.c} = 2\,m$

$\sigma_{x.g.max.1.test.c} := \sigma_{x.g.test.c}\left(x_{g.max.1.test.c}\right) = 15.787\cdot MPa$

The maximum stress in span 1

Stress in mid-span:

$x_{max.gmid.test.c} := 1 + \frac{1}{2}$

Approximate location where the derivates is zero

Given

$\left(d\sigma_{x.g.test.c}\left(x_{max.gmid.test.c}\right) = 0\right)$

The max where the derivates is zero

$x_{g.max.mid.test.c} := \text{Find}\left(x_{max.gmid.test.c}\right)$

Find the location of the zero derivates

$x_{g.max.mid.test.c} = 9.055\,m$

$\sigma_{x.g.max.mid.test.c} := \sigma_{x.g.c}\left(x_{g.max.mid.test.c}\right) = 118.162\cdot MPa$

The maximum stress in mid-span

Stress in span 3:

$x_{max.g3.test.c} := 21 + \frac{1}{2}$

Approximate location where the

Given

derivates is zero

$\left(d\sigma_{x.g.test.c}\left(x_{max.g3.test.c}\right) = 0\right)$

The max where the derivates is zero

$x_{g.max.3.test.c} := \mathrm{Find}\left(x_{max.g3.test.c}\right)$

Find the location of the zero derivates

$x_{g.max.3.test.c} = 15.431\,m$

$\sigma_{x.g.max.3.test.c} := \sigma_{x.g.c}\left(x_{g.max.3.test.c}\right) = 246.235 \cdot MPa$

The maximum stress in mid-span

Stress at supports:

$\sigma_{x.g.B.test.c} := \sigma_{x.g.test.c}(l) = -142.082 \cdot MPa$

$\sigma_{x.g.C.test.c} := \sigma_{x.g.test.c}(2 \cdot l) = -177.603 \cdot MPa$

B 11.7 Comparing with Values from Abaqus

Comparing the reaction forces:

$R_{A.Ab.test.c} := R_{A.Ab.test} = 0.557 \cdot kN$ $\qquad R_{A.test.c} = 0.556 \cdot kN$

$R_{B.Ab.test.c} := R_{B.Ab.test} = 10.828 \cdot kN$ $\qquad R_{B.test.c} = 10.833 \cdot kN$

$R_{C.Ab.test.c} := R_{C.Ab.test} = 21.68 \cdot kN$ $\qquad R_{C.test.c} = 21.682 \cdot kN$

$R_{D.Ab.test.c} := R_{D.Ab.test} = 11.954 \cdot kN$ $\qquad R_{D.test.c} = 11.929 \cdot kN$

$R_{A.Ab.test} + R_{B.Ab.test} + R_{C.Ab.test} + R_{D.Ab.test} = 45.02 \cdot kN$

$R_{A.test.c} + R_{B.test.c} + R_{C.test.c} + R_{D.test.c} = 45 \cdot kN$

$$\frac{q_{test.C} \cdot 3l}{2} = 30 \cdot kN$$

Comparing the moments:

$x_{root.test.1.c} = 2\,m$ — Location of maximum field moment in span 1

$x_{root.test.mid.c} = 9.055\,m$ — Location of maximum field moment in span 2

$x_{root.test.3.c} = 15.431\,m$ — Location of maximum field moment in span 3

$2l = 12\,m$ — Location of maximum support moment

$2l - a_{joint} = 10.732\,m$ — Location of joint

$M_{B.Ab.test.c} := M_{B.Ab.test} = 6.655 \cdot kN \cdot m$ $\qquad M_{B.test.c} = 6.667 \cdot kN \cdot m$

$M_{C.Ab.test.c} := M_{C.Ab.test} = 8.336 \cdot kN \cdot m$

$M_{C.test.c} = 8.428 \cdot kN \cdot m$

$M_{AB.Ab.test.c} := M_{AB.Ab.test} = -0.744 \cdot kN \cdot m$

$M_{AB.test.c} := M_{Ed.g.max.test.1.c} = -0.741 \cdot kN \cdot m$

$M_{BC.Ab.test.c} := M_{BC.Ab.test} = -3.748 \cdot kN \cdot m$

$M_{BC.test.c} := M_{Ed.g.max.test.mid.c} = -5.544 \cdot kN \cdot$

$M_{CD.Ab.test.c} := M_{CD.Ab.test} = -14.997 \cdot kN \cdot m$

$M_{CD.test.c} := M_{Ed.g.max.test.3.c} = -11.554 \cdot kN \cdot m$

$M_{k.f} \cdot b_s = 15.16 \cdot kN \cdot m$

$M_{k.s} \cdot b_s = 20.768 \cdot kN \cdot m$

Comparing the stresses at support B and C:

$\sigma_{B.Ab.test} = -123.2 \cdot MPa$

$\sigma_{x.g.B.test.c} = -142.082 \cdot MPa$

$$\sigma_{B.Ab.calc.test.c} := \frac{-M_{B.Ab.test.c}}{W_{el.g.Ab}} = -141.978 \cdot MPa$$

$\sigma_{C.Ab.test} = -154.3 \cdot MPa$

$\sigma_{x.g.C.test.c} = -177.603 \cdot MPa$

$$\sigma_{C.Ab.calc.test.c} := \frac{-M_{C.Ab.test.c}}{W_{el.g.Ab}} = -177.833 \cdot MPa$$

Comparing the stresses at the location of the joint:

$\sigma_{joint.Ab.test.l} = -7.298 \cdot MPa$

$\sigma_{joint.test.l.c} := \sigma_{x.g.test.c}(1 + a_{joint}) = 3.835 \times 10^{-14} \cdot MPa$

$\sigma_{joint.Ab.test.r} = 8.205 \cdot MPa$

$\sigma_{joint.test.r.c} := \sigma_{x.g.test.c}(21 - a_{joint}) = -1.551 \times 10^{-13} \cdot MPa$

Placement of joints vs. the location of the zero moment:

$l + a_{joint} = 7.268\,m$

$l + a_{test.l} = 7.315\,m$

$2 \cdot l - a_{joint} = 10.732\,m$

$l + a_{test.r} = 10.774\,m$

B 11.8 Deflection of the Tested Sheet

Deflection of the 3-span continuous sheet, distributed loads:

$q_{test.A.c} = 0 \cdot \frac{kN}{m}$ $q_{test.B.c} = 1.667 \cdot \frac{kN}{m}$ $q_{test.C.c} = 3.333 \cdot \frac{kN}{m}$ $q_{test.D.c} = 5 \cdot \frac{kN}{m}$

$q_{test.joint.c.l} = 2.019 \cdot \frac{kN}{m}$ $q_{test.joint.c.r} = 2.981 \cdot \frac{kN}{m}$

$R_{A.test.c} = 0.556 \cdot kN$

$R_{B.test.c} = 10.833 \cdot kN$ $M_{B.test.c} = 6.667 \cdot kN \cdot m$

$R_{C.test.c} = 21.682 \cdot kN$ $M_{C.test.c} = 8.428 \cdot kN \cdot m$

$R_{D.test.c} = 11.929 \cdot kN$

$l = 6\,m$

$E_s = 2.1 \times 10^5 \cdot MPa$

$I_g = 6.648 \times 10^6 \cdot mm^4$

$x_{test} := 0m, 0.1m .. L$

$a_m(x_{test}) := x_{test} - l$ $a_3(x_{test}) := x_{test} - l \cdot 2$ $a_c(x_{test}) := x_{test} - l - a_{joint}$

Deflection of left part cantilever, based on two integrals of the moment:

$$EI \frac{d^2 y}{dx^2} = R_{A.test.c} \cdot x_{test} - \frac{q_{test.c}(x_{test}) \cdot x_{test}^2}{2 \cdot 3}$$

$$EI \frac{dy}{dx} = R_{A.test.c} \cdot \frac{x_{test}^2}{2} - \frac{q_{test.c}(x_{test}) \cdot x_{test}^3}{18} + C_{1.test.l}$$

$$EI\,y(x) = R_{A.test.c} \cdot \frac{x_{test}^3}{6} - \frac{q_{test.c}(x_{test}) \cdot x_{test}^4}{72} + C_{1.test.l} \cdot x_{test} + C_{2.test.l}$$

Boundary conditions at y(0)=0 and at y(l)=0 gives the valus for C1 and C2

$C_{2.test.l} := 0kN \cdot m^3$

$$C_{1.test.l} := \frac{\left(-R_{A.test.c} \cdot \frac{l^3}{6} + \frac{q_{test.c}(l) \cdot l^4}{72}\right)}{l} = 1.667 \cdot kN \cdot m^2$$

Deflection of right part cantilever, based on two integrals of the moment:

$$EI\frac{d^2y}{dx^2} = R_{A.test.c}\cdot x_{test} - \frac{q_{test.c}(x_{test})\cdot x_{test}^2}{2\cdot 3} + R_{B.c}\cdot(x_{test} - l) + R_{C.test.c}\cdot(x_{test} - 2l)$$

$$EI\frac{dy}{dx} = \frac{R_{A.test.c}\cdot x_{test}^2}{2} - \frac{q_{test.c}(x_{test})\cdot x_{test}^3}{18} + \frac{R_{B.test.c}\cdot(x_{test} - l)^2}{2} \ldots$$
$$+ \frac{R_{C.test.c}\cdot(x_{test} - 2l)^2}{2} + C_{1.test.r}$$

$$EI\,y(x) = \frac{R_{A.test.c}\cdot x_{test}^3}{6} - \frac{q_{test.c}(x_{test})\cdot x_{test}^4}{72} + \frac{R_{B.test.c}\cdot(x_{test} - l)^3}{6} \ldots$$
$$+ \frac{R_{C.test.c}\cdot(x_{test} - 2l)^3}{3} + C_{1.test.r}\cdot x_{test} + C_{2.test.r}$$

Boundary conditions at y(L)=0 and at y(2l)=0 gives the valus for C1 and C2

$$C_{1.test.r} := \frac{\left[\frac{R_{A.test.c}\cdot(2l)^3}{6} - \frac{q_{test.c}(2l)\cdot(2l)^4}{72} \ldots + \frac{R_{B.test.c}\cdot[(2l) - l]^3}{6} + \frac{R_{C.test.c}\cdot[(2l) - 2l]^3}{3}\right]}{(2l)} = -34.167\cdot kN\cdot m^2$$

Calculating the start at finish for the middle sheet, in-between the joints:

$$y_1 := \frac{\left[\frac{R_{A.test.c}\cdot(l + a_{joint})^3}{6} - \frac{q_{test.c}((l + a_{joint}))\cdot(l + a_{joint})^4}{72} \ldots + \frac{R_{B.test.c}\cdot[(l + a_{joint}) - l]^3}{6} + C_{1.test.l}\cdot(l + a_{joint})\right]}{(E_s\cdot I_g)} = -19.266\cdot mm$$

$$y_r := \left[\begin{array}{l}\frac{-q_{test.joint.c.r}\cdot\left(a_{joint}\right)^4}{24\cdot E_s\cdot I_g}\cdot\left[\frac{6\cdot\left(a_{joint}\right)^2}{a_{joint}^{\ 2}}-\frac{4\left(a_{joint}\right)^3}{a_{joint}^{\ 3}}+\frac{\left(a_{joint}\right)^4}{a_{joint}^{\ 4}}\right]\ldots \\ +\frac{-\left(q_{test.C.c}-q_{test.joint.c.r}\right)\cdot\left(a_{joint}\right)^4}{120\cdot E_s\cdot I_g}\cdot\left[\begin{array}{l}\frac{10\cdot\left(a_{joint}\right)^2}{a_{joint}^{\ 2}}\ldots \\ +\frac{-10\cdot\left(a_{joint}\right)^3}{a_{joint}^{\ 3}}\ldots \\ +\frac{-5\left(a_{joint}\right)^4}{a_{joint}^{\ 4}}+\frac{\left(a_{joint}\right)^5}{a_{joint}^{\ 5}}\end{array}\right]\ldots \\ +\frac{-P_{test.r}\cdot a_{joint}^{\ 2}\cdot a_{joint}}{2\cdot E_s\cdot I_g}\cdot\left(1-\frac{a_{joint}}{3\cdot a_{joint}}\right)\end{array}\right] = -2.911\cdot mm$$

$$y\left(x_{test}\right) := \frac{y_1+1.15mm}{1-2\cdot a_{joint}}\cdot a_c\left(x_{test}\right)$$

$$\delta_{test.c}\left(x_{test}\right) := \left\|\begin{array}{ll}\frac{\left(\frac{R_{A.test.c}\cdot x_{test}^{\ 3}}{6}-\frac{q_{test.c}\left(x_{test}\right)\cdot x_{test}^{\ 4}}{72}+C_{1.test.l}\cdot x_{test}\right)}{\left(E_s\cdot I_g\right)} & \text{if } 0\le x_{test}\le l \\ \frac{\left[\begin{array}{l}\frac{R_{A.test.c}\cdot x_{test}^{\ 3}}{6}\ldots \\ +\frac{-q_{test.c}\left(x_{test}\right)\cdot x_{test}^{\ 4}}{72}\ldots \\ +\frac{R_{B.test.c}\cdot\left(x_{test}-l\right)^3}{6}+C_{1.test.l}\cdot x_{test}\end{array}\right]}{\left(E_s\cdot I_g\right)} & \text{if } l\le x_{test}<l+a_{joint} \\ \left[\begin{array}{l}y_1-y\left(x_{test}\right)\ldots \\ +\frac{-\left(\begin{array}{l}q_{test.c}\left(x_{test}\right)\ldots \\ +-q_{test.joint.c.l}\end{array}\right)\cdot a_c\left(x_{test}\right)\cdot\left(1-2\cdot a_{joint}\right)^3}{360\cdot E_s\cdot I_g}\cdot\left[\begin{array}{l}7\ldots \\ +\frac{-10\cdot a_c\left(x_{test}\right)^2}{\left(1-2a_{joint}\right)^2}\ldots \\ +\frac{a_c\left(x_{test}\right)^4\cdot 3}{\left(1-2a_{joint}\right)^4}\end{array}\right]\ldots\end{array}\right. & \text{if } l+a_{joint}\le\end{array}\right.$$

$$+\frac{-\left(q_{test.joint.c.l}\right)\cdot a_c\left(x_{test}\right)\cdot\left(l-2\cdot a_{joint}\right)^3}{24\cdot E_s\cdot I_g}\cdot\left[1\ \ldots+\frac{-2\cdot a_c\left(x_{test}\right)^2}{\left(l-2a_{joint}\right)^2}\ \ldots+\frac{a_c\left(x_{test}\right)^3}{\left(l-2a_{joint}\right)^3}\right]$$

$$\frac{-q_{test.joint.c.r}\cdot a_{joint}{}^4}{24\cdot E_s\cdot I_g}\cdot\left(\frac{6\cdot a_m\left(x_{test}\right)^2}{a_{joint}{}^2}\ \ldots+\frac{-4\,a_m\left(x_{test}\right)^3}{a_{joint}{}^3}\ \ldots+\frac{a_m\left(x_{test}\right)^4}{a_{joint}{}^4}\right)\ \ldots\quad \text{if } 2l-a_{jc}$$

$$+\frac{-\left(q_{test.C.c}-q_{test.joint.c.r}\right)\cdot a_{joint}{}^4}{120\cdot E_s\cdot I_g}\cdot\left(\frac{10\cdot a_m\left(x_{test}\right)^2}{a_{joint}{}^2}\ \ldots+\frac{-10\cdot a_m\left(x_{test}\right)^3}{a_{joint}{}^3}\ \ldots+\frac{-5\,a_m\left(x_{test}\right)^4}{a_{joint}{}^4}+\frac{a_m\left(x_{test}\right)^5}{a_{joint}{}^5}\right)\ \ldots$$

$$+\frac{-P_{test.r}\cdot a_m\left(x_{test}\right)^2\cdot a_{joint}}{2\cdot E_s\cdot I_g}\cdot\left(1-\frac{a_m\left(x_{test}\right)}{3\cdot a_{joint}}\right)$$

$$\frac{-q_{test.c}\left(a_3\left(x_{test}\right)\right)\cdot\left(a_3\left(x_{test}\right)\right)\cdot l^3}{24\cdot E_s\cdot I_g}\cdot\left[1-\frac{2\left(a_3\left(x_{test}\right)\right)^2}{l^2}+\frac{\left(a_3\left(x_{test}\right)\right)^3}{l^3}\right]\ \ldots\quad \text{if } l\cdot 2\le x_{test}$$

$$+\frac{-\left(q_{test.D.c}-q_{test.c}\left(a_3\left(x_{test}\right)\right)\right)\cdot\left(a_3\left(x_{test}\right)\right)\cdot l^3}{360\cdot E_s\cdot I_g}\cdot\left[7\ \ldots+\frac{-10\left(a_3\left(x_{test}\right)\right)^2}{l^2}\ \ldots+\frac{\left(a_3\left(x_{test}\right)\right)^4\cdot 3}{l^4}\right]\ \ldots$$

$$M_{C.test.c}\cdot\left[1-\left(a_3\left(x_{test}\right)\right)\right]\cdot l\left[\ \ldots\ \left[1-\left(a_3\left(x_{test}\right)\right)\right]^2\right]$$

$$+\frac{}{6\cdot E_s\cdot I_g}\cdot\left[1-\frac{}{l^2}\right]$$

$d\delta_{test.c}(x_{test}) := \frac{d}{dx_{test}}\delta_{test.c}(x_{test})$

The derivates of the deflection

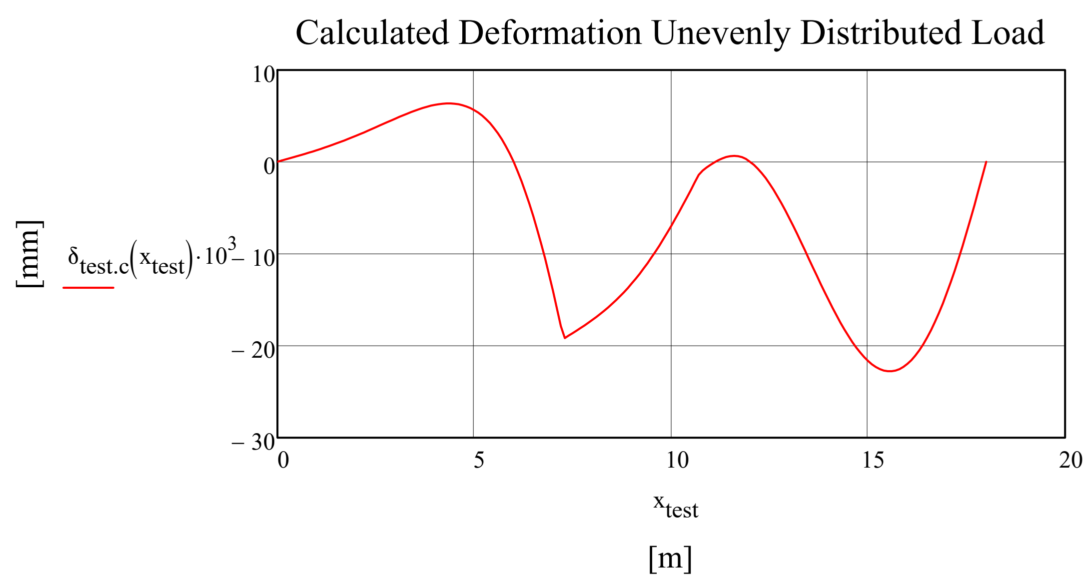

Maximum deflection first span:

$x_f := 1$

Approximate location where the derivates is zero in the first span

Given

$(d\delta_{test.c}(x_f) = 0)$

The derivates is zero where the deflection is its max or min

$x_{root.test.1} := \mathrm{Find}(x_f)$

Find the location of the maximum deflection

$x_{root.test.1} = 4.354\ \mathrm{m}$

$\delta_{test.1.c} := \delta_{test.c}(x_{root.test.1}) = 6.348\cdot\mathrm{mm}$

The maximum deflection in span 1

Maximum deflection span 3:

$x_f := L - \frac{1}{2}$

Approximate location where the derivates is zero in the first span

Given

$(d\delta_{test.c}(x_f) = 0)$

The derivates is zero where the deflection is its max or min

$x_{root.test.3} := \mathrm{Find}(x_f)$

Find the location of the maximum deflection

$x_{root.test.3} = 15.55\ m$

$\delta_{test.3.c} := \delta_{test.c}(x_{root.test.3}) = -22.798 \cdot mm$

The maximum deflection in span 3

Maximum calculated deflection in each span:

$\delta_{calc.test.1.c} := \delta_{test.c}(x_{root.test.1}) = 6.348 \cdot mm$

$\delta_{calc.test.mid.c} := \delta_{test.c}(x_{root.test.mid}) = -12.731 \cdot mm$

$\delta_{calc.test.3.c} := \delta_{test.c}(x_{root.test.3}) = -22.798 \cdot mm$

B 12 Design of a Trapezoidal Steel Sheet

B 12.1 Effective Cross-section:

We assume that the dimensions of the grooves, which act like stiffeners, are made with regard to the fact that these must not buckle. In order to account for buckling the effective cross-section will be calculated according to SS-EN 1993-1-5.

The upper flange:

The grooves are considered internal stiffeners and according to SS-EN 1993-1-3 5.5.3.3 (4) the flange can be assumed as simply supported, giving an evenly distributed effective area. The effective area is considered in the compressed part of the cross-section i.e. the top flange and parts of the web.

$b_e := 2 \cdot b_{p1} + b_{p2} + 2 \cdot s_{go}$

$b_1 := b_{p1} + 0.5 \cdot b_{go}$

Effective cross-section is calculated on the parts of the sheet which are compressed; the top flange the upper part of the web as well as part of the middle part of the web decided by the NA.

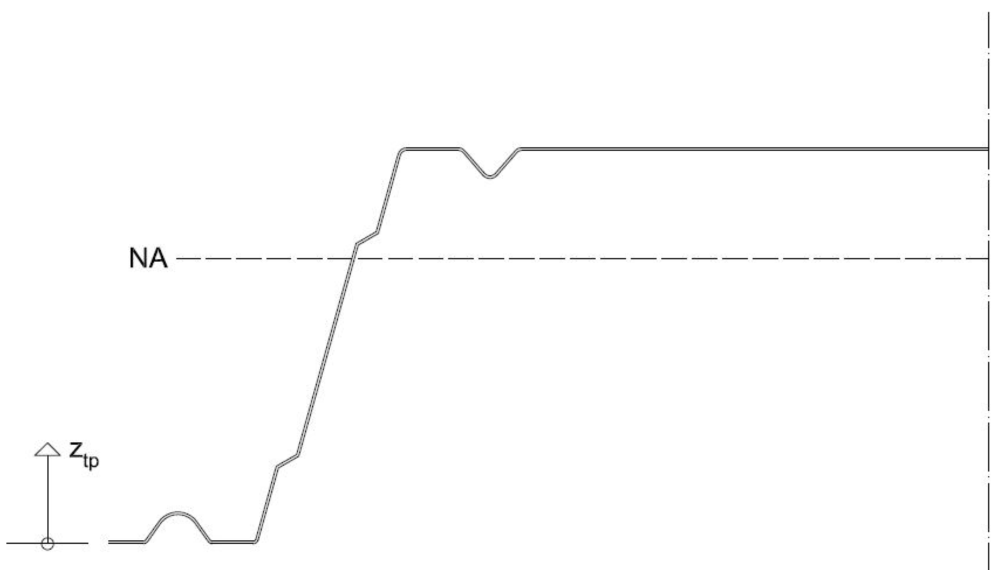

$A_g = 4.222 \times 10^3 \cdot mm^2$

$z_{tp} = 141.021 \cdot mm$

$I_g = 6.648 \times 10^6 \cdot mm^4$

The top flange is in evenly distributed compression

$\psi := 1$

$(3 + \psi) \geq 0 = 1$

$k_\sigma := 4.0$

Outer side of the top flange is part 1:

$$\lambda_{p.fo.1} := \frac{\frac{b_{p1}}{t_s}}{28.4 \cdot \varepsilon \cdot \sqrt{k_\sigma}} = 0.55$$

$$\rho_{fo.1} := \begin{cases} 1.0 & \text{if } \lambda_{p.fo.1} \leq 0.673 \\ 1.0 & \text{if } \dfrac{\lambda_{p.fo.1} - 0.055(3 + \psi)}{\lambda_{p.fo.1}^2} \geq 1.0 \\ \dfrac{\lambda_{p.fo.1} - 0.055(3 + \psi)}{\lambda_{p.fo.1}^2} & \text{otherwise} \end{cases} \qquad \rho_{fo.1} = 1$$

The middle part of the top flange is part 2:

$$\lambda_{p.fo.2} := \frac{\frac{b_{p2}}{t_s}}{28.4 \cdot \varepsilon \cdot \sqrt{k_\sigma}} = 8.731$$

$$\rho_{fo.2} := \begin{cases} 1.0 & \text{if } \lambda_{p.fo.2} \leq 0.673 \\ 1.0 & \text{if } \dfrac{\lambda_{p.fo.2} - 0.055(3 + \psi)}{\lambda_{p.fo.2}^2} \geq 1.0 \\ \dfrac{\lambda_{p.fo.2} - 0.055(3 + \psi)}{\lambda_{p.fo.2}^2} & \text{otherwise} \end{cases} \qquad \rho_{fo.2} = 0.112$$

The effective widths of the cross-section then becomes the following:

$b_{eff.fo.1} := \rho_{fo.1} \cdot b_{p1} = 29.23 \cdot mm$

$b_{eff.fo.2} := \rho_{fo.2} \cdot b_{p2} = 51.771 \cdot mm$

$$A_{sc.eff} := 2A_{fu} + A_{gu} + 2A_{wu} + 2\cdot A_{w.fu} + 2\cdot A_{wm} + 2\cdot A_{w.fo} + 2\cdot A_{wo} \dots$$
$$+ t_s\cdot\left(b_{eff.fo.1}\cdot 2 + b_{eff.fo.2}\right) + 2\cdot A_{go}$$

$$A_{eff} := A_{sc.eff}\cdot\left(1 - \delta_{sc}\right) = 866.193\cdot mm^2$$

With consideration to sharp corners

$$z_{tp.eff} := \frac{\begin{array}{l}2A_{fu}\cdot\left(z_{fu}\right) + A_{gu}\cdot\left(z_{gu}\right) + t_s\cdot\left(b_{eff.fo.1}\cdot 2 + b_{eff.fo.2}\right)\cdot\left(z_{fo}\right) \dots \\ + 2\cdot A_{go}\cdot z_{go} + 2A_{wu}\cdot\left(z_{wu}\right) + 2A_{wm}\cdot\left(z_{wm}\right) + 2\cdot A_{wo}\cdot\left(z_{wo}\right) \dots \\ + 2A_{w.fu}\cdot z_{w.fu} + 2\cdot A_{w.fo}\cdot\left(z_{w.fo}\right)\end{array}}{A_{eff}} = 113.464\cdot mm$$

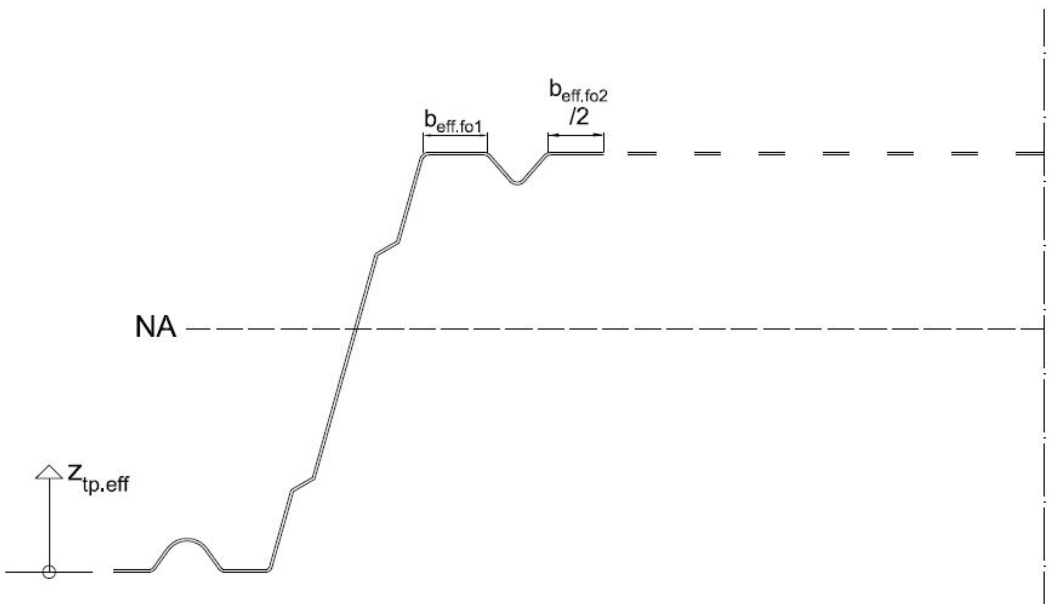

Effective cross-sectional area for a compressed groove

$$A_s := t_s\cdot\left(s_{go} + 0.5b_{eff.fo.1} + 0.5b_{eff.fo.2}\right)$$

$$z_{tp.s} := \frac{\left(t_s\cdot 0.5\cdot b_{eff.fo.1}\right)\cdot\left(\frac{t_s}{2} + h_{go}\right) + \left(t_s\cdot 0.5\cdot b_{eff.fo.2}\right)\cdot\left(\frac{t_s}{2} + h_{go}\right) + \left(s_{go}\cdot t_s\right)\cdot\left(\frac{h_{go}}{2}\right)}{A_s} = 10.598\cdot mm$$

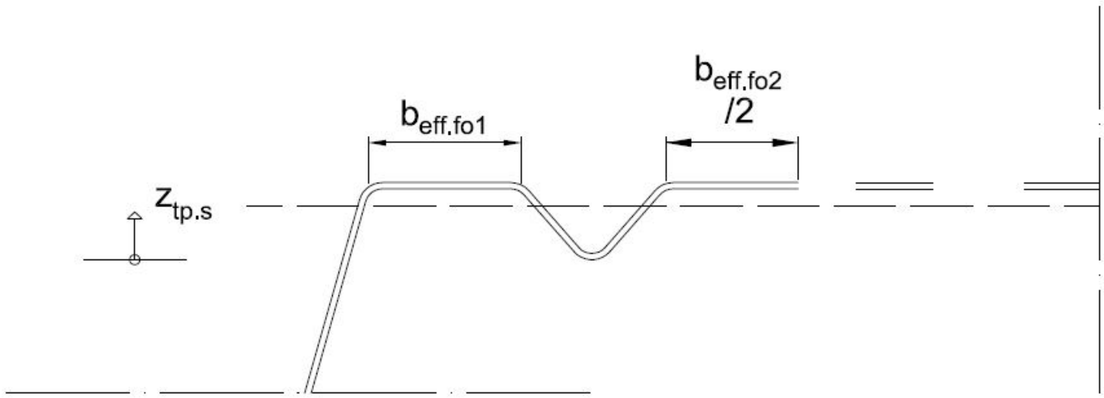

When calculating the second moment of area, I, for the groove; for the outer flange a width of 15t is contributing and for the inner the minimum width of 15t or 0.5beff is contributing, according to SS-EN 1993-1-3 5.5.3.4.2

$$\left(15 \cdot t_s \le 0.5 \cdot b_{eff.fo.2}\right) = 1$$

The second moment of area is calculated excluding the bt^3/12 part, since its contribution is very small.

$$I_s := 2\left[t_s \cdot \left(15 \cdot t_s\right) \cdot \left(h_{go} + \frac{t_s}{2} - z_{tp.s}\right)^2\right] + \left[t_s \cdot s_{go} \cdot \left(z_{tp.s} - \frac{h_{go}}{2}\right)^2\right] = 1.332 \times 10^3 \cdot mm^4$$

The critical stress for a flange with two symmetrically placed grooves, SS-EN 1993-1-3 5.5.3.4.2(3):

$$l_b := 3.65\left[\frac{I_s \cdot b_1^{\,2} \cdot \left(3 \cdot b_e - 4 \cdot b_1\right)}{t_s^{\,3}}\right]^{\frac{1}{4}}$$

Buckling length for a flange with two symmetrical grooves

$$s_w := \left(h_s - t_s\right) \cdot \sin\left(\phi_w\right) = 186.244 \cdot mm$$

The length of the angled web

$$k_{wo} := \sqrt{\frac{\left(2 \cdot b_e + s_w\right) \cdot \left(3 \cdot b_e - 4 \cdot b_1\right)}{b_1 \cdot \left(4 \cdot b_e - 6 \cdot b_1\right) + s_w \cdot \left(3 \cdot b_e - 4 \cdot b_1\right)}}$$

$$k_w := \begin{cases} k_{wo} & \text{if } \dfrac{l_b}{s_w} \geq 2 \\ k_{wo} - (k_{wo} - 1)\cdot\left[\dfrac{2\cdot l_b}{s_w} - \left(\dfrac{l_b}{s_w}\right)^2\right] & \text{otherwise} \end{cases}$$

kw can be put to 1 to be on the safe side.

$$\sigma_{cr.s} := \frac{4.2\cdot k_w\cdot E_s}{A_s}\cdot\sqrt{\frac{I_s\cdot t_s^{\,3}}{8\cdot b_1^{\,2}\cdot(3\cdot b_e - 4\cdot b_1)}}$$

Critical stress for the groove

The web:

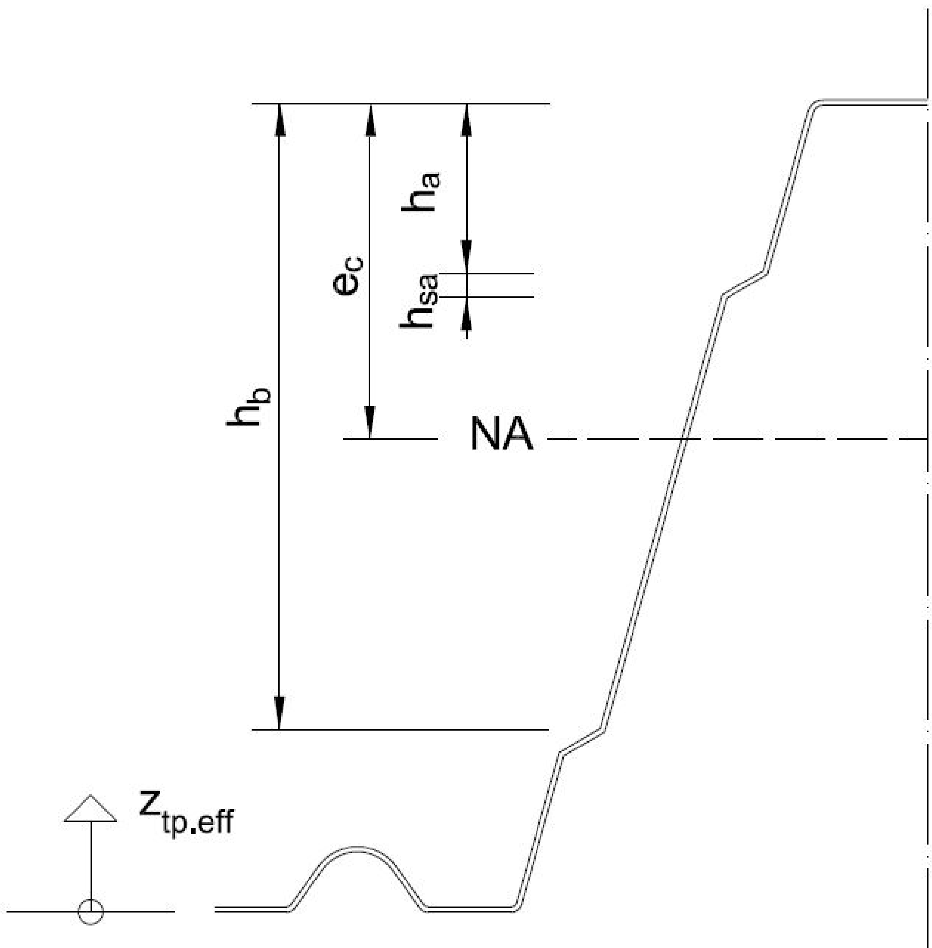

$$e_c := h_s - z_{tp.eff} - \frac{t_s}{2}$$

$h_a := l_{wo} \cdot \sin(\phi_w)$

$h_{sa} := h_{w.fo}$

$h_b := h_a + h_{sa} + l_{wm} \cdot \sin(\phi_w)$

Deciding which parts are in the compressed zone:

$e_c > h_a = 1$

$e_c > h_b = 0$

Effective cross-sectional area for a compressed fold in the web, according to SS-EN 1993-1-3 5.5.3.4.3:

$$\sigma_{com.Ed} := \frac{f_{yb}}{\gamma_{M0}}$$

Stress in the compressed flange when the capacity of the cross-section is reached

$$s_{eff.0} := 0.76 \cdot t_s \cdot \sqrt{\frac{E_s}{\gamma_{M0} \cdot \sigma_{com.Ed}}} = 21.243 \cdot mm$$

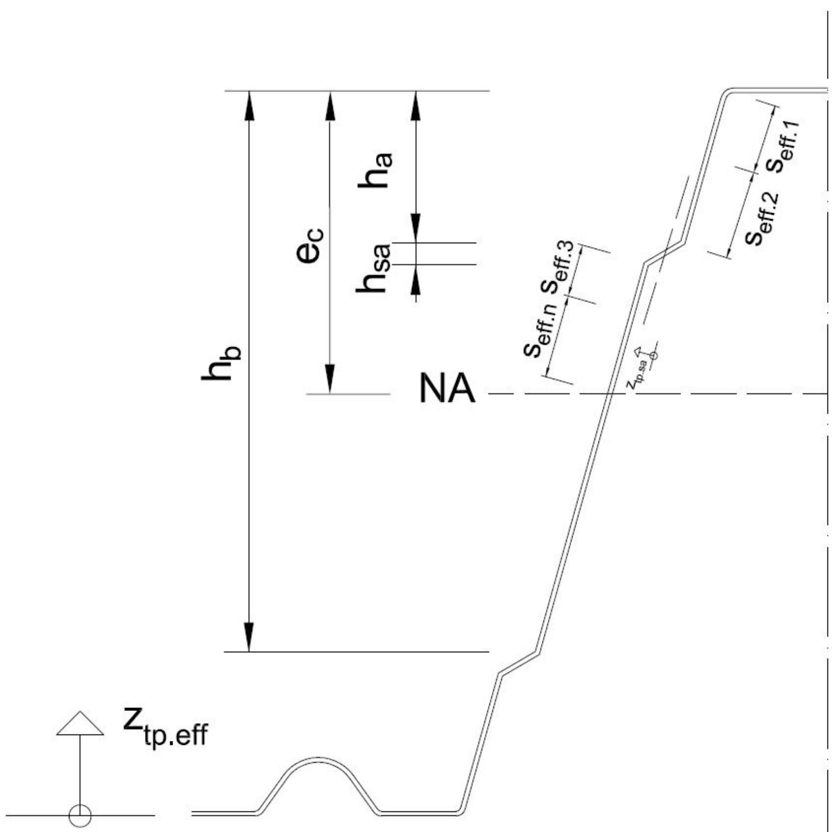

The web is fully effective for this thickness of the sheet, however the dimensions are first determined according to SS-EN 1993-1-3 5.5.3.4.3(5) and then revised according to (6). The bottom web fold is in tension therefore when calculating we assume one fold.

$e_c = 80.911 \cdot mm$

$h_a = 40.757 \cdot mm$

$h_b = 150.999 \cdot mm$

$h_{sa} = 5.8 \cdot mm$

$$s_n := \frac{\left(l_{wu} \cdot \sin(\phi_w) + h_{w.fu} + l_{wm} \cdot \sin(\phi_w)\right) - \left(z_{tp.eff} - \frac{t_s}{2}\right)}{\sin(\phi_w)} = 37.225 \cdot mm$$

$s_{eff.1} := s_{eff.0} = 21.243 \cdot mm$

$$s_{eff.2} := \left(1 + \frac{0.5 \cdot h_a}{e_c}\right) \cdot s_{eff.0} = 26.593 \cdot mm$$

$$s_{eff.3} := \left[1 + 0.5 \cdot \frac{(h_a + h_{sa})}{e_c}\right] \cdot s_{eff.0} = 27.354 \cdot mm$$

$s_{eff.n} := 1.5 \cdot s_{eff.0} = 31.864 \cdot mm$

The whole part is effective if true; giving updated measurements:

$s_{eff.1} + s_{eff.2} \geq l_{wo} = 1$

$$s_{eff.1} := \frac{l_{wo}}{2 + 0.5 \cdot \frac{h_a}{e_c}} = 18.829 \cdot mm$$

$$s_{eff.2} := l_{wo} \cdot \frac{\left(1 + \frac{0.5 \cdot h_a}{e_c}\right)}{2 + \frac{0.5 \cdot h_a}{e_c}} = 23.571 \cdot mm$$

$l_{wo} = 0.042\ m$

$s_{eff.1} + s_{eff.2} = 0.042\ m$

The whole part of the web is effective if true; the values need to be revised:

$s_{eff.3} + s_{eff.n} \geq s_n = 1$

$$s_{eff.3} := s_n \cdot \frac{\left(1 + 0.5 \cdot \frac{h_a + h_{sa}}{e_c}\right)}{2.5 + \frac{0.5 \cdot (h_a + h_{sa})}{e_c}} = 17.195 \cdot mm$$

$$s_{eff.n} := \frac{1.5 \cdot s_n}{2.5 + \frac{0.5 \cdot (h_a + h_{sa})}{e_c}} = 20.03 \cdot mm$$

$s_n = 37.225 \cdot mm$

$s_{eff.n} + s_{eff.3} = 37.225 \cdot mm$

$$A_{sa} := t_s \cdot \left(s_{eff.2} + s_{eff.3} + l_{w.fo}\right) = 65.27 \cdot mm^2$$

Effective area of the top web fold:

$$A_{sb} := t_s \cdot \left(s_{eff.n} + \frac{l_{wu}}{2} + l_{w.fu}\right) = 64.379 \cdot mm^2$$

Not relevant since the bottom web fold is in tension

The local axis of the gravity center for the upper web fold ((parallel to the web):

$$z_{tp.sa} := \frac{\left(t_s \cdot l_{w.fo}\right) \cdot \left(\sin(\phi_f) \cdot \frac{l_{w.fo}}{2} + \frac{t_s}{2}\right) + \left(t_s \cdot s_{eff.2}\right) \cdot \frac{t_s}{2} + \left(t_s \cdot s_{eff.3}\right) \cdot \left(\sin(\phi_f) \cdot l_{w.fo} + t_s\right)}{A_{sa}}$$

$z_{tp.sa} = 4.322 \cdot mm$ $\quad h_f := \sin(\phi_f) \cdot l_{w.fo} + 2t_s = 10.454 \cdot mm$

The second moment of area is calculated excluding the bt^3/12 part, since its contribution is very small.

$$I_{sa} := t_s \cdot s_{eff.2} \cdot \left(z_{tp.sa} - \frac{t_s}{2}\right)^2 + t_s \cdot s_{eff.3} \cdot \left(h_f - z_{tp.sa} - \frac{t_s}{2}\right)^2 \ldots = 1.066 \times 10^3 \cdot mm^4$$
$$+ t_s \cdot l_{w.fo} \cdot \left(z_{tp.sa} - \frac{h_f}{2}\right)^2$$

Critical stress for the fold, according to SS-EN 1993-1-3 5.5.3.4.3(7):

$$s_1 := l_{wo} + l_{w.fo} + l_{wm} + 0.5 \cdot \left(l_{w.fu} + l_{wu}\right)$$

$$s_2 := s_1 - l_{wo} - 0.5 \cdot l_{w.fo}$$

$$k_f := 1$$

$$\sigma_{cr.sa} := \frac{1.05 \cdot k_f \cdot E_s \cdot \sqrt{I_{sa} \cdot t_s^3 \cdot s_1}}{A_{sa} \cdot s_2 \cdot (s_1 - s_2)} = 313.708 \cdot MPa$$

Reduced areas with regard to distortion buckling:

$$\beta_s := 1 - \frac{(h_a + 0.5 \cdot h_{sa})}{e_c}$$

The modified stress with regard to flange grooves and web folds in a sheet, according to SS-EN 1993-1-3 5.5.3.4.4. This value is used for the distortional buckling and when checking the capacity of the sheet later.

$$\sigma_{cr.mod} := \frac{\sigma_{cr.s}}{\left[1 + \left(\beta_s \cdot \frac{\sigma_{cr.s}}{\sigma_{cr.sa}}\right)^4\right]^{\frac{1}{4}}} = 216.805 \cdot MPa$$

The slenderness with regard to web folds and flange grooves:

$$\lambda_d := \sqrt{\frac{f_{yb}}{\sigma_{cr.mod}}} = 1.392$$

Reduction factor χ, according to SS-EN 1993-1-3 5.5.3.1(7)

$$\chi_d := \begin{array}{|l} 1.0 \text{ if } \lambda_d \le 0.65 \\ (1.47 - 0.723 \cdot \lambda_d) \text{ if } 0.65 < \lambda_d \le 1.38 \\ \frac{0.66}{\lambda_d} \text{ if } \lambda_d \ge 1.38 \end{array} \qquad \chi_d = 0.474$$

$$A_{s.red} := \chi_d \cdot A_s \cdot \frac{f_{yb}}{\gamma_{M0} \cdot \sigma_{com.Ed}} = 47.313 \cdot mm^2 \qquad A_{s.red} := \min(A_s, A_{s.red}) = 47.313 \cdot mm^2$$

$$t_{s.red} := \begin{array}{|l} t_s \cdot \frac{A_{s.red}}{A_s} \text{ if } A_{s.red} < A_s \\ t_s \text{ otherwise} \end{array} \qquad t_{s.red} = 0.593 \cdot mm$$

$$A_{sa.red} := \frac{\chi_d \cdot A_{sa}}{1 - \frac{(h_a + 0.5 \cdot h_{sa})}{e_c}} = 67.221 \cdot mm^2 \qquad A_{sa.red} := \min(A_{sa}, A_{sa.red}) = 65.27 \cdot mm^2$$

$$t_{sa.red} := \begin{array}{|l} (\chi_d \cdot t_s) \text{ if } A_{sa.red} < A_{sa} \\ t_s \text{ otherwise} \end{array} \qquad t_{sa.red} = 1.25 \cdot mm$$

Values of the effective cross-section where the full web is load-carrying but only an effective part of the top flange is load carrying, and Rounded corners will be considered by a simplification of the area with sharp corners, according to SS-EN 1993-1-3 5.1(5):

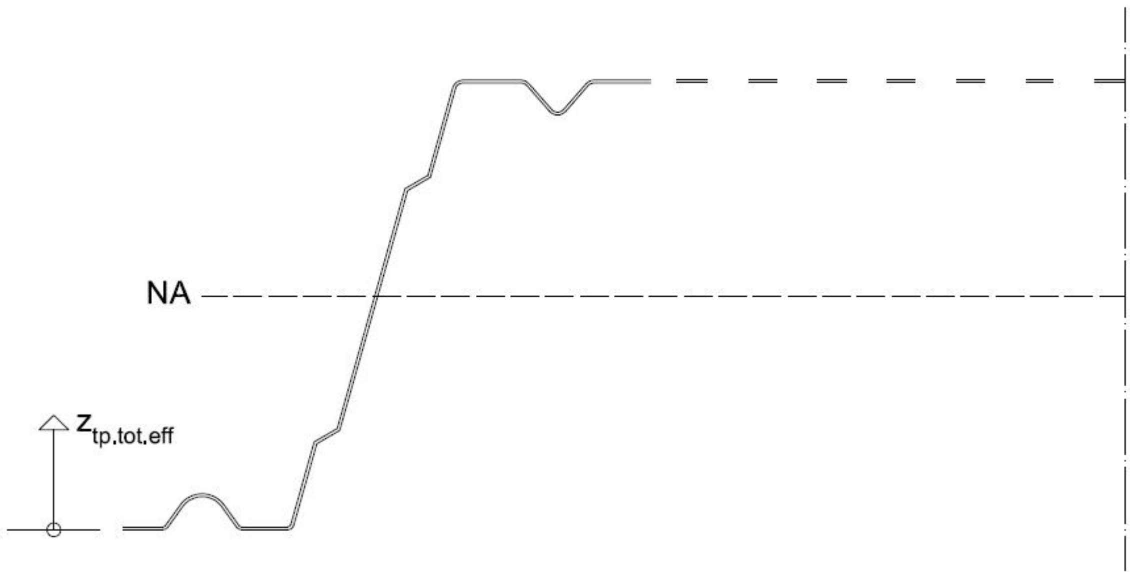

Distances for calculating the z.tp location:

$$s_1 := \frac{t_s}{2}$$

$$s_2 := t_s + \frac{h_{gu}}{3}$$

$$s_3 := t_s + \frac{l_{wu}}{2} \cdot \sin(\phi_w)$$

$$s_4 := t_s + l_{wu} \cdot \sin(\phi_w) + \frac{h_{w.fu}}{2}$$

$$s_5 := t_s + l_{wu} \cdot \sin(\phi_w) + h_{w.fu} + \frac{z_{tp.eff} - h_{w.fu} - l_{wu} \cdot \sin(\phi_w) - t_s}{2} \cdot \sin(\phi_w)$$

$$s_6 := t_s + l_{wu} \cdot \sin(\phi_w) + h_{w.fu} + \left(z_{tp.eff} - h_{w.fu} - l_{wu} \cdot \sin(\phi_w) - t_s + \frac{s_{eff.n}}{2}\right) \cdot \sin(\phi_w)$$

$$s_7 := t_s + l_{wu} \cdot \sin(\phi_w) + h_{w.fu} + \left(l_{wm} - \frac{s_{eff.3}}{2}\right) \cdot \sin(\phi_w) = 0.142 \text{ m}$$

$$s_8 := t_s + l_{wu} \cdot \sin(\phi_w) + h_{w.fu} + l_{wm} \cdot \sin(\phi_w) + \frac{h_{w.fo}}{2}$$

$$s_9 := t_s + l_{wu} \cdot \sin(\phi_w) + h_{w.fu} + l_{wm} \cdot \sin(\phi_w) + h_{w.fo} + \frac{s_{eff.2}}{2} \cdot \sin(\phi_w)$$

$$s_{10} := h_s - t_s - \frac{s_{eff.1}}{2} \cdot \sin(\phi_w)$$

$$s_{11} := h_s - \frac{t_s}{2}$$

$$s_{12} := h_s - (h_{go} + t_s - z_{tp.s})$$

$$A_{c.eff} := 2 \cdot t_s \cdot s_{eff.n} + 2 \cdot A_{sa.red} + 2 \cdot t_s \cdot s_{eff.1} + 2 \cdot t_s \cdot 0.5 b_{eff.fo.1} + 2 \cdot A_{s.red} = 358.849 \cdot mm^2$$

$$A_{fo.eff} := 2 \cdot t_s \cdot 0.5 b_{eff.fo.1} + 2 \cdot A_{s.red} = 131.163 \cdot mm^2$$

$$\begin{aligned} A_{tot.sc.eff} := {} & 2 \cdot A_{fu} + A_{gu} + 2 \cdot A_{wu} + 2 \cdot A_{w.fu} \cdots \\ & + 2 \cdot t_s \cdot \left(z_{tp.eff} - h_{w.fu} - l_{wu} \cdot \sin(\phi_w) - t_s\right) \cdots \\ & + 2 \cdot t_s \cdot s_{eff.n} + 2 \cdot A_{sa.red} + 2 \cdot t_s \cdot s_{eff.1} + 2 \cdot t_s \cdot 0.5 b_{eff.fo.1} + 2 \cdot A_{s.red} \end{aligned} = 771.693 \cdot mm^2$$

$$A_{tot.eff} := A_{tot.sc.eff} \cdot (1 - \delta_{sc}) = 755.21 \cdot mm^2$$

$$z_{tp.tot.eff} := \frac{\begin{aligned} & 2 \cdot A_{fu} \cdot (s_1) + A_{gu} \cdot (s_2) + 2 \cdot A_{wu} \cdot (s_3) + 2 \cdot A_{w.fu} \cdot (s_4) \cdots \\ & + 2 \cdot t_s \cdot \left(z_{tp.eff} - h_{w.fu} - l_{wu} \cdot \sin(\phi_w) - t_s\right) \cdot (s_5) + 2 \cdot t_s \cdot s_{eff.n} \cdot (s_6) \cdots \\ & + 2 \cdot t_{sa.red} \cdot s_{eff.3} \cdot (s_7) + 2 \cdot t_{sa.red} \cdot l_{w.fo} \cdot (s_8) + 2 \cdot t_{sa.red} \cdot s_{eff.2} \cdot (s_9) \cdots \\ & + 2 \cdot t_s \cdot s_{eff.1} \cdot (s_{10}) + 2 \cdot t_s \cdot 0.5 b_{eff.fo.1} \cdot (s_{11}) + 2 \cdot A_{s.red} \cdot (s_{12}) \end{aligned}}{A_{tot.eff}} = 102.086 \cdot mm$$

The second moment of area is calculated excluding the bt^3/12 part when its contribution is very small.

$$
\begin{aligned}
I_{tot.sc.eff} := {} & 2\cdot A_{fu}\cdot\left(z_{tp.tot.eff}-s_1\right)^2 + A_{gu}\cdot\left(z_{tp.tot.eff}-s_2\right)^2 \ldots \\
& +2\cdot\left[\frac{t_s\cdot\left(l_{wu}\cdot\sin(\phi_w)\right)^3}{12} + A_{wu}\cdot\left(z_{tp.tot.eff}-s_3\right)^2\right]\ldots \\
& +2\cdot\left[\frac{t_s\cdot\left(h_{w.fu}\right)^3}{12} + A_{w.fu}\cdot\left(z_{tp.tot.eff}-s_4\right)^2\right]\ldots \\
& +2\left[\begin{array}{l}\dfrac{t_s\cdot\left(z_{tp.eff}-h_{w.fu}-l_{wu}\cdot\sin(\phi_w)-t_s\right)^3}{12}\ldots \\ +t_s\cdot\left(z_{tp.eff}-h_{w.fu}-l_{wu}\cdot\sin(\phi_w)-t_s\right)\cdot\left(z_{tp.tot.eff}-s_5\right)^2\end{array}\right]\ldots \\
& +2\cdot\left[\frac{t_s\cdot\left(s_{eff.n}\right)^3}{12} + t_s\cdot s_{eff.n}\cdot\left(s_6-z_{tp.tot.eff}\right)^2\right]\ldots \\
& +2\cdot\left[\frac{t_{sa.red}\cdot\left(s_{eff.3}\right)^3}{12} + t_{sa.red}\cdot s_{eff.3}\cdot\left(s_7-z_{tp.tot.eff}\right)^2\right]\ldots \\
& +2\left[\frac{t_{sa.red}\cdot\left(l_{w.fo}\right)^3}{12} + t_{sa.red}\cdot l_{w.fo}\cdot\left(s_8-z_{tp.tot.eff}\right)^2\right]\ldots \\
& +2\cdot\left[\frac{t_{sa.red}\cdot\left(s_{eff.2}\right)^3}{12} + t_{sa.red}\cdot s_{eff.2}\cdot\left(s_9-z_{tp.tot.eff}\right)^2\right]\ldots \\
& +2\cdot\left[t_s\cdot s_{eff.1}\cdot\left(s_{10}-z_{tp.tot.eff}\right)^2\right] + 2\cdot t_s\cdot 0.5b_{eff.fo.1}\cdot\left(s_{11}-z_{tp.tot.eff}\right)^2\ldots \\
& +2\cdot A_{s.red}\cdot\left(s_{12}-z_{tp.tot.eff}\right)^2
\end{aligned}
$$

$I_{tot.eff} := I_{tot.sc.eff}\cdot\left(1-2\cdot\delta_{sc}\right) = 3.682\times10^6\cdot mm^4$

$I_{comp} := I\cdot b_s = 5.408\times10^6\cdot mm^4$ Compare value with that from Lindab

B 12.2 Moment and Shear Force Distribution

Applied evenly distributed load on the global beam model and the resulting moment and shear force distribution.

$M_{Ed.g}(x)$ The distributed moment

$V_{Ed.g}(x)$ The distributed shear force

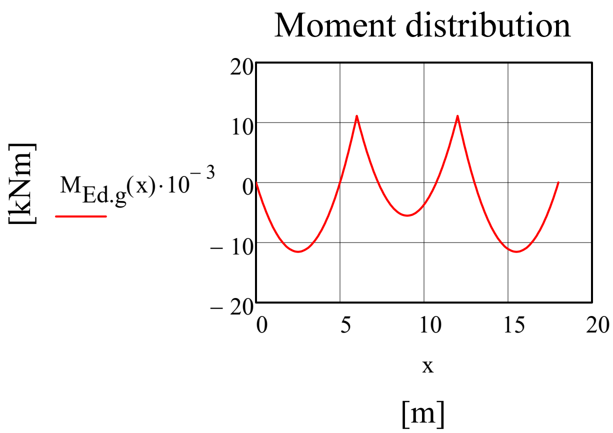

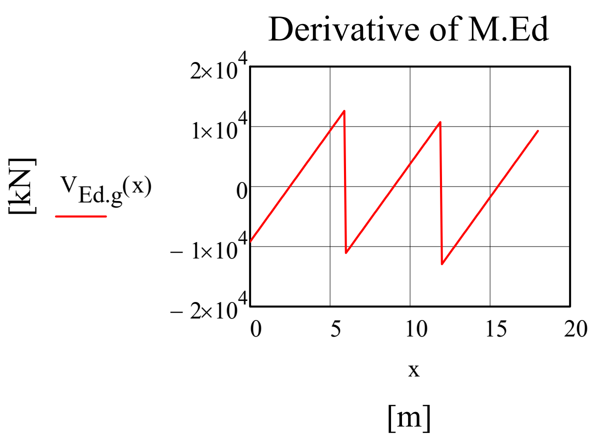

$R_A = 9.25\cdot kN$ $\quad M_A := 0kN\cdot m$ $\quad M_{AB} := M_{Ed.g.max.1} = -11.563\cdot kN\cdot m$

$R_B = 24.05\cdot kN$ $\quad M_B = 11.1\cdot kN\cdot m$ $\quad M_{BC} := M_{Ed.g.max.mid} = -5.55\cdot kN\cdot m$

$R_C = 24.05\cdot kN$ $\quad M_C = 11.1\cdot kN\cdot m$ $\quad M_{CD} := M_{Ed.g.max.1} = -11.563\cdot kN\cdot m$

$R_D = 9.25\cdot kN$ $\quad M_D := 0kN\cdot m$

$$R_{Ed.g} := \max(R_A, R_B, R_C, R_D) = 24.05\cdot kN$$

$$M_{Ed.g.s} := -\max(M_A, M_B, M_C, M_D) = -11.1\cdot kN\cdot m$$

$$M_{Ed.g.f} := -\min(M_{AB}, M_{BC}, M_{CD}) = 11.563\cdot kN\cdot m$$

B 12.3 Capacity of the Sheet:

Moment capacity:

$$W_{eff} := \frac{I_{tot.eff}}{\left(h_s - z_{tp.tot.eff}\right)} = 3.963 \times 10^4 \cdot mm^3 \qquad W_{el} = 3.918 \times 10^5 \cdot mm^3$$

$$W_{eff} < \frac{W_{el}}{3} = 1$$

The moment capacity for compression and when taking into account the effect of modified critical stress depending on stiffeners in both the flanges and the webs for calculating distortional slenderness.

$$M_{c.Rd} := \frac{f_{yb}}{\gamma_{M0}} \cdot W_{eff} = 16.644 \cdot kN \cdot m \qquad \frac{f_{yb}}{\gamma_{M0}} = 420 \cdot MPa$$

$$M_{Rd.mod} := \frac{\sigma_{cr.mod}}{\gamma_{M0}} \cdot W_{eff} = 8.591 \cdot kN \cdot m \qquad \frac{\sigma_{cr.mod}}{\gamma_{M0}} = 216.805 \cdot MPa$$

The effect of shear deformations:

According to SS-EN 1993-1-5 the shear deformations should be regarded.

$L_1 := 6m$ $\qquad$ $L_2 := 6m$ $\qquad$ Length of span 1 and 2

$$b_0 := \frac{b_{fo}}{2} \qquad L_e := 0.25 \cdot \left(L_1 + L_2\right)$$

Shear deformations need to be regarded if the following criteria is not met:

$$b_0 < \frac{L_e}{50} = 0$$

$$\alpha_0 := \sqrt{1 + \frac{2A_s}{b_0 \cdot t_s}}$$

$$\kappa := \frac{\alpha_0 \cdot b_0}{L_e} = 0.12$$

$$\beta_{pos} := \begin{cases} 1.0 & \text{if } \kappa \le 0.02 \\ \dfrac{1}{1 + 6.4 \cdot \kappa^2} & \text{if } 0.02 < \kappa \le 0.70 \\ \dfrac{1}{5.9 \cdot \kappa} & \text{if } \kappa > 0.70 \end{cases} \qquad \beta_{neg} := \begin{cases} 1.0 & \text{if } \kappa \le 0.02 \\ \dfrac{1}{1 + 6.0 \cdot \left(\kappa - \dfrac{1}{2500 \cdot \kappa}\right) + 1.6 \cdot \kappa^2} & \text{if } 0.02 < \kappa \le 0.70 \\ \dfrac{1}{8.6 \cdot \kappa} & \text{if } \kappa > 0.70 \end{cases}$$

$\beta_0 := \min\left[\beta_{pos}, \left(\frac{0.55 + 0.25}{\kappa}\right)\cdot\beta_{pos}\right]$ At the edge supports

$b_{eff} := \beta_{pos}\cdot b_0 = 264.733\cdot mm$

$b_{eff.fo.2} + b_{eff.fo.1} \le b_{eff} = 1$ Criterion fulfilled and we do not need to check shear deformations!

The combination of buckling and shear can be regarded by calculating an effective area of the compressed flange:

$$\alpha_0 := \sqrt{\frac{\left(b_{eff.fo.1}\cdot 2 + b_{eff.fo.2}\right)\cdot t_s}{b_0\cdot t_s}}$$

$$\kappa := \frac{\alpha_0\cdot b_0}{L_e} = 0.06$$

$$\beta_{pos} := \begin{cases} 1.0 & \text{if } \kappa \le 0.02 \\ \dfrac{1}{1 + 6.4\cdot\kappa^2} & \text{if } 0.02 < \kappa \le 0.70 \\ \dfrac{1}{5.9\cdot\kappa} & \text{if } \kappa > 0.70 \end{cases} \qquad \beta_{neg} := \begin{cases} 1.0 & \text{if } \kappa \le 0.02 \\ \dfrac{1}{1 + 6.0\cdot\left(\kappa - \dfrac{1}{2500\cdot\kappa}\right) + 1.6\cdot\kappa^2} & \text{if } 0.02 < \kappa \le 0.70 \\ \dfrac{1}{8.6\cdot\kappa} & \text{if } \kappa > 0.70 \end{cases}$$

$\beta_{pos} = 0.978$ $\beta_{neg} = 0.756$ $A_{c.eff} = 3.588 \times 10^{-4}\, m^2$

$A_{eff.fo} := A_{fo.eff}\cdot\beta_{pos} = 128.256\cdot mm^2$

$A_{c.eff} := A_{eff.fo} + \left(2\cdot t_s\cdot s_{eff.n} + 2\cdot A_{sa.red} + 2\cdot t_s\cdot s_{eff.1}\right) = 355.942\cdot mm^2$

$s_p := \max\left(l_{wu}, l_{wm}, l_{wo}\right)$

$s_d := l_{wu} + l_{w.fu} + l_{wm} + l_{w.fo} + l_{wo} = 213.937\cdot mm$

$s_w = 186.244\cdot mm$

$$k_r := 5.34 + \frac{2.10}{t_s}\cdot\left(\frac{I_{sa}\cdot 2}{s_d}\right)^{\frac{1}{3}}$$

slenderness of the web:

$$\lambda_w := \max\left[\left(0.346 \cdot \frac{s_d}{t_s} \cdot \sqrt{\frac{5.34}{k_r} \cdot \frac{f_{yb}}{E_s}}\right), \left(0.346 \cdot \frac{s_p}{t_s} \cdot \sqrt{\frac{f_{yb}}{E_s}}\right)\right] = 1.345$$

We assume that the continuous sheet in practice is supported with stiffeners at the ends giving the following capacity:

$$f_{bv} := \begin{vmatrix} (0.58 \cdot f_{yb}) \text{ if } \lambda_w \le 0.83 \\ \left(0.48 \cdot \dfrac{f_{yb}}{\lambda_w}\right) \text{ if } 0.83 < \lambda_w < 1.40 \\ \left(0.48 \cdot \dfrac{f_{yb}}{\lambda_w}\right) \text{ if } \lambda_w \ge 1.40 \end{vmatrix}$$

$$f_{bv} = 149.892 \cdot \text{MPa}$$

$$V_{b.Rd} := \frac{\dfrac{h_w}{\sin(\phi_w)} \cdot t_s \cdot f_{bv}}{\gamma_{M0}} = 37.765 \cdot \text{kN}$$

Reaction forces:

Buckling due to support moment and concentrated loads must be considered i.e. crippling of the web. The local resistance for transverse loads is calculated according to SS-EN 1993-1-3 6.1.7.4.

$e_{max} := 4.49\text{mm}$ $\quad$ $e_{min} := 2.79\text{mm}$ $\quad$ Eccentricity of the fold relative the system line of the web

$2 < \dfrac{e_{max}}{t_s} < 12 = 1$ $\quad$ The condition is fulfilled!

The resistance is calculated first like an un stiffened sheet and the multiplied with a reduction factor to compensate for the folds in the webs.

$b_d := 2 \cdot b_{fu} + b_{gu} = 79.154 \cdot \text{mm}$ $\quad$ Width of area where the load is applied

$$\kappa_{as.R} := \min\left(1.45 - 0.05 \cdot \frac{e_{max}}{t_s}, 0.95 + 35000 \cdot t_s^{\,2} \cdot \frac{e_{min}}{b_d^{\,2} \cdot s_p}\right) = 1.174$$

At the supports

Conditions to be fulfilled:
- the clear distance from the reaction force/point load to a free edge must be 40 mm or more.
- the cross-section must fulfill the criteria according to SS-EN 1993-1-3 6.1.7.3 below

$$\frac{\max(r_{gu}, r_{go}, r_{wo}, r_{wu})}{t_s} \le 10 = 1$$

$$\frac{h_w}{t_s} \le 200 \cdot \sin(\phi_w) = 1$$

$$45deg \le \phi_w \le 90deg = 1$$

Since the sheeting is continuous over the supports we assume category 2 according to Figure 6.9 SS-EN 1993-1-3

$l = 6\,m$ Length of first span

$\alpha := 0.15$ Category coefficient

$s_s := 150mm$ The size of the support

$$\beta_v := \frac{\left|V_{Ed.g}\left(1 - \frac{s_s}{2}\right)\right| - \left|V_{Ed.g}\left(1 + \frac{s_s}{2}\right)\right|}{\left|V_{Ed.g}\left(1 - \frac{s_s}{2}\right)\right| + \left|V_{Ed.g}\left(1 + \frac{s_s}{2}\right)\right|} = 0.079$$

$$l_a := \begin{cases} s_s & \text{if } \beta_v \le 0.2 \\ (10mm) & \text{if } \beta_v \ge 0.3 \\ \frac{(0.3 - \beta_v)\cdot(s_s - 10mm)}{0.1} & \text{if } 0.2 < \beta_v < 0.3 \end{cases}$$

$$r := \min(r_{wo}, r_{wu}) = 2 \cdot mm$$

$$R_{w.Rd} := \frac{\alpha \cdot t_s^2 \cdot \sqrt{f_{yb} \cdot E_s} \cdot \left(1 - 0.1 \cdot \sqrt{\frac{r}{t_s}}\right) \cdot \left(0.5 + \sqrt{0.02 \cdot \frac{l_a}{t_s}}\right) \cdot \left[2.4 + \left(\frac{\phi_w}{90deg}\right)^2\right]}{\gamma_{M1}} = 12.12 \cdot kN$$

$R_{w.Rd.R} := R_{w.Rd} \cdot \kappa_{as.R} = 14.23 \cdot kN$ Capacity for one web with regard to support reactions.

Combined bending moment and concentrated force according to SS-EN 1993-1-3 6.1.11:

$M_{Ed.g.f} = 11.563 \cdot kN \cdot m$ Maximum moment in field

$M_{Ed.g.s} = -11.1 \cdot kN \cdot m$ Maximum moment at support

$M_{c.Rd} = 16.644 \cdot kN \cdot m$ Moment capacity

$R_{Ed.g} = 24.05 \cdot kN$ Maximum reaction force at support

$2R_{w.Rd.R} = 28.46 \cdot kN$ Capacity of two webs

$V_{b.Rd} = 37.765 \cdot kN$ Shear capacity with regard to buckling

$M_{d.f} = 15.16\, m \cdot kN$ Maximum moment in field according to Lindab

$M_{d.s} = 20.768\, m \cdot kN$ Maximum moment at support according to Lindab

$$\frac{-M_{Ed.g.s}}{M_{c.Rd}} \le 1 = 1$$

$$\frac{R_{Ed.g}}{2R_{w.Rd.R}} \le 1 = 1$$

$$\frac{M_B}{M_{c.Rd}} + \frac{R_B}{2R_{w.Rd.R}} \le 1.25 = 0 \qquad \frac{M_A}{M_{c.Rd}} + \frac{R_A}{2R_{w.Rd.R}} \le 1.25 = 1$$

The combination of moment and reaction force at the support sets the limit of what the beam can handle. No reduction with regard to the peak has been taken. The moments are lower than the capacity given by Lindab.

B 12.4 Moment Capacity of the Sheeting:

$$P_{cr} = \frac{q_{cr} \cdot \left(1 - 2 \cdot a_{joint}\right)}{2}$$ Point load acting at the end of the cantilever due to mid sheet

$$M_{B.cr} = q_{cr} \cdot \frac{a_{joint}^{2}}{2} + a_{joint} \cdot P_{cr}$$ Support moment B

$$R_{B.cr} = q_{cr} \cdot a_{joint} + P_{cr} + M_{B.cr} \cdot \frac{1}{1} + q_{cr} \cdot \frac{1}{2}$$ Reaction force support B

$$\frac{M_{B.cr}}{M_{c.Rd}} + \frac{R_{B.cr}}{2R_{w.Rd.R}} = 1$$ The moment and shear capacity with regard to 100 % utalisation.

$$\frac{q_{cr}\cdot\frac{a_{joint}^2}{2}+a_{joint}\cdot\frac{q_{cr}\cdot(l-2\cdot a_{joint})}{2}}{M_{c.Rd}} \ldots \quad = 1$$
$$+\frac{q_{cr}\cdot a_{joint}+\frac{q_{cr}\cdot(l-2\cdot a_{joint})}{2}+\left[q_{cr}\cdot\frac{a_{joint}^2}{2}+a_{joint}\cdot\frac{q_{cr}\cdot(l-2\cdot a_{joint})}{2}\right]\cdot\frac{1}{l}+q_{cr}\cdot\frac{l}{2}}{2R_{w.Rd.R}}$$

$$q_{cr} := \frac{1}{\left[\frac{\frac{a_{joint}^2}{2}+a_{joint}\cdot\frac{(l-2\cdot a_{joint})}{2}}{M_{c.Rd}} \ldots + \frac{a_{joint}+\frac{(l-2\cdot a_{joint})}{2}+\left[\frac{a_{joint}^2}{2}+a_{joint}\cdot\frac{(l-2\cdot a_{joint})}{2}\right]\cdot\frac{1}{l}+\frac{l}{2}}{2R_{w.Rd.R}}\right]} = 2.447\cdot\frac{kN}{m}$$

The critical load given the combination of moment and shear at the support.

$q_{cr} = 2.447\cdot\frac{kN}{m}$ Critical load for evenly distributed load

$P_{cr} := \frac{q_{cr}\cdot(l-2\cdot a_{joint})}{2} = 4.239\cdot kN$ Point load acting at the end of the cantilever due to mid sheet

$M_{B.cr} := q_{cr}\cdot\frac{a_{joint}^2}{2}+a_{joint}\cdot P_{cr} = 7.341\cdot kN\cdot m$ Support moment B

$R_{A.cr} := -M_{B.cr}\cdot\frac{1}{l}+q_{cr}\cdot\frac{l}{2} = 6.118\cdot kN$ Reaction force support A

$R_{B.cr} := q_{cr}\cdot a_{joint}+P_{cr}+M_{B.cr}\cdot\frac{1}{l}+q_{cr}\cdot\frac{l}{2} = 15.906\cdot kN$ Reaction force support B

$M_{AB.cr} := -R_{A.cr}\cdot l+q_{cr}\cdot\frac{l^2}{2} = 7.341\cdot kN\cdot m$

B 12.5 Diaphragm Action:

Diaphragm action is not needed to be combined with the transversal load-bearing capacity, however it must fulfill the following criteria:

Stress in the edge beam consist of a force couple meaning that the shear flow is evenly distributed.

$$S(x) := \frac{V_{Ed.g}(x)}{b_s}$$ Shear flow in the sheet

$$\tau_{Ed}(x) := \frac{V_{Ed.g}(x)}{b_s \cdot t_s}$$ Shear due to diaphragm action

$$\tau_{Ed}(0m) \le 0.25 \cdot \frac{f_{yb}}{\gamma_{M1}} = 1$$

Force in connectors (controls were also made in chapter 8):

$$F_{v.Ed} := \frac{\frac{M_{Ed.g}(l)}{m}}{4 \cdot a_{joint} \cdot \sin(\phi_w)} \cdot b_s = 1.821 \cdot kN$$ Vertical force on the connectors

Shear capacity of the screws

$$F_{v.Rd} = 7.84 \cdot kN$$

$$F_{v.Ed} \le F_{v.Rd} = 1$$

Local buckling of the web:

$$R_{Ed.g} \le 2R_{w.Rd.R} = 1$$

Global buckling:

$$V_{Ed.g}(l) \le \frac{\left(V_{b.Rd} \cdot L_{tot}^{2}\right)}{L_{tot}^{2}} = 1$$

B 13 Summary of Section Modulus

Sectional modulus for:
1. shell without hinge, including transversal grooves
2. shell without hinge, flat flange
3. solid without hinge
4. shell with hinge
5. solid elastic with hinge
6. solid plastic with hinge
7. beam model.

	Measured values from Abaqus:	Calculated values:	Calculated values (disregard rounded corners):
1	$W_{Ab.tg} = 2.043 \times 10^5 \cdot mm^3$	$W_{el.tg} = 1.406 \times 10^5 \cdot mm^3$	$W_{el.sc} = 1.469 \times 10^5 \cdot mm^3$
2	$W_{Ab.flat} = 1.588 \times 10^5 \cdot mm^3$	$W_{el.flat} = 1.406 \times 10^5 \cdot mm^3$	$W_{el.sc} = 1.469 \times 10^5 \cdot mm^3$
3	$W_{Ab.s} = 1.349 \times 10^5 \cdot mm^3$	$W_{el.s} = 1.267 \times 10^5 \cdot mm^3$	$W_{el.s.sc} = 1.324 \times 10^5 \cdot mm^3$
4	$W_{Ab.l} = 3.652 \times 10^5 \cdot mm^3$	$W_{el.l} = 3.918 \times 10^5 \cdot mm^3$	$W_{el.l.sc} = 4.093 \times 10^5 \cdot mm^3$
5	$W_{Ab.s.l} = 1.492 \times 10^5 \cdot mm^3$	$W_{el.s.l} = 1.267 \times 10^5 \cdot mm^3$	$W_{el.s.l.sc} = 1.324 \times 10^5 \cdot mm^3$
6	$W_{Ab.s.l.p.2} = 1.336 \times 10^5 \cdot mm^3$	$W_{el.s.l.p} = 1.267 \times 10^5 \cdot mm^3$	$W_{el.s.l.sc} = 1.324 \times 10^5 \cdot mm^3$
7	$W_{el.g.Ab} = 4.688 \times 10^4 \cdot mm^3$	$W_{el.g} = 4.692 \times 10^4 \cdot mm^3$	

	ratio:	ratio:
1	$\frac{W_{Ab.tg}}{W_{el.tg}} = 1.453$	$\frac{W_{Ab.tg}}{W_{el.sc}} = 1.391$
2	$\frac{W_{Ab.flat}}{W_{el.flat}} = 1.129$	$\frac{W_{Ab.flat}}{W_{el.sc}} = 1.081$
3	$\frac{W_{Ab.s}}{W_{el.s}} = 1.064$	$\frac{W_{Ab.s}}{W_{el.s.sc}} = 1.019$
4	$\frac{W_{Ab.l}}{W_{el.l}} = 0.932$	$\frac{W_{Ab.l}}{W_{el.l.sc}} = 0.892$

5 $\frac{W_{Ab.s.l}}{W_{el.s.l}} = 1.177$ $\frac{W_{Ab.s.l}}{W_{el.s.l.sc}} = 1.127$

6 $\frac{W_{Ab.s.l.p.2}}{W_{el.s.l}} = 1.054$ $\frac{W_{Ab.s.l.p.2}}{W_{el.s.l.sc}} = 1.009$

7 $\frac{W_{el.g.Ab}}{W_{el.g}} = 0.999$

The solid models seem to correlate very well between the calculated values based on the disregard of rounded corners (which Eurocode demands for the cross-section).

B 14 Comparing Lindab and the Numerical Model

The moments that Lindab set to be the capacity over support and in field compared to the numerical values retrieved from Abaqus.

$M_{d.s} = 20.768 \cdot kN \cdot m$ $\qquad M_{k.s} = 25.96 \cdot \frac{kN \cdot m}{m}$ Support moment capacity according to Lindab

$-M_{d.f} = -15.16 \cdot kN \cdot m$ $\qquad M_{k.f} = 18.95 \cdot \frac{kN \cdot m}{m}$ Field moment capacity according to Lindab

$M_{max.s} := 40.6143 kN \cdot m$ Maximum support moment in beam model

$M_{mid.f} := -21.9106 kN \cdot m$ Maximum field moment in mid-span

$M_{max.f} := -41.9872 kN \cdot m$ Maximum field moment in outer span

The conclusion is that the capacity of the beam element model computed in Abaqus has a higher capacity than what Lindab assumes.

Calculated capacities for the cross-section with regard to the combination of shear and moment over the support:

$M_{AB.cr} = 7.341 \cdot kN \cdot m$ Maximum calculated field moment

$M_{B.cr} = 7.341 \cdot kN \cdot m$ Maximum calculated support moment

$M_{c.Rd} = 16.644 \cdot kN \cdot m$ Compressional capacity of the sheet

Load in Abaqus when yielding over the support:

$q_{yield} := 0.33 \cdot 20 \frac{N}{mm} = 6.6 \cdot \frac{kN}{m}$ $\qquad M_{yield} := 20 kN \cdot m$